H24/3689

MONASH UNIVERSITY
THESIS ACCEPTED IN SATISFACTION OF THE
REQUIREMENTS FOR THE DEGREE OF
DOCTOR OF PHILOSOPHY

ON..... [redacted] 16 September 2003 .....

.....[redacted].....

Sec. Research Graduate School Committee

The Vacuum Swing Adsorption Process for Oxygen Enrichment. A Study into the Dynamics, Modelling and Control.

Christopher Chun Keong Beh
Bachelor of Engineering (Mechanical) (Auckland)

A thesis submitted in partial fulfillment of the requirements for the degree of
Doctor of Philosophy

Department of Chemical Engineering
Monash University
Australia

June 2003

Statement

The work presented in this thesis for the Degree of Doctor of Philosophy in Chemical Engineering is, to the best of my knowledge and belief, original, except as acknowledged in the text, and that the material has not been submitted, either in whole or in part, for a degree at this or any other university.

Chris Beh.

Acknowledgements

Firstly, the author would like to acknowledge the financial support of his industrial sponsor, Air Products and Chemicals, Inc., throughout the course of this research effort. The author is indebted to the help and useful discussion from both existing and past members of the Monash Adsorption Research Group especially Dr. Paul A. Webley (thesis supervisor), Dr. Simon J. Wilson, Dr. Jianming He, Mr. Richard Shannon Todd and also to Mr. Graeme Short for useful suggestions regarding process analysis. A special thanks is owed to Dr. K. Satheesh Kumar for the very beneficial discussions on various numerical techniques and methods and also to Mr. Francis Greg Shinskey for his contribution in assisting the author's understanding of process control theory and practical application.

The author wishes to thank the workshop staff in the Department of Chemical Engineering especially Mr. Paul Beardsley, Mr. Peter Froud, Mr. John Barnard Mr. Roy Harrip, Mr. Gamini Ganegoda, Mr. Ron Graham and Mr. Ross Ellingham, because without their continued assistance this research effort would not have been able to proceed. The role of the administrative staff is often overlooked, yet their contribution smoothed many of the administrative hurdles during the course of this work from efficient placement of purchase orders to overseas travel assistance. The author, therefore, would like to gratefully acknowledge the roles of Mrs. Yvonne Arnold, Mrs. Judy Lawlor, Mrs. Irene Murray and Mr. Stelios Konstantinidis for their help throughout the tenure of the project.

Last but never the least, the author wishes to thank his parents and family for their support throughout the term of this project and especially Ms. Mary Kim for her efforts in proof reading this thesis and Ms. Emma Kim for cross-checking the consistency of the references.

Thank you!

Abstract

The literature on the application of control theory to pressure swing adsorption (VSA/PSA) processes contains very little published work. Given the relative importance of this technology, a barrier between the developers of current control theory (which has been a fruitful area of research) and the adsorption community exists. Why this is so, is largely unknown but some of the reasons for this curious fact probably stems from the late maturity of this technology (the late 1980's showed a resurgence in its use) compared to other systems such as distillation and that most gas companies utilise their own proprietary control techniques. Another reason could be the relative complexity and variations in the configurations (i.e. different cycle arrangements and number of adsorber columns) of these systems compared to other unit operations and the deficiency in the control literature regarding batch process control.

Most PSA/VSA systems are multiple-output-multiple-input (MIMO) processes, meaning that there is more than one control objective, which in turn is a function of each boundary condition in the process. Unlike most commonly encountered control problems, the control of pressure and vacuum swing adsorption systems is exceptionally challenging due to the cyclic, bulk gas separation nature of the process and its inherent nonlinearities (operates under non-equilibrium, non-steady state, non-isothermal conditions). Performance targets such as product oxygen purity, production and pressure as demanded by the customer is a strong function of process disturbances such as seasonal and diurnal temperature changes, inlet pressure, changes in customer requirements and processing conditions. The application of decentralised control using multiple, individual PID controllers has been the traditional method for control of these processes in the field. Difficulties with these controllers still occur due, in part, to the incorrect implementation of the PID blocks, incorrect choice and pairings of both manipulated and controlled variables and a general lack of understanding of the control problem at hand.

To better understand the complex nature of the process, part of the focus of this research effort was to characterise the system and determine the variables of importance to aid process modelling. This was attempted on two levels: through the application of artificial neural networks (an empirical modelling technique) and the development of an isothermal, lumped parameter, coupled tank model. Although both methods showed satisfactory predictive ability, the computational requirements for real-time application in a process control structure hindered practical implementation. Instead, simple first and second-order models were employed in the kernel of the model predictive control structure discussed below. In addition, a simple method was developed (based on experimental observations) that permitted estimation of the location and shape of the adsorption front to aid process monitoring and plant diagnostics.

The originality of this thesis stems from the fact that it represents the first known contribution in the field of process control of these systems and embodies both building and commissioning of an experimental pilot oxygen VSA plant and process modelling. Consequently, there are several objectives involved with this research with the ultimate goal being the development of a robust controller structure. The initial finding from this project is that both single-input-single-output (SISO) and MIMO PID controllers, if implemented correctly, can control to a satisfactory degree. The PID algorithm was then compared to a novel MPC controller developed in the course of this work. Although the preliminary results showed that MPC control offered only comparable performance to multiple loop PID, it is recommended that further research into the application of more traditional model-based architectures be conducted as well as investigating the advantages and limitations of the current MPC structure. It is also reasoned that given the nonlinearity of the process, control with PID at high product concentrations (> 90%) may indicate larger disparities between the two competing techniques and in this case PID control because of its linear, decentralised nature, may fail. Lastly, the use of both full and one-way decoupling as method for separating interaction and thereby assisting MIMO PID was not met with any success. Model errors caused unstable loop behaviour and resulted in the failure of PID with control loop decoupling.

List of Publications

International Refereed Journals

Beh, C.C.K. and P. Ranganathan, "Comments on "An Artificial Neural Network as a Model for Chaotic Behavior of a Three-Phase Fluidized Bed"", *Chaos, Solitons and Fractals*, **17**, 985-986, 2003

Beh, C.C.K., K.A. Smith and P.A. Webley, "The VSA Process for Oxygen Enrichment: Process Description and Dynamic Modeling Using Neural Networks", *International Journal of Smart Engineering System Design*, **5**, 1-9, 2003

Beh, C.C.K. and P.A. Webley, "A Method for the Determination of Composition Profiles in Industrial Air Separation, Pressure Swing Adsorption Systems", *Adsorption Science and Technology*, **21**, 35-52, 2003

Beh, C.C.K. and P.A. Webley, "The Dynamics and Characteristics of an Oxygen Vacuum Swing Adsorption Process to Step Perturbations. Part 1. Open Loop Responses", *Adsorption Science and Technology*, **21**, 319-347, 2003

Beh, C.C.K. and P.A. Webley, "The Dynamics and Characteristics of an Oxygen Vacuum Swing Adsorption Process to Step Perturbations Part 2. Sensitivity Analysis and Controller Pairings", *Adsorption Science and Technology*, **21**, 349-362, 2003

Beh, C.C.K. and P.A. Webley, "A Practical Method for the Dynamic Determination of the Product Oxygen Concentration in Pressure-Swing Adsorption Systems", *Industrial and Engineering Chemistry Research*, in press, 2003

Beh, C.C.K. and P.A. Webley, "Control of the Oxygen Vacuum Swing Adsorption Process. Part 1. Single Loop Control", *Control Engineering Practice*, submitted for review, 2003

Beh, C.C.K. and P.A. Webley, "Control of the Oxygen Vacuum Swing Adsorption Process. Part 2. Multiple Loop Control", *Control Engineering Practice*, submitted for review, 2003

Todd, R.S., J. He, P.A. Webley, C.C.K. Beh, S.J. Wilson and M.A. Lloyd, "Fast Finite Volume Method for PSA/VSA Cycle Simulation – Experimental Validation", *Industrial and Engineering Chemistry Research*, **40**, 3217-3224, 2001

Wilson, S.J., C.C.K. Beh, P.A. Webley and R.S. Todd, "The Effects of a Readily Adsorbed Trace Component (Water) in a Bulk Separation PSA Process: The Case of Oxygen VSA", *Industrial and Engineering Chemistry Research*, **40**, 2702-2713, 2001

International Refereed Conferences

Beh, C.C.K., R.S. Todd, P.A. Webley, "Capturing Mass Transfer Effects Using Neural Network Models. Case Study - Breakthrough Fronts for N_2/O_2 Separation", *Proceedings of the Sixth World Congress in Chemical Engineering*, Paper No. 228, ISBN 0 7340 2201 8, 2001

Beh, C.C.K., K.A. Smith and P.A. Webley, "Dynamic Modelling Using Neural Networks. Case Study – Pilot Scale VSA Process for Oxygen Production", *Smart Engineering System Design: Neural Networks, Fuzzy Logic, Evolutionary Programming, Data Mining and Complex Systems*, C.H. Dagli, A.L. Buczak, J. Ghosh, M.J. Embrechts, O. Ersoy and S. Kercel (Eds.), ASME Press, New Jersey, **11**, pp. 551-556, 2001

Beh, C.C.K. and P.A. Webley, "On-Line Modelling of an Oxygen Vacuum Swing Adsorption Process Using Neural Networks", *Proceedings of the Sixth World Congress in Chemical Engineering*, Paper No. 226, ISBN 0 7340 2201 8, 2001

Beh, C., S. Wilson, P. Webley and J. He, "The Control of the Vacuum Swing Adsorption Process for Air Separation", *Proceedings of the Second Pacific Basin Conference on Adsorption Science and Technology*, D. Do (Ed.), World Scientific, Singapore, pp. 663-667, 2000

Webley, P., C. Beh, J. He, S. Wilson and S. Todd, "Numerical Simulation and Experimental Validation of Multiple-Layer, Non-Isothermal, Bulk gas Pressure Swing, Adsorption", *Proceedings of the Second Pacific Basin Conference on Adsorption Science and Technology*, D. Do (Ed.), World Scientific, Singapore, pp. 658-662, 2000

International Conferences

Beh, C.C.K. and P.A. Webley, "Open Loop Dynamics of an Oxygen Vacuum Swing Adsorption Process", *AIChE Annual Meeting*, November, Paper No. 121e, 2002

Local Refereed Conferences

Beh, C.C.K. and P.A. Webley, "Control of Periodic Adsorption Processes – A Review and Some Recent Developments", *Proceedings of the 31st Annual Australasian Chemical Engineering (Chemeca) Conference*, September, Paper No. 253, 2003

Todd, R.S., C.C.K. Beh, S.J. Wilson and P.A. Webley, "Simplified Modelling of Pressure Driven Flow in Pressure Swing Adsorption Process", *Proceedings of the Melbourne Graduate Fluids Conference*, 5 July, pp. 5-8, 2001

Table of Contents

List of Figures

List of Tables

Chapter One

Introduction

Separation by adsorption of fluid mixtures is a widely accepted practice. It has gone from a lab curiosity in the early part of this century, to a viable alternative technology for the production of nitrogen, hydrogen and oxygen to name a few applications. Reduced cost and high efficiency are the main advantages this technology has to offer over its competitors such as cryogenic distillation. This chapter will briefly introduce the concept of adsorption and the processes that incorporate this phenomenon and the scope and objectives of this study.

1.1 WHAT IS ADSORPTION?

Adsorption is the interaction between the species present in a fluid phase (either gas or liquid), and a solid surface [Tien, 1984]. It involves the selective uptake of one or more of the species within the fluid (the adsorbate) onto the solid surface. The species is then defined as being adsorbed. The use of this phenomenon as a method of separation is not new with the Egyptians and Sumerians (around 3750 BC) applying this method for the reduction of copper, zinc and tin ores using charcoal for the manufacture of bronze [Dabrowski, 2001]. However, over the past twenty years there has been a significant increase in the number of patents and publications in this field [Sircar, 2000].

There are various types of adsorbents both of the organic and inorganic forms. Activated carbon, polymeric adsorbents and even cellulose and wool form part of the family of organic adsorbents. On the other hand, silica gel and alumina are two of the more common forms of inorganic adsorbents [Farooq *et al.*, 1994]. There is an important class of inorganic adsorbents called zeolites that have gained much popularity because of the nature of its adsorptive, selective and regenerative properties. It is this class of adsorbents and their use in the separation of oxygen from air that will form the basis of this investigation.

Zeolites are generally aluminosilicates [Yang, 1987], (stoichiometric compounds of silica and aluminium). Internally, zeolites are crystalline and exhibit micropores, (within the crystals) of dimensions so uniform that they can distinguish between molecules of nearly identical size. It is because of this nature they are often referred to as molecular sieves.

The empirical formula for a zeolite containing a single cation, M, of valence, n, is:

$M_{2/n}.Al_2O_3.xSiO_2.yH2O$

where x is the silica-to-alumina ratio and y is the molar water of hydration.

Zeolites are available in a variety of structures such as 5A (Ca cation) and 13X (Na cation), where the 'A' and 'X' denote different crystalline framework and hence differences in the diameter of the pores. Zeolite development has arguably had the greatest influence in the air separation industry. Beginning with the use of the more traditional zeolites such as 13X and 5A through to the development of LiX and its consequent derivative, LiLSX (the "L" denoting low silica to alumina ratio), zeolites have improved process efficiency immensely. Furthermore, the new lithium based zeolitic sieves currently under study, which promise increased selectivities and adsorption capacities for nitrogen [Hutson *et al.*, 1999; Yang, 2000], is further establishing this technology as a viable non-cryogenic source of oxygen. However so, due to the importance of oxygen for industrial use, (oxygen is the third largest man-made chemical commodity following nitrogen), there is still sufficient interest, both industrial and academic, to understand and refine the process to accommodate the newer molecular sieve materials.

Additional information on adsorption for the interested reader can be found in the following references: Ruthven (1984), Tien (1984) and Yang (1987) with Dabrowski (2001) providing a very thorough review of adsorption from its humble beginnings to its many and varied process applications. Cassidy and Holmes (1984), Sircar (2001) and Shelley (1991), outline the many commercial applications of various adsorption processes and describes the future trends in adsorption technology including novel applications of hybrid systems. A review of the competing technologies such as distillation and membranes is summarised by Koros and Mahajan (2000) while Michael (1997) investigates the practical aspects of selecting the correct separation technology. In both articles, the authors admit that adsorption processes are more economically viable over membrane and cryogenic distillation systems for the production of oxygen at purities between 90%-95% and 20-150 metric tonnes per day. The work by Ray (2000), contains a large bibliographical listing of publications encompassing most fields of adsorption including the theory, types of adsorbents, ion exchange and various adsorption processes (both gas and liquid phases).

1.2 PRESSURE SWING ADSORPTION

A process that harnesses the physics of the adsorption phenomenon is termed pressure swing adsorption, (PSA). PSA is now a widely accepted unit operation for the purification of various chemical commodities such as methane, nitrogen and hydrogen, [Cassidy and Holmes, 1984; Sircar, 2001; Sircar, 2002] with one of the first patents dating back to Skarstrom in the 1950's [Farooq *et al.*, 1994]. It is generally accepted that there are three principal steps involved in operation of a PSA cycle -

1. *Adsorption*, which involves pressurising the bed with the feed stream to pressures well above atmospheric. This causes the preferentially adsorbed species to be selectively adsorbed from the bulk gas to solid phase.
2. *Desorption*, which allows the adsorbent bed to be regenerated for use during the next adsorption step by reduction of the adsorption bed total pressure to near or at atmospheric pressure.
3. *Purge*, which permits further desorption by lowering the partial pressure of the adsorbable species and forces contaminants (the adsorbate), in the fluid phase, down the bed by allowing a purge stream (typically product gas), containing relatively low concentrations of the adsorbable species, into the product end of the bed. The purge gas is normally sourced from the top of a bed that has undergone adsorption or from the product tank.

In addition to the steps mentioned above, most patented and industrial PSA cycles utilise a series of intermediary steps such as a low pressure purge and bed-to-bed equalisation to increase efficiency of production, increase oxygen recovery and decrease power costs to name but a few.

Arguably, the primary paradox of a PSA process is that the customer generally requires continuous production rate. However as described above, the PSA cycle operates in a batch-wise manner whereby transient pressure and flow conditions exist between each step. In order to achieve this, either more beds are required or the steps times and hence overall cycle time, is decreased. Typically, an adequately sized product buffer tank is provided in industrial installations to dampen the fluctuations caused by the unsteady nature of the process. A steady state situation, termed cyclic steady state (CSS), can exist in PSA operation and it is defined as a point when the operating variables, (such as flows, pressures and temperatures), are constant from cycle to cycle (refer to Chapter 2, §2.1.1 for a detailed definition).

1.3 VACUUM SWING ADSORPTION - FOR AIR SEPARATION

Since its inception as a patented process (with one of the first patents issued in October 1970 [Kumar, 1996]), vacuum swing adsorption (VSA) has gained popularity and is the system of choice for small to medium size oxygen enrichment plants. VSA is one of the few industrial processes available that has the capacity to produce high purity oxygen greater than 90% and offers a cost effective and efficient source of enriched oxygen product for applications

requiring less than 100 tons per day of contained oxygen [Kumar, 1996]. Bed volume becomes the limiting factor in terms of capital cost for larger installations [Smith and Klosek, 2001]. The drive for low-power, cost efficient oxygen production by Japanese steel arc furnaces during the 1980's, led to further research and development of this technology [LaCava *et al.*, 1998]. VSA is a derivative of PSA and thus operates in a similar manner except that the adsorption is performed at or slightly above atmospheric pressures while desorption occurs at pressures below atmospheric. As with PSA, continual change has occurred such as cycle development, step time refinement and most notably, the reduction in the number of beds. However, the development of adsorbents with increased selectivity and capacity, (i.e. the ability of the adsorbent to preferentially adsorbed nitrogen over oxygen), has kept VSA as the process of choice over other oxygen production processes such as cryogenic distillation and electrolysis of water for low purity oxygen [Kumar, 1996].

The VSA process was developed to exploit both the adsorptive capacity and the selectivity of the sieve to adsorbed nitrogen over oxygen at sub-atmospheric conditions. An example is illustrated in Figure 1.3a, which illustrates the capacity and selectivity of the CaX zeolite over a pressure window of 1 Bar for both the PSA and VSA process. It can clearly be seen in this simple example, that VSA has a higher relative loading of N_2 (0.46 mol/kg sieve), compared to a PSA cycle (0.26 mol/kg sieve) with similar relative loading of oxygen in both cases. In terms of the selectivity of the sieve, which is the ratio of the quantity of nitrogen adsorbed over the quantity of adsorbed oxygen, the VSA process yields a selectivity of 13 compared to the ratio of 9.5 in the PSA pressure window shown. It is clear that this particular sieve is more favourable for use in a VSA rather than a PSA environment because of its larger relative capacity for nitrogen adsorption and its larger selectivity ratio. The nonlinearity of the CaX isotherm means that increasing the pressure window in a PSA system, (say from 1 Bar.A to 3 Bar.A), in a bid to increase the relative loading, does not result in an as high a loading as a VSA system with the same pressure window. Also, the sharp gradient of the isotherm at pressures below atmospheric can be exploited by the use of deeper vacuums in a VSA system to further increase the amount of nitrogen adsorbed.

Further disadvantages of PSA for the use of oxygen production is that the amount of co-adsorbed oxygen increases with pressure, thus reducing the oxygen recovery, (ratio of quantity of oxygen in product stream over the quantity of oxygen in feed stream). In terms of capital cost, a PSA system requires a compressor to pressurise the inlet stream from atmospheric to the appropriate adsorption pressure, which also impacts on the running cost of the system due to this additional power requirement. Typically, an air blower is used in most industrial VSA installations (see Figure 1.3b). Lastly, the bed volumes can be kept to minimal dimensions in a VSA environment due to the higher gains in adsorption capacity and selectivity.

Figure 1.3b shows a typical process flow diagram of a dual bed, oxygen VSA system consisting of a feed blower, vacuum pump, product tank and associated on/off and control valves. The product composition perceived by the customer is measured downstream of the product vessel and varies periodically with time as adsorption and desorption of the adsorbent columns occurs. Thus, the volume of the product tank dictates this composition swing over the cycle with greater damping resulting from a larger tank. The reason for this variation originates from the axial composition profiles in the bed. As shown in Figure 1.3c, the shape of the cyclic steady state adsorption front in the bed at any point in the cycle is a function of the cycle boundary conditions (i.e. the step conditions). During the feed step (where product gas is removed from the adsorption column and flows into the product vessel) the composition leaving the adsorber changes with time as the adsorption front pushes its way through the bed (see Figure 1.3d). Hence, it is apparent that the distributed nature of the product mole fraction entering the product vessel and mixing with the gas already present in the tank causes downstream temporal fluctuations in oxygen purity.

As a slight digression from the discussion of 'standard' VSA processes whereby nitrogen is preferentially adsorbed, it is useful to mention the literature on the development of an oxygen selective adsorbent. The current literature on this topic is predominantly contained within the patent database but so far the problems have been the toxicity of the manufacturing process, the toxicity of the sieves themselves and the slow oxygen desorption kinetics. In essence, this still remains as the 'Holy Grail' of oxygen production industry. Alternatively, patents such as Golden *et al.* (1992 and 1995) discuss the manufacture of oxygen selective sieves using porous carbon substrates (carbon molecular sieves or CMS) for air separation. Use of these sieves is discussed in the Baksh and Notaro (1998) patent for the production of nitrogen from air. The limitation of their technique is that the separation process is kinetically governed and the resulting adsorbate stream is only oxygen enriched and consequently not suitable for processes requiring high purity oxygen.

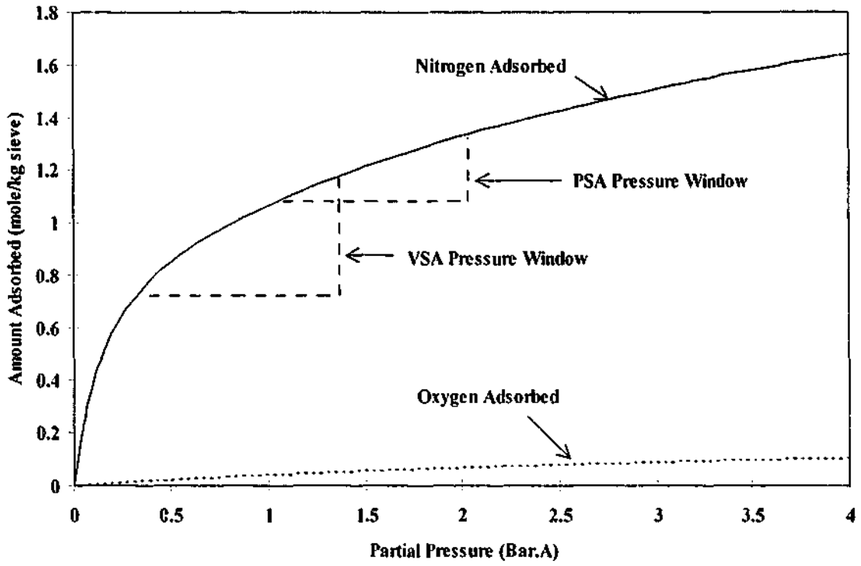

Figure 1.3a. Comparative adsorptive capacities of PSA V's VSA processes at equilibrium, isothermal (293K) conditions on CaX zeolitic sieve.

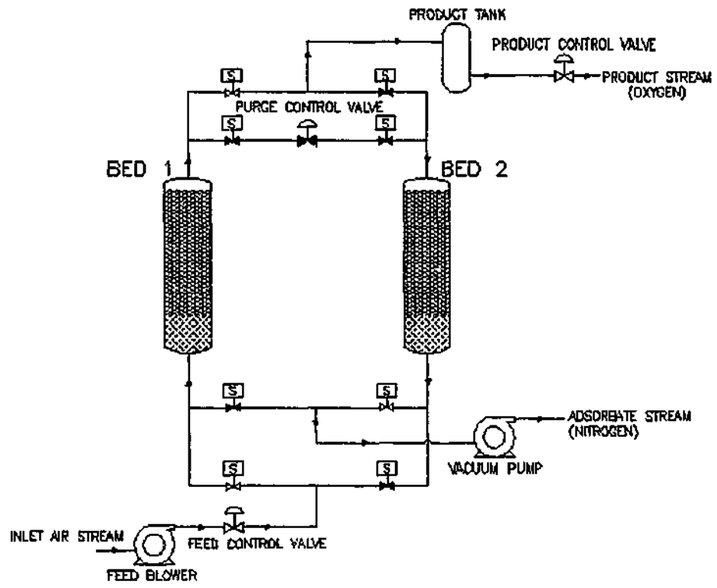

Figure 1.3b. A typical dual bed O_2 VSA process flow diagram.

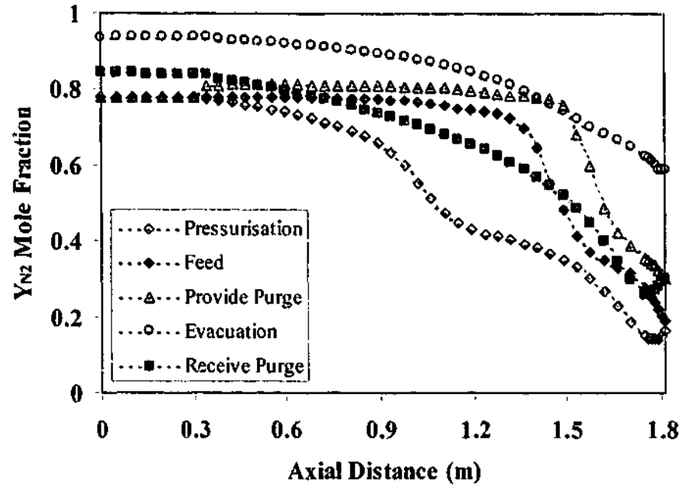

Figure 1.3c. End of step N_2 composition profile resulting from a simulated five step, single bed O_2 VSA cycle.

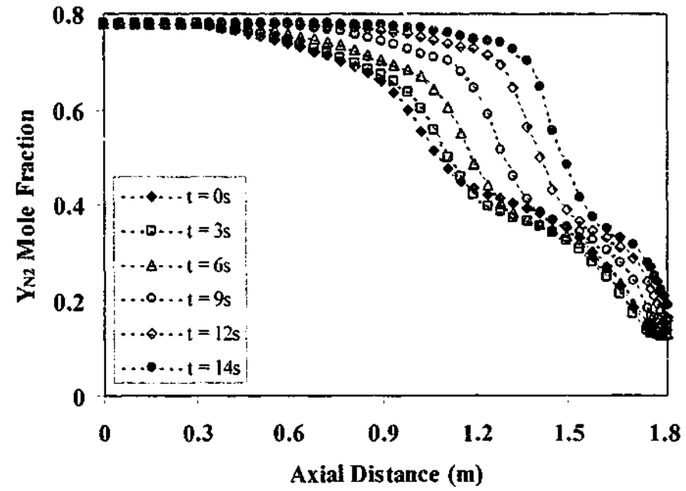

Figure 1.3d. N_2 composition profile during the feed step resulting from a simulated five step, single bed O_2 VSA cycle.

1.4 THE CONTROL PROBLEM FORMULATION

The importance of O_2 VSA as a unit operation is evident from the previous section with the customer requiring tight tolerances on the output variables. It is clear, therefore, that appropriate control strategies are necessary to meet the customer's requirements with the end control objectives to supply a product gas at the set point purity, pressure and flow. How this is achieved is not immediately obvious, as the following analysis will show.

Consider the six step cycle as shown in Figure 1.4a. The variables to be controlled are the product purity, pressure and production rate over the cycle. The manipulated variables (MV) in this case are valve positions CV1 at step 1, CV1 at step 2, CV4 at step 2 and CV3 at step 3.

The following assumptions are usually made in devising a control scheme:

1. No control of the vacuum flow by valve CV2 is permitted. This is consistent with industrial practice where plants are designed with a vacuum pump of fixed capacity with no flow regulation. Valve CV2, therefore, is fixed at a designated position throughout the cycle as determined by design considerations.
2. It is assumed that the beds, piping and valves are symmetrical thus allowing the manipulated variables for bed 2 to be equal to the values determined by the controller for bed 1.
3. Control action is not continuous with time but occurs once every cycle. It is meaningless to adjust valve position continuously if the step during which the valve is used (e.g. feed step) is not occurring. The cycle time, τ, must therefore be used as the appropriate "time" variable. This is an important point to note since most third-party PID controllers request real-time as input – use of these controllers may therefore require severe detuning when applying the PID loops to a PSA process. To overcome this deficiency, it may be prudent to implement ones own PID algorithms.
4. To simplify the control problem further, it is assumed that CV1 during step 1 is fixed and not available for control. This reduces the problem down to a multiple-input-multiple-output (MIMO) scenario of three inputs with three outputs.

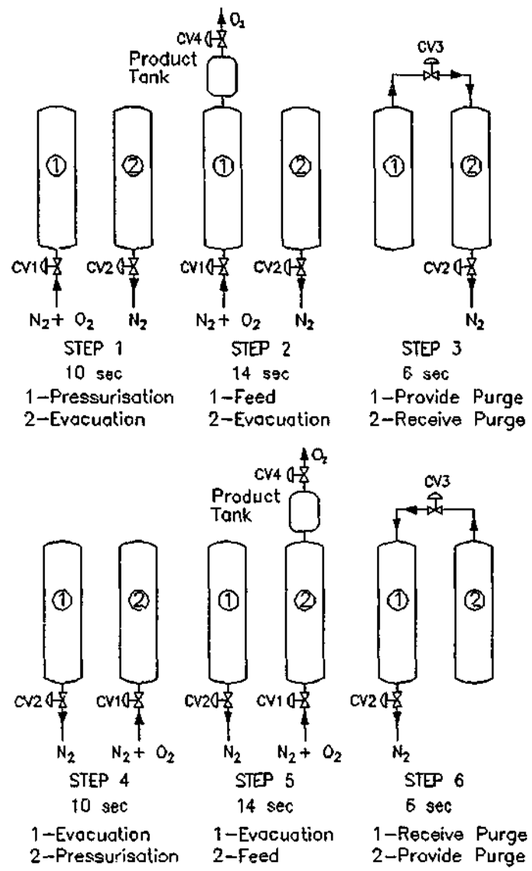

Figure 1.4a. A dual bed, 6 step oxygen VSA cycle.

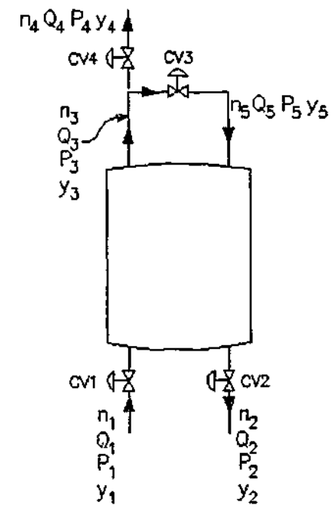

Figure 1.4b. A hypothetical continuous, isothermal VSA process.

A control strategy can be developed by viewing the VSA process as a pseudo-continuous, isothermal system as shown in Figure 1.4b. A total and species mass balance (Eqs. (1.4a) and (1.4b) respectively) gives

$$\dot{n}_1 = \dot{n}_2 + \dot{n}_4 \tag{1.4a}$$

$$\dot{n}_1 y_1 = \dot{n}_2 y_2 + \dot{n}_4 y_4 \tag{1.4b}$$

where n denotes flow rate and y mole fraction of oxygen.

The following equations and relationships describe a mass balance around the product end of the bed

$$\dot{n}_3 = \dot{n}_4 + \dot{n}_5 \tag{1.4c}$$

and $y_3 = y_4 = y_5 = y_p$ which is the product composition. Also, $y_1 = y_f$ = feed composition = constant, Q_2 = constant as CV2 is fixed (constant flow vacuum pump) and $P_1 = P_f$ = feed pressure = constant.

Let us determine which MV to use to control the oxygen production rate for example. From the species balance, Eq. (1.4b), in terms of volumetric flow, Q, and pressure, P, becomes

$$\frac{P_4 y_p Q_4}{RT} = \frac{P_f y_f Q_1}{RT} - \frac{P_2 y_2 Q_2}{RT} \tag{1.4d}$$

Since Q_2 is fixed by CV2, only Q_1 (CV1) and Q_4 (CV4) can affect the oxygen production rate, $\dot{n}_4 y_p$. But

$$\dot{n}_4 = \dot{n}_3 - \frac{P_5 Q_5}{RT} \tag{1.4e}$$

The production rate, therefore, can also be influenced by Q_5 (CV3). A similar argument can be composed for the case of product purity and product pressure. It is clear from this very simple analysis that the oxygen VSA processes is not only MIMO but also interacting (i.e. the perturbation of a single MV while keeping all other MV's constant, impacts upon all CV's). Typically, industrial practice has been to simply employ the product valve to control product purity or flow rate but this argument has shown that this strategy may not be the correct or most

stable controller pairing. Hence, the question of loop pairing and extent of loop interaction and decoupling will be a significant part of this study.

1.5 PLANT DISTURBANCES

As well as the loop interactions as described in the section previous, process disturbances, whether it is natural or customer induced, can have significant and prolonged effects on the performance of the VSA system. They can be classed into four categories:

1. customer influence
2. ambient effects
3. equipment malfunction
4. process conditions

1. Customer Influence

By demanding more or less product gas from the plant, the process experiences a change in load and is subsequently forced to operate at different conditions.

Typical customer requests are -

- higher/lower product purity
- more/less production rate

2. Ambient Effects

The variation in inlet/ambient temperature due to climatic/seasonal and diurnal changes and to a lesser extent, inlet/ambient pressure fluctuations, can have adverse effects on system performance by altering the thermal profiles within the bed, (as the sieves are a strong function of temperature), and increasing/decreasing the molar flow rate of the inlet air.

3. Equipment Malfunction

Valve failure, whether be it a solenoid or control valve, is another disturbance to the plant. The philosophy held by industry is that the controller should be able to maintain system performance within allowable tolerances until the problem has been rectified. Another disturbance due to equipment failure is contamination of the adsorbent sieve. This is normally attributed to contact with moist air due to leaks in the bed or convective mass transport of water from the pre-layer by the gas phase or an increase in humidity of the inlet air stream. This poses a more difficult problem for the control system to deal with as the moisture is irreversibly adsorbed onto the sieve and the cause of the problem is very difficult to diagnose.

4. Process Conditions

One of the most significant problems faced by VSA plants is the formation of the 'cold-spot' where temperatures as low as -56°C have been recorded [Kumar, 1996]. This phenomena severely affects the thermal profiles within the bed and hence the plant performance, and is observed in large industrial plants where the size of the beds cause them to operate adiabatically. Initiation of the problem is at the interface between an inert pre-layer, (non- or lesser adsorbing sieve) and the adsorbent sieve. Differences between the loading of the adsorbate phase and the heat of adsorption between the two layers causes the cold spot to form, where the severity of the 'cold-spot' is a function of the difference in adsorbent characteristics. Figure 1.5a is an example of an experimental thermal profile, for the case of a VSA cycle with an adsorbent and inert layer. The process is an eight step, dual bed cycle using a CaX (UOP VSA-2) zeolite above a layer of alumina (Alcan AA300 5mm beads). The temperature swing from adsorption (feed step) to desorption (receive purge gas) can be clearly observed as well as the temperature depression at 0.2m, which was measured to be as low as -7°C during the purge stage. The location of the 'cold-spot' coincides exactly with the position of the adsorbent/pre-layer interface. The occurrence of 'cold-spots' is not only limited to beds of multiple layers but can occur in a single layered bed when a strongly adsorbed component, (such as water in air or a ternary mixture), saturates the first few centimetres of sieve and thus alters its adsorption characteristics to the point that it behaves very much like an inert layer [Wilson, 2001].

Past efforts to eliminate the problem of 'cold-spots' have not been successful or practical. This includes methods such as the insertion of thermal conducting plates to transfer heat from the hot to the cold sections of the bed and the installation of a heat exchanger in the bed [Kumar, 1996]. On the other hand, researchers have tried to take advantage of the cold spot phenomena by layering the beds with differing adsorbents so that the temperature conditions favour the adsorption characteristics of the particular sieve [Park *et al.*, 1998a; Notaro *et al.*, 1998]. The reference by Wilson (2001) contains detailed explanations of the formation of the 'cold-spot' effect and a review of the past studies and its applications.

The disturbances to a VSA system are numerous and varied and thus a highly robust controller is required. Table 1.5a lists some of the typical responses employed in industry in the event of controller failure and reveals the large costs it is associated with.

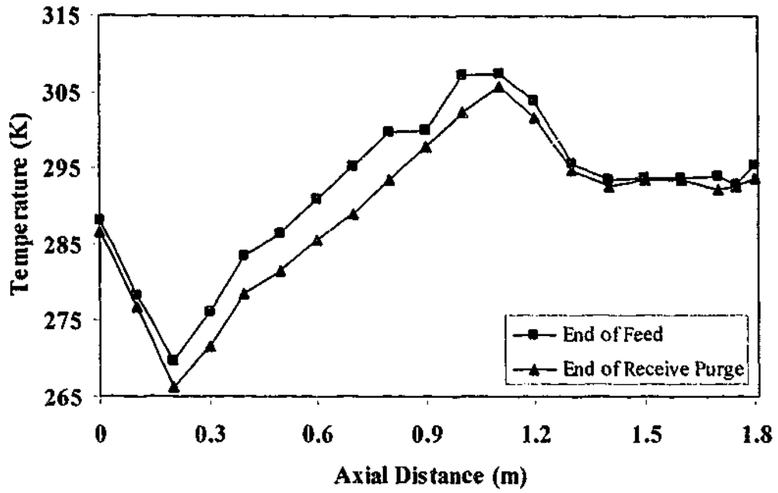

Figure 1.5a. Thermal profile of bed 1 gathered from a pilot VSA plant running an 8 step, dual bed cycle with a CaX adsorbent and an alumina pre-layer.

Table 1.5a. Typical industrial responses to controller failure.

Type of Failure	Response	Impact
Failure to achieve product purity.	Vent product gas and provide liquid oxygen, (LOX) back up.	High capital cost of LOX. Wastage of product and power.
Turndown problems due to a decrease in customer demand for product gas.	Vent proportion of product gas.	Wastage of product and power.
Failure to achieve pressure/flow.	Provide LOX back up.	High capital cost of LOX.
Start Up (low product purity).	Vent product gas and provide LOX back up.	High capital cost of LOX. Wastage of product and inefficient use of power.
Thermal effects cause a deterioration in performance due to the 'cold-spot' problem (studies have shown that this can be up to 20% [Watson *et al.*, 1996]).	Plant shutdown to allow thermal equilibrium to be reached (for large plants this may take up to a week).	Loss of production.

1.6 PAST VSA/PSA CONTROL STRATEGIES

The published literature to date contains an abundance of information on adsorption mass transfer and numerical modelling of various adsorption processes but lacks material relating to the control of adsorption systems. The attitude of the academic community to this largely ignored but important field of research, is reflected in the commentary paper by Ruthven (2000). In his paper, he suggests that the future challenges in terms of process development will be in the form of process miniaturization utilising rapid cycle technology [Sircar and Hanley, 1995] and states that most of the major problems associated with process modelling and simulation have been overcome. However, the reduction in cycle time has several limitations (equipment design and mass transfer being the some of the important factors) and has not been employed in large-scale oxygen production processes. The reference Todd (2003) contains an in-depth discussion on the limitations and problems encountered by rapid cycle PSA. In contrast, the many problems still faced by the industrial engineer (see Table 1.5a above which lists the industrial responses to controller failure) have been overlooked by academia. Furthermore, control theory with respect to batch processes in general, is still in its infancy. For example, the U.S. standard ISA S88.01-1995 [The International Society for Measurement and Control, 1995] and its international equivalent IEC 61512-1 [International Electrotechnical Commission, 1997] was composed because of the need to define the common terminology and models to use in batch manufacturing. They also provide a means for defining flexible manufacturing systems and good engineering practices in the operation of batch facilities. Although the two standards are useful in defining the terminology of batch control, they do not identify the most appropriate method to use in the control of specific processes.

In a review of the current literature, both open and in the patent database, it was discovered that the word "control" has been used fairly liberally. It is the aim of this section to rigorously define the terminology so as to avoid confusion with other interpretations. Figure 1.6a shows a flowsheet of the plant control hierarchy. From the perspective of this thesis, it is entry D that shall be defined as "process control" since it is at this point in the flowsheet when process control theory and algorithms are applied. Categories B and C in Figure 1.6a, represent circumstances whereby a plant must be operated outside of its normal/design conditions and attaining these new set points cannot be achieved purely by changes in the manipulated variables. In practice the use of heuristics and/or variables that are not normally engaged during normal operation are employed to accomplish the new conditions. When the updated conditions are met, the process controller, D, continues with its regulatory task. An overall plant control algorithm, A, manages both the process and abnormal condition algorithms. Procedural control, category F in Figure 1.6a, is defined as the PSA/VSA cycle conditions incorporating cycle and step times and flow configurations controlled by various on/off and one-way valves and

pressure, flow or concentration switches. This is usually automated in the field via a programmable logic controller (PLC) and/or a supervisory control and data acquisition system (SCADA). The remaining entries in the flowsheet are self-explanatory. A summary of the current control literature available in the public domain on PSA/VSA control is provided in Table 1.6b. All the entries in this table correspond to category D in Figure 1.6a (i.e. process control algorithms) and in some cases embodies other entries below it.

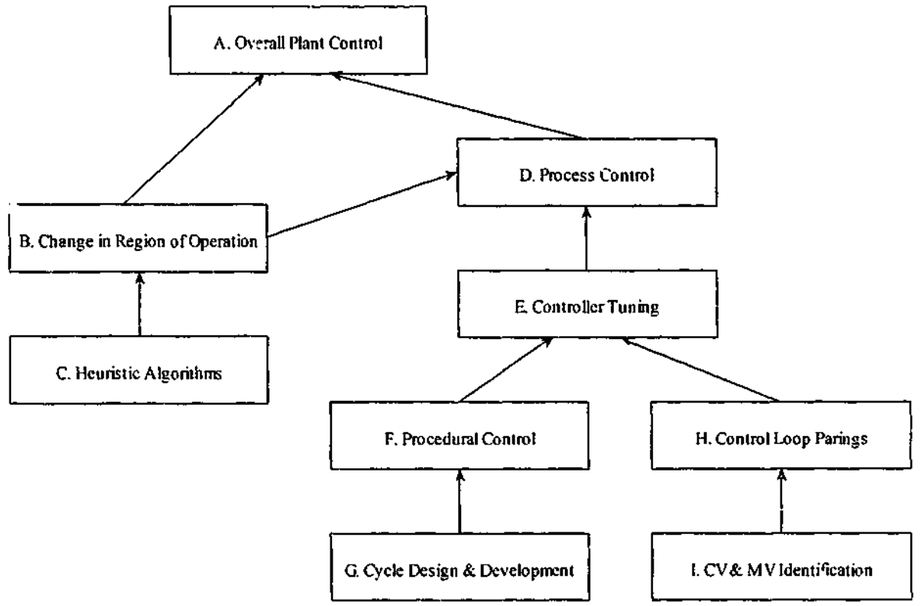

Figure 1.6a. The PSA/VSA plant control hierarchy.

Klatt *et al.* (2000), Klatt *et al.* (2002) and Natarajan and Lee (2000) illustrate the application of model-based control methods to a simulated moving bed (SMB) chromatography system whilst Nagrath *et al.* (2003) applied model predictive control to a liquid chromatography process. Although chromatography is an adsorption-related process, the nature of this system is quite different from PSA/VSA. Firstly, the SMB process is continuous whereas the VSA process is a batch system and secondly, the chromatography process is for liquid phase separations whilst bulk gas separation occurs in the VSA system. These two factors simplify the control problem immensely in terms of model reduction (energy balance can be neglected and constant fluid velocity can be assumed) and hence the computational requirements and the availability of control tools and theory for continuous systems can be used. As a result, the work of these researchers is not relevant in this field of study and can be omitted.

On the other hand, Zone and Kirkby (1994) in a study entitled "Controlling the Pressure Swing Adsorption Process" presented a simple model (where the model is solved using the Method of Characteristics) and then compared this to a more detailed numerical model and pilot plant data. No control schemes were proposed in their publication. They concluded that a form of model based control will be required to efficiently control PSA processes. In a similar vein, Kowler and Kadlec (1972) proposed a method to control a cyclic adsorber by the manipulation of cycle times. The process under study was a rapid PSA system (cycle times of around three seconds) for the separation of a binary mixture of nitrogen/methane where the component to be maximised was the product nitrogen with methane being preferentially adsorbed. They performed various experiments by varying the feed step time to optimise the cycle based on the product composition and flow rate. Once again their strategy was not a control methodology as such but an optimisation study.

A mechanistic approach to the control of PSA systems was proposed in the paper by Matz and Knaebel (1987). The researchers recognised the dependence of the product composition on the location of the thermal fronts generated by adsorption and assumed coincidence of the thermal and mass transfer waves and the composition gradient in the bed. They then proposed a method based entirely on measurements of the axial temperature profile to control the product purity by manipulation of the length of time for the feed step. The ultimate time for the feed step was calculated as a function of the bed length and the coefficients of a polynomial regression to fit the axial positions of the thermocouples to the occurrence of the thermal shifts. They applied this technique to a single column experimental unit, however, the cycle under study was not a true pressure swing cycle as a separate reservoir of pure light component was used to both pressurise and purge the bed. This deprives the cycle of transient responses whereby the product purity would asymptote to a final value and was performed because the researchers were concerned about the failure of their method under more realistic cycle conditions. They also reported difficulties in controlling the purge step due to the smaller changes in enthalpy and the diffuse nature of the thermal wave during this step. Therefore, the use of temperature measurements alone is insufficient for the control of industrial PSA/VSA processes.

The only true model predictive control (MPC) architecture developed to deal with the control of PSA processes currently available in the public domain has been presented in the works of Bitzer *et al.* (2001), Bitzer and Zeitz (2002a) and Bitzer *et al.* (2002). These researchers studied two different cycle arrangements for the separation of oxygen from air as typically encountered in medical oxygen generators. In the first cycle, a dual bed, two step system with continuous production was investigated. The primary objective of their controller was to ensure control of the purity variable despite disturbances by manipulation of the overall

cycle time. The product flow was assumed to be constant and therefore the product purity was calculated as the integrated value averaged over the cycle. The control strategy consisted of a feedforward and feedback controller, which corrects the predictions made by the feedforward controller. The feedforward control structure comprised of a function relating the product purity to cycle time at CSS, (which was determined by direct numerical simulation of the process studied), whilst a PID controller was used for the feedback control scheme. Finally the trajectory of this mixed control architecture was predetermined over a fixed time horizon and the method demonstrated excellent control in spite of a +60% step change in the production rate.

A slightly different strategy was invoked by Bitzer and Zeitz (2002a) and Bitzer *et al.* (2002) for the control of a dual bed cycle whereby product was recovered in two of the four steps. In a similar vein to the method above, both a feedforward and feedback controller was employed. The feedforward model this time was a function of not only the cycle time and product concentration but also of the product flow rate. As in the previous discussion, a PID controller was chosen for feedback stabilisation however, the production/purge step time was the manipulated variable in this case. The researchers demonstrated the performance of their controller scheme for various disturbances such as variations in product flow rate, changes to the inlet composition, ambient fluctuations and set point adjustments. For all the disturbances the controller performed favourably.

Nevertheless, the methods discussed above have numerous deficiencies to be applicable to field operation. The researchers have reduced the order of the control problem by only investigating a single-input-single-output (SISO) system with product purity as the controlled variable and cycle time being manipulated. However, as discussed in §1.4, the customer typically requires many variables to be tightly controlled (flow and pressure for example). Also, the cycles studied by the researchers are simple and are not representative of the cycles run in large air separation plants. The cycles contained numerous operations in the one step such as adsorption, production and purge, and the manipulated variable was either the cycle time (if a continuous cycle was chosen) or the step time of the production/purge step. However, in order to improve purity, product recovery and lower power requirements, the industrial convention is to divide the various operations such as production and purge into separate steps. In this case, the timings of each individual step would need to be controlled and at the same time the control scheme would have to avoid the predicament of scheduling the steps to avert problems without causing the beds to run out of phase and be imbalanced. The alteration of cycle (and consequently step times), furthermore, can cause problems such as fluidisation and hence increased attrition of the sieve material.

Also in oxygen VSA, a constant volumetric flow pump is used for desorption of the heavy component. This essentially imposes fixed physical bounds on the minimum step and cycle time. Therefore, the manipulation of cycle or step times to control the MIMO industrial oxygen VSA process is not a practical alternative. Furthermore, it is unusual that the researchers did not consider comparing their control scheme with that of single loop PID, which is typical in most control studies when demonstrating the performance of a new controller. A final closing remark on the work conducted by the researchers Bitzer *et al.* (2001), Bitzer and Zeitz (2002a) and Bitzer *et al.* (2002) is that so far all their proposed control strategies have been applied to a numerically simulated processes, which are considerably more sympathetic environments than the severe conditions (such as multiple load disturbances) experienced in the field.

Communication with industry has revealed that the conventional control method for the VSA process consisted of multiple continuous PID loops. As a starting point for this study, this methodology was implemented and tested on a pilot plant since no published literature on this scheme exists [Beh *et al.*, 2000]. The aim was to be able to control product purity, product flow and product pressure as well as regulation of the pressure profiles within each step. The addition of this subordinate control task (i.e. bed pressure control) is in essence a crude procedure to adjust the position of the composition front. An eight step, sixty second VSA cycle (see Figure 2.2b in Chapter 2 for a schematic representation) for oxygen enrichment was investigated in this study using two steel-walled columns loaded with 10kg of CaX and 1.3kg of an inert layer (alumina) per bed. For this case, a total of nine PID loops was used, four to control the end-of-step pressures for each of the four steps experienced by each of the two beds with the product valve controlling the product purity in the ninth loop. The eight PID loops controlling the bed pressures operate only for the duration of the appropriate step whilst the purity controller was continuous in operation. Calculation of the PID algorithm was based on the error generated by the difference between the set point and the value of the controlled variable at the previous cycle. Controller tuning was based on step responses with each controller tuned independently and then detuned by an appropriate amount. Table 1.6a lists the pairings of the controlled and manipulated variables and the performance of the process in open and closed loop modes is presented in Figure 1.6b for a disturbance in the inlet temperature.

Figure 1.6b shows that the performance of the VSA system with and without control as the inlet feed temperature in both cases dropped by approximately 2.5°C. It reveals that in the open loop case, the product purity decreased by approximately 1% and had no corrective action been taken, would have continued to decrease. On the other hand in the closed loop scenario, the control scheme was able to maintain the purity to within 0.5% of its set point (90%). Whilst this simple illustration serves to demonstrate that this form of multiple PID control was effective for modest disturbances, the unusual purity response in the open loop mode seen in Figure 1.6b

should also serve as a warning that more severe disturbances would be difficult to control with simple PID. The purity in open loop mode was seen to decrease initially, then increase, and then decrease again. Such inverse response has been frequently observed in the VSA process. Short time-scale changes in feed temperature (i.e. day to night variations) resulted in only minor variations in bed temperature since the thermal capacity of the beds was very large. However, a lower gas inlet temperature corresponded to more dense gas being fed into the beds and thus the potential for premature breakthrough of the nitrogen front existed. Changes in ambient temperature also impacted on the temperature of the gas involved in the purge and pressure equalisation steps and resulted in a complex thermal interaction in the beds.

The researchers also performed step changes by varying the vacuum levels through the use of a control valve connected to the inlet of the vacuum pump. The different vacuum levels produced much more dramatic changes in the plant performance, which was observed to be proportional to controller performance. The researchers concluded in their study by stating that multiple loop PID was only suitable for modest disturbances and that a model based control structure may be necessary to achieve more satisfactory results. However, this method of PID implementation used an unnecessary number of PID blocks and thus over-constrained the control problem. In the scenarios studied, the main controller failure was due to severe loop interaction. For example, a change in the operating conditions may cause the purity variable to drift. The purity control block responds to maintain set point. However, this then impacts on the system flows and pressures (and eventually the thermal balance) but the bed pressure controls still attempts to maintain previous levels no matter how much the operating conditions have changed. It is clear from this scenario, that PID controllers implemented in this manner may try to achieve unrealistic controller goals. Hence, a rethink of the current PID implementation strategy is required.

Table 1.6a. Controller set points and loop pairings.

Controlled Variable	Manipulated Variable	Set Point (kPa.A)
End of Feed Step Pressure	Feed Valve	130
End of Evacuation Step Pressure	No Control. Fixed step times & vacuum pump capacity.	44
End of Purge Step Bed-Bed Pressure Difference	Purge Valve	50
End of Pressure Equalisation Step Bed-Bed Pressure Difference	Purge Valve	16
Oxygen Product Purity (%)	Product Valve	90

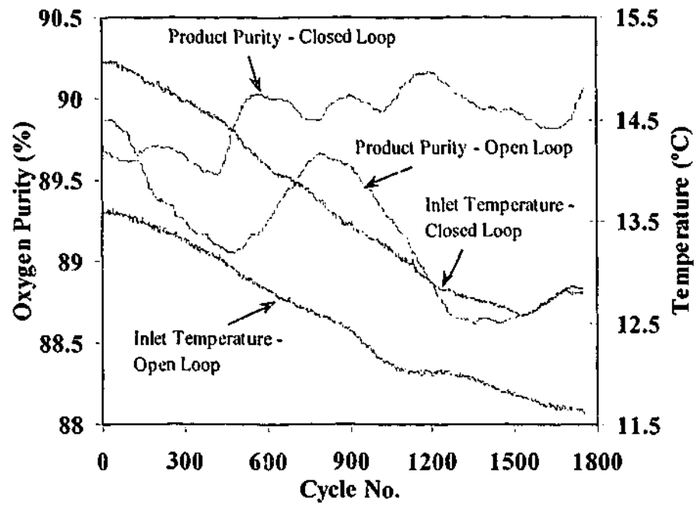

Figure 1.6b. Open and closed loop response of the product oxygen purity to a change in feed temperature.

The patent database provides some insight into control systems that have been or are currently implemented in the field. Although useful and insightful, patents have the drawbacks of being written with the intention to hide details and lack the depth and specifics in areas crucial to the design and implementation. Nevertheless, a number of patents have been critiqued by the author and although the list is not exhaustive, the patents embody a broad cross-section of control strategies and techniques covering all entries in Figure 1.6a except category A. Only one patent describes a true process control algorithm, Schaub *et al.* (1995), and will be discussed in detail later. Table 1.6c provides a summary of the main findings. The use of proprietary control techniques is hypothesized as the principal reason why no process control algorithms, relevant to this thesis (as defined by category D in Figure 1.6a), have been patented.

Some patents contain the terms: "control" and/or "PSA" and/or "adsorption" in their titles but in actuality the authors described inventions that are tangential to the focus of this work. For example, the methods established by Asztalos (1982) and Servido *et al.* (1993) represents a class of techniques for the procedural control of an adsorbent system using three-way valves. In another patent, Li *et al.* (1993) has the misleading title of "Programmable Control and Operation Equipment of Swing Pressure Adsorption Process". No process control algorithms classifiable as category D in Figure 1.6a are introduced in the work but instead the authors discuss a robust and hermetically reliable programmable control valve and its associated

assembly for use in PSA systems. An in-depth discussion of these patents will therefore be excluded from this thesis.

Grader (1987) described the control of oxygen product flow begins by designing the PSA process for a maximum oxygen product to feed air ratio. When the customer demand has fallen from the design flow level, the oxygen product to feed air ratio was increased. The correct oxygen flow was supplied to the customer but the downside is that oxygen purity was not maintained at a constant level.

Gunderson (1988), on the other hand, used cycle times to manipulate inlet feed flows to control product purity. Besides affecting other steps within the process, a reduction in feed gas, with all other processing variables kept constant, would result in a corresponding reduction in product flow.

Miller *et al.* (1987) utilised a more advanced control strategy. The co-current depressurisation or pressure equalisation gas was analysed to determine whether a product purity problem exists. They outlined three approaches in correcting the purity problem:

1. adjust adsorption time
2. adjust PE step to avoid impurity breakthrough
3. adjust the amount of purge gas entering adsorbent beds

The main drawback of this scheme was the need for an additional oxygen analyser to measure breakthroughs during the pressure equalisation step, which is especially difficult in VSA processes. Also, the tuning procedure outlined in this patent is a long process (12-24 hrs) and requires several iterations.

The Smolarek (1991) patent endeavoured to produce predominantly nitrogen (with a lower purity oxygen co-product) by PSA separation of air under variable demand conditions and to provide an improved PSA process and system for enhancing the efficiency of air separation operations under reduced nitrogen product gas conditions. Utilisation of a variable volume, product storage tank and the manipulation of cycle times was employed to determine variation in user demand and to control the steps within the PSA cycle. A minimum of two beds was required for this method and the beds operated 180 degrees out of phase. By controlling step times and consequently the overall cycle time determined the pressure and hence purity profile of both beds. The difficulties associated with this control method relates to the fact that because the beds are coupled, alteration of the time for a particular step also affected the end of step variables such as pressure and hence the purity of all other steps. Also, the patent was unclear on just how adjustments should be made (i.e. which step to change and by how much), to maintain set point.

Schebler and Hart (1986) proposed the use of a small bleed valve in conjunction with an oxygen partial pressure sensor in order to control the partial pressure of oxygen in the product stream. If the partial pressure were to rise above a set point, the bleed valve would open and allowed a small portion of product gas to vent into the atmosphere. This impacted on the PSA plant by causing it to produce more gas, which in turn lowered the oxygen purity in the product stream and thus decreases the oxygen partial pressure in the product stream. The limitation, therefore, of this patent was that multivariable control issues were not addressed.

Naheiri (2001) presented a method for controlling the flow of gas between an adsorbent vessel and a gas storage tank using check valves. The check valves are installed in parallel between each vessel and each check valve allowed gas to flow either from the adsorber to the tank or from the tank to the adsorber as a function of the differential pressure and the check valve setting. The advantage of this method was that it allowed product gas to leave the adsorber beds only when a specified pressure differential had been attained. It also allowed some product gas to enter back into the beds as purge stream during the cycle, from the product vessel at a different pressure differential that corresponded to the setting of the second check valve. This method is not true a process control technique in the definition of this thesis but is a concept for process improvement.

The technique developed by Myers *et al.* (1982) presented a method of adsorber pressure control through the use of a pressure transducer located in the supply line to the beds. The objective of this patent was to ensure that each bed is operating at matching efficiencies as it was observed in practice that beds of adsorbent materials are nearly always different. The pressure signal was fed back to a control system that regulated the length of time for which an inlet solenoid valve was opened. This patent undertakes to pair a particular control loop with bed pressure although it may also be employed in feedforward control, the authors did not discuss this.

A patent in the similar vein as the one above, suggested the use of a differential pressure measurement as a signal to allow the control of product gas flow via a control valve [Abel *et al.*, 1991]. It did not describe how other variables of importance, such as concentration, are to be controlled. This patent, once again, proposed single loop pairings and in this case differential pressure was matched to the product valve.

Stocker and Whysall (1988) presented an alternative process configuration whereby they claim that the reliability of the system was improved with reduced cost through the introduction of a control valve that automatically controlled product repressurisation and also product gas released from the adsorber vessel. This patent falls into the categories H and I in Figure 1.6a.

A procedure for the independent control of product flow rate and concentration was claimed in the McCombs (1998) patent. In this patent, descriptions of the control loop pairings for

oxygen PSA processes are given including explanations of how and why they were chosen. It was suggested that the product and bed-to-bed purge be used to control the product concentration and a product control valve and pressure regulator, coupled with low and high pressure switches, employed to maintain product flow. Although the process was described in some detail and the control problem was formulated, no detail on the actual process control algorithm was provided.

Sircar (1984) postulated a control strategy that employed numerous control loops for the regulation of an equivalent number of control objectives. This rather complete description of the proposed control system utilised a sequential or procedural routine that was based on limit switches and solenoid actuated valving for the control of the adsorption air fractionation process. Controller pairings discussed by the author included control of the adsorption step by sensing the adsorber product composition, terminating the rinse step based on a predetermined detected oxygen composition and the use of pressure level to control the evacuation and pressurisation steps. The limitation of this method is that fine regulation of the process was not available due to the lack of use of control valves and the assumption that bed pressure corresponded directly to the position of the adsorption front. The regulation of the bed pressure levels combined with oxygen purity control can cause significant interactions between the control loops (especially when disturbances occur) resulting in control loop failure (discussed in detail by Beh *et al.* (2000)). Also, it is perceived that unbalanced conditions could occur with the use of this control strategy caused by different step times employed for each bed. Finally, the technique outlined in this patent would be classed in category F as a procedural control methodology rather than a true process control algorithm.

For cyclic PSA processes comprising of two or more adsorber vessels, Tan (1996) suggested that control of the product oxygen concentration can be established by periodically varying the duration of the purge stage of one or more beds. A sensor located in the waste or evacuation stream was used to determine the extent to which the purge step time was altered. The patent further proposed that if two beds are used then the purge period of both beds are to be adjusted. In the case of multiple adsorbers, the purge duration of the two worst performing beds are adjusted. The author did not discuss how problems with beds being out of balance due to differences in purge timings are circumvented. As with the case for most of the patent literature, the author did not detail the exact algorithm used for control, and multivariable demands had not been addressed.

In another control strategy, a cyclic VSA system for the fractionation of air was controlled by monitoring the pressure in the product vessel [Koch, 1985]. The adsorption feed step time was automatically regulated based on this measured signal to control the production rate. As stated previously, altering the step times for each bed can cause scheduling problems (i.e. cycle

becomes unbalanced). A final deficiency of this patent is that it did not consider conditions where multiple objectives are of interest especially when the product concentration is also of concern.

A control scheme presented by Aylsworth *et al.* (1998) provided an interesting alternative for the control of an oxygen concentrator (particularly for medical use) by using the measured product gas purity and feeding this signal back into a control algorithm. The controller then altered the speed of an AC motor, which varied the molar flow of feed gas entering the system. The authors claim that the control system was general enough that it can be applied to both continuous and periodic processes from adsorption systems to membranes, electrolysis and ceramic-based technologies. Like most patents, Aylsworth *et al.* (1998) lack detailed on the actual control algorithm that updates the motor speed and once again, did not address any multiple loop control issues.

Rouge and Teuscher (2001) presented a method that attempted to satisfy multiple loop objectives for the control of the product output and maintenance of constant product pressure. The authors adjusted both the duration of gas fed into the adsorbers and the duration of the gas stream exiting the adsorber as product (as a function of the feed and make product step lengths and the ratio of the actual production rate to the nominal amount), to control the product pressure and production rate respectively. The principal goal of the control algorithm was to optimise or minimise specific energy at a constant product pressure. Control of the product concentration, which is arguably the variable of most importance to a customer, was not detailed in the patent and issues related with scheduling of multiple adsorber beds were not addressed.

Schaub *et al.* (1995) presented a fairly detailed algorithm and procedure for the control of oxygen PSA/VSA systems. In fact this patent is the only one that would qualify as a process control algorithm in the context of this thesis. The authors utilised the measurement of the axial temperature profiles in each absorbent bed for the determination of whether a gas purity imbalance existed. They initially assume that all the beds are similarly packed and if there are negligible external disturbances then the axial temperature profile in each column would be identical. An irregularity in a particular adsorber would cause a difference in the temperature profiles. The valve positions (and hence flow rates) during the pressure equalisation, oxygen repressurisation, purge and/or product feed steps for each adsorber were adjusted by employing temperature and pressure dependent relationships. During the production step, the product valve was adjusted for each bed by an amount in proportion to the difference in the temperature at the bottom of each bed and the rate of change in temperature difference at the bottom of the bed of interest in response to a disturbance. The thermal sensors at the feed end of the columns was selected as they had been determined or had been observed to have the fastest response

time to a change. The authors further proposed that gain values be used to further refine the output of the controller to the valve such that satisfactory control would result. Equation (1.6a) describes the valve adjustment procedure.

$$\Delta m_{Valve(\%)}\Big|_{t+\Delta t_c} = G_P\left(T_{B1}-T_{B2}\right)_t + R_P\left[\left(T_{B1}-T_{B2}\right)_t - \left(T_{B1}-T_{B2}\right)_{t-\Delta t_c}\right] \quad (1.6a)$$

where $\Delta m_{Valve(\%)}$ is the percentage change in control valve position, T_{B1} and T_{B2} are the bottom bed temperatures of bed 1 and 2 respectively, t is real-time, Δt_c is the controller sample interval ("every few hours" has been suggested the authors), G_P is the gain value and R_P is the reset value. Both G_P and R_P are numerical tuning constants that are similar in function to the proportional and reset time gains in a PI algorithm.

The control of the purge flow (and presumably the pressure equalisation stage), however, had been defined as a function of the average bed pressure. This is because the authors state the importance of maintaining a lower pressure in the evacuated bed (i.e. the bed receiving purge gas) than the bed or vessel providing purge. The controller equation relating to the change in purge valve position is given by

$$\Delta m_{PurgeValve(\%)}\Big|_{t+\Delta t_c} = G_P\left(\Delta P_{Desired} - \Delta P_{Measured}\right)_t \quad (1.6b)$$

where $\Delta m_{Valve(\%)}$ in this case is the percentage change in the purge control valve, $\Delta P_{Desired}$ is the desired pressure rise over the step, $\Delta P_{Measured}$ is the measured/actual pressure rise over the step and G_P is as previously defined. Tuning of the controller gains was not discussed in any detail by the authors but it seems to have been performed on an ad-hoc basis on each plant. Also, it should be mentioned that the authors maintained that the control algorithm is applicable to PSA/VSA systems where more than two adsorbers are involved.

It appears that the proposed control scheme was designed with multivariate objectives in mind by controlling both product flow per bed and purge amounts to maintain production rate and product concentration, which are indirectly inferred from the axial temperature profiles and adsorber pressure. The limitation of this method is that it is constructed in the form of a linear, decentralised control structure (just like PID) and consequently is prone to the severe control loop interactions that plague oxygen VSA/PSA systems. For example, if a disturbance occurred it may cause the process to shift to a point of operation whereby the set pressure change over the purge step may not be achievable. If this happens both purge and/or product valves may saturate in value.

McCombs (1995), Pietruszewski (1979), Doong and Brenskelle (1998) and Shirley and LaCava (1993) postulated methods for plant operation outside of normal conditions. In each patent, traditional process control theory was not invoked as the methods considered the circumstances when the process required operation outside of its normal/design region. McCombs (1995) allowed the operating capacity of the PSA system to be varied so that the operating cost of the unit was reduced. This was achieved by varying the intake to the feed compressor by restricting the flow by some means (e.g. through the use of a valve). Pietruszewski (1979) presented a method for controlling an adsorption system during periods of reduced product demand by advancing or adjusting the cycle time to reduce capacity. Doong and Brenskelle (1998), on the other hand, achieved this same goal of product turndown by the inclusion of an idle step on the feed compressor/vacuum pump at the end of the bed-to-bed equalisation step.

An alternative technique to incorporate varying customer demand was offered by Shirley and LaCava (1993). In this patent, the authors proposed the pairing of the feed/inlet gas stream for the control of product concentration for minor fluctuations and also to meet changes in customer demand (turndown) at a desired purity. Moreover, the patent did not disclose or suggest the type of control algorithm and as with many of the patents reviewed, a major limitation of this patent was that multivariable objectives were not considered.

Table 1.6b. A summary of the current published VSA/PSA control strategies.

Methodology	Limitations	Reference
Control of the thermal gradients in the bed to maintain product purity.	The cycle studied was not realistic of the PSA cycles practised as the researchers were concerned with the failure of their method. Experienced problems in controlling the purge step (even with this simple cycle) due to small changes in enthalpy and diffuse nature of the thermal waves.	Matz and Knaebel (1987)
Cycle/step times manipulated to maintain product purity. Feedforward (a simple CSS empirical model) and feedback controller (PID) used to alter the cycle or the relevant step time.	Simplistic cycle arrangement chosen by the researchers, which is of limited practical relevance in industrial PSA systems. Development of this method is required for the application to industrial cycles where the production and purge steps occur separately. Alteration of cycle time only affected the production rate. The affects of altering the step time cascades to the other steps of the cycle, which can cause an unstable situation if a MIMO system is being controlled. Controlling step times leads to a difficult optimisation problem to avoid beds being run out of phase and becoming unbalanced and also in avoiding problems such as fluidisation. The addition of the vacuum pump in the VSA process imposes physical bounds on the minimum allowable step time. Only applied to a single control variable (purity) whereas VSA/PSA processes are MIMO. Did not compare the performance of their MPC controller against that of single loop PID. Their control strategies have yet to be tested in field operation.	Bitzer *et al.* (2001) Bitzer and Zeitz (2002a) Bitzer *et al.* (2002)
Control using multiple loop PID (including pressure level controls) to maintain product purity. PID control applied with respect to continuous time.	The numerous PID blocks can over-constrain the control problem and lead to severe loop interaction (due to unrealistic control targets) and controller failure. Application of PID in continuous time to a batch process requires considerable detuning of controller gains leading to poor controller performance.	Beh *et al.* (2000)

Table 1.6c. A summary of the current VSA/PSA patented control techniques.

Methodology	Limitations	Reference
System was designed for the maximum oxygen product to feed air ratio.	In the event of a customer requiring less product gas, the oxygen product to feed air ratio was increased. Although the product flow was maintained, the product purity dropped.	Grader (1987)
Cycle times manipulated to alter inlet feed flows to control product purity.	Affected other steps within the process. A reduction in feed gas, with all other variables kept constant, would result in a corresponding reduction in product flow.	Gunderson (1988)
The co-current depressurisation or pressure equalisation gas was analysed to determine whether there was a problem with the product purity. Three approaches used in correcting the purity problem: 1. adjust adsorption time. 2. adjust PE step to avoid impurity breakthrough. 3. adjust the amount of purge gas entering adsorbent beds.	An additional oxygen analyser was required to measure breakthroughs during the pressure equalisation step. System tuning was a long process (12-24 hrs), requiring several iterations.	Miller *et al.* (1987)
By controlling step times and hence the overall cycle time, the pressure and hence purity profile of the both beds are determined.	Beds are coupled, alteration of the time for a particular step also affected the end of step variables such as pressure and hence purity of all other steps. Patent was unclear on just how adjustments should be made (i.e. which step and by how much) to maintain set point.	Smolarek (1991)
A small bleed valve in conjunction with an oxygen partial pressure analyser was used to control the partial pressure of oxygen in the product stream. If the partial pressure were to rise above a set point, the bleed valve would open and allowed a small portion of product gas to vent into the atmosphere.	Caused the plant to produce more gas, which in turn lowered the oxygen purity in the product stream. The overall oxygen partial pressure in the product stream was also lowered. Multivariate control issues not addressed.	Schebler & Hart (1986)
Check valves used to control the flow of gas between an adsorbent vessel and a gas storage tank.	Not a process control algorithm but a concept for process improvement.	Naheiri (2001)

Table 1.6c. A summary of the current VSA/PSA patented control techniques (continued).

Methodology	Limitations	Reference
Use of adsorber pressure control for the overall regulation of purity and product flow. Measurement of the pressure in the supply line to the adsorbent beds was fed back to a control system that regulated the length of time for which an inlet solenoid valve was opened.	Patent undertakes to pair a particular control loop with bed pressure and is therefore not a process control algorithm as defined in this context.	Myers *et al.* (1982)
Differential pressure measurement used to vary the position of the product control valve to control product gas flow.	This patent suggests a possible loop pairing and is not a process control algorithm as such.	Abel *et al.* (1991)
System reliability was improved with reduced cost through the introduction of a control valve that automatically controlled product repressurisation and also product gas exiting an adsorbent column.	Patent is best classified as process improvement or development.	Stocker and Whysall (1988)
A procedure for the independent control of product flow rate and concentration was claimed. Bed-to-bed purge used to control purity and a product control valve, pressure regulator and low and high pressure switches were employed to maintain product flow.	Control problem was formulated but no detail on the actual process control procedure was provided.	McCombs (1998)
Postulated a control strategy with numerous control objectives. Utilised a sequential/procedural control routine based on limit switches and solenoid actuated valving for the control adsorption step by sensing the adsorber product composition and terminating the rinse step based on a predetermined detected oxygen composition. Also utilised pressure level to control the evacuation and pressurisation steps.	Fine regulation of the process was not available due to the lack of use of control valves and the assumption that bed pressure corresponded directly to the position of the adsorption front. The regulation of the bed pressure levels combined with oxygen purity control can cause significant interactions between the control loops (especially when disturbances occur) causing control loop failure (discussed in detail by Beh *et al.* (2000)). Unbalanced conditions could occur caused by different step times employed for each bed. The technique outlined in this patent would be classed in category F as a procedural control methodology rather than a true process control algorithm.	Sircar (1984)

Table 1.6c. A summary of the current VSA/PSA patented control techniques (continued).

Methodology	Limitations	Reference
Varying the duration of the purge stage of one or more beds controlled the product oxygen purity. Sensor located in the waste stream used to determine extent to which the purge step was altered.	Did not offer any solutions for the possibility of unbalanced beds. The control algorithm was not detailed. Multivariable demands not addressed.	Tan (1996)
By measuring the product tank pressure and employing this to automatically regulate the adsorption feed step time to control the production rate.	Altering step times can cause scheduling problems. Conditions where multiple objectives are of importance were not addressed.	Koch (1985)
Purity control of general oxygen production processes by variation of the speed of an AC motor driving the feed compressor or blower.	Lacked details on the actual control algorithm. Suggested single loop pairing for control. Does not address multiple loop issues.	Aylsworth *et al.* (1998)
Product pressure and production rate are controlled by adjusting the duration of gas fed into the adsorbers and the duration of the gas stream exiting the adsorber as product (as a function of the feed and make product lengths and the ratio of the actual production rate to the nominal amount). Principal goal of the control algorithm was to optimise or minimise specific energy at a constant product pressure.	Control of the product concentration not detailed in the patent. Issues related with scheduling of multiple adsorber beds were not addressed.	Rouge and Teuscher (2001)
Only patent to address multivariate control issues and employed two linear, decentralised algorithms based on adsorber axial temperature and pressure measurements to control the product flow and purity. Control valve positions were altered per bed during the make product and purge steps.	Controller tuning was not discussed in detail and an ad-hoc procedure would probably be used. Severe loop interactions that are inherent in O_2 VSA/PSA processes may cause the linear, decentralised control scheme to fail.	Schaub *et al.* (1995)

Table 1.6c. A summary of the current VSA/PSA patented control techniques (continued).

Methodology	Limitations	Reference
Several methods postulated for plant operation outside of normal conditions. This is typically defined as "turndown". 1. Intake flow to the feed compressor was restricted (e.g. by a valve) to vary operating capacity [McCombs, 1995]. 2. Cycle time advanced to reduce to reduce capacity [Pietruszewski, 1979]. 3. Idle step included at the end of the bed-to-bed equalisation step for the compressor/vacuum pump to vary capacity [Doong and Brenskelle, 1998].	Traditional control theory not applied as the methods considered operation outside the normal/design conditions of the plant.	McCombs (1995) Pietruszewski (1979) Doong and Brenskelle (1998)
Inlet gas flow varied to control both the purity about an operating point or used to meet changes in customer demand (turndown) at a desired purity.	Patent does not disclose or suggest the type of control algorithm. Multivariate objectives were not considered.	Shirley and LaCava (1993)

1.7 PROJECT DEFINITION AND SCOPE OF THE STUDY

As discussed in the prior sections, the limitations of current control schemes, coupled with the increasing importance of VSA/PSA as a unit operation in the chemical industry, emphasises the necessity for further research in this field. There are several factors that make the VSA process difficult for the application of conventional control strategies and they are:

- strongly nonlinear
- cyclic, batch operation
- transient, non-equilibrium operation
- multiple-input-multiple-output system
- strong loop interaction
- large time constants
- non-isothermal operation
- difficult to model (process/model mismatch exists)

The focus of this work is to develop both a firm understanding of the process and of the control problem at hand. The knowledge obtained in this initial effort is then utilised to

research and develop appropriate controller structures that address the control issues. The performance of these controllers are assessed on an experimental pilot plant. In order to achieve these goals, the research is divided into four distinct parts. The objectives of this thesis are summarised in Figure 1.7a where a roadmap of the project is presented. The first section of the thesis involves an investigation into the physics of the process through the use of a pilot plant and a full numerical simulator. This will be followed by a study into empirical modelling techniques (artificial neural networks in particular) to aid online control. The study will also investigate the development and applicability of a simple mechanistic process model. The ability of this simple model to predict experimental trends will be tested using step and frequency responses leading to an analysis of the system stability and loop interaction to elucidate control loop pairings and possible decoupling strategies.

The third section of this thesis concentrates on the design of appropriate controller structures that will satisfy design objectives. In this research effort, both single and multiple loop control will be investigated and the performance of a decentralised (PID) controller, with and without the use of an explicit decoupling algorithm, and a centralised (MPC) controller is tested. All control schemes presented in this thesis are implemented on a pilot oxygen VSA plant and tested by applying various disturbances reminiscent of field operation.

The final and concluding section of this thesis presents a method for process monitoring and diagnostics. This technique allows the composition gradient to be inferred based on natural observations (measurement of pressure and temperature) and a simple mathematical algorithm. It is envisaged that this knowledge will provide the process engineer and plant operator invaluable heuristics in which to diagnose problems with the control variables and aid in establishing their cause.

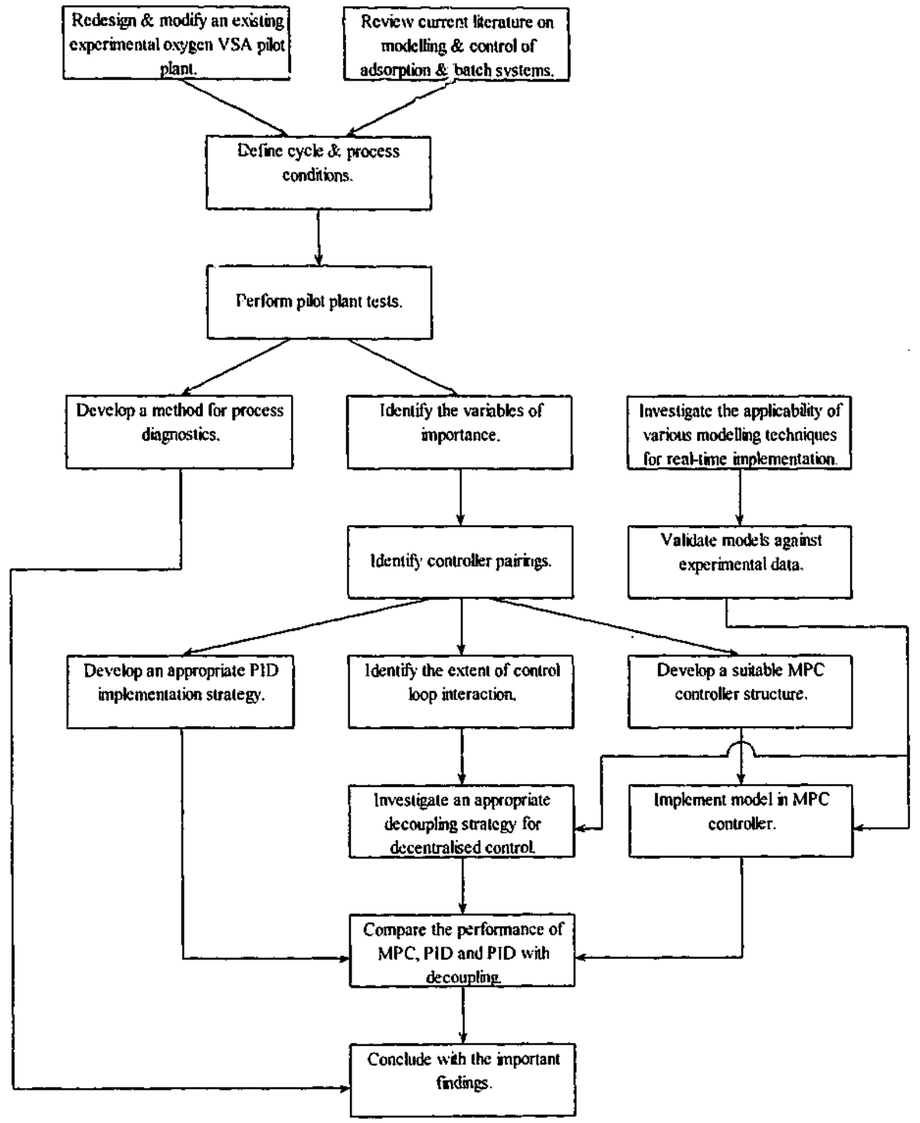

Figure 1.7a. The project roadmap.

The objectives above are addressed in the nine chapters to ensue and their content and goals are outlined as follows:

Chapter Two – Pilot Plant and Equipment

- Re-design an existing pilot oxygen VSA plant to ensure robustness and repeatable performance under continuous operation. This includes design and construction of PVC columns, implementation and testing of improved flow metering equipment and updating of the control logic and hardware configurations.
- Commission and operate the pilot plant.

Chapter Three – Process Modelling

- Aid the development of a detailed mechanistic model and examine the precision of the model against experimental data.
- Investigate the applicability of reduced-order physical models.
- Investigate the use of artificial neural networks as an alternative empirical method for modelling VSA systems.

Chapter Four – Open Loop Dynamics and Characteristics

- Discuss the development of a simplified mechanistic adsorption process model and use it to explain the observed experimental trends gathered from step response experiments on the laboratory plant.
- Establish the parameters of importance in the VSA process for oxygen enrichment.
- Determine the sensitivity of the system from an artificial neural network fit to pilot plant responses.
- Calculate the relative gain (RGA) matrix to ascertain control loop pairings.
- Confirm the robustness of the RGA through statistical means.

Chapter Five – Frequency Response to Cyclic Disturbances

- Use frequency response techniques to characterise the system and determine the significance of particular factors in a VSA cycle.
- Demonstrate the open loop stability of the VSA process.
- Perform additional validation of the simple model developed in Chapter 4.

Chapter Six – Single Loop Control

- Describe the implementation of control techniques in batch systems.
- Define the PID algorithm used, its features and tuning.
- Discuss the development of a novel model predictive control (MPC) structure and detail the tuning procedure tuning.
- Demonstrate the performance of both PID and MPC, in single loop form, in terms of load rejection and set point change on a pilot-scale oxygen VSA plant.

Chapter Seven – Multiple Loop Control

- Discuss the development and validation of simple empirical models for use in the tuning and simulation of controller dynamics.
- Derive a general, explicit decoupling algorithm for use in conjunction with decentralised controller structures in both full and one way configuration.
- Review current MIMO tuning practices and describe the control loop parings and tuning procedures practised.
- Compare the load rejection performance of PID, PID with explicit decoupling and MPC control implemented on a pilot-scale oxygen VSA plant.

Chapter Eight – A Simple Method to Construct the Composition Profile

- Discuss the development of a simplified adsorption process model to aid process monitoring and plant diagnostics.
- Apply the simple model to an industrial system (simulated numerically) and discuss its benefits and limitations.

A note to the reader is that the layout of this thesis is somewhat unconventional with each chapter being self-contained. No separate chapter is given for the literature review rather, the literature review is interspersed throughout the thesis and only discussed in the relevant chapter. The benefit of this structure is that it allows ease of reading, as the scope of this research topic is broad, covering several key areas. The important findings and the achievement of the original goals are summarised in the final chapter, Chapter 9, in addition to recommendations for future work in this area.

NOMENCLATURE

$\dot{n}$	mole rate (mol/s)
P	pressure (kPa.A)
Q	volumetric flow rate (m^3/s)
R	universal gas constant (kJ/mol/K)
T	temperature (K)
y	composition

Subcripts

1	feed stream
2	vacuum stream
3	bed product off-take
4	product stream
5	purge stream
f	feed
p	product

Chapter Two

Pilot Plant and Equipment

A pilot-scale VSA plant was designed and built in-house in a previous PhD project [Wilson, 2001] and refined further by the author for experimental purposes. The intention of the pilot plant was to accurately capture the effects observed by its industrial size equivalents and allow study of the physics to aid the on-going modelling effort within the adsorption group. A significant portion of this research effort involved the redesign of major equipment (such as the adsorbent beds, valving, pipework and flow metering equipment) and the PLC and SCADA software to ensure robustness, enable continuous online operation and the implementation of multiple loop controllers.

2.1 THE VSA PILOT PLANT

A pilot-scale unit was built to accommodate the main characteristics observed in plants in the field. Typically, industrial VSA units span two to three meters in height and one to two meters in diameter. This ensures essentially "short-term" adiabatic operation (although seasonal and diurnal temperature fluctuations do affect process performance), due to the small ratio of the surface to volume and the low conductivity of the zeolite sieve. Wilson (2001), had successfully designed and used polyurethane columns for sections of his research, however issues with mechanical robustness associated with the research objectives of this study such as continuous cyclic operation, meant that more mechanically sturdy beds were required. With this in mind, the beds for the pilot plant were designed and fabricated using 110mm O.D. x 3.0mm w.t. PVC pipe that has an effective working height of 1.81m. The beds were further insulated with fibre glass wool with reflective aluminium outer. The wall thickness was also kept to a minimum to reduce axial conduction due to source and sink effects and the Peclet number, (which defines the extent of axial dispersion), was kept reasonably high (>100), to ensure plug flow but below the incipient fluidisation velocity. Details of the columns and column internals, (including the sieve hold-down mechanism), are provided in Appendix C. A study using numerical simulation by Wilson (2001), shows that the PVC columns compare very well to the polyurethane columns in terms of capturing the axial temperature profile of a true adiabatic bed with an inert and adsorbent layer. The analysis also included a column fabricated from carbon steel, which showed significant deviation from adiabatic conditions. Furthermore, the overall

heat transfer coefficient for the polyurethane, PVC and metal columns was determined to be 0.22 W/(m^{2}K), 1.1 W/(m^{2}K) and 3.9 W/(m^{2}K) respectively and showed that the PVC material approximated polyurethane quite well. [Wilson, 2001; Wilson and Webley, 2002b]. It should be noted, however, that for the purposes of this study, true adiabaticity was not the chief requirement, (unlike in the case of Wilson (2001) whose main research objective was to study the cause and effect of the 'cold spot'), and therefore use of adsorbent beds manufactured from PVC was sufficient.

To allow comparison with numerical simulation and model validation and to ensure precise control, accurate flow metering equipment was required. This seemingly trivial task is complicated by the unsteady states that exists between each step of the process even at cyclic steady state (refer to §2.1.1). The inability of most common measurement equipment to discern the large spikes in gas flow which occurs between an evacuated bed coming online to a high pressure inlet stream, provides an example of the problems faced in the design of VSA plants. A pitot tube flowmeter provided by Rosemount from their "Annubar" series was selected, coupled with a sensitive differential pressure transmitter placed inline with the inlet and evacuation streams. This setup proved to be the best combination and provided regular mass balance closure between 1% and 3% compared to the >10% measured using turbine flowmeters. Also, unlike other forms of pressure drop devices such as orifice and turbine flowmeters, the "Annubars" allowed greater turndown ratios (defined as the ratio between highest and lowest measured flow) and are fairly robust in design as they contain no mechanical parts. Furthermore, a laminar flowmeter was utilised on the product line as the flow conditions on this stream was far less severe due to the damping provided by the 60L product buffer tank. Comparisons between the product flow sensor and a 4L soap bubble flowmeter showed excellent correlation.

The design of the on/off (solenoid) valves proved to be another major hurdle in the design of a VSA plant. Continual valve cycling caused the rapid demise of the stainless steel ball valves originally used for sequential control. The valves were recorded to fail (leaking stem or body seals) within four to five days of operation depending on the cycle studied. However, the change to globe valve designs had been met with considerable success.

A P&ID diagram of the pilot plant with dual bed operation is shown in Figure 2.1a (while a detailed version of the actual experimental assembly is included in Appendix B). The experimental plant was able to admit up to three beds and was valved such that both bed-to-bed purge and product purge steps were available. A control valve, located before the vacuum pump, allowed various vacuum conditions to be simulated (the control valve is not normally included with industrial plants and therefore a vacuum blower of fixed capacity is used). House air was supplied via a compressor and refrigerant dryer to the inlet stream to the pilot plant but further dried (to -50°C dew point at atmospheric conditions) and cleaned through a zeolite

(NaX) PSA dryer, oil knockout pots and particulate filters. The dryer also removed carbon dioxide and slightly enriched the inlet air stream to the VSA unit to a constant oxygen mole fraction of 22%. Therefore, the underlying assumption used throughout this thesis that the inlet fluid stream consisted of a binary mixture of oxygen and nitrogen was justified as only oxygen, argon and nitrogen were allowed to enter the VSA. Oxygen and argon have similar kinetics and adsorption characteristics and hence can be lumped together as a single component [Miller, 1973]. The argon content of air is about 1%, which means that the feed stream, in this case, had a nitrogen content of approximately 77%. This value for the nitrogen mole fraction was employed in numerical simulations.

The inlet air stream from the dryer was regulated in pressure before entering a 60L feed buffer tank with a centrally positioned, PID controlled, electric heater element used to maintain the fluid temperature in the vessel (VSA inlet temperature variation ~±1°C). A pressure regulator located downstream of the feed tank further ensured that constant inlet pressure was experienced by the VSA system. Heat loss from the feed tank and inlet piping was minimised by insulation consisting of fibre glass wool with reflective aluminium outer. The pressure regulation valves, heater element and insulation were additions to and in the case of the downstream regulator a modification to, the original plant design. All new components were sized and set based on previous operational data.

In addition, the software and hardware environment associated with the experimental plant was representative of industrial units with fully instrumented pressure, temperature, flow and product oxygen (paramagnetic) sensors. Junction exposed, T-type thermocouples are located axially along the length of the adsorbent beds to aid additional analysis of axial temperature profiles (see Appendix B for details of their location). An on-board programmable logic controller (PLC) allowed procedural control of the process, determination of mass balance closure and real-time performance calculations. Furthermore, the PLC had been programmed to handle various interlocks and trips (such as high and low pressure/flow) to avoid compromising both plant and user operation and safety. Lastly, the data was logged remotely via a supervisory, control and data acquisition (SCADA) package (Citect version 5.21, Service Pack E). A schematic of the communications highway is depicted in Figure 2.1b with a picture of the experimental VSA pilot plant shown in Figure 2.1c. A list of all the instrumentation and equipment used in this study including their range, errors and scaling is included in Appendix A.

The quality of the molecular sieves employed throughout this study was verified before use by experimental equilibrium adsorption measurements using a *Micromeretics ASAP 2010* porosimeter. The obtained isotherm was matched to known dual-site Langmuir parameters and if different, the zeolite sieve was regenerated via a flow-through furnace. A flow of dry air at a dew point of -50°C at atmospheric conditions (distributed through the bottom of the furnace and

exiting its way through one inch hole in the lid) was used to remove the desorbed contaminants (i.e. water). Furthermore, the characterisation of various types of zeolites (surface area, pellet and bed voidage, pore distribution), the regression of isotherm parameters if not available, establishment of the conditions for regeneration and the sizing and design of a 30L flows-through furnace that permitted simultaneous regeneration of the molecular sieve required for two adsorption columns were all slight but necessary digressions from the primary objectives of this research project. Details of the flow-through furnace system are contained in Appendix D.

2.1.1 Cyclic Steady State Definition

The following definition of cyclic steady state (CSS) was formulated for direct application on the experimental VSA plant and had been coded into the logic of the PLC. It differed slightly to the CSS criteria used in the MINSA numerical adsorption process simulator [Todd *et al.* 2001b] in that only the absolute errors are considered for the variables of interest. The determination of CSS is described as follows –

1. Minimal mass balance error (based on product and vacuum), (±3% deviation).
2. Constant oxygen concentration between $cycle_X$ and $cycle_{X+N}$, (±1% deviation) where the subscript N represents the sample interval (measured in cycles) of the CSS verification routine.
3. Balanced cyclic bed pressures between adsorber bed 1 and adsorber bed 2 and individual bed pressure profiles are constant from $cycle_X$ to $cycle_{X+N}$ (±1% deviation).
4. The adsorbent bed axial temperature profiles are constant from $cycle_X$ to $cycle_{X+N}$ (±0.5% deviation).
5. A constant product gas molar flow per cycle exists from $cycle_X$ to $cycle_{X+N}$, (±50 mmole/cycle deviation).
6. Both the inlet pressure and temperature are constant between $cycle_X$ and $cycle_{X+N}$ (±1% and ±0.5% deviation, respectively).

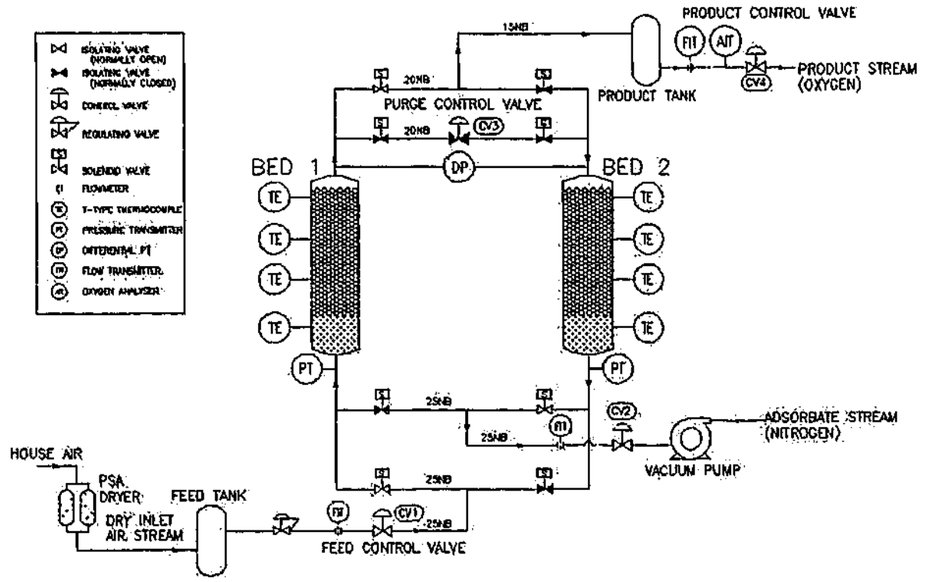

Figure 2.1a. P&ID of the experimental VSA pilot plant.

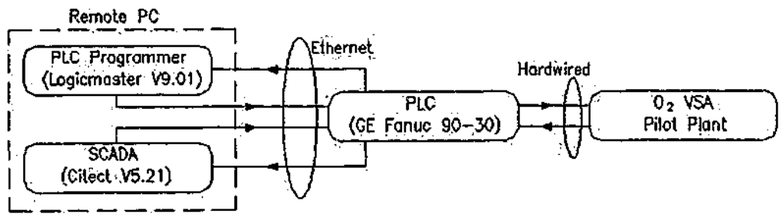

Figure 2.1b. Software and hardware communications highway of the O_2 VSA pilot plant.

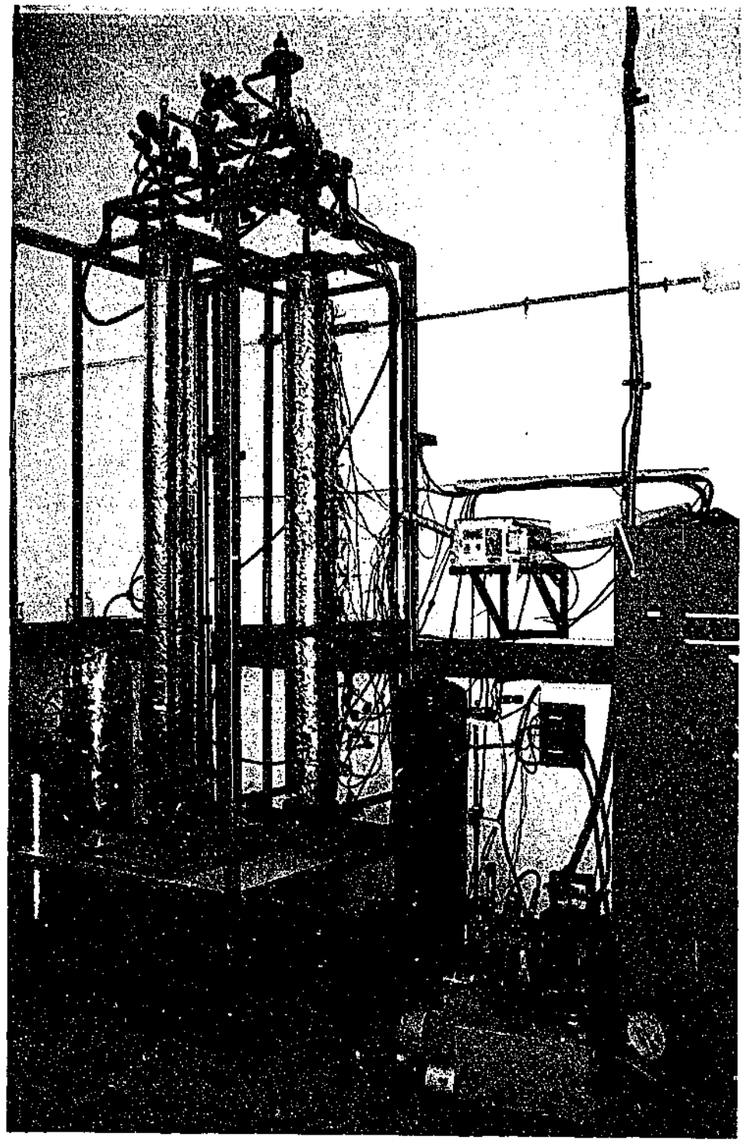

Figure 2.1c. **The experimental VSA Pilot Plant. Dual bed operation, the vacuum pump (foreground on the floor), feed (background – insulated) and product (foreground – black in colour) tanks, the paramagnetic oxygen analyser (mounted on a stand attached to the wall), PLC cabinet (behind pump – orange in colour), top valve train and product line can be observed.**

2.2 THE VSA CYCLES

Various VSA cycles had been studied, experimentally and numerically, throughout the course of this research effort and included both single and dual bed scenarios. Figures 2.2a to 2.2c represent schematics of the three main cycles employed. The three cycle arrangements shown in this section possess many similar features. The single bed cycle utilised product gas to purge the bed (Figure 2.2a) and the eight step cycle incorporated a pressure equalisation (PE) step to decrease power requirements and increase product recovery (Figure 2.2b). This eight step process is an example of a commonly used industrial cycle. The bulk of the work, however, will entail the use of the oxygen VSA cycle shown in Fig 2.2c as it contains all of the major steps of importance (adsorption, desorption and purge as discussed in §1.2) and while maintaining realistic industrial operation. Moreover, the cycle shown in Figure 2.2c ensured that the analysis was not clouded by additional information from secondary steps such as PE.

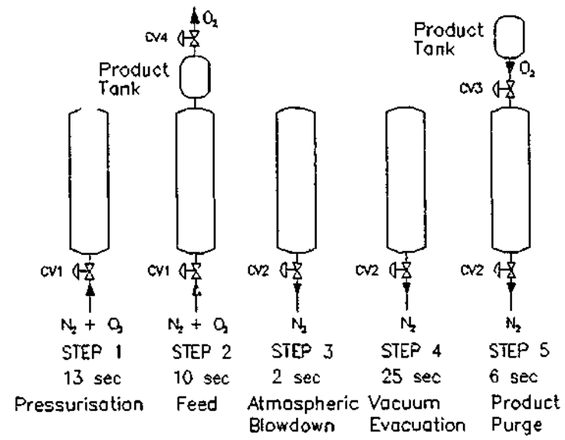

Figure 2.2a. **Sequence diagram for a single bed, 5 step cycle O_2 VSA cycle with product purge. Total cycle time 56 seconds.**

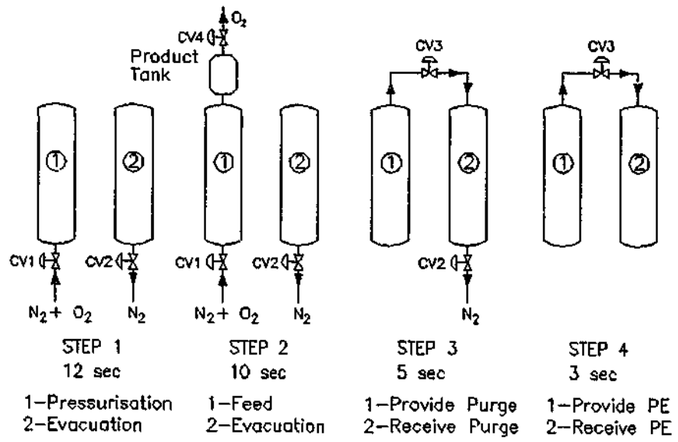

Figure 2.2b. **Sequence diagram for a dual bed, 8 step O_2 VSA cycle. First four steps are shown with the following four steps being mirror images of the first four for bed 2. Total cycle time 60 seconds.**

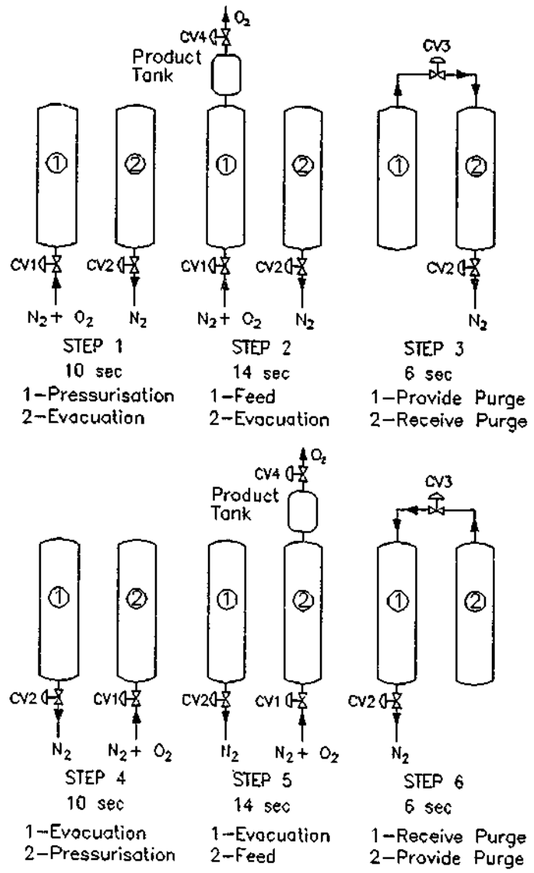

Figure 2.2c. **Sequence diagram for a dual bed, 6 step O_2 VSA cycle. Total cycle time 60 seconds. This is the principal cycle used in this study.**

In the discussion to follow, a description of the primary cycle of interest (Figure 2.2c) only will be provided as similar explanations can be provided for the other two cycles (Figures 2.2a and 2.2b). Being a semi-batch process, product off-take occurred during steps two (bed 1) and five (bed 2), with the flow into the bed controlled by valve CV1 and product flow controlled by valve CV4. Desorption of the adsorbate (nitrogen in this case) occurred during steps three and four and was controlled via valve CV2. The purge step, here shown in steps three (bed 1) and five (bed 2), is important for the maintenance in product purity. It forces contaminants (nitrogen) in the fluid phase down from the top of the bed and allows further adsorbate desorption to occur by lowering the partial pressure of nitrogen around the sieve. Control of the product purge stream was via valve CV3. Pressurising the bed with dry air in steps one (bed 1) and three (bed 2) completed the cycle. It should be noted that a product tank was present downstream of the beds. Control valve CV4, therefore, regulated flow from the product tank. Although product gas was provided to the product tank during steps two and five only, product withdrawal from the tank through CV4 was continuous. Fixed valve coefficient switch valves connect the beds, feed and product tanks only. An additional point of note is that the cycle studied did not include a pressure equalization step. Such a step is often included in large-scale PSA cycles to enhance recovery and reduce power requirements. Since the goal of this study was not to optimise power requirements or recovery of the process, this step had been omitted for purposes of simplicity. However, bed-to-bed coupling (important for studying system dynamics) had been retained through the inclusion of the purge step.

2.3 CHOICE OF FIXED PROCESS VARIABLES

As this thesis represents a first approach to the control problem, the scope of this study will be limited by fixing certain process variables. The discussion in Chapter 1 and in the preceding sections reveals that there are several variables that contribute to process performance. However, some of these variables are design variables (such as the adsorbent or the number of beds) while other variables, such as step time, can be both utilised for eith control or plant design. In the discussion to ensue, the major system parameters are described and the reasons given for the choices made.

Number of Beds

Although the pilot plant facilitated the use of three beds, single and two bed cycles were practiced. This reflects the current industrial practice to move away, where possible, from multiple beds in an effort to decrease capital costs. Large industrial installations, however, still consist of two or more beds as capital costs are incurred when designing a single bed plant for high throughputs and relatively high purity. This represents an additional argument for the

selection of the dual bed cycle shown in Figure 2.2c in §2.2 above, as the principal cycle of study.

Cycle Time

The current direction in the gas market is towards faster cycle times to increase production rates with the maintenance of product purity, which is understandable given the performance of the current molecular sieves. A cycle time of 60 seconds (or 56 seconds for the single bed case) is consistent with present industrial practice.

Steps & Step Time

Throughout the course of this study, the step times and hence the overall cycle time will remain fixed. The possibilities of varying step times for both control and optimisation of adsorption processes was not part of this investigation. In Chapter 1, §1.6, the issues regarding the control of step times was discussed and shown that depending on the cycle configuration, problems associated with unbalanced adsorber pressures can result. Use of this variable for control unnecessarily complicates the control problem at hand. Thus, the step times of the cycles studied will be equivalent to that shown in §2.2 or stated otherwise.

Adsorbent

For the majority of the experiments discussed throughout the text, a single layer of commercially available lithium based zeolitic sieve (~9.1 kg/bed) placed above a prelayer of alumina (~0.5kg/bed) was used unless stated otherwise. In industry, the prelayer's function is to remove moisture from the air stream, preventing contamination of the main bed. Whilst the inlet air stream to the laboratory plant was predried, the prelayer was retained in order to duplicate the unusual temperature profiles created by a prelayer of material in a bulk gas separation system [Wilson *et al.*, 2001].

2.4 CONCLUDING REMARKS

A pilot oxygen VSA plant, originally designed and built in a previous study [Wilson, 2001], was modified to ensure both robustness for continuous cyclic operation and reasonable mass balance closure. In addition, software logic allowed the online determination of CSS, performance calculation and communication to auxiliary equipment and third-party programs.

The cycle chosen for the majority of this study was a six step, dual bed cycle shown in Figure 2.2c. Also, several variables such as cycle and step time and the adsorbent were fixed to enable preliminary investigation into modelling and process control.

Chapter Three
Process Modelling

There are several limitations associated with most process modelling techniques whether it is by mechanistic or empirical means and no one method can be definitively regarded as superior over the other. Careful consideration of the process and the sensitivity of the factors involved can be rewarded by an increased understanding of the system investigated. It must be further stressed that all process models, whether physical or based on empirical fits, should be tested against measured data of sufficient quality in order to verify their value. The advent of adsorption and its associated processes has spurred much interest in the academic community mainly due to the severely nonlinear behaviour (introduced in Chapter 1). Various analytical tools have been used and developed in the past for the solution of the governing equations. This chapter will review some of these methods and discuss their benefits and limitations. In addition, a description and the performance of a numerical simulator (MINSA) and dynamic neural network (DySONN), both developed in-house, will be discussed.

3.1 MECHANISTIC MODELS

PSA and VSA processes represent a class of systems that has attracted much academic interest due to their complexity. The following section highlights the use of various analytical and numerical methods for the modelling of adsorption processes and discusses their strengths and limitations.

Analytical Techniques

The use of elegeant analytical techniques to solve the conservation equations and the boundary conditions which describe the operation of the PSA/VSA cycle has had limited success. Slow PSA/VSA cycles, coupled with various assumptions (such as that of equilibrium) reduces the equation set to a series of first-order hyperbolic equations which can be solved using the Method of Characteristics [Abbott, 1966]. The application of this method to model trace component removal and develop analytical solutions [LeVan, 1995; Subramanian and Ritter, 1998] had been met with moderate success. For example, Wilson *et al.* (2001) proposed a hybrid method for the solution estimation of the adsorbent front position for a strongly adsorbed trace component (water). By solving a species balance for the adsorbed component using the

Method of Characteristics, and imposing the boundary condition of an equivalence in the moles of water entering and leaving the bed over a cycle at steady state and that this amount was equal to the measured number of moles of water entering during the feed (adsorption) steps, the position of the water loaded zone could be iterated from an initial guess. Estimates by the characteristics model was in good agreement with both numerical analysis and direct physical measurement of the amount of water adsorbed on the molecular sieve.

For bulk separation processes such oxygen enrichment, the analysis was not so easily determined. Knaebel and Hill (1985) studied a theoretical two-bed air separation cycle for the enrichment of oxygen presented an example of the use of this technique. They assumed isothermal operation, slow cycle (and hence equilibrium operation), negligible axial pressure gradients and dispersion (and consequently sharp adsorption fronts) and used linear isotherms. Furthermore, the initial and boundary conditions were simplified by assuming a clean bed (i.e. no composition profiles of the more readily adsorbed component) and complete purge (using product gas consisting of 100% of oxygen) of the heavier component (nitrogen) in the bed. By assuming a product tank of sufficient volume, they were able to solve analytically for the pressurisation step using product gas only but solution of the equations using feed gas pressurisation required simultaneous solution of nonlinear equations and numerical integration due to the composition profiles induced by the feed stream. Chiang (1996) extended the work of Knaebel and Hill (1985) to include the more realistic operation of incomplete purging of the beds to enhance recovery of the lighter (oxygen) component. The obvious benefits of such methods is that it allows better appreciation of the physics of the process compared to numerical solutions where the underlying physics can be lost due to a proliferation of data and concerns with numerical convergence. Also, an added benefit of analytical solutions is that they permit a semi-rigorous check for the numerical model and tests the validity and accuracy of its outputs. However, the complexity and nonlinearity of the governing equations, the difficulties associated with the changing boundary conditions due to the cyclic nature of the process and the fact that bulk gas separation occurs in oxygen VSA, has meant that analytical solutions have had limited applications to industrial air separation cycles. Consequently, due to the poor match of analytical models to the air separation processes their use in model-based control structures is impractical.

Numerical Methods

Numerical procedures for the integration of the governing equations presents several methods that can overcome the many limitations faced by analytical techniques. In order to understand the process and to accurately capture the physics of the process, the Adsorption Group at Monash University designed and built a VSA/PSA simulation package called MINSA (Monash Integrated Numerical Simulator for Adsorption). The numerical model has been tested

and verified using both analytical expressions from simplified adsorption models (such as the exact solution for a breakthrough of a dilute component [Ruthven, 1984] and BLI [Knaebel and Hill, 1985]) and data collected from pilot plant studies [Webley *et al.*, 2000; Todd *et al.*, 2001b]. By specifying the initial and boundary conditions, the boundary condition type, the number of beds, the steps and the step times within a cycle, most PSA/VSA cycles could be simulated for the binary mixture of nitrogen and oxygen. Assuming ideal gas behaviour, the non-isothermal system mass balance is expressed in the simulator in terms of pressure as

$$\frac{\partial P}{\partial t} - \frac{P}{T}\left(\frac{\partial T}{\partial t}\right) = -\frac{T}{\varepsilon_t}\frac{\partial\left(\frac{uP}{T}\right)}{\partial z} - \frac{\rho_b RT}{\varepsilon_t}\sum_{i=1}^{2}\frac{\partial n_i}{\partial t} \qquad (3.1a)$$

where n_i is the moles of species i adsorbed per unit mass of adsorbent, ε_b and ε_t is the bed and total voidage respectively and u the superficial velocity. The component balance for an adsorbable species i is written as

$$P\left(\frac{\partial y}{\partial t}\right) + y\left(\frac{\partial P}{\partial t}\right) - \frac{Py}{T}\left(\frac{\partial T}{\partial t}\right) = -\frac{T}{\varepsilon_t}\frac{\partial\left(\frac{uPy}{T}\right)}{\partial z} - \frac{\rho_b RT}{\varepsilon_t}\left(\frac{\partial n_i}{\partial t}\right) \qquad (3.1b)$$

Second order effects such as axial dispersion in the gas phase were not included in the above equation as dispersion of the mass transfer front was dominated by mass transfer kinetics with axial dispersion playing only a minor role in the regions of interest. Also, diffusion was implemented through the determination of the mass transfer rate coefficient, k_i, which rendered a separate dispersion term redundant. The uptake term, $\partial n_i/\partial t$, on the right hand side of Eqs. (3.1a) and (3.1b) can be approximated by the Linear Driving Force (LDF) assumption which describes the mass transfer as a simple first order model [Glueckauf and Coates, 1947] given by

$$\frac{\partial n_i}{\partial t} = k_i\left(n_i^{eq} - n_i\right) \qquad (3.1c)$$

The MINSA model allows the option of linear, single-site Langmuir and coupled dual-site Langmuir isotherms for use in modelling the pressure, temperature and composition dependence of the equilibrium loading, n_i^{eq}, in solving for the actual loading, n_i. Furthermore, two options have been included in the process model based on the limiting mass transfer resistance. For macropore diffusion control, the gas accumulation in the pellet voids was included in the

isotherm calculation and the voidage in the mass balance equations (3.1a and 3.1b) became the external bed voidage. Alternatively, for micropore diffusion control, the gas accumulation in the pellet voids was not included in the isotherm calculation but was implicitly included in the overall balance equations by using the total voidage. However, macropore resistance was generally assumed for conventional PSA/VSA cycles where bidisperse molecular sieve zeolites were used and as a result, the mass transfer coefficient, k_i, becomes (Ruthven, 1984)

$$k_i = \frac{60 D_i}{d_p^2} \tag{3.1d}$$

$$\text{where } D_i = \frac{\varepsilon_p}{\tau}\left(\frac{1}{D_m} + \frac{1}{D_{k,i}}\right)^{-1} \tag{3.1e}$$

The molecular, D_m, and Knudsen, $D_{k,i}$, diffusion coefficients were calculated by use of standard expressions for these quantities (Sherwood *et al.*, 1975).

The bulk separation nature of the oxygen VSA/PSA system warranted the addition of the energy conservation balance. Equation (3.1f) describes the energy balance formulation used in MINSA based on the assumption of local equilibrium between the gas, adsorbed and solid phases. Kumar and Sircar (1984) have investigated the conditions over which this assumption holds and this covers the region of interest throughout this work.

$$\rho_b\left(\frac{\partial U_b}{\partial t}\right) + \varepsilon_t\left(\frac{\partial \rho_g U_g}{\partial t}\right) + \rho_b\left(\frac{\partial U_{ads}}{\partial t}\right) = -\frac{\partial\left(u\rho_g H_g\right)}{\partial z} - \frac{4h_w}{D}\left(T - T_{amb}\right) \tag{3.1f}$$

$$U_b = C_{pb}\left(T - T_{ref}\right)$$

$$U_g = H_g - \frac{P}{\rho_g}$$

where

$$U_{ads} = C_{pa}\left(\sum_{i=1}^{2} n_i\right)\left(T - T_{ref}\right) - \int_0^n \lambda dn$$

$$H_g = C_{pg}\left(T - T_{ref}\right)$$

and λ is the heat of adsorption evaluated at the reference temperature. Currently, there are two methods implemented in MINSA in evaluating the heat of adsorption – either as a constant or the isosteric heat of adsorption was estimated through the use of the Clausius-Clapeyron relationship (Eq. (3.1g)).

$$\lambda_i = -\frac{RT^2}{p_i}\left(\frac{\partial p_i}{\partial T}\right)_{n_i, n_j} \tag{3.1g}$$

By taking the derivative of the equilibrium isotherm using chain-rule expansion, where $n_i^{eq} = f(p_i, (1-p_i), T)$ and p_i is the partial pressure of component i, the partial derivative on the right hand side of Eq. (3.1g), $(\partial p_i / \partial T)_{n,w}$, was determined. The intensive computational requirements of this derivative at each time step and for each spatial node was avoided by approximating λ_i as a polynomial in terms of loading and temperature in a pre-processing calculation.

For convective flow through a packed bed, pressure drop becomes the dominant mechanism for momentum transfer and neglecting it can result in incorrect estimation of the axial composition profile [Chahbani and Tondeur, 2001]. The empirical correlation of Ergun [Ergun, 1952] for bed pressure drop had been used in the past with much success [Sereno and Rodrigues, 1993 and Todd *et al.*, 2001a], and provided a simplified approach to modelling one-dimensional, steady state flow through a bed packed with molecular sieve zeolite or activated carbon.

$$-\frac{\partial p}{\partial z} = \left[\frac{1.75\rho_g M_g\left(1-\varepsilon_b\right)}{\phi_p \varepsilon_b^3 d_p}\right]u^2 + \left[\frac{150\mu_g\left(1-\varepsilon_b\right)^2}{\phi_p^2 \varepsilon_b^3 d_p^2}\right]u \tag{3.1h}$$

Here, d_p and ϕ_p are the diameter and shape factor respectively for the particles, μ_{ga} the fluid dynamic viscosity and M_g the molecular weight of the gas. The finite volume approximation was used to solve the coupled partial differentials (Eqs. (3.1a) to (3.1h)) and had been shown to be particularly suited for modelling the hyperbolic conservation equations [Webley and He, 2000]. Implementation of the finite volume scheme requires discretisation in the axial domain and the resulting ordinary differential equations were then solved in the temporal domain using LSODA [Petzold, 1983] or DVODE [Brown *et al.*, 1989], stiff/non-stiff, variable time step, first-order, backward difference integrator packages. The solution strategy implemented utilised a higher order conservative interpolation scheme (QUICK – quadratic upstream interpolation with convective kinetics) [Leonard, 1979] for estimation of the control volume wall values which dampens the level of numerical dispersion. In addition, oscillatory results are smoothed using a SMART scheme based on the work by Gaskell and Lau (1988) [Webley and He, 2000], especially in regions of sharp gradients (e.g. in the region around the adsorption front). Additional information of the numerical simulator can be found in the reference Webley and He (2000) which provides details of the finite volume method, the interpolation scheme, the

solution adaptive strategy and the implementation of the various boundary conditions. Also, the node refinement scheme, the method utilised for cyclic steady state determination and the control technique employed to adjust the value of the boundary conditions such that desired specifications are met are discussed by Todd *et al.* (2001b).

Nevertheless, there are still several limitations associated with such numerical simulators for the purposes of control and process monitoring. To minimise computational requirements many process simulators including MINSA, model multiple bed systems using a single bed. In cycles where bed-to-bed interactions occur, the history of the purge stream exiting the bed providing purge gas is stored as a time dependent vector and then used as input during the step when the second bed receives the purge stream. This ultimately introduces errors in the prediction of transient responses and for advanced control algorithms may cause incorrect or unfavourable changes. In addition, use of rigorous single bed simulators does not satisfy real-time computing requirements. For example, a process discretised into 20 nodes throughout the main adsorbent bed and utilising the cycle conditions described in Figure 2.2c of Chapter 2, a simulation would take longer to run than the actual process on a Dec Alpha 667 MHz, Unix based computer. In addition, the pilot plant and most industrial systems incorporate pressure/flow regulators and feed and product tanks as auxiliary items to the adsorbers, which was not modeled in MINSA. The consequence of the inclusion of these components implies additional computing resources to cope with the extra differential equations that describe these items. The final disadvantage of detailed numerical models was the large number of unknown parameters that require accurate determination from experiments. Factors such as the isotherm parameters, various components of the Ergun equation and mass transfer coefficients represent some of the "fitting" parameters available in the numerical system. This does not include the complexities of correctly selecting the boundary conditions (e.g. setting valve flow coefficients) such that the numerical model can be calibrated to field data.

3.2 EMPIRICAL MODELLING – USE OF ARTIFICIAL NEURAL NETWORKS

Empirical modelling techniques, in particular artificial neural networks (ANN), offer an attractive alternative for systems such as the VSA process for oxygen production, where the creation of a model is difficult and its solution is complicated. The development of different neural network algorithms, since their conception in the mid-1900's, have been many and varied and references outlining their operation are just as abundant [Zurada, 1992; Masters, 1993; Hassoun, 1995; Graupe, 1997; Haykin, 1999]. The universality of ANN's for function approximation has been proven and discussed by Stinchcombe and White (1989) and Hornik *et al.* (1989). They demonstrated through the use of the Stone-Weierstrass Theorem, which is

based on function space theory, that a three-layer feedforward neural network is able to generalise any Borel measurable function, M, to any desired degree of accuracy, independent of the activation functions used. The researchers admitted the following assumptions/limitations to their proof:

1. The activation function, G, may be any continuous non-constant function (not necessarily a squashing function (e.g. sigmoidal or Tanh)).
2. The function that is to be modelled by the artificial neural network is both smooth and continuous, (i.e. C^r is $\mathcal{H}$ to $\mathcal{H}$ for $r \in N \equiv \{1,2, \ldots\}$).

This proof, coupled with the numerous successful applications of feedforward ANN's, resulted in the development of an in-house multi-layer perceptron (MLP) artificial neural network with a single hidden layer (DySONN – **Dy**namic and **S**tatic **O**peration **N**eural **N**etwork). The ANN is designed to enable the creation of non-linear relationships between the inputs and outputs from data sets in both static and dynamic modes. It furthermore permits any number of input, hidden and output neurons together with sigmoid, hyperbolic tangent and linear activation functions. Neural networks consist of a number of interconnected processing elements (PEs) or neurons that perform parallel computation and data processing [Haykin, 1999]. Figure 3.2a shows the typical structure of a three layer MLP architecture where the inputs are denoted as X and the outputs as Y. The inputs and outputs are related nonlinearly through the hidden neurons, h. A bias term B (a constant generally set to 1), is added to the ANN and passed via a weighted link to every hidden and output neuron in order to increase the approximation capabilities of the model [Haykin, 1999].

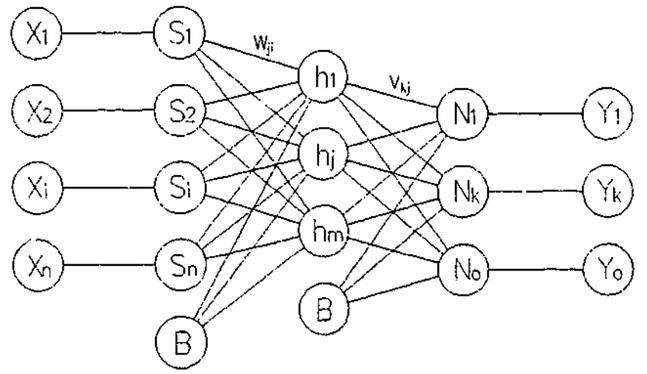

Figure 3.2a. Architecture of a three layer MLP neural network.

For a typical MLP neural network, the relationships between the input and hidden neurons is given by

$$S_i = d(X_i) \tag{3.2a}$$

$$h_j = f\left(\left(\sum_{i=1}^{I} w_{ji} S_i\right) + w_{jB} B\right) \tag{3.2b}$$

Similarly, the hidden neurons are related to the output neurons by

$$Y_k = c(N_k) \tag{3.2c}$$

$$N_k = g\left(\left(\sum_{j=1}^{J} v_{kj} h_j\right) + v_{kB} B\right) \tag{3.2d}$$

To further aid neural network learning, the measured inputs and outputs are normalised (generally based on the sample mean and standard deviation) as the weight change is proportional to the error gradient. This is represented by the function *d()* above and *c()*, which is the inverse of *d()*. DySONN permits the use of either sigmoidal (logistic), Tanh, standard statistical normalisation and also allows simpler scaling functions such as those based on the maximum value or the range. However, it is more common to use sigmoidal and Tanh functions as they may be helpful in reducing the effects of outliers and have an additional advantage in that no new data, no matter how large, is ever clipped or scaled out of range. The sigmoidal scaling function, which normalises the data between (0,1) and used for model determination, is represented below.

$$S_i = \frac{1}{1 + e^{-\left(\frac{X_i - \bar{X}_i}{\sigma_i}\right)}} \tag{3.2e}$$

and the Tanh scaling function which normalises the data between (-1,1) is written as

$$S_i = \frac{e^{2\left(\frac{X_i - \bar{X}_i}{\sigma_i}\right)} - 1}{e^{2\left(\frac{X_i - \bar{X}_i}{\sigma_i}\right)} + 1} \tag{3.2f}$$

In addition, to add nonlinearity to the process modelling, the sigmoidal (logistic) was employed for the activation functions *f()* and *g()*. The sigmoidal function compresses values between (0,1) and is expressed as follows

$$h_i = f\left(\left(\sum_{i=1}^{I} w_{ji} S_i\right) + w_{jB} B\right) = \frac{1}{1 + e^{-\left(\left(\sum_{i=1}^{I} w_{ji} S_i\right) + w_{jB} B\right)}} \tag{3.2g}$$

In a similar fashion, the Tanh function compresses its output values between (-1,1) and is described as follows

$$h_i = f\left(\left(\sum_{i=1}^{I} w_{ji} S_i\right) + w_{jB} B\right) = \frac{e^{\left(\left(\sum_{i=1}^{I} w_{ji} S_i\right) + w_{jB} B\right)} - 1}{e^{\left(\left(\sum_{i=1}^{I} w_{ji} S_i\right) + w_{jB} B\right)} + 1} \tag{3.2h}$$

How do Artificial Neural Networks learn?

The backpropagation algorithm is arguably the most popular numerical method for the training of feedforward ANN's even though other methods such as Levenberg-Marquardt and conjugate gradient exist. Nevertheless, it has been demonstrated that the backpropagation algorithm is robust enough to approximate any nonlinear input-output mapping [Hecht-Nielsen, 1989] although slightly computationally inefficient when compared to other numerical techniques. Alternatives to the numerical computation of the weight coefficients are genetic algorithms (GA), which are able to overcome the problems associated with numerical techniques such as convergence on local minimas by locating global minimas [Man *et al.*, 1999]. GA's are in essence smart guessing schemes that utilise the biological analogy whereby the members with the least errors (sets of weight coefficients in this case) are "bred" by swapping "genes" (the weight coefficients) with other members with similarly low error values. The main limitation to the use of GA's is the initial size of the population of weighting coefficients and spread of values. This limits the use of GA's to problems that are relatively small or to where large computing power is available. Also, for dynamic problems, GA's can prove to be highly cumbersome. It is for t[illegible]e reasons that the backpropagation algorithm is used as the basis of neural network generalisation. During the training of the ANN, relationships between inputs and outputs are created through the use of a gradient descent method to update each of the weight coefficients by back propagating the mean squared error of the associated ANN output, (E_k – defined by Eq. (3.2i)), with respect to the weights, W_{ji} and V_{kj}, for the data set. The chain rule for derivatives is used to obtain an analytical expression for the pattern-by-pattern update of the weight coefficients as described by Eqs. (3.2j) to (3.2m). A minus sign is

used for the change in weight as it is a gradient descent in weight space, which seeks a value of the weight coefficient such that the value of E_k is minimised [Haykin, 1999]. To further ensure that a minima is not overstepped, the generalised delta rule is applied by using a learning rate, λ, of constant value where $0< \lambda \leq 1$. Furthermore, a constant momentum coefficient, μ, is applied to the weight update in order to speed convergence where $0\leq \mu \leq 1$. The momentum coefficient is analogous to a second-order term that acts upon the gradient of the previous weight change.

$$E_k = \frac{1}{2}(O_k - Y_k)^2 \tag{3.2i}$$

$$\Delta v_{kj}(e) = -\frac{\partial E_k}{\partial v_{kj}} = -\frac{dE_k}{dY_k}\frac{dY_k}{dN_k}\frac{\partial N_k}{\partial v_{kj}} = (O_k - Y_k)h_j \frac{dY_k}{dN_k}\frac{dN_k}{dg_k} \tag{3.2j}$$

$$\Delta v_{kj}(e) = \lambda(O_k - Y_k)h_j \frac{dY_k}{dN_k}\frac{dN_k}{dg_k} + \mu\frac{\partial E_k}{\partial v_{kj}}(e-1) \tag{3.2k}$$

$$\Delta w_{ji}(e) = -\sum_{k=1}^{K}\frac{\partial E_k}{\partial w_{ji}} = -\sum_{k=1}^{K}\frac{dE_k}{dY_k}\frac{dY_k}{dN_k}\frac{\partial N_k}{\partial h_j}\frac{\partial h_j}{\partial w_{ji}} = S_i\frac{dh_j}{df_j}\sum_{k=1}^{K}\left[(O_k - Y_k)v_{kj}\frac{dY_k}{dN_k}\frac{dN_k}{dg_k}\right] \tag{3.2l}$$

$$\Delta w_{ji}(e) = \lambda S_i\frac{dh_j}{df_j}\sum_{k=1}^{K}\left[(O_k - Y_k)v_{kj}\frac{dY_k}{dN_k}\frac{dN_k}{dg_k}\right] + \mu\frac{\partial E_k}{\partial w_{ji}}(e-1) \tag{3.2m}$$

The new weights for the input and output layers are updated in the following manner

$$v_{kj}(e+1) = v_{kj}(e) + \Delta v_{kj}(e) \tag{3.2n}$$

$$w_{ji}(e+1) = w_{ji}(e) + \Delta w_{ji}(e) \tag{3.2o}$$

The computation is performed every epoch (e - defined as a single pass of the training set), until either the average mean squared error over the patterns, $\hat{E}$, or R^2 satisfies a set tolerance or the number of training epochs has been attained. R^2 is a measure of the accuracy of the ANN output to a benchmark model, wherein the prediction is the average of all outputs in the training set and is calculated by the following relationship

$$R^2 = 1 - \left[\frac{\sum_{k=1}^{K}(O_k - Y_k)^2}{\sum_{k=1}^{K}(O_k - \overline{O}_k)^2}\right] \tag{3.2p}$$

where O_k is the measured output value, $\overline{O}_k$, in Eq. (3.2p) above represents the mean of the measured output values and Y_k the ANN prediction.

Constructing an Artificial Neural Network

Unlike other parametric curve fitting methods such as regression analysis, ANN's require no *a priori* knowledge of the functional form of the data. This flexibility has been criticised by some in the mathematical field due to the lack of a rigorous algorithmic approach in designing the optimal ANN structure for a particular data set. However, the use of ANN's is still relatively new and it is only in more recent times that their uses and limitations have been studied in further detail. For example the paper by Reich and Barai (2000) attempts to answer particular fundamental questions concerning the use of ANN's and the authors offer advice on empirical modelling building. On the other hand, the researchers Bhat and McAvoy (1992) tackled the problem of having an excessively large ANN by developing an algorithm called StripNet to reduce the number of weight coefficients such that the ANN is of the simplest possible structure whilst retaining its generalistic abilities. These two references should assist the reader's awareness in the use of ANN's though construction of an ANN can be summarised as follows:

- Collect a sufficient amount of representative data.
- Set the initial weights to random values.
- Select the neuron activation functions and data scaling parameters.
- Experiment with tolerances (such as the mean squared error tolerance) during the training process.
- Experiment with the number of hidden neurons.
- Experiment with learning and momentum rates.
- Test trained ANN against a test set (i.e. data not used during the training process).

The advantages of using ANN's are –

- Provides accurate and expeditious prediction.
- Can model any data set provided that the underlying function is smooth and continuous.
- Can provide accurate information of the first and n^{th} order derivative of the data/function being modelled.
- Useful for system diagnostics.

The limitations of ANN's are –

- No proper mathematical basis for selection of architecture – problem dependent.
- Can over-learn or over-fit the data set.
- For large and complicated data sets, much computing power required for training.
- Cannot extrapolate beyond the region of the data used to fit the ANN.
- ANN's are only as good as the training data used and hence data of sufficiently high quality only should be utilised.

The paper by Otawara *et al.* (2002) is an example of how ANN's can be misused. The researchers applied a three layer feedforward neural network to model a three-phase fluidised bed undergoing chaotic behaviour. They successfully trained the network on experimentally determined data values at three different gas superficial velocities but at each point the system undergoes severe chaotic behaviour. The authors employed their trained ANN model to predict the behaviour of the system and in some cases extrapolate beyond the region trained They also observed the occurrence of bifurcations in their ANN model in some regions of operation. Furthermore, the gas velocities associated with these predicted bifurcations were not confirmed by experimentation. The applicability of ANN's, therefore, for this type of system has been questioned as it violates the condition of smooth functionality of the underlying system [Beh and Ranganathan, 2003]. Chaotic systems are largely dependent on the initial conditions and even initial conditions that are close will lead to quite divergent trajectories and hence large variations in the output parameter. This is valid even if a sufficiently small distance, ε_m, separates the input condition used from an input condition presented to the ANN during the training phase. The reason for this difference is that ANN's interpolate between the values of the training set and hence fit a smooth and continuous function over that surface. In a chaotic system, however, two nearby trajectories will diverge from each other over time by an amount, which is an exponential function of the system's Lyapunov exponents. In their defence, the authors concede that the predicted bifurcations may not be quantitatively equivalent to the real system but maintain that the ANN may show similar qualitative trends as field operation [Otawara *et al.*, 2003]. No additional experiments were presented or planned to justify their claims. As demonstrated by this example, a proper understanding of the use and limitations of ANN's is necessary for its application to various problems.

Applications of Artificial Neural Networks to Adsorption Studies

The application of neural networks in the modelling of adsorption systems is not new. Several researchers have used this technique to successfully model fundamental adsorption characteristics [Carsky and Do, 1999; Yang *et al.*, 1996], utilised it for the prediction of

multicomponent isotherms [Faur-Brasquet *et al.*, 2001], shown its ability to better model pressure drop in activated carbon cloth than the Ergun equation [Faur-Brasquet and Le Cloirec, 2003] while others have shown its applicability in modelling single step breakthrough experiments on trace component, liquid systems [Basheer and Najjar, 1996; Brasquet and Le Cloirec, 2000]. The use of neural networks in studying breakthrough characteristics was extended by Beh *et al.* (2001b) to the more complicated bulk gas separation of nitrogen from air on NaX molecular sieve. The ANN was successfully trained using eleven training breakthrough data sets (composed of various pressures, temperatures, flowrates and composition), satisfying the conditions of a low overall mean squared error and ensuring a good fit of the data set as measured by the R^2 value (Eq. (3.2p)). An example of the ability of the trained ANN against test data is presented in Figure 3.2b, which shows satisfactory approximation of the experimental breakthrough curve.

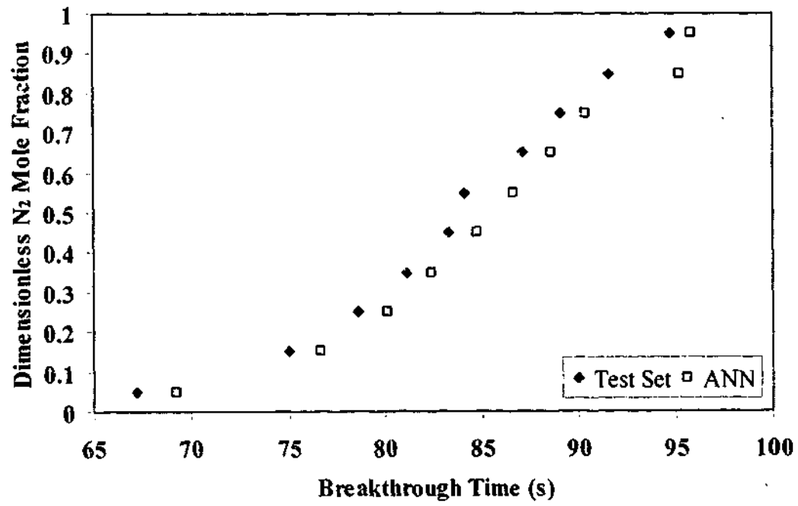

Figure 3.2b. Comparison of ANN against measured breakthrough time (34.3 kPa.G, 22.9°C, 1.7 mmole/s, 0.1 N_2 mole fraction).

Lewandowski *et al.* (1998) applied neural networks in the simulation and optimisation of a nitrogen PSA process, while Sundaram (1999) successfully trained several neural networks on various adsorption processes such as nitrogen and hydrogen purification. Figures 4.6a to 4.6c in the subsequent chapter demonstrates the application of an ANN in modelling cyclic steady state responses of the oxygen purification process. Dynamic modelling using neural networks, however, has not been applied in this field thus far. There have been some inroads into investigating the use of neural networks as dynamic models in various chemical engineering

processes such as reactors and anaerobic digesters [Xinggui *et al.*, 1998; Shaw *et al.*, 1997; Zorzetto *et al.*, 2000] (a short review of some of applications of ANN's in chemical engineering processes is discussed by Nikravesh *et al.* (1997)) but these processes do not share the complexity of an adsorption cycle. The next section will discuss the application of ANN's to the time variant VSA system.

3.2.1 Dynamic Modelling of the O_2 VSA Process

The implementation and performance of a dynamic neural network model on a numerically simulated VSA and an experimental pilot oxygen vacuum swing adsorption process will be discussed in this section. In both cases, a single layer of adsorbent material without a pre-layer was utilised and a single bed cycle similar to Figure 2.2a in Chapter 2 was studied. The inputs chosen for neural network training were the end of step pressures and temperatures at the bed entrance, the valve positions at each step and the total number of moles of gas fed into the bed over a cycle. The ANN outputs were based on customer driven interests such as oxygen purity (measured as percentage), recovery (moles of oxygen in the product stream divided by the moles in the feed stream) and production rate (kgPDc – kilograms per day of contained oxygen). The ANN applied to the pilot plant had an additional output, the average product pressure (measured in kPa.A). Seven hidden neurons were used for both cases to avoid problems of over-fitting the data (the ANN learning noise) and computational burdens. This number of hidden neurons was experimentally determined to be sufficient and avoids starving the network of weights when building relationships between inputs and outputs. In order for the ANN to generalise well, it must be trained on an adequate operating surface that includes areas of operation that are outside normal processing conditions. The response surface method (RSM) [Box *et al.*, 1978] was used to develop a series of experiments whereby once the simulation or plant had reached cyclic steady state (CSS – quantitatively defined by Todd *et al.* (2001b) and experimentally defined in §2.1.1 of Chapter 2), perturbations to the manipulated variables were made about CSS. Thirty perturbations to the valve and temperature boundary conditions were made to the process in open loop mode. The system was brought back to its original state after each change. Overall, 30000 cycles were used to train the ANN as it has been suggested in past studies that at least 800 cycles are required to fully assess the impact on performance of a singular process change due to the slow transient behaviour of a PSA bulk gas separation process [Wilson *et al.*, 2001].

Upon completion of the training phase, the ANN trainer module was halted and the on-line predictor module activated. Using the stored training weights and statistics, disturbances to the process conditions were made within the bounds of the training set. The ANN and process outputs were logged every cycle for comparison. To incorporate conditions realistic of field

operation, the following scenarios (that are within the training surface but not explicitly used to train the ANN) were applied as test cases for the trained ANN and are described as follows –

For the Numerical Simulator

Case 1. 10% increase in product valve (CV4) position during step 1. This scenario represents a situation whereby the customer demands an increase in product delivery.

Case 2. 10% increase in purge valve (CV3) position during 3. The amount of purge stream introduced to a bed has a significant effect on product purity and represents a situation whereby purge is used as a form of purity control (as investigated in the past by various researchers [Tan, 1996]).

Case 3. 5°C increase in inlet stream temperature. This final case study simulates the diurnal and seasonal changes experienced during VSA operation.

For the Pilot Plant

Case 4. 50% decrease in product valve (CV4) position during step 2. This scenario represents a situation whereby the customer reduces product demand.

Case 5. 20% increase in feed valve (CV1) position during step 2. The case study attempts to simulate the fluctuations in inlet pressure, which is a common occurrence in the field.

It should be noted that the scenarios listed above are by no means exhaustive of the varying conditions experienced by a VSA plant during operation but they do encapsulate the important situations that cause fluctuations in performance. To aid brevity, only the responses of the oxygen purity variable will be discussed with the following references available for specific information – Beh and Webley (2001), Beh *et al.* (2001a) and Beh *et al.* (2003).

Figures 3.2.1a and 3.2.1b illustrate the dynamic response of the oxygen VSA system to the perturbations above and the dynamic response of the trained neural network. The discussion will begin with results obtained from the implementation of the ANN on the numerical simulator. With reference to Figure 3.2.1a, for each case, the ANN was able to accurately capture the system dynamics. This includes the initial transients of the first 100 cycles where an inverse response (i.e. the initial response is in a direction opposite to the condition at CSS), occurs in the system. This interesting phenomenon emphasises the strong non-linearities that are abundant in the process. This is observed in the dynamics of the oxygen purity value (as shown in Figure 3.2.1a). From a control perspective, these inverse responses may cause problems if controllers such as PID are used. A final observation is the variance in system responses to differing disturbances. For Case 1, wherein the product valve was perturbed by 10%, fluctuations in the output conditions ceased within 50 cycles. Similarly, perturbation of the purge valve in Case 2 produced rapid asymptotic convergence in both oxygen recovery and production rate but a

slower response in oxygen purity, which took approximately 1000 cycles to steady. A change to the inlet temperature, however, had a very different effect. A gradual convergence to the steady state value is observed in all parameters, taking approximately 1500 cycles. This case study illustrates the strong but slow temperature dependence of the sieve and hence the process overall. Research into this area of study has revealed that this is mainly due to the low thermal conductivity and high thermal capacitance of the zeolitic sieve [Wilson, 2002a]. Once again from a control standpoint, the changes in process conditions have varying time constants with the added complexity that these perturbations may occur simultaneously or within the transient periods of each other.

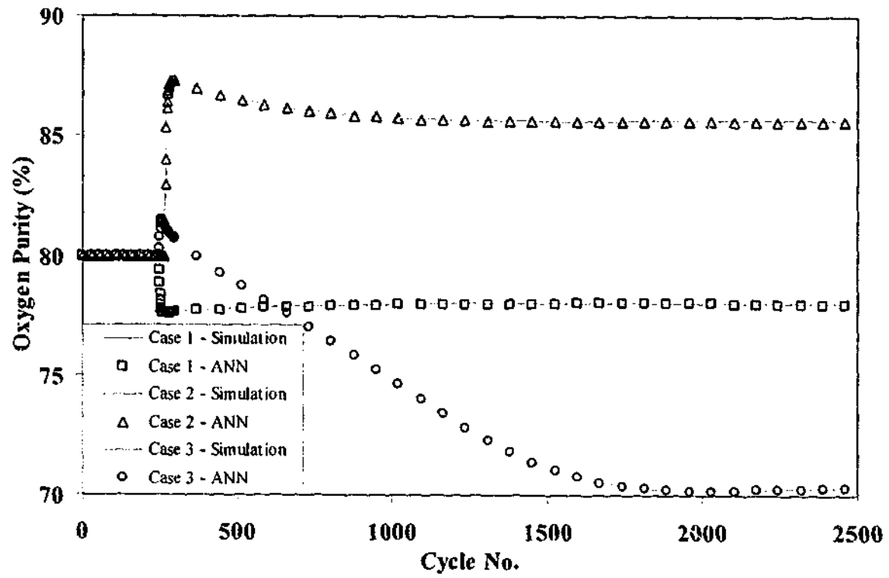

Figure 3.2.1a. Comparison of the dynamic response of the ANN and numerical simulation to fluctuations in oxygen purity for Cases 1, 2 and 3.

For the pilot plant study and with reference to Figure 3.2.1b, closing the product valve, as in Case 4, increases the back pressure on the system and hence provides an equivalent increase in product pressure. The product oxygen purity also improves from 91.8% to around 94.3% caused by this increase in bed pressure (as there is an equivalent increase in N_2 adsorption) and hence inhibits axial movement of the adsorption front. An increase in the feed valve position in Case 5, however, causes a decrease in oxygen purity from 92% to 89.6% and an increase in production rate for the equivalent product pressure as for Case 4. This reduction in purity is

mainly attributed to the saturation of the adsorbent bed and hence breakthrough of the nitrogen front occurs during step two of the cycle.

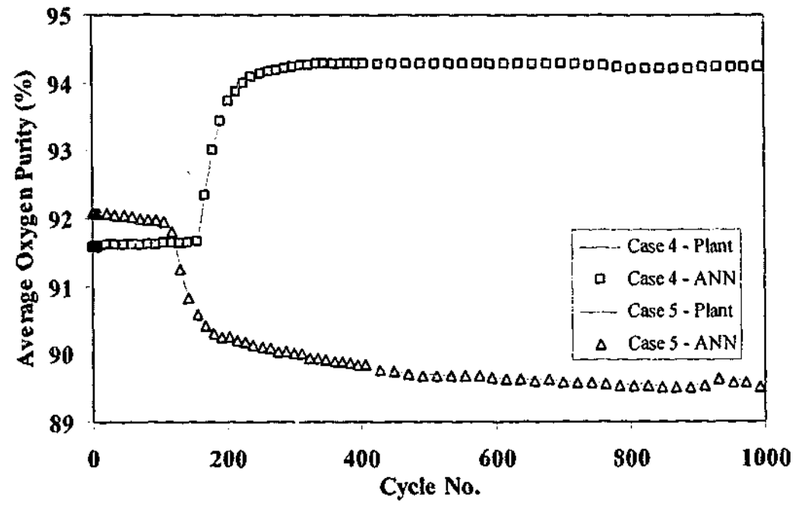

Figure 3.2.1b. Comparison of the dynamic response of the ANN and pilot plant to fluctuations in oxygen purity for Cases 4 and 5.

The data presented in this section shows that ability of neural networks in capturing the dynamics of this process lends itself to future studies as the basis for model predictive control of PSA/VSA systems. Some of the limitations of ANN's under dynamic conditions pertain to the large computer memory required to store training data with time and also the ever increasing computing power to train the ANN from such a large database. Consequently, ANN algorithms better suited to time-series data should be utilised instead of the MLP algorithm chosen. Lastly, the case studies investigated were sufficiently close to the training data that reliable prediction was provided. Thus, the predictive ability of the ANN was, unfortunately, never severely tested.

3.2.2 Sensitivity Analysis Using Neural Networks

The magnitude of the ANN weight coefficients indicates the extent of interaction between input and output variables. The ability to interpret these values, therefore, increases the applicability of neural networks not only for modelling but also for sensitivity analysis. It is curious to note that there seems to be very little published literature (non-existent in most texts describing the fundamentals and operation of neural networks) on the employment of neural networks in this field.

One of the earlier methods introduced to analyse the weight coefficients was the Hinton diagram. This is a simple process of viewing weights and basically involves the use of colours to highlight the magnitude of the connection weight. Thus, the deeper or darker the colour, the larger the weight. This visual method, however, lacks the ability to quantitatively comprehend the influence a particular input has on an output. The complex pairing of input and output neurons further demonstrates this. For example, with reference to Figure 3.2a, if the weigh connecting input one and output two is large, the sum of the weighted inputs to output neuron one may be smaller than that of output neuron two simply because of the magnitude of the input values. This is further complicated if hidden neurons rest between input and output streams and therefore there will be a minimum of two sets of weights. In this situation, it would be impossible to determine the network sensitivity based on colour changes. In essence, Hinton diagrams are "static" methods where only the magnitude of the coefficient is analysed. In the text to follow, several quantitative static methods will be reviewed and a generalised jacobian matrix will be derived for a feedforward neural network.

The method proposed by Garson (1991) to interpret the effect of input factors on outputs is arguably the most well known, static weight analysis technique. By assuming a single output neuron and partitioning the sum of effects on the output layer, the relative importance of each causal variable can be examined. Equation (3.2.2a) describes an extension of the formulation proposed by Garson (1991) which has been generalised by the author for N number of inputs, hidden neurons and outputs. It shows how the output k is affected by input i.

$$J_{ik} = \frac{\sum_{b=1}^{J}\sum_{a=1}^{I}\left[\left(\frac{w_{ba}}{\sum_{n=1}^{J}\sum_{m=1}^{I} w_{nm}}\right) v_{kb}\right]}{\sum_{i=1}^{I}\left[\sum_{b=1}^{J}\sum_{a=1}^{I}\left[\left(\frac{w_{ba}}{\sum_{n=1}^{J}\sum_{m=1}^{I} w_{nm}}\right) v_{kb}\right]\right]} \qquad (3.2.2a)$$

Gedeon (1997) reviews a number of other static analysis techniques and redefines Garson's formulae such that the contribution of positive and negative weights, do not cancel each other out. Tchaban *et al.* (1998) proposed a simpler relationship to establish the impact of a particular input on the output (Eq. 3.2.2b).

$$J_{ik} = \frac{X_i}{O_k}\sum_{j=1}^{J} w_{ji} v_{kj} \qquad (3.2.2b)$$

The absolute values of the weights are used in the two previous equations. The method of weight partitioning and that of Tchaban *et al.* (1998), although simple, neglects the value of the system inputs. Conditions may exist in a system or process whereby the sensitivity of a particular output to input changes because the system or process is in a different operating regime. An analysis of the surface gradient is therefore required. In the equations to follow, a general expression is a derived resulting in a jacobian matrix, which corresponds to the derivatives at a particular region on the surface.

The use of an adequately trained ANN to correctly report information on the actual system sensitivity (derivative at a particular point) has been mathematically proven by Hornik *et al.* (1990). Thus, once an ANN generalises a system sufficiently, the derivatives obtained from the trained ANN are equivalent to the derivatives of the system being modelled. An analytical expression for the sensitivity coefficients (gradient about a particular operating region) can be obtained through the application of the chain rule for derivatives to Eqs. (3.2a) through (3.2d) to yield the derivative of Y_k with respect to X_i described by Eq. (3.2.2c). The bias term and its resulting weight coefficients are ignored in this procedure as the bias is constant and therefore has no corresponding impact on the derivatives of the system.

$$\frac{\partial Y_k}{\partial X_i} = \sum_{j=1}^{J} \frac{dY_k}{dN_k}\frac{\partial N_k}{\partial h_j}\frac{\partial h_j}{\partial S_i}\frac{dS_i}{dX_i} \qquad (3.2.2c)$$

Each partial derivative in Eq. (3.2.2c) can be solved analytically from the equations in §3.2 to yield the following expression

$$\frac{\partial Y_k}{\partial X_i} = \sum_{j=1}^{J} \frac{dY_k}{dN_k}\frac{\partial N_k}{\partial g_k}\frac{\partial g_k}{\partial h_j}\frac{\partial h_j}{\partial f_j}\frac{\partial f_j}{\partial S_i}\frac{dS_i}{dX_i} = \sum_{j=1}^{J} c_k' g_k' v_{kj} f_j' w_{ji} d_i' \qquad (3.2.2d)$$

Therefore the Jacobian matrix of partial derivatives is comprised of Eq. (3.2.2d) describing each element as given by Eq. (3.2.2e) below.

$$J_{ik} = \begin{bmatrix} \frac{\partial Y_1}{\partial X_1} & \cdot & \cdot \\ \cdot & \frac{\partial Y_k}{\partial X_i} & \cdot \\ \cdot & \cdot & \frac{\partial Y_K}{\partial X_I} \end{bmatrix} \qquad (3.2.2e)$$

The result is a matrix of sensitivities whereby the value of its members determines the magnitude of the influence of a particular input to the outputs and the degree of interaction. Figure 3.2.2a illustrates the use of an ANN that has been trained on the function $y = \mathrm{Sin}(4x)$ (a single-input-single-output system) and through the application of Eq. (3.2.2d) the derivative, $y' = 4\mathrm{Cos}(4x)$ is approximated. Figure 3.2.2b shows a satisfactory match between the analytical solution and the differentiated ANN (a point of note: the ANN was not regressed on the analytical derivative).

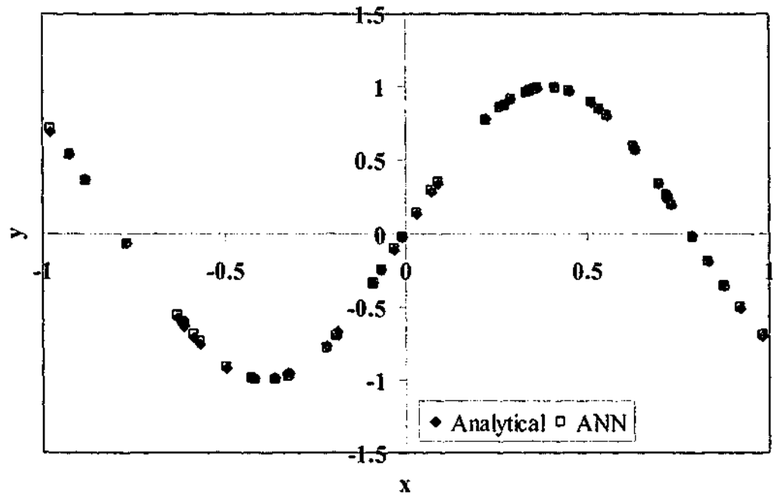

Figure 3.2.2a. Comparison between analytical solution and ANN for y=Sin(4x).

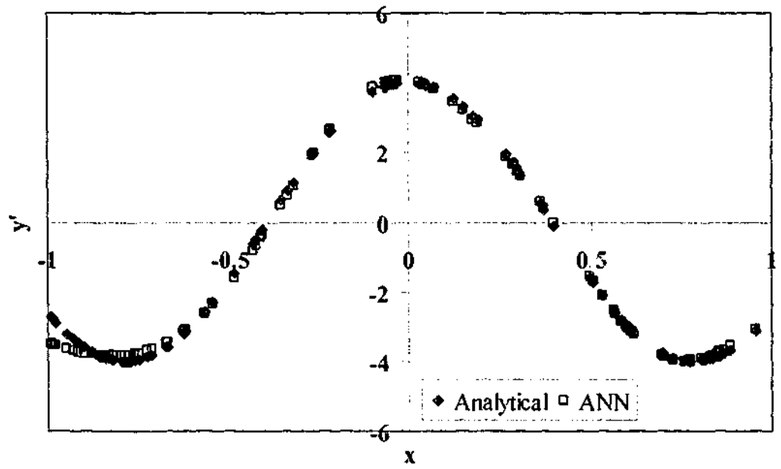

Figure 3.2.2b. Comparison between analytical solution and ANN for y'=4Cos(4x).

The equation (Eq. (3.2.2e)) established above represents a true derivative, which can in some cases be a strong function of the region of operation. In order to smooth the effects of the input conditions and to obtain an overall sensitivity matrix, Zurada *et al.* (1994) has proposed various objective functions evaluated for the set X (which represents the set of input vectors X_i at different inlet conditions). The mean square average sensitivity, the absolute value average sensitivity, the average sensitivity and the maximum sensitivity can be determined using Eqs. (3.2.2f) to (3.2.2i) respectively.

$$\bar{J}_{ik} = \sqrt{\frac{\sum_{n=1}^{N}\left(\left.\frac{\partial Y_k}{\partial X_i}\right|_n\right)^2}{N}} \tag{3.2.2f}$$

$$\bar{J}_{ik} = \sqrt{\frac{\sum_{n=1}^{N}\left|\left.\frac{\partial Y_k}{\partial X_i}\right|_n\right|}{N}} \tag{3.2.2g}$$

$$\bar{J}_{ik} = \frac{\sum_{n=1}^{N}\left.\frac{\partial Y_k}{\partial X_i}\right|_n}{N} \tag{3.2.2h}$$

$$\bar{J}_{ik} = \max_{n=1\ldots N}\left\{\left.\frac{\partial Y_k}{\partial X_i}\right|_n\right\} \tag{3.2.2i}$$

An example of the application of these averaged sensitivities is illustrated in the following problem. Equations (3.2.2j) and (3.2.2k) represent a third order interacting polynomial system consisting of three inputs (X_1,X_2,X_3) and two outputs (Y_1,Y_2).

$$\begin{aligned} Y_1 = {} & aX_1 + bX_1^2 + cX_1^3 + dX_2 + eX_2^2 + fX_2^3 + \\ & gX_3 + hX_3^2 + iX_3^3 + jX_1X_2 + kX_1X_3 + lX_2X_3 + \\ & mX_1X_2X_3 \end{aligned} \tag{3.2.2j}$$

$$\begin{aligned} Y_2 = {} & nX_1 + oX_1^2 + pX_1^3 + qX_2 + rX_2^2 + sX_2^3 + \\ & tX_3 + uX_3^2 + vX_3^3 + wX_1X_2 + xX_1X_3 + yX_2X_3 + \\ & zX_1X_2X_3 \end{aligned} \tag{3.2.2k}$$

The ANN was trained on a pattern set of 200 and tested against 50 input variables that were not used in the training stage. The overall system sensitivity for 200 inputs was calculated for the analytical solution of Eqs. (3.2.2j) and (3.2.2k) and compared to the derivative of the ANN model as shown in Figure 3.2.2c. Both analytical and empirical formulations were based on the mean square average sensitivity (Eq. (3.2.2f). Once again the excellent correlation was between the ANN and the analytical result which further emphasises the use of this empirical modelling tool for sensitivity analysis of complicated systems such as oxygen VSA.

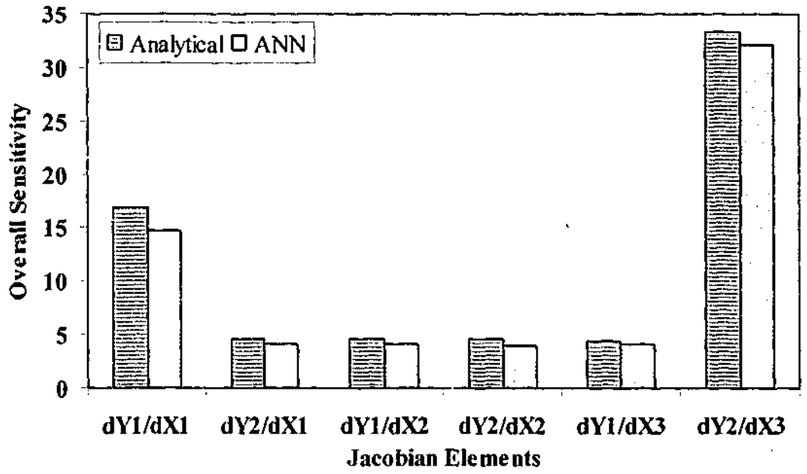

Figure 3.2.2c. Sensivity of inputs to outputs for an increase in coefficients *c* and *t* (with all other coefficients = 1) for a third order interacting polynomial.

The ability to analyse a system empirically that is too complicated to model physically and/or there are some unknown parameters within the model (such as mass or heat transfer coefficients) and also to gain information on the relationships between inputs and outputs makes artificial neural networks a powerful tool. Sensitivity analysis allows the user to determine which input has the least impacts on the output variables and therefore can be neglected (further simplifying the ANN and the analysis). It can also be used to identify process/model mismatch (for example if the derivative calculated by a model does not match that of the process which is modelled by the ANN). In terms of process control, the sensitivity information gained from the ANN can be utilised to determine control loop pairings and lead the way in the design of techniques for control loop decoupling algorithms.

3.3 CONCLUDING REMARKS

Several methods have been tested in this chapter for the possible use as an online modelling procedure in model-based control algorithms. Unfortunately, due to the complexity of the oxygen VSA process, this study has not been able to define an appropriate modelling technique for this system. It has been shown that analytical methods are not able to cope with the governing equations and that numerical solution of these equations is limited by computational requirements and further undermined by process/model mismatches due to the many ill-defined parameters within the model and certain unmodelled process dynamics. On the other hand, empirical methods such as artificial neural networks have the advantage that the physics of the process are not required as it forms relationships between the measured inputs and outputs that is purely empirically based. Once again, as experienced with numerical simulators, large memory storage and processing power are required, hindering the attractiveness of this alternative. Nevertheless, the ability of ANN's for the calculation of the process derivative does make them useful as a process control tool. This suggests, therefore, that a compromise is made by reducing the complexity of the physical model, incorporating some empirical information and utilising ANN's to model certain features where necessary. In the chapter to follow, a greatly simplified version of the rigorous model described in §3.1 is presented and combined with an ANN to gather sensitivity information.

NOMENCLATURE

Minsa Nomenclature

C_{pb}	bed heat capacity (J/kg/K)
C_{pa}	adsorbed phase heat capacity (J/kg/K)
C_{pg}	gas heat capacity at constant pressure (J/mol/K)
d_p	pellet diameter (m)
D	bed diameter (m)
$D_{k,i}$	Knudsen diffusion coefficient (m^2/s)
D_i	overall diffusion coefficient (m^2/s)
D_m	molecular diffusion coefficient (m^2/s)
h_w	heat transfer coefficient ($J/(m^2.s.K)$)
H_g	gas enthalpy (J/mol)
k_i	mass transfer coefficient for oxygen and nitrogen
M_g	gas molecular weight (kg/mol)
n_i	nitrogen and oxygen adsorbed loading (mol/kg)
n_i^{eq}	nitrogen and oxygen adsorbed equilibrium loading (mol/kg)
p	partial pressure (bar.A)

P	pressure (bar.A)
R	universal gas constant (m^3.bar/mol/K)
t	time variable (s)
T	temperature (K)
u	superficial velocity (m/s)
U	Internal energy (J/mol)
y	adsorbable component mole fraction (nitrogen)
z	axial location in bed (m)
ε_b	bed voidage
ε_p	pellet voidage
ε_t	total voidage
ϕ_p	particle shape factor
λ	heat of adsorption (J/mol)
ρ_b	bed density (kg/m^3)
ρ_g	gas density (mol/m^3 or kg/m^3)
μ_g	dynamic viscosity (Pa.s)
τ	tortuosity

Minsa Subcripts

ads	adsorbed phase
amb	ambient conditions
b	bed or solid phase
g	gas phase
i	adsorbed component
ref	reference conditions

ANN Nomenclature

B	neural network bias term
e	epoch
E_k	mean squared error and average mean squared error based on the patterns respectively
f_j	hidden neuron activation function
g_k	output neuron activation function
h_j	j^{th} hidden neuron
J_{nk}	jacobian matrix element
n	n^{th} pattern

N	number of patterns used for average sensitivity calculation
O_k	k^{th} measured output value
$\overline{O}_k$	k^{th} mean measured output value
R^2	measure of the accuracy of the ANN output to a benchmark model wherein the prediction was the average of all outputs in the training set
w_{ji}	neural network weight coefficient relating input neurons to hidden neurons
v_{kj}	neural network weight coefficient relating hidden neurons to output neurons
X_i, S_i	i^{th} input and normalised input neuron respectively
$\overline{X}_i$	mean value of the i^{th} input
Y_k, N_k	k^{th} output and normalised output neuron respectively
Δw_{ji}, Δv_{kj}	change in neural network weight coefficients
λ	learning rate
μ	momentum term
σ	standard deviation of measured inputs and outputs

Chapter Four

Open Loop Dynamics and Characteristics

The analysis of step responses of manipulated variables provides valuable information for the study of system dynamics, extent of interaction and control loop pairings. The first part of this chapter will present data from input perturbations gathered from a pilot-scale experimental oxygen VSA process. The interesting time-variant temperature profiles and bed and system pressures, flows and purity will be the main focus of the discussion. A simple mechanistic model is derived and used as a quantitative tool for interpretation of the observed trends. In addition, the possible applications of this knowledge for heuristic based control will be discussed. The objective of the second section of this chapter is to characterise the step response data gained using empirical modelling techniques. This information will be employed to analyse the sensitivity of the input variables and therefore permit determination of the extent of closed loop interaction and identification of suitable controller parings.

4.1 INTRODUCTION

The focus of previous research efforts in air separation adsorption processes has been primarily on the determination of cyclic steady state conditions. Thus, the optimisation of design and operating conditions has required detailed investigation of steady state conditions leading to the development of process simulators and a large amount of experimental information. In contrast, the investigation of dynamic responses of an adsorption process to changes in manipulated variables and external disturbances has been almost non-existent. Unfortunately, it is this dynamic behaviour which is the feature of most interest to the operator and process engineer once the plant has been built and is in operation. Since multiple control objectives must be met during the operation of an O_2 VSA process (typically oxygen purity, flow rate, and pressure), and many variables (typically valve positions) are available for manipulation, it is important to understand the impact of these variables on purity, flow and pressure as well as identify potential interactions which may diminish the quality of the control scheme. In industry, multiple PID loops are commonly employed to control individual parameters in the O_2 VSA process with the assumption that these loops are independent but this may not be the case. The purpose of this chapter, which is based on previous work [Beh and

Webley, 2002; Beh and Webley, 2003b; Beh and Webley, 2003c; Beh and Webley, 2003d], is to examine and present the experimental dynamic response of the O_2 VSA system (particularly product purity, flow, and pressure) to step changes in manipulated variables and load with a view to using this information to pair and tune control loops.

The chapter is organised in the following manner. Firstly, the process and perturbation scenarios will be described followed by a discussion of the development of a simple process simulator to aid interpretation of trends in the data. Next, the open loop dynamics and the results gained from modelling of the system with an artificial neural network (ANN) will be discussed. The values elucidated from the ANN will be used to determine the system gain and this sensitivity matrix will then be utilised to compute a relative gain matrix to establish control loop pairings and aid the design of loop decoupling algorithms. The chapter will conclude by summarising the important findings.

4.2 THE VSA CYCLE AND CASE STUDIES

The primary VSA cycle studied in this chapter bears the main characteristics typical of industrial practice and is described in detail in Chapter 2, §2.2 and shown in Figure 2.2c. In order to understand and characterise the process, the following scenarios were investigated with perturbations about cyclic steady state –

Case 1. An increase of 5% in the feed valve (CV1) position during the feed steps (steps 2 and 5).

Case 2. An increase of 3% in the purge valve (CV3) position during the purge steps (steps and 3 and 4).

Case 3. A decrease of 10% in the product valve (CV4) position during the feed steps (steps 2 and 5).

Case 4. Product load disturbance of 5 kPa via water level in a load tank.

The magnitudes of the perturbations of the manipulated variables were chosen based on previous experience in O_2 VSA operation and are upper limits of what would typically be needed to control purity, flow, and pressure.

The responses measured were bed pressures, flow rates, temperatures and product composition as a function of absolute time and cycle time. Of particular interest are product composition, product flow rate and product pressure since these directly impact upon the customer and are usually the variables selected for control. Furthermore, it should be noted that the case studies above are by no means exhaustive of the varying conditions experienced by a VSA plant during operation but they do encapsulate the important situations that cause

fluctuations in performance. Also, these valves are typically used for the purposes of control in the VSA process to ensure purity, flow and pressure targets are met.

4.3 MECHANISTIC MODEL DEVELOPMENT

To help understand the observed responses it was considered important to develop a computationally simple yet physically representative model. The model should account for the direction of the response (increase or decrease) as well as the approximate magnitude (steady state gain) and response time (number of cycles needed to reach 95% of the final value). The eventual use of this model will be in a model predictive structure for future on-line model-based control. It is worthwhile elaborating on the need for an appropriate model since there is already an abundance of adsorption models in the literature. The reader is therefore justified in questioning the need for an additional model. Explanation of the ***dynamic*** response of a cyclic adsorption system and development of a control model can be done on at least three different levels:

a. Detailed solution of the governing differential conservation equations with appropriate time varying boundary conditions.
   There have been many adsorption simulators developed over the last decade [Todd *et al.*, 2001b]. This modelling approach is not appropriate in the current study for at least three reasons:
   1. The vast majority of adsorption simulators (including our own, MINSA [Todd *et al.*, 2001b]) are unfortunately single bed simulators. As mentioned earlier, multi-bed systems are modelled in one bed simulators by storing information on beds providing gas and using this information later when needed for modelling beds receiving gas. This approach is entirely appropriate when only information at cyclic steady state is required since eventual convergence on the correct profiles would be achieved for moderate computational demand. When bed coupling is present (as in the current study), however, a true multi-bed simulator is needed to correctly model the short-term/dynamic (1 to 5 cycles) response of the system. The computational demands of a full multi-bed simulator are excessive and would not satisfy the need for future on-line model-based control. Doong and Propsner (1998) discussed the benefits of multi-bed adsorption process simulators with demonstration on a dual bed PSA process. Although their model was a single bed simulator, they attempted to demonstrate the effects of asymmetric operation by adjusting the position of the bed-to-bed valve during the bed-to-bed purge and pressure equalisation steps such that each

bed would experience differing purge flows throughout the cycle. Their study showed that operation asymmetry resulted in vastly different performance from that of a symmetric process simulation. In the field, asymmetric operation is a more common scenario due to the slight variances in piping arrangements, bed packing and volume and valve positions (especially in the case of the purge valve which is generally designed to flow in a unilateral direction but in a VSA/PSA process bilateral flow between beds is permitted). The authors also admit that their single bed simulator with variable bed-to-bed boundary conditions still did not provide a true representation of the dynamics of a multi-bed system.

2. A distributed model is useful when information on distributed variables or variables directly dependent on distributed parameters is needed. In this study, the main variables of interest are purity, flow rate, and pressure. Oxygen purity is strongly dependent on the concentration behaviour in the adsorption bed (a distributed variable) and if this were the sole variable of interest, then a distributed model would be required. However, product flow rate and pressure are also variables of interest. These are lumped or integrated variables governed largely by flows to and from coupled adsorption tanks with only weak dependence on the spatial information in the beds. Use of a spatially distributed model therefore is unnecessarily complicated and a lumped parameter model (see c. below) is more appropriate.
3. Numerical solution of the coupled conservation equations is sufficiently complex to conceal the physics upon which the equations are based. Tracing which terms in the equations were responsible for predicted behaviour as a function of time is difficult and extremely tedious. A simpler (perhaps less accurate) model which contains the essence of the physics would be more appropriate.

b. Ad hoc arguments followed by construction of an entirely empirical model using correlations between input manipulated variables and responses.

Some of the responses of the system (pressure and flow) can be explained using ad hoc arguments and indeed, these arguments will be used from time to time. However, these arguments can provide at best the direction of the response, not the magnitude nor the time scale of the response. At worst, ad hoc arguments can be completely incorrect. In addition, ad hoc arguments have no predictive power. While black-box type empirical models can be used for prediction (and control purposes), they hold only for situations which match exactly the experimental conditions for which they were derived. They

contain no underlying physics and hence provide no ability to predict the effect of perturbations outside the scope of that studied. It is for these reasons that black-box models are only used in process control structures if reliable mechanistic models are not available or that the physical model requires impractical computing resource or if mechanistic models are difficult to develop (refer to Chapter 2 in the section which discusses the use of ANN's).

c. Solution of a spatially lumped model.

It is hypothesized that a lumped model (not spatially distributed) based on a true multi-bed system (including associated gas storage tanks) will serve to explain the direction, magnitude, and time scales of the pressure and flow rate responses since these are integrated quantities determined mainly by integrated (or average) bed properties. Such a model is therefore appropriate for the goals of this study since it is computationally rapid, has underlying physics and can be used to help explain observed responses. The price that is paid with these simplifications is the loss of purity prediction (a spatial variable) as well as the loss of *a priori* prediction. Some parameters of the model must be adjusted to "calibrate" the model to the experimental data – in the present study, these parameters are valve Cv's and pressure boundary conditions, as explained below. It should be stressed that such a calibration is done purely to fix absolute values of pressure and flow for future control purposes and is not necessary for predicting the change in pressure and flow nor the time scale of the response. The model is firmly grounded in the physics of pressure driven flow to/from coupled tanks, some of which contain adsorbents.

The lumped model, termed SoCAT – Simulator of Coupled Adsorptive Tanks, was developed with the aforementioned goals in mind. As mentioned above, this model does not replace simulators that are intended to provide an *a priori* match to experimental data. The model is not unique – there are several variations that are possible. The process model is based on the flow sheet illustrated in Figure 4.3a and the similarities between the model process flow diagram and the pilot plant P&ID as depicted in Figure 2.1a can be seen. SoCAT consists of a feed tank which is connected via control and on/off valves to the two adsorber tanks. The adsorbers are connected to each other to enable the simulation of bed-to-bed interactions and are both also connected to a product tank. Furthermore, adsorbate evacuation is simulated via stream 8.

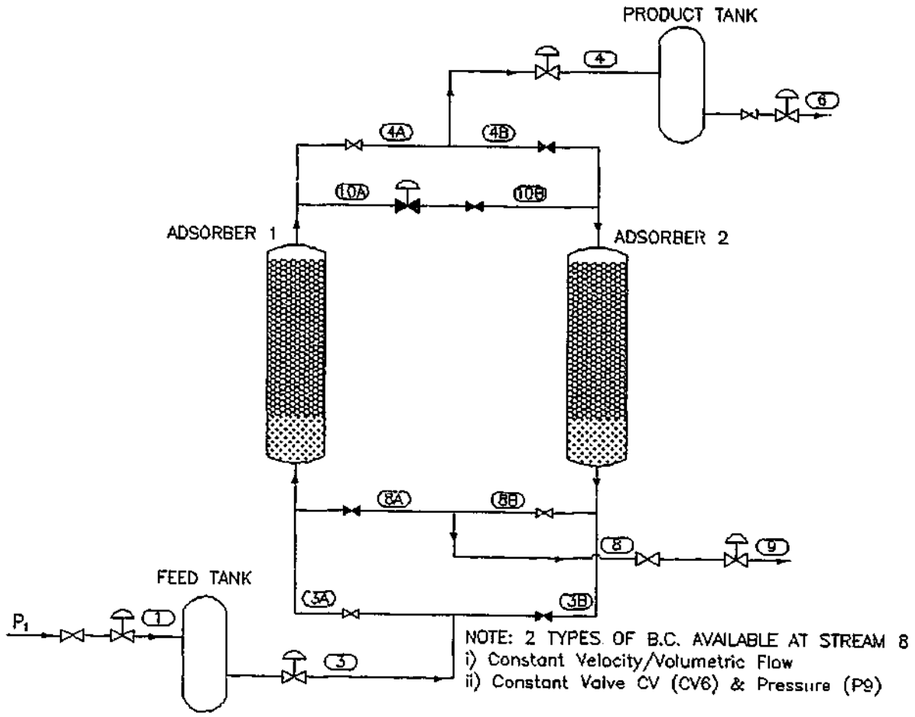

Figure 4.3a. Process flow diagram of the dynamic model - SoCAT.

The following assumptions were made to allow the development of the model –

- Constant feed pressure (P_1).
- Gases obey the ideal gas law.
- Inlet gas stream consists of a binary mixture of nitrogen and oxygen (argon and oxygen was assumed to have similar kinetics and adsorption characteristics and therefore lumped together as a single component).
- Constant gas phase composition (y_{N2}=0.77) prevails in the bed during all steps.
- Isothermal conditions exist throughout the cycle operation (T=299.15K).
- There is negligible ambient heat transfer.
- Near equilibrium conditions exist in the adsorbers due to the relatively long cycle times. Large mass transfer coefficients are consequently employed for the calculation of the adsorption rate.

The assumption of isothermality requires justification and a digression at this point is appropriate. It is well known that the O_2VSA process is highly non-isothermal. Since adsorption is an exothermic process, all bulk gas separation systems will be non-isothermal. While inlet

temperatures are typically near ambient, the heat of adsorption of nitrogen is sufficiently high (together with the large amounts of nitrogen adsorbed and desorbed) for the temperature swing at a point in the bed to exceed 10°C. The large bed diameters ensures essentially adiabatic operation. Large bulk flows up and down the bed convect the heat of adsorption slowly through the bed with a time scale significantly longer than pressure and flow responses. In addition, changes in feed/purge temperature from the boundaries propagate though the bed at even slower time scales. Multilayer beds lead to unusual axial temperature profiles due to regenerative heat exchange and the occurrence of a "cold spot"at the interface between the pre-layer and main layer is common. As a result of these coupled thermal phenomena, there are at least two different time scales inherent in the full response of an O_2 VSA system:

a. "Short" time scale.
   This scale (on the order of a few cycles) is a characteristic of the major portion of pressure and flow responses. As valve positions change, pressure driven flows change and bed and tank pressures change. The short term temperature swing (on a one cycle basis – adsorption and desorption) at some points in the bed will also change rapidly as the mass transfer front moves in the bed. However, valve perturbations will lead to relatively small changes in the position of the mass transfer front and the bulk of the bed will experience unchanged temperature swings on the short time scale.

b. "Long" time scale.
   This scale (of the order of 500 to 800 cycles) is a characteristic of the thermal propagation velocity due purely to convection from the boundary through the bed. The very low thermal velocities are simply a result of the high ratio of bed-to-gas thermal capacity. The convection leads to a change in the axial temperature profile.

The decoupling of these time scales can be accomplished through multiple scale analysis as shown by Wilson and Webley (2002a). It is important to note that even though true thermal cyclic steady state is only accomplished after the long time scale, flows and pressures are at an approximate "cyclic steady state" after the short time scale. Thus, the mass balance is approximately satisfied very soon while the energy balance is only satisfied at the completion of the long time scale. Since the simple lumped model is aimed at addressing flows and pressures (not purity), and the temperature swing changes are modest on this time scale, it is appropriate to use a "constant temperature swing" model for short time scale prediction. As such, a "constant temperature swing" model is defined as an isothermal model in this study.

Due to the assumptions above, it is expected that there will be a mismatch between the model and pilot plant, with the principal error arising from the fixed value for the composition

used in the model (y_{N2} at the end of purge and evacuation steps is assumed equal to 0.77 whereas it is known to be different). The assumption of isothermal conditions will also introduce errors as described above. It is, therefore, expected that the lumped model will be unable to correctly capture the effects of the purge step. In reality, a composition profile exists in the gas leaving the bed providing purge (which can be between 10% to 20% N_2) and entering the bed receiving the purge gas. This difference in composition lowers the partial pressure of N_2 at the top of the bed undergoing purge and causes nitrogen to desorb from the zeolite, adding to the total bed pressure. The lumped model, on the other hand, assumes a fixed gas phase nitrogen composition of 77% independent of the current step and hence does not correctly capture the true effects of the purge. As discussed above, SoCAT is incapable of capturing the effects of any process disturbance on oxygen purity since this requires modelling the composition profile within the bed. However, the oxygen purity can be modelled by an appropriate extension to SoCAT and will be discussed in §4.4.

The model derivation begins by firstly considering material balances around the feed and product tanks (Eqs. (4.3a) and (4.3b) respectively, with reference to Figure 4.3a).

$$\frac{dP_F}{dt} = \frac{1}{V_F}\left(P_1Q_1 - P_3Q_3\right) \tag{4.3a}$$

$$\frac{dP_P}{dt} = \frac{1}{V_P}\left(P_4Q_4 - P_6Q_6\right) \tag{4.3b}$$

where Q_i is the volumetric flow rate of stream i and V_F and V_P are the volumes of the feed and product tank respectively.

A material balance around the adsorber vessels yields two equations which includes the sink/source term due to adsorption/desorption. For convenience, the mass balance for the first adsorbent bed only is shown (Eq. (4.3c)) as a similar relationship exists for the second bed.

$$\frac{dP_{A1}}{dt} = \frac{1}{\varepsilon_b V_{A1}}\left(P_{3A}Q_{3A} - \left(P_{4A}Q_{4A} + P_{8A}Q_{8A} + P_{10A}Q_{10A}\right) - MRT\sum_{i=1}^{2}\frac{dn_i}{dt}\right) \tag{4.3c}$$

The linear driving force, LDF, model [Sircar and Hufton, 2000] is frequently used to model the rate of mass transfer of the adsorbate into the zeolitic sieve. It describes the uptake rate as the product of the mass transfer coefficient, k_i, and the difference in adsorbate loading from equilibrium conditions as given by Eq. (4.3d).

$$\frac{dn_i}{dt} = k_i\left(n_i^{eq} - n_i\right) \tag{4.3d}$$

In this instance, the actual form of the mass transfer relationship is irrelevant since "large" values for k_i are used, hence implying essentially equilibrium conditions. The dual-site Langmuir relationship for the two species, (oxygen and nitrogen) was used to characterise the equilibrium loading, n_i^{eq}.

$$n_i^{eq} = \frac{m_1 b_i Py_i}{1+\sum_{i=1}^{2} b_i Py_i} + \frac{m_2 d_i Py_i}{1+\sum_{i=1}^{2} d_i Py_i} \tag{4.3e}$$

$$\text{where } b_i = b_{o_i} e^{\frac{Q_{1i}}{RT}};\ d_i = d_{o_i} e^{\frac{Q_{2i}}{RT}} \tag{4.3f}$$

While simpler isotherm forms could certainly be used, the above isotherm form and parameters were available for the sieve used in this study and represented very little additional computational burden. Square wave output (representing the on/off valves) boundary conditions are used in order to simulate the various steps in the cycle (refer to Figure 2.2c) as well as fixed valve coefficients (which represent the control valves on the plant). For this cycle, however, a constant volumetric flow rate boundary condition was assumed for stream 8 (due to a constant volumetric flow rate rotary vane pump used in the pilot plant). Calculation of the volumetric flow rates is given by the valve equation as specified by the Fluids Control Institute. For pressure driven flow, the volumetric flow rate, Q (NL/s), is described by

$$Q = 77.01C_v\sqrt{\frac{P_U^{\ 2} - P_D^2}{S_g T}} \qquad P_D \geq 0.53P_U \tag{4.3g}$$

where P_U and P_D is the upstream and downstream pressures of the valve respectively. For conditions experiencing choked flow, Q is represented by

$$Q = 65.31C_v P_U\sqrt{\frac{1}{S_g T}} \qquad P_D < 0.53P_U \tag{4.3h}$$

However, if the upstream pressure is greater than the downstream pressure, a "No Flow" condition is employed. This simulates logic in the experimental plant whereby solenoid valves

are not opened until the downstream pressure is greater than the upstream pressure to avoid backflow.

$$Q = 0 \qquad P_U \leq P_D \qquad (4.3i)$$

The dynamic model consists of eight coupled time-variant ODE's (representing molar flows, tank pressures and adsorbate species uptake) with an additional fifteen ODE's to allow verification of numerical mass balance closure and achievement of cyclic steady state. The set of ODE's are solved in the time domain using LSODA [Petzold, 1983] or DVODE [Brown *et al.*, 1989], stiff/non-stiff, variable time step, first-order, backward difference integrator packages.

4.4 DEVELOPMENT OF AN OXYGEN PURITY MODEL

The simplified process model, SoCAT as discussed in the previous section, can be extended to predict oxygen product purity, which is arguably the most important variable for control [Beh and Webley, 2003d]. The following derivation details a practical yet simple method for the dynamic prediction of oxygen concentration and is implemented in SoCAT without any additional complexity or requiring significant computing resource.

The model derivation begins by performing a component mass balance around the product tank yielding

$$\frac{d(N_p y_p)}{dt} = n_i y_i - n_o y_o \qquad (4.4a)$$

where $N_p y_p$ are the moles of oxygen in the product tank.The unknown variables in Eq. (4.4a) are mole fractions y_i, y_p and y_o. In the case where perfect mixing is assumed in the product tank, the mole fraction of oxygen (y_o) in the stream leaving the tank is equal to the mole fraction in the tank (y_p). The total moles in the product tank, N_p, and the mole rates into and out of the tank, n_i and n_o respectively, are obtained by integration of the total mass balances around the feed, product and adsorber vessels and are performed in SoCAT. Equation (4.4a) is therefore decoupled (i.e. solution of the system mass balances is not influenced by y_p) from the equations describing bulk flows in the system and can be solved independently. To solve (4.4a), knowledge of the inlet oxygen mole fraction, y_i is required. In order to estimate the inlet mole fraction, y_i, it was assumed that while the VSA response may take several cycles, the actual response of the adsorber beds to perturbations is 'instantaneous' (i.e. movement of the adsorbate front occurs in the same cycle that the disturbance is made). The capacity and the flows into and

out of the product tank dampen this response. This assumption is valid because control action is taken on a cycle-based time scale, not on an instantaneous time scale. When a perturbation to the process occurs, there is change to the number of moles produced by the bed undergoing feed. This change in number of moles is accompanied by an increase or decrease in purity according to whether the adsorption front moved through the end of the bed or was retained within the bed. Thus, the "pulse" of product gas produced by the bed will have a new purity (and quantity) produced on the **same cycle that the perturbation was made**. The relationship between average purity and number of moles produced from the bed is therefore the same dynamically and at cyclic steady state. Of course, the product vessel from which the customer supply of oxygen is ultimately taken contains "pulses" of product gas of varying purity from several previous cycles and so does not reach cyclic steady state within the same cycle as the perturbation. It is this lag between the "instantaneous" response of the bed and the accumulated history of previous cycles "stored" in the product tank that equation (4.4a) attempts to represent. The main reason why product vessels are employed in an industrial situation is to dampen the pressure, flow and product concentration swing. Typically, these large installations can have product tanks sized between 4 – 5 times the volume of the adsorber beds and it is this large capacity that permits the suppression of fluctuations.

Figure 4.4a shows the cyclic steady state oxygen purity as a function of number of moles of product produced with a 2nd order polynomial fit through the data points. It shows reasonable correlation (R^2=0.79) although the difference between the model and the experimental values can be up to ±2% in some cases which may cause some errors in the model approximation. Figure 4.4b shows the extrapolation of this model for a larger range of product flows with bounds placed on the empirical fit such that compositions less than and greater than that physically attainable are not permitted (i.e. 21% ≤ y_i ≤ 95%). It should be noted that the maximum obtainable oxygen purity using PSA is 95% as argon shares similar equilibrium adsorption properties to oxygen. Typically, the product concentration is measured downstream of the product tank, as this is the only value of interest to the customer. However, oxygen inlet mole fraction, y_i, that is obtained from Figure 4.4b is an averaged value and hence the instantaneous mole rate and composition is estimated by

$$n_i \approx \bar{n}_i = \frac{N_i}{\tau_c} \qquad (4.4b)$$

$$y_i \approx \bar{y}_i \qquad (4.4c)$$

where τ_c is the total cycle time.

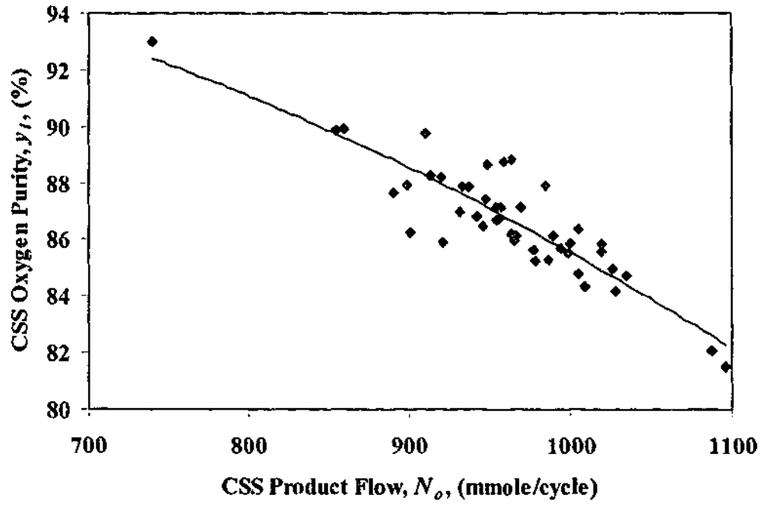

Figure 4.4a. Cyclic steady state relationship between product flow per cycle and oxygen purity. Comparison of the empirical fit to pilot plant data – $R^2 = 0.79$.

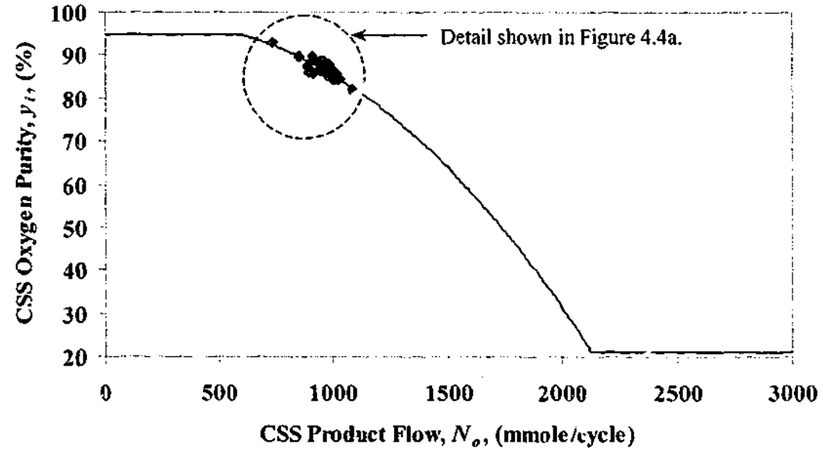

Figure 4.4b. Extrapolation of the empirical fit across the range of flow conditions with bounds on the minimum and maximum allowable values of y_i.

To solve Eq. (4.4a) correctly, a relationship for $n_i y_i$ is required and is approximated by the averaged value as described in Eq. (4.4d).

$$n_i y_i \approx \bar{n}_i \bar{y}_i = \frac{N_i \bar{y}_i}{\tau_c} \tag{4.4d}$$

In reality, the gas entering the product tank is not fed continuously but enters as a non-uniform pulse of fixed period due to the ad/desorption steps required in VSA/PSA processes., Equation (4.4d), therefore, is better represented by Eqs. (4.4e) and (4.4f). These equations account for the steps in which product gas from the adsorbers is either being fed into the product vessel (Eq. (4.4e)) (therefore the average molar flow of the component of interest is calculated), or not being fed (hence the molar flow for the species is zero) (Eq. (4.4e))).

$$\bar{n}_i \bar{y}_i = \frac{N_i \bar{y}_i}{\tau_p} = C \qquad t = t_p \tag{4.4e}$$

$$\bar{n}_i \bar{y}_i = 0 = C \qquad t \neq t_p \tag{4.4f}$$

where C is a constant based on Eqs. (4.4e) and (4.4f), τ_p is the product feed time and t_p is the instantaneous time corresponding to the production step in the cycle. Therefore, over a cycle the assumption of an average $n_i y_i$ holds as

$$\int_0^{\tau_c} n_i y_i dt = \int_0^{\tau_c} C dt = N_i \bar{y}_i \tag{4.4g}$$

It should be noted that the instantaneous mole fraction, y_i, entering the product vessel within the cycle does not correspond to actual/measured values due to the assumption of averaged mole fraction as given by Eq. (4.4h).

$$y_i = f(n_i(t)) \neq \bar{y}_i = g(\bar{n}_i(\tau_c)) \tag{4.4h}$$

From Eqs. (4.4e) and (4.4f), Eq. (4.4a) can be re-written as

$$\frac{V_p}{RT} \frac{d(P_p y_p)}{dt} = C - n_o y_o \tag{4.4i}$$

Assuming that the tank is well-mixed then $y_o = y_p$ and therefore Eq. (4.4i) can be re-arranged to yield

$$\frac{dy_p}{dt} = \frac{\frac{RT}{V_p}\left(C - n_o y_p\right) - y_p \frac{dP_p}{dt}}{P_p} \qquad (4.4j)$$

Equation (4.4j), with application of the assumption for y_i (determined empirically from Figure 1), provides a simple relationship for y_p, which is entirely decoupled from the total mass balance of the adsorber-tank system (to re-iterate the mass balance equations are not dependent on the solution of y_p).

A final note with regards to the implementation of this method, is that once the total mass balances are solved to determine the molar parameters in Eq. (4.4a) (i.e. integrate for N_o), the time integrator must be reset to the initial conditions at the commencement of the cycle. The solution vector from the ODE solver now includes Eq. (4.4j).

4.5 OPEN LOOP RESULTS AND DISCUSSION

The results of the open loop perturbations are organised as follows. Firstly, transient and cyclic steady state profiles are shown for each of the system responses (bed pressure, product tank pressure, product flow, feed flow, evacuation flow, oxygen purity and thermal responses) with a discussion of the results for each of the responses. It is worthwhile noting that the correct time variable to use in all of the following discussion is cycle time and not absolute time. Due to the batch nature of the process, each bed cycles through several steps but product is only provided during the feed step. Hence, it is only of interest to show the bed and product pressure during the feed step during successive cycles. Therefore, from the standpoint of process control, real time must be replaced by cycle time.

4.5.1 Effect of Process Disturbances on Bed and Product Tank Pressure

For purposes of brevity, only the transient and cyclic steady state responses for a step change in feed valve position are shown (refer to Figures 4.5.1a to 4.5.1d) as the system responses for the other perturbations yielded similar results. An increase in the feed valve position directly increased the bed and product tank pressure as depicted in Figures 4.5.1a and 4.5.1c. This was due to additional moles of gas entering the bed and therefore caused an equivalent increase in the amount of adsorbate and the product species (oxygen) available for uptake. This resulted in a rise in the bed pressure and hence an equivalent rise in the product tank pressure. The main observations to note are the fast system response to the valve change (negligible dead time), short time constant (steady state reached within two cycles) and that the response appears to be first-order. The trends exhibited by the pilot plant are captured by the model including the rapid

response, asymptotic closure to steady state and the delta change from the initial conditions (~4.5 kPa and ~3.9 kPa for the pilot plant bed and tank profiles respectively compared with 4.65 kPa and 4.54 kPa for the model). The mismatches observed between the experiment and model was due predominantly to the assumption of constant composition (as discussed previously). This was highlighted during the purge steps (steps 3 and 6) as depicted in Figure 4.5.1b. The model does not correctly capture the increase in bed pressure due to the purge effect as the constant composition profile of the entering purge stream ensures a larger amount adsorbed than what occurs experimentally. Consequently, the bed pressure does not rise as much as that observed experimentally. This variance in the bed pressure profile was manifested in the product tank pressure and resulted in similar mismatches between the plant and model as shown in Figure 8. Although the difference between the model and plant pressure history (Figure 4.5.1b) appeared to be large, it is important to note that the pressure scale was deliberately exaggerated to help highlight the differences. In addition, it should be remembered that the true "long time scale" cyclic steady state had not yet been attained within the 12 cycles shown in Figures 4.5.1a and 4.5.1c. Despite this, the pressures had reached a constant value and, interestingly, retained these values even at true cyclic steady state. Whilst the data depicted in Figures 4.5.1a through to 4.5.1d do not necessarily validate the SoCAT model, they certainly do not substantially conflict with its predictions of response times and magnitude of change.

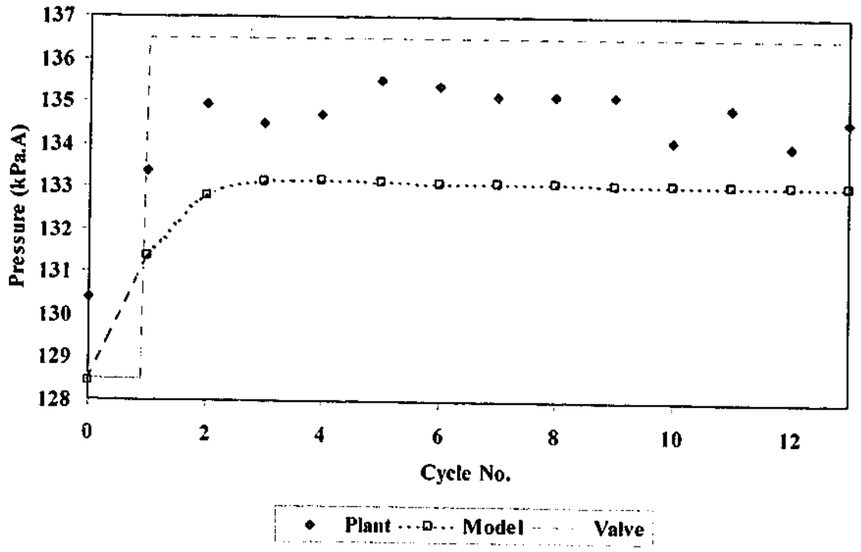

Figure 4.5.1a. Bed 1 pressure history while undergoing feed (step 2) for a step change in the feed valve position – comparison of plant and model. Change in pressure: pilot plant ~4.5 kPa and model 4.65 kPa.

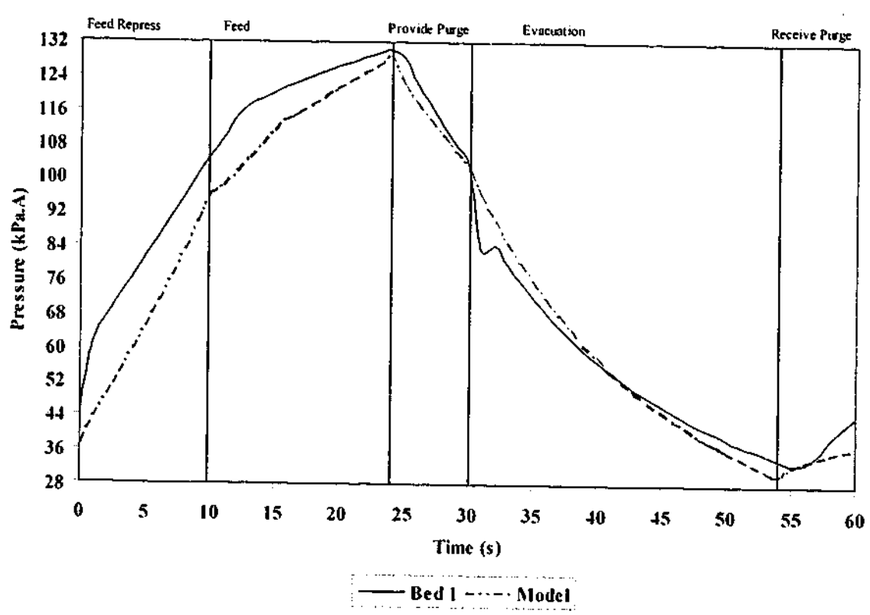

Figure 4.5.1b. Bed 1 CSS pressure history. Comparison of plant and model over a single cycle.

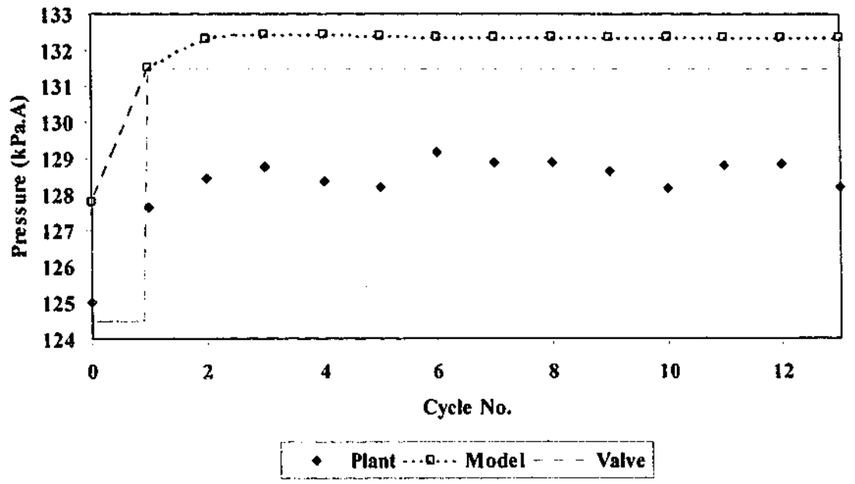

Figure 4.5.1c. Product tank pressure history while undergoing feed from bed 2 (step 5) for a step change in the feed valve position – comparison of plant and model. Change in pressure: pilot plant ~3.9 kPa and model 4.54 kPa.

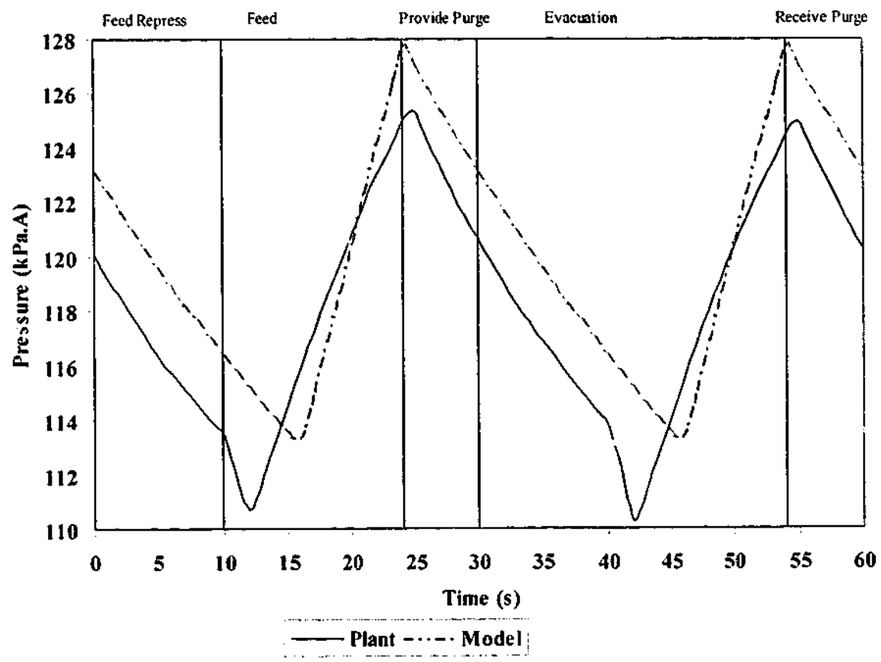

Figure 4.5.1d. Product tank pressure history at CSS over a cycle. Comparison of plant and model.

4.5.2 Effect of Process Disturbances on System Flows

Figures 4.5.2a to 4.5.2f shows the response of process cyclic molar flows (mmole/cycle) to feed and product valve perturbations. The response to purge valve and load variation are not shown for the sake of brevity but the steady-state gains for these open loop tests are included in Table 4.5.2a. An analysis of the response curves represented by Figures 4.5.2a to 4.5.2f revealed that the system response to the changes was rapid, with negligible dead time and very short time constants ("short time scale" steady state was attained within five to ten cycles in all cases). This is consistent with the pressure variations discussed previously. These time-variant trends are correctly reproduced by the model (note: the model had not been fitted to the dynamic data) along with the magnitude of the changes between initial baseline conditions and the final steady state as shown in Table 4.5.2a. Once again, while this is not sufficient to validate the model, it does suggest that an equilibrium model can adequately describe a major portion of the VSA (flow and pressure) response with flow to and from the adsorber tanks. There was no need to invoke complex mass transfer arguments to explain the bulk of the pressure and flow response (direction and magnitude) to changes in process variables.

The mass balance error, which is the difference between in-flow and out-flows as a percentage of in flow, is shown for the case of the feed valve change in Figure 4.5.2g. Once again, this illustrates the ability of the model in simulating bulk flow conditions (mass balance error is of similar magnitude for both model and experiment) and shows that steady state was attained within seven cycles in the pilot plant and within four cycles in the model. The mismatch in the molar feed flow value for all cases with the exception of the feed valve perturbation condition, was caused by the presence of a pressure regulation valve fitted between the control valve and the feed tank (refer to Figure 2.1a) in the pilot plant. This feature was not modelled in the process simulator (refer to Figure 4.3a). Since the feed tank was at a much higher pressure than the adsorbent beds, choked flow conditions occurred in the process model, which resulted in a constant volumetric flow rate and subsequent molar rate as described by Eq. (4.3h). On the other hand, the pressure regulator fitted on the pilot plant decreased the feed tank pressure as experienced by the adsorbent beds and pressure-driven flow resulted as described by Eq. (4.3g). The final point to note is that the response of the product stream flow to closure of the product valve and changes in load are very similar (not shown here). This is useful from a control perspective as it means that a product load disturbance can be simulated in the field by adjustment of the product valve alone. This is much easier to do in practice than the application of an actual load disturbance. This result was expected.

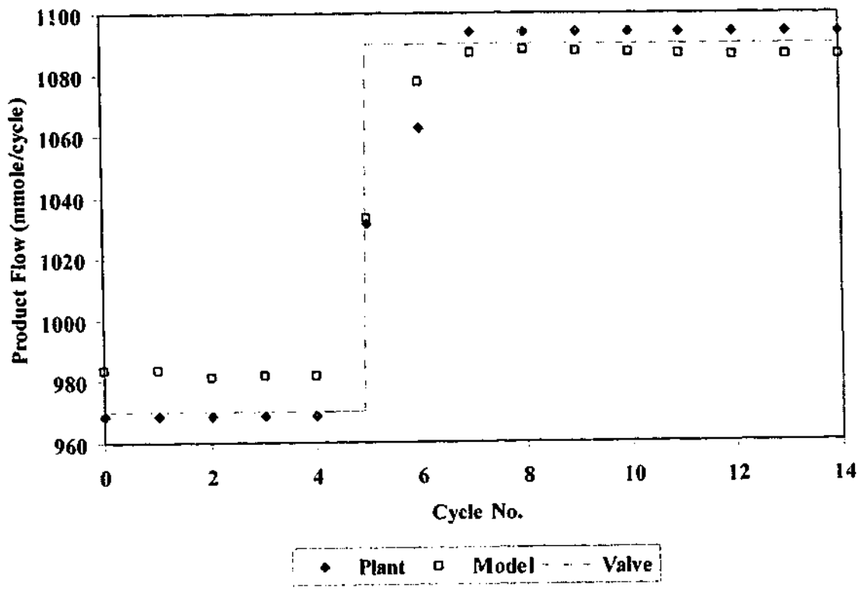

Figure 4.5.2a. Change in product moles per cycle due to a 5% increase in feed valve position – pilot plant 125 mmole/cycle and model 102 mmole/cycle.

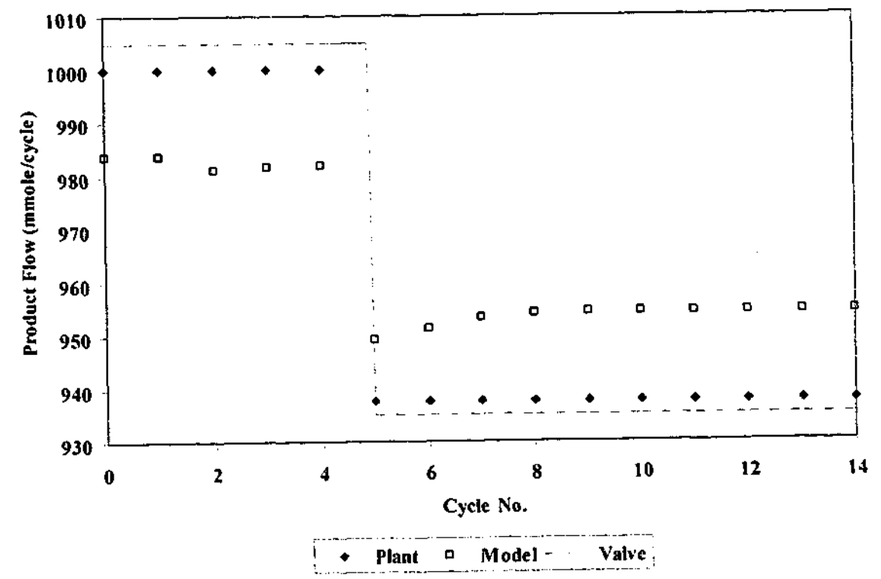

Figure 4.5.2b. Change in product moles per cycle due to a 10% decrease in product valve position – pilot plant 63 mmole/cycle and model 30 mmole/cycle.

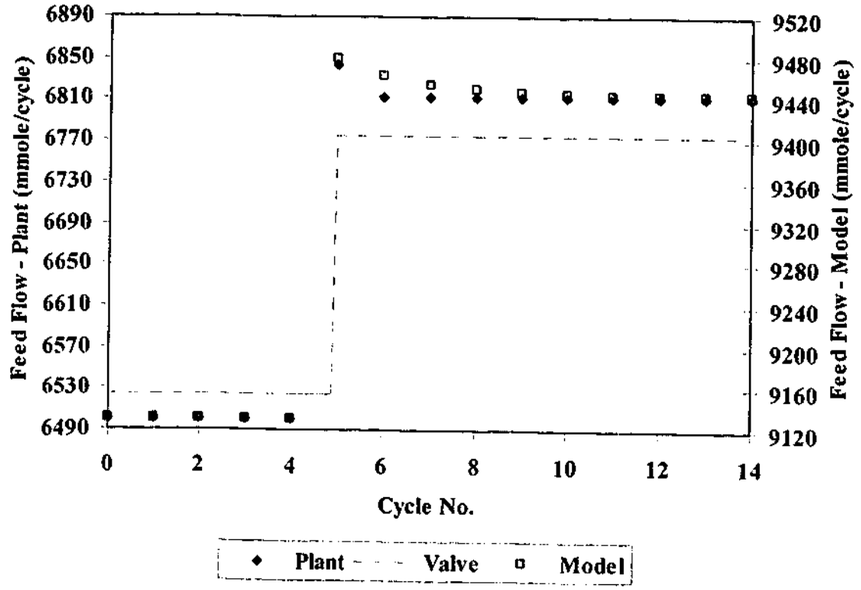

Figure 4.5.2c. Change in feed moles per cycle due to a 5% increase in feed valve position – pilot plant 313 mmole/cycle and model 313 mmole/cycle.

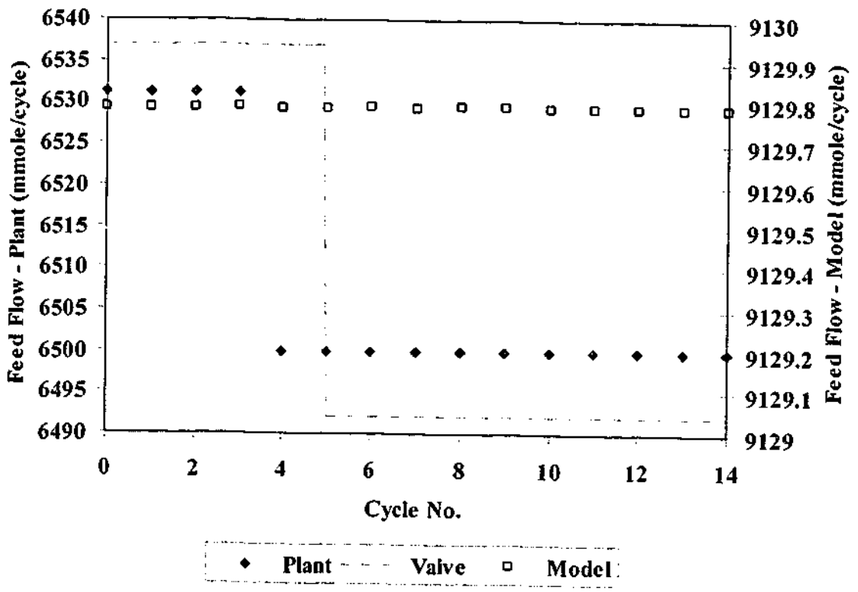

Figure 4.5.2d. Change in feed moles per cycle due to a 10% decrease in product valve position – pilot plant 31 mmole/cycle and model 0 mmole/cycle.

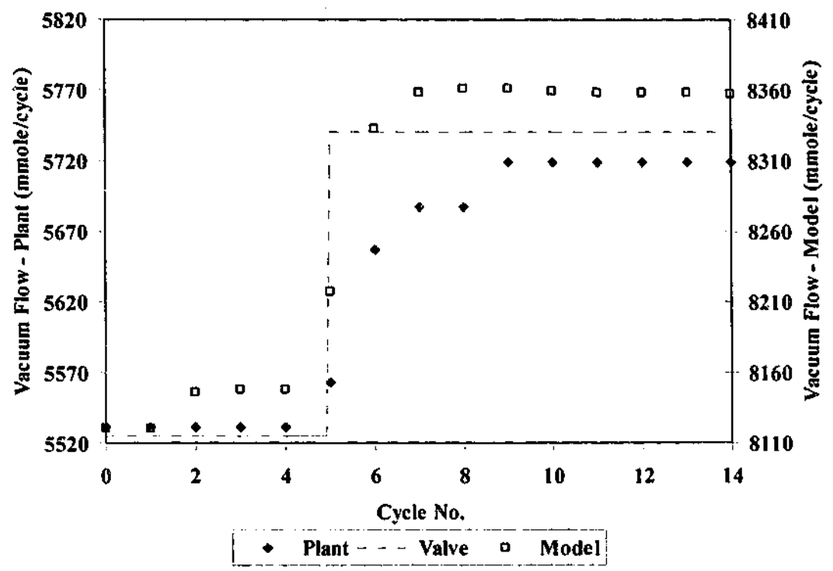

Figure 4.5.2e. Change in evacuation moles per cycle due to a 5% increase in feed valve position – pilot plant 188 mmole/cycle and model 237 mmole/cycle.

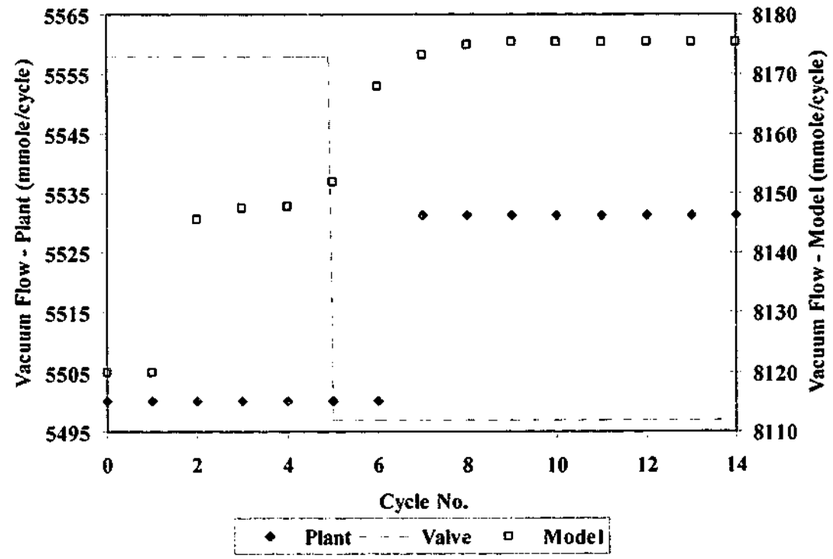

Figure 4.5.2f. Change in evacuation moles per cycle due to a 10% decrease in product valve position – pilot plant 31 mmole/cycle and model 56 mmole/cycle.

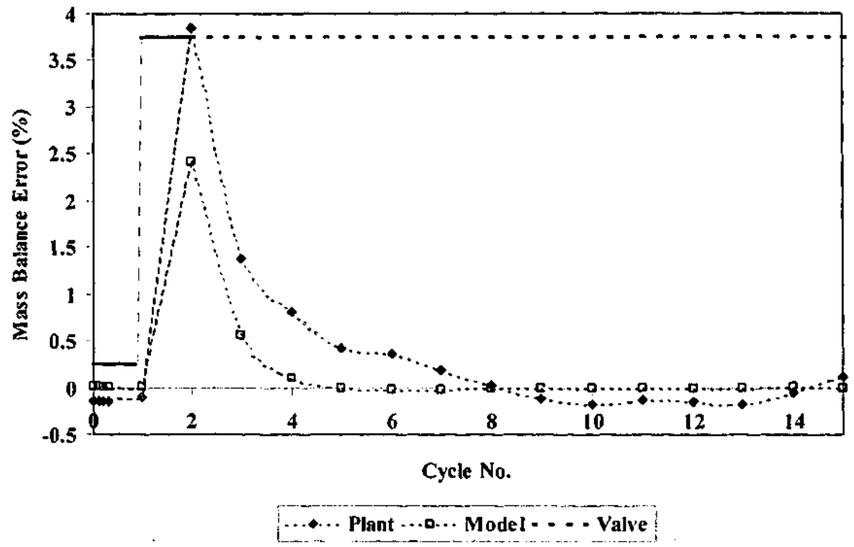

Figure 4.5.2g. Change in the system mass balance due to a 5% step in the feed valve position – comparison of pilot plant versus model. Pilot plant cyclic steady state attained in 7 cycles. Model cyclic steady state attained in 4 cycles.

Table 4.5.2a. Effect of disturbances on VSA system CSS flows. Comparison of experiment and model.

		Feed Flow mmole/cycle	Product Flow mmole/cycle	Evacuation Flow mmole/cycle	Mass Balance Error %
Baseline	Plant	6601.8	960.81	5577.29	0.97
	Model	9129.79	981.92	8147.87	-6.45E-05
Feed Valve, 5% Increase	Plant	+ 313	+ 125	+ 188	0.56
	Model	+ 313	+ 102	+ 237	-4.34E-04
Purge Valve, 3% Increase	Plant	- 125	+ 31	- 125	1.1
	Model	0	+ 35	- 35	-2.72E-04
Product Valve, 10% Decrease	Plant	- 31	- 63	+ 31	0.43
	Model	0	- 30	+ 56	-2.96E-04
5kPa Product Load Disturbance	Plant	- 31	- 63	+ 63	0.43
	Model	0	- 70	+ 70	-1.07E-04

4.5.3 Effect of Process Disturbances on Oxgen Purity

Product concentration (%O_2) is arguably the most important variable from a customer's perspective and subsequently demands tight control tolerances (typically ±1% to 2% of set point). Figures 4.5.3a to 4.5.3d represent system responses to the four scenarios. Unlike the pressure and flow responses shown previously, oxygen purity has a measurable delayed reaction to the change (dead times between one to three cycles) and a significantly slower return to cyclic steady state (time constants of around four to six cycles). The concentration of oxygen in the product gas leaving a bed was governed by the extent with which the mass transfer front was allowed to breakthrough. In the experiments, a baseline of 85% oxygen purity was used indicating that some breakthrough of the mass transfer front had been permitted. Since the mass transfer front was relatively sharp (10 to 20cm as indicated from detailed simulations), any shift in the position of the mass transfer front will produce a "pulse" of product gas with slightly different composition from 85%. The flow rate in the bed and the adsorptive capacitance of the bed dictate the position of the mass transfer front. Hence, any perturbations that affect flow and pressure would influence the position of the mass transfer front and consequently affect oxygen purity.

As seen from the earlier response studies, the flows from the beds and the bed pressures respond quickly, (within three to five cycles), to perturbations in valve positions and hence equally rapid changes in oxygen purity would be expected. If the oxygen purity immediately downstream of the beds (and upstream of the product tank) is measured, such rapid responses are indeed seen. It should be recalled, however, that the oxygen product flows into a large product tank and the oxygen purity reported here (and of interest to the customer) was measured ***downstream*** of the product tank. The oxygen response was therefore strongly influenced by the mixing patterns in the product tank. In the case of the oxygen VSA pilot plant, flow into the 60 litre product tank was fed by half inch tubing running perpendicular to the vessel wall located near the top of the tank whilst the exit stream was located near the bottom of the vessel and also runs perpendicular via a half inch tube. No baffling or internal mixing was used in the tank. On average, for the set of experiments conducted, approximately 20 litres of product gas entered and exited the tank per cycle at CSS. If the conditions were dominated by pure plug flow, then a step change in the exit product valve position would result in a stepwise change in flow after a delayed period (dead time of around three cycles in this case ≡ volume of product vessel/volume of gas exiting the vessel per cycle). On the other hand, if conditions within the product vessel were well-mixed then the measured exit composition would follow an asymptotic relationship with the time constant of the response being a function of the capacity of the tank.

As the results show, however, a condition somewhere in between plug flow and well-mixed existed. This condition was not constant but was a function of the flow dynamics and depended on the magnitude and type of perturbations as characterised by the different measured time

delays (refer to Table 4.5.3a). For completeness, the full response time (time to reach 100% of value) of the paramagnetic analyser and connecting tubing was measured and found to be about 25 to 30 seconds for a step change in composition at constant flow. As the response of the analyser was much less than the period of the cycle studied (total cycle time was 60 seconds), this further demonstrated that the observed delay was attributed to poor mixing in the tank. By varying the size of the product vessel and altering the flow configurations, the system responses can therefore be sharpened or dampened. It is important to note that the distributed nature of the packed-bed adsorber system was separated from that of the tank through the definition of time as cycle time, not absolute time. Essentially, the adsorbent beds provided pulses of gas into the tank at a particular composition over the cycle and hence the time-variant dynamics of the solute as a function of axial position in the bed can be ignored when considering the product tank.

There are also second-order effects that influence the oxygen response. As shown later, the bed temperature profile is changed by the perturbations – rapid changes in the position of the mass transfer front will generate rapid changes in the temperature swing at particular points in the bed which in turn will subtly change the convective flows through the bed leading to overall re-adjustment of the bed profiles. These temperature shifts change the adsorptive capacity of the sieve leading to pressure and flow changes and eventually alters the oxygen purity. However, readjustment of the thermal profiles was very slow (hundreds of cycles) and consequently their influence was not sufficiently significant to contribute to the bulk of the oxygen response. An additional second order affect is the coupling of the beds. In step 3 (Figure 2.2c), the purge gas leaving the bed providing purge has a trailing composition relatively high in nitrogen (low in oxygen) as the mass transfer front moves through. This "tail" enters the bed receiving gas and resides at the product end of that bed. Thus, on the subsequent feed step, this "tail" will exit first and enter the product tank followed by high purity oxygen and later the portion of the mass transfer zone. One half cycle later, the reverse occurs – the bed providing purge now receives purge and vice versa. This coupling of the beds and "exchange" of impure oxygen gas acts to further delay the overall response.

Typically, simulations (such as the MINSA adsorption simulator [Todd *et al.*, 2001b] and SoCAT) assume perfect mixing in vessels such that the exit composition is equivalent to that within the tank. However, non-idealities such as non-uniform mixing and various process delays should be accounted for to ensure that dynamic information is not lost as this will affect the field performance of control algorithms, which are usually implemented and tuned offline. If such large unit operations were operated under less than ideal flow configurations then dead time would dominate the response causing unnecessary difficulties in the design and tuning of various control algorithms (both model-based and PID). The presence of time delay in a process

causes a reduction from the theoretical maximum controller gain (i.e. a system with no dead time) and may consequently result in sluggish controller performance.

As discussed earlier, the SoCAT model has been extended through the use of an empirical relationship between CSS flow and purity to model the oxygen response (refer to §4.4). This model, with assistance from MINSA [Todd *et al.*, 2001b] will be used to quantitatively explain the observed trends whilst a simple and purely empirical model is utilised for future controller design. It is the objective of this section to demonstrate the usefulness of both the extended SoCAT model and a first-order model with dead time (FODT) in capturing the step response data. Although both methods can be utilised in a model predictive structure, the FODT is the simplest to implement (dead time can be incorporated relatively easily) and is also the least computationally intensive. The first-order with dead time model, as described by Eq. (4.5.3a), was solved in terms of deviation variables ($O \equiv$ change in product oxygen concentration and $V \equiv$ change in valve position) producing the analytical solution, Eq. (4.5.3b).

$$\frac{dO(t)}{dt} + \frac{1}{\tau_p} O(t) = \frac{K_p}{\tau_p} V(t - \tau_D) \tag{4.5.3a}$$

$$O(t) = K_p V(t - \tau_D)\left(1 - e^{\frac{-t}{\tau_p}}\right) \tag{4.5.3b}$$

where K_p is the process gain, τ_p the process time constant, τ_D the system time delay and t in this case has the time units of cycle number (i.e. $t \in$ N, where N = 0, 1, 2, 3, ...).

The SoCAT model was calibrated to a single "baseline", experimental set and perturbations made about this point. The FODT model, on the other hand, was calibrated to four experimental data sets, each of which represents the four disturbances studied. Each FODT model was then perturbed about the empirically fitted value. The performance of the FODT model is summarised in Table 4.5.3a and the performance of the SoCAT model is shown in Figures 4.5.3a to 4.5.3d. The integral absolute error, IAE, was used as a measure of performance of the first-order model in comparison with plant data and is described by Eq. (4.5.3c).

$$IAE = \int_0^T |y_a - y_m| dt \tag{4.5.3c}$$

Table 4.5.3a. 1st order with dead time model parameters and performance.

		K_p (%O_2/%Valve Open)	τ_p (cycles)	τ_D (cycles)	IAE (%O_2)
Feed Valve	5% increase from baseline†	-0.765	5	2	3.16
	5% decrease back to baseline				3.45
	3% decrease back to baseline				9.55
Purge Valve	3% increase from baseline†	-0.3167	4	1	2.80
	3% decrease back to baseline				3.05
	5% decrease back to baseline				11.82
Product Valve	10% decrease from baseline†	-0.2925	6	3	2.29
	10% increase back to baseline				3.66
	7% increase from baseline				6.92
Product Load Disturbance		0.69 %O_2/kPa Load	6	3	2.16

† Used for FODT fit.

The FODT model describes the oxygen response characteristics observed in field operation well (see Figures 4.5.3a to 4.5.3d) even though the product tank was of a higher order due to the occurrence of non-ideal mixing. Failure of the FODT model in capturing the responses that are clearly measured after the initiation of the step change are highlighted in Figures 4.5.3a to 4.5.3d (the FODT model shows sharp changes in the process variable initially after the time delay whereas the plant exhibits smoother transitions). Better representation may be achieved using higher order approximations such as N^{th} order models or a series of interacting first-order lags (each with different time constants). However, the satisfactorily low IAE and the observed approximation of the FODT model was sufficient to justify its use over more computationally expensive higher order methods. Furthermore, due to process/model mismatch, additional fine-tuning of the controller parameters is required once implemented in the field. The main use of the FODT model should be to enable the determination of approximate gains that seek to minimise the IAE.

The SoCAT empirical oxygen purity model yields reasonable results, capturing the qualitative effects of the step change and the observed trends. Figures 4.5.3a to 4.5.3d indicate

that the SoCAT model, however, does not correctly simulate the absolute average purity value. This process/model mismatch is in part due to the accuracy of the initial calibration of the SoCAT model. For instance, Table 4.5.2a shows that there is a discrepancy of 20 mmole/cycle between experimental data and model which amounts to approximately 0.60% difference in the absolute value between plant and model. In addition to the problems associated with the initial model calibration, incorrect estimations of the change in magnitude of the boundary conditions (e.g. valve flow coefficients or product backpressure) accounts, in part, for some of the mismatch. Referring once again to Table 4.5.2a, a difference of up to 33 mmole/cycle for a step change between the change in product flow predicted by the model in comparison with the plant was observed. By assuming a linear relationship over time (i.e. on a per cycle basis), 33 mmole/cycle corresponds to a 1.0% difference in the predicted purity. Another cause of discrepancy between the model and plant data was the reliability of the experimental data, which showed some scatter of approximately 2% at the same product flow (refer to Figure 4.4a). Consequently, the empirical fit obtained may result in similar differences when compared to the pilot plant. What is encouraging though, as signified in Figures 4.5.3a to 4.5.3d, was the ability of the model to correctly predict trends in the transient responses. These differences in the estimation of the absolute value of the composition variable are sufficiently small such that the application of this technique in the field for process monitoring or control would yield useable results as the oxygen purity is commonly permitted to drift within 1% to 2% of set point. It is cautioned, however, that for faster cycles such as rapid PSA, the assumption of 'instantaneous' product concentration leaving the adsorber vessels may no longer hold.

As discussed previously, the simplified purity model assumes ideal mixing conditions within the adsorber vessel and therefore any disturbances will manifest themselves instantaneously with some damping. In order to attain a match with the plant, the model output was delayed between one and three cycles as shown in Figures 4.5.3a to 4.5.3d. The principal error, as is in case of the FODT model, was due to the poor mixing characteristics that occur within the product tank. The difficulty in delaying the model output is that the system dead time, which is a function of both the volume of flow into and out of the product tank and of the flow profiles within the tank itself, is not constant as shown in Table 4.5.3a but varies.

In process engineering, tracer experiments are often used to characterise the transport capability of reactor vessels usually assuming steady state relationships [Fogler, pp. 759-795, 1992]. However, these general methods are difficult to apply to the unsteady state oxygen VSA process because it is these transient, instantaneous flows that alters the composition profile in the product vessel. In order to estimate the extent of mixing or to establish models for mixing, the time-variant pressure profile of the tank, the flows in (which are a series of non-uniform pulses) and out would have to be physically simulated all the while ensuring that the tracer is non-intrusively introduced. Various permutations of the flow and pressure regimes would have

to be tested to eventually obtain a dynamic model of mixing. Work into the development of simple mixing models for PSA/VSA systems might be useful for the initial 'grass roots' design and costing of industrial installations.

This inability to characterise the mixing profile in the product tank can lead to severe controllability problems. The typical industrial convention is to use multiple PID loops to control variables such as purity, flow and pressure [Beh *et al.*, 2000]. Once the controller pairings have been made and decouplers are applied, controller tuning becomes the principal control problem. In the case of PID controllers there are two main tuning methodologies – open loop step responses and frequency perturbations (open or closed loop) [Åström and Hägglund, 1995]. For each of the methods mentioned, there exist numerous algorithms in which to establish estimates of the controller settings [Åström and Hägglund, 1995]. However, most of these methods assume that the system can be identified by an empirical fit through an 'experimental' data set (which can be gathered from either the field or model data) or by direct synthesis of the model and controller to obtain appropriate gains [Chen and Seborg, 2002a]. If model parameters such as the system lag, gains or time delays varied with time (due to material deterioration or fouling for example) then the calculated controller gains would no longer be valid for the system. This may result in major robustness problems and controllability issues. Various methods have been developed in the past that involve the auto-tuning of controller settings or gain scheduling to help overcome some of these difficulties [Åström and Hägglund, 1995]. However, as shown above in the case of oxygen VSA, it makes no sense in incorporating a gain schedule for example that updates the controller settings as a function of the flow and disturbance regime. Other issues such as the controller 'kick' arise, which may result in deficiencies in control.

In the case of oxygen enrichment, the primary variable of importance to the customer is the product concentration with the majority of commodity gas users being large industrial installations processing up to 5 to 20 metric tonnes of contained oxygen per day at 93% to 95% purity [Parkinson *et al.*, 1999]. Hence, product vessel capacities range from several hundred to thousands of cubic meters for these large users. In these cases, the inlet and outlet flow arrangements and possibly the internals should be designed such that uniform composition occurs throughout the tank and concentration gradients are avoided. This can be achieved by the appropriate layout of piping, design of baffling and mixing points to minimise non-idealities. It is envisaged that the additional outlay in cost spent designing well-mixed product vessels would quickly pay itself back with reduced rework, fewer control problems and a generally satisfied customer.

Finally, it is important to note that feed, purge and product valves all affect the oxygen purity with different process dynamics. Using these valves to control other variables (such as product

flow and pressure), therefore would lead to strong coupling between the control loops – the extent of this coupling is investigated in §4.6and §4.7 of this chapter.

The individual responses shown in Figures 4.5.3a to 4.5.3d will now be discussed. The decrease in oxygen purity following an increase in feed (Figure 4.5.3a) and purge (Figure 4.5.3b) valve positions was due to differing causes. In the event of an increase in the feed valve position, an increase in moles of gas entering the bed caused movement of the adsorption front further towards the product end of the bed. This shift in the position of the front caused more moles of nitrogen to leave the bed as product and to enter the bed undergoing purge, adding further to the moles of nitrogen ready to be released as product during the feed step of the second bed. Figure 4.5.3a shows the product purity dropping from an initial value of 85% and asymptotically converging to a steady value of around 81%, 20 cycles after the valve perturbation was made. However, in the case where the purge valve increased, movement of the front during the purge step allowed nitrogen to contaminate the top of the bed receiving purge as discussed earlier. The convergence of this condition was faster (15 cycles) with a slight decrease in purity (87.2% to 86.2% in Figure 4.5.3b).

It should be noted that the purge step is implemented in a cycle to allow maintenance of product purity by essentially "cleaning" the top of the bed receiving the purge stream. The change of 3% in this case therefore is significantly large for this region of operation and so smaller variations in the purge stream would yield higher product concentrations. Furthermore, it is clear, for the region of operation, that an increase in product moles per cycle would result in a decrease in oxygen purity (refer Table 4.5.3a). The product mole rate is a fast-acting variable while the oxygen purity is slow due to the capacity of the product tank and therefore feedforward action can be utilised to ensure product purity is within tolerance. However, the use of product flow alone as a feedforward process variable may not be sufficient to determine the effect on purity. For example, if the cycle was operated under disparate conditions (i.e. use of different adsorbents, different process conditions, differing bed height, etc) whereby the adsorption front was held further into the bed (as the case for a high purity scenario), the removal of more product gas may not necessarily affect the product concentration. It is therefore theorised that measurements of the product flow as well as another variable that yields information on the position of the adsorption front is sufficient to determine whether the product concentration would rise or fall.

The last point to note is that reduction of the product valve or reduction of product load causes increased product purity with similar characteristic responses (compare Figure 4.5.3c with Figure 4.5.3d). An opposite effect from the feed valve change occurs whereby the adsorption front is pushed further back into the bed hence providing a greater region for product oxygen in the bed.

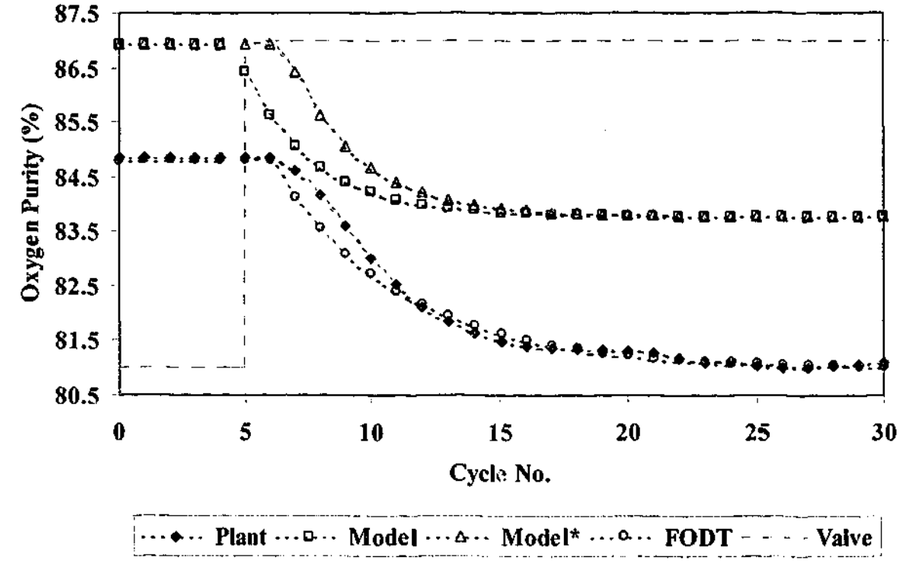

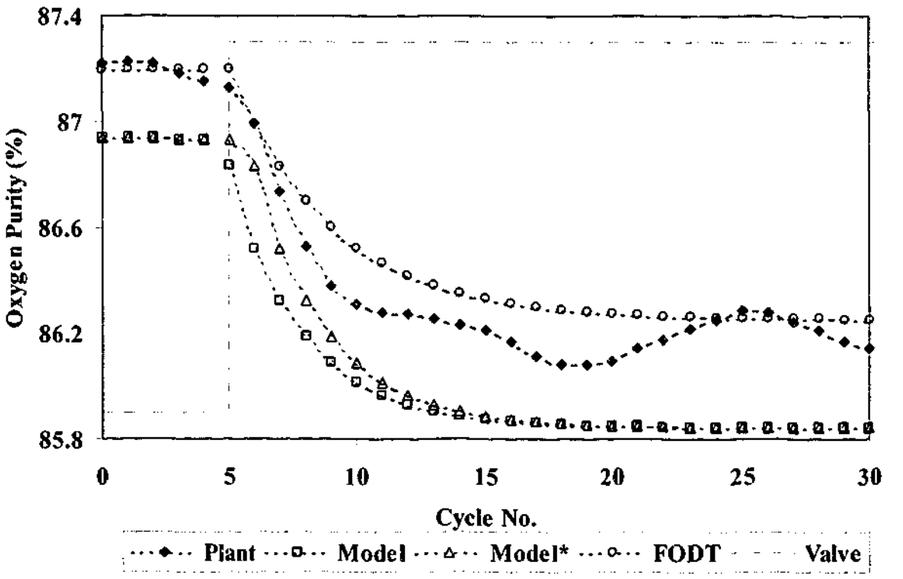

Figure 4.5.3. **(a) The response of the cycle averaged oxygen purity to a 10% step change in feed valve position. (b)The response of the cycle averaged oxygen purity to a 3% step change in purge valve position. Triangle and circle data points shows SoCAT and FODT output delayed by two cycles (a) and one cycle (b) respectively. Step change initiated at cycle 5. Squares shows model response with no delay.**

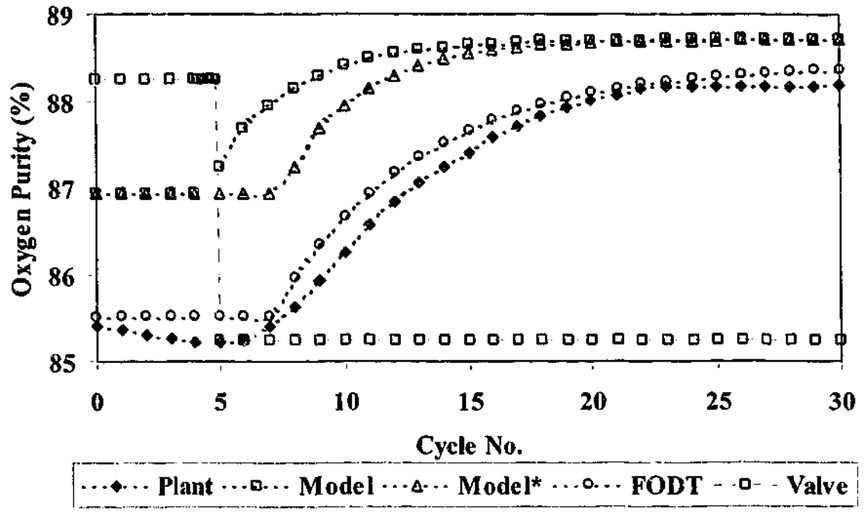

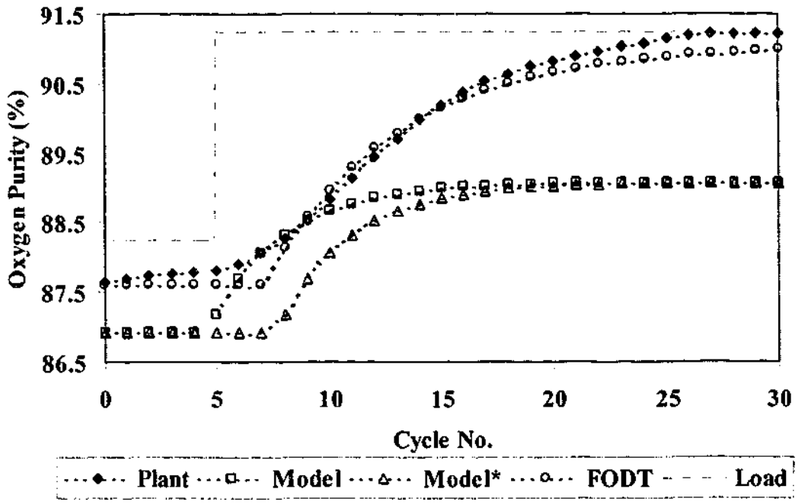

Figure 4.5.3. **(c) The response of the cycle averaged oxygen purity to a 10% step change in product valve position. (d) The response of the cycle averaged oxygen to a 5 kPa product load disturbance. Triangle and circle data points shows SoCAT and FODT output delayed by three cycles for both (c) and (d). Step change initiated at cycle 5. Squares shows model response with no delay.**

4.5.4 Effect of Process Disturbances on Production Rate

The production rate variable is a derived quantity that is defined in terms of the product concentration and cyclic molar flow. The units used for large industrial VSA plants are tonnes per day of contained oxygen (TPDc) but will be re-defined in this study as kilograms per day of contained oxygen (kgPDc) because of much reduced capacity of the pilot plant as revealed in Eq. (4.5.4a).

$$PR = \frac{0.0864 M_{O_2}}{\tau_c} \left(\int_t^{t+\tau} n_p y_{O_2} dt \right) \qquad (4.5.4a)$$

where M_{O2} is the molar mass of oxygen (taken to be 31.999 kg/kmole), τ_c is the cycle time, y_{O2} is the mole fraction of oxygen in the product and n_p is the instantaneous molar product flow rate.

The responses to the three case studies reveals that the oxygen production rate variable changes within the same cycle of the perturbation. This bears some similarity to the graphs showing the product flows per cycle where an instantaneous response is observed. However, unlike the product flow variable, the production rate exhibited more complicated behaviour as illustrated in Figure 4.5.4c where an inverse response to the change was observed or a damped oscillatory behaviour as shown in Figures 4.5.4a and 4.5.4b. The response to the product load disturbance of Case 4 is not shown in this section as previous discussion (refer to §4.5.2 and §4.5.3) have demonstrated that a step change in the product valve produced equivalent response. The complexity of the production rate variable can be simply explained by examining Eq. (4.5.4a), which shows that the production rate is a function of both the product flows per cycle and the average product concentration over the cycle. As discussed in the previous section, a first-order model yields reasonable correlation to the dynamics of the product purity variable and this first-order approximation can also be utilised to model the product flow per cycle (using small values for the model time constant). In essence the production rate variable may be modelled with either two first-order systems representing oxygen purity and product flow or a second-order system with a primary and secondary time constant – a second-order with dead time model (SODT). The failure of a FODT model in capturing the process dynamics and the correct response shown by the SODT model provided additional proof that the response was not first-order as shown in the three figures below. The dominant variable, as observed in Figures 4.5.4a to 4.5.4c, was the system product flow per cycle, which was due to the relative magnitudes of the changes in y_{O2} and n_p (a 100 mmole/cycle change in product flow may result in a 4% change in product purity). The influence of the product flow per cycle was further reflected in the speed of response of the production rate (no time delay was observed).

The advantages of using a reduced-parameter model such as SoCAT along with the empirical purity model, is highlighted in Figures 4.5.4a to 4.5.4c, which shows satisfactory correlation between process and model especially in the initial regions of the response where a second-order or inverse response was observed. This is significant from the plant and control engineer's perspective as the oxygen production rate is a variable of importance to the customer. The errors associated with the simplified SoCAT model can be attributed predominantly to inaccuracies in estimating the relationship between the oxygen concentration as a function of flow and the inaccuracies involved with the calibration of the product purity and flow to baseline conditions as discussed in the previous section. The time delays associated with mixing in the product tank, which is not modelled in SoCAT, caused minor problems with process/model mismatch. Finally, the oscillations observed at steady state in the pilot plant are attributed to errors in the product flow sensor.

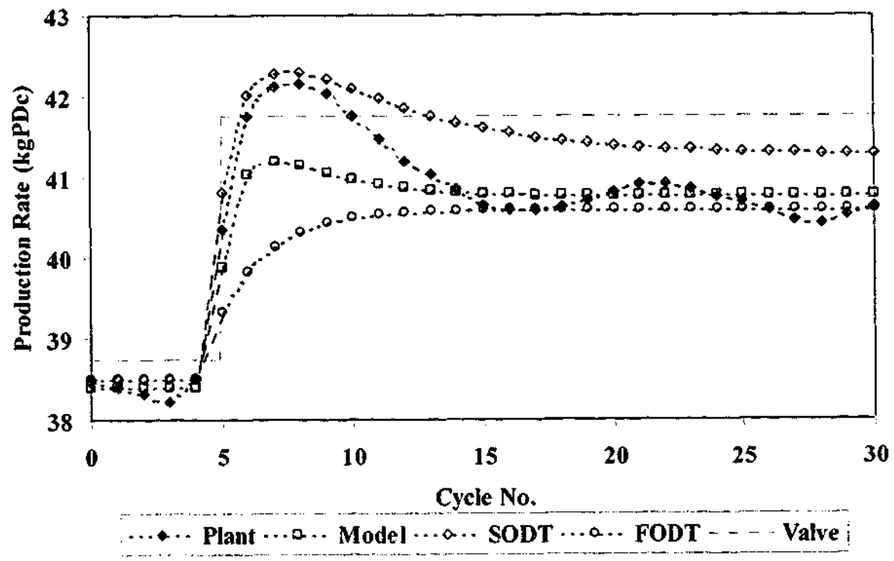

Figure 4.5.4a. Production rate response to a 5% increase in the feed valve.

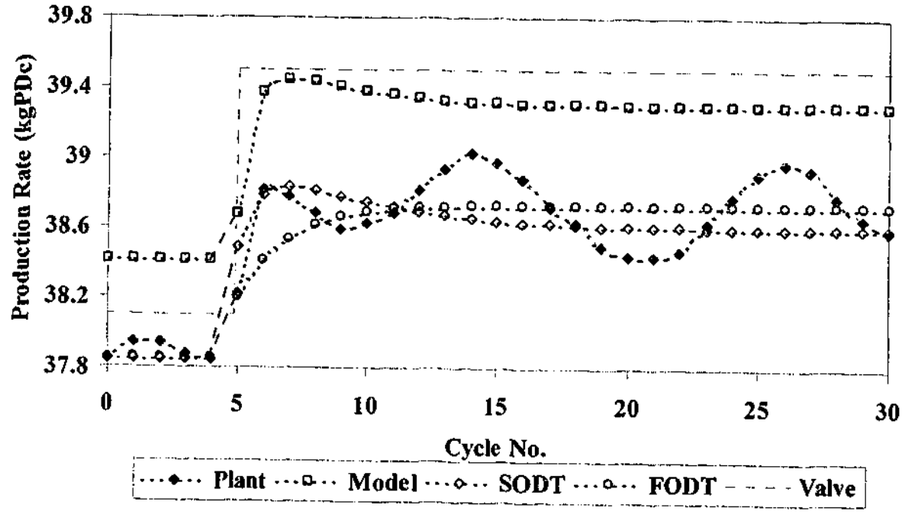

Figure 4.5.4b. Production rate response to a 3% increase in the purge valve.

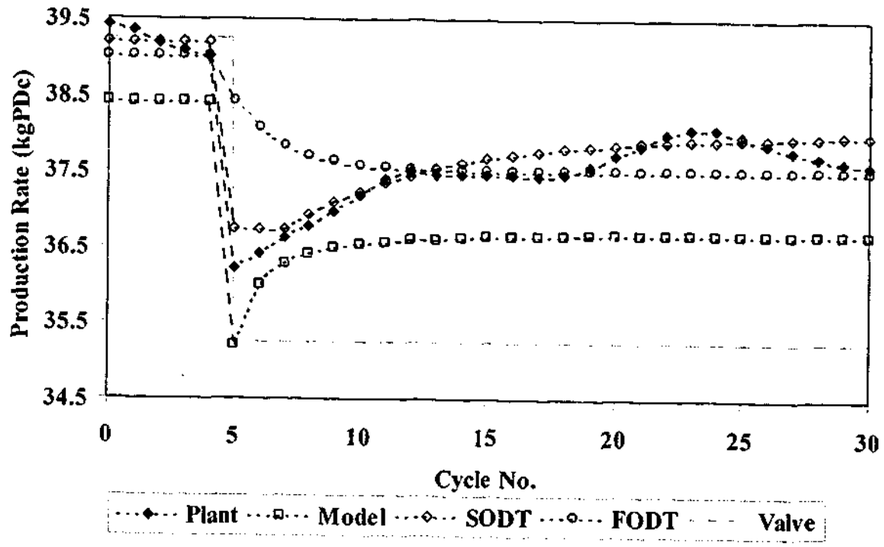

Figure 4.5.4c. Production rate response to a 10% decrease in the product valve.

4.5.5 Effect of Process Disturbances on Thermal Evolution

While the thermal evolution and response of the beds to process disturbances is of no direct interest to the customer, they are an important source of diagnostic information and offer potential for control. The temperature profile in the bed at the end of each step in the cycle for the baseline condition (before perturbations) is shown in Figure 4.5.5a. The cold spot at the interface between the layers was clearly observed (at 0.3m) – the causes of this cold spot have been extensively discussed [Wilson and Webley, 2002b]. The temperature swing between feed and evacuation was 4 to 6°C in the main section of the bed (0.4 to 1.2m) and only 1 to 1.5°C at the top of the bed. This was expected since the oxygen rich gas was kept at the product end of the bed and little adsorption/desorption occurs here. Upon receiving perturbations in valve positions, the bed flows and pressures change and as a result, the temperature profiles change. The final cyclic steady state temperature profile was established in such a way that the overall energy balance was satisfied at each point in the bed for the boundary conditions at each end of the bed.

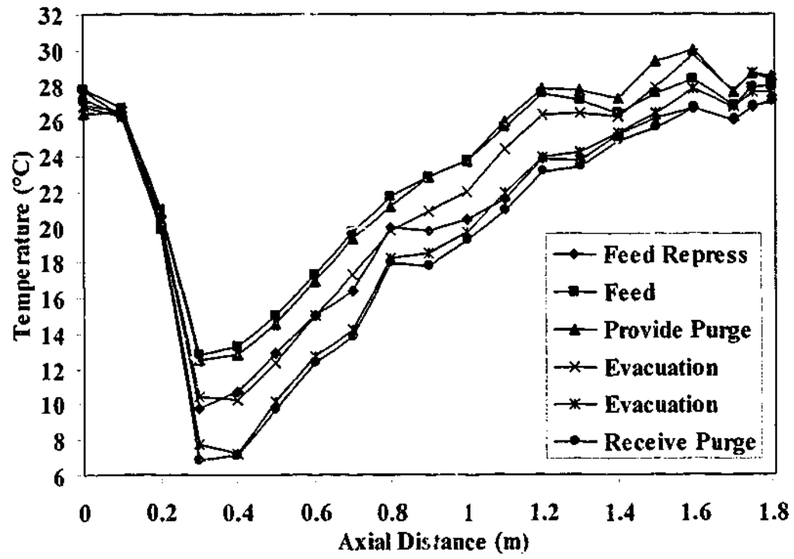

Figure 4.5.5a. Cyclic steady state axial temperature profile at baseline conditions.

Figure 4.5.5b shows the change in bed temperature (from its baseline value as shown in Figure 4.5.5a) at cyclic steady state after a 5% increase in feed valve position. The maximum change in temperature was small (2°C) with very little change occuring between 0.8 and 1.6m indicating little change in adsorptive behavior in this section of the bed. As shown earlier, the

oxygen product purity had dropped for this perturbation indicating a movement of the mass transfer zone towards the end of the bed. This movement manifested itself as an increase in the temperature near the top of the bed (1.6m onwards). The slightly higher main bed temperatures lead to heating of the prelayer on desorption and thus, slightly elevating the temperature of the prelayer (0 to 0.4m). It is interesting to note that the temperature swing at the top of the bed which was 1 to 1.5°C before the perturbation has now increased to 2 to 3.5°C reflecting the movement of the mass transfer zone and subsequent heat generation by nitrogen adsorption. While Figure 4.5.5b shows the final cyclic steady state temperature, Figure 4.5.5c shows the transient approach of the system towards cyclic steady state at three points in the bed: 0.3m, 0.7m, and 1.6m, respectively.

The feed valve perturbation was made at cycle 47. All three thermocouples (0.3m, 0.7m and 1.6m) show an immediate initial response (most easily identified by the thermocouple at 1.6m) followed by a more gradual approach to cyclic steady state. The temperature at 0.3m (in the prelayer) takes 250 cycles to reach cyclic steady state and that at 0.7m was essentially unchanged. The response at 1.6m was over after 2 to 3 cycles. The varying response time for the different locations was a result of the different causes of the temperature change. In the prelayer, no adsorption/desorption takes place and the temperature shift was entirely due to (slow) convective heating of the bed. At 1.6m, the response was rapid because movement of the mass transfer zone had led to enhanced temperature changes due to increased adsorption/desorption. Therefore, there is no one time scale for the temperature changes in the bed – as discussed earlier, there are multiple time scales involved in O_2 VSA responses.

Figure 4.5.5d shows the change in bed temperature (from its baseline value as shown in Figure 4.5.5a) at cyclic steady state after a 3% increase in purge valve position. Even though the purity response was similar (compare Figures 4.5.3a and 4.5.3b), the bed temperature response was entirely different. Temperatures in the main portion of the bed had increased by about 1.5°C with little change in temperature of the cold spot. Once again, the temperature swing at the exit of the bed has increased reflecting the presence of the mass transfer zone.

The transient response of the system to a 3% increase in purge valve is shown in Figure 4.5.5e. The thermocouple at 0.7m now shows a significant dead time (absent in the feed valve responses) and a cyclic steady state approached only after about 310 cycles. It is clear that significantly different transient and steady state temperatures are attained as a result of different perturbations.

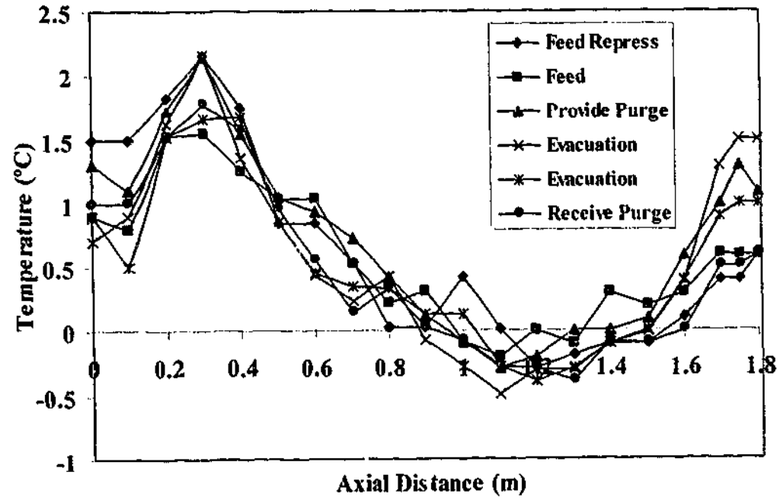

Figure 4.5.5b. Cyclic steady state change in adsorbent bed temperature as a result of a 5% increase in feed valve position.

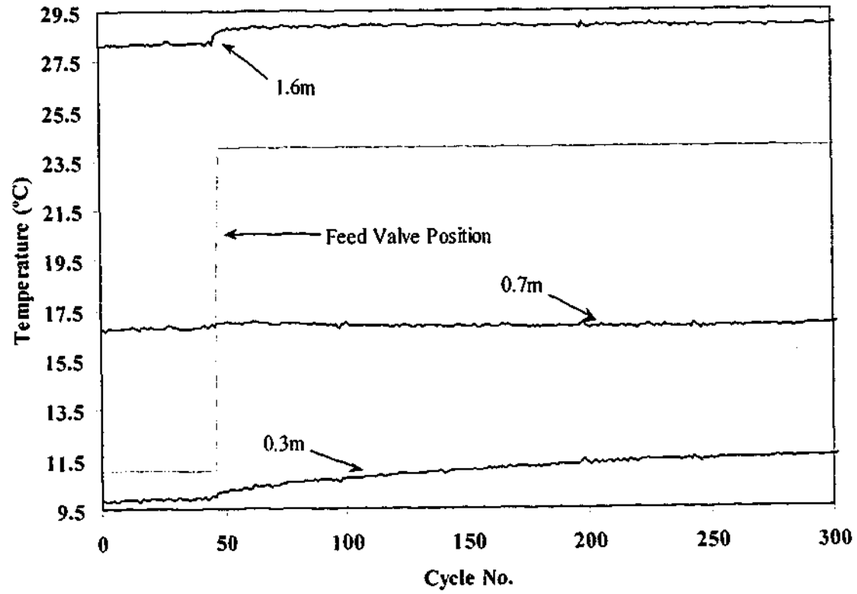

Figure 4.5.5c. Transient temperature response at various axial locations in adsorber bed 1 for a 5% increase in feed valve position.

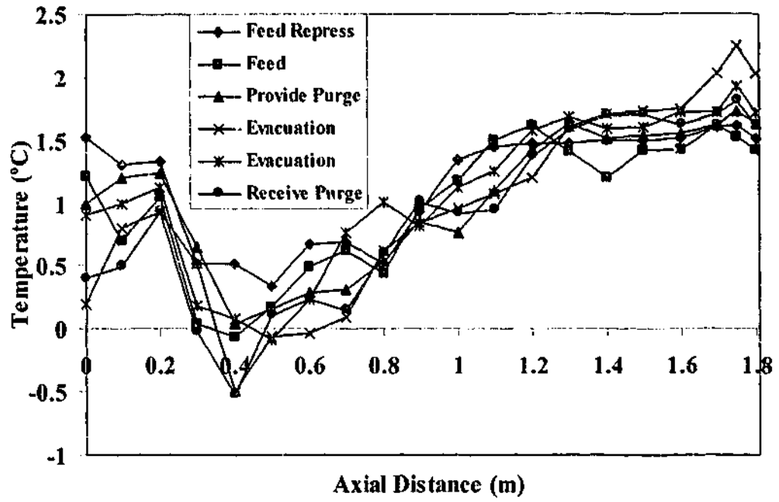

Figure 4.5.5d. Cyclic steady state change in adsorbent bed temperature as a result of a 3% increase in purge valve position.

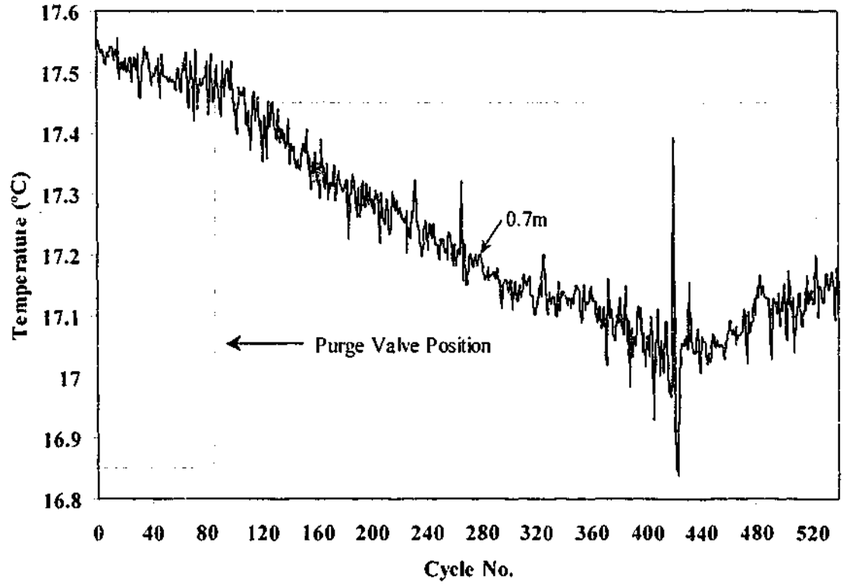

Figure 4.5.5e. Thermal history in the middle of bed 1 for a 3% increase in purge valve. Dead time 50 cycles, CSS attained in ~ 310 cycles.

Wilson and Webley (2002a) have discussed a simple method for the determination of cyclic steady state profiles following a change in boundary conditions that can be used to explain some the effects resulting from these case studies. These complications in thermal transients can however be neglected by the control engineer as it was observed that although the time-variant thermal energy profiles had not yet attained an asymptotic value, their closure had a negligible impact on the controlled variables (such as oxygen purity, flow and product pressure). This is principally because the cyclic steady state temperature closure is within two °C of its initial value and is either not significant enough to cause a difference in the output variables and/or is within the error tolerance of the sensors.

The close coupling of short-term temperature responses and location of the mass transfer front raises interesting options for diagnoses and control. By monitoring the axial thermal profiles at each instance in time, coupled with the measurements of the product flow, valuable heuristic information on the movement of the adsorption front and the likely impact on product concentration can be established. This can be utilised in a feedforward manner by the control engineer for the maintenance of product purity. The assumption of this method is that the velocity of the concentration wave and the subsequent thermal (adsorptive) wave are coincident, which is the case for bulk gas separation processes such as O_2 VSA and is substantiated from a previous analysis [Basmadjian, pp.57-59, 1997]. Use of the thermal fronts for control of the feed step for an air separation cycle had been proposed by Matz and Knaebel (1987), which was based entirely on measurements of the axial temperature profile and the premise above. A review of their work has been discussed in detail in §1.6 of Chapter 1. An additional use of the axial temperature profiles is as a powerful diagnostic tool to monitor sieve contamination (and subsequent deactivation) by either leaks at various sections of the bed or through impurities carried through the feed stream. This last example would cause a shift in the 'cold spot' further into the bed and a decrease in performance due to a diminished adsorptive capacity.

4.6 ANN MODELLING AND SENSITIVITY ANALYSIS

In order to smooth the experimental responses and to obtain sensitivities, an artificial neural network (ANN) model of the adsorption system was developed using experimentally determined data at cyclic steady state (CSS – defined in Chapter 2, §2.1.1) where perturbations were made and then returned to the baseline conditions. A description of the ANN is given in Chapter 3, §3.2.

An ANN model of the adsorption system was developed using a data set consisting of fifty five cyclic steady state runs, gathered from the pilot plant, where perturbations were made and then returned to the baseline conditions. In order to capture the effects of the perturbations correctly, the ANN architecture was represented by not only the changes in the absolute

measurements of both the inputs and the outputs but also as a function of the change from the baseline condition (i.e. ANN $\equiv f(X_i, \Delta X_i, O_k, \Delta O_k)$. Hence, the MLP structure consisted of twelve physical input neurons (six absolute measurements of the three valve positions, the average ambient temperature, the average inlet temperature, average inlet pressure and six neurons representing their change due to the step response) as well as six output neurons (three for the absolute values and three for the changes to the oxygen purity, product pressure and production rate measured in kg of contained oxygen per day (kgPDc)). Lastly, sixteen hidden neurons were used for this case study to avoid problems of over-fitting the data (the ANN learning noise) and computational burdens. The ANN was successfully trained, satisfying the conditions of a low overall mean squared error and ensuring a good fit of the data set as measured by the R^2 value. The approximation ability of the trained ANN is illustrated in Figures 4.6a to 4.6c, which compares the ANN to seven test sets not used during the training stage. The overall averaged MSE and R^2 for the ANN on the test sets are 0.12 and 0.91 respectively.

Due to the difficulties in attaining duplicate baseline conditions for every case (as a result of slight differences in ambient and inlet temperatures and pressures and valve position due to valve 'chatter'), seven baseline scenarios were used and their sensitivities calculated individually. The overall average system gain was then determined by Eq. (3.2.2h). Table 4.6a shows the results of the sensitivity analysis using the trained ANN.

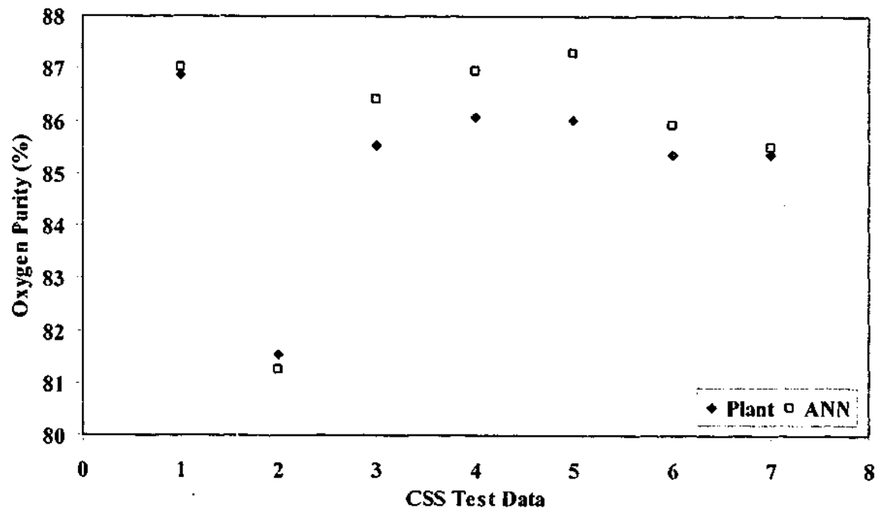

Figure 4.6a. Comparison of pilot plant oxygen purity with the trained ANN prediction.

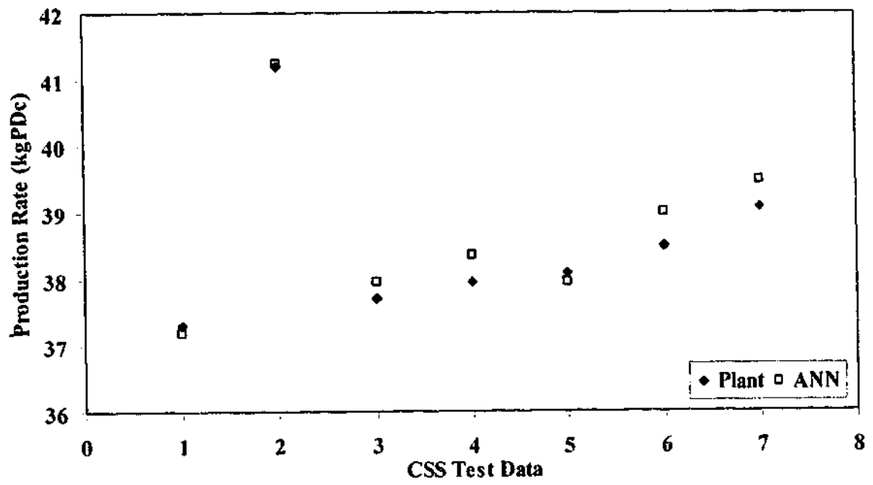

Figure 4.6b. Comparison of pilot plant production rate with the trained ANN prediction.

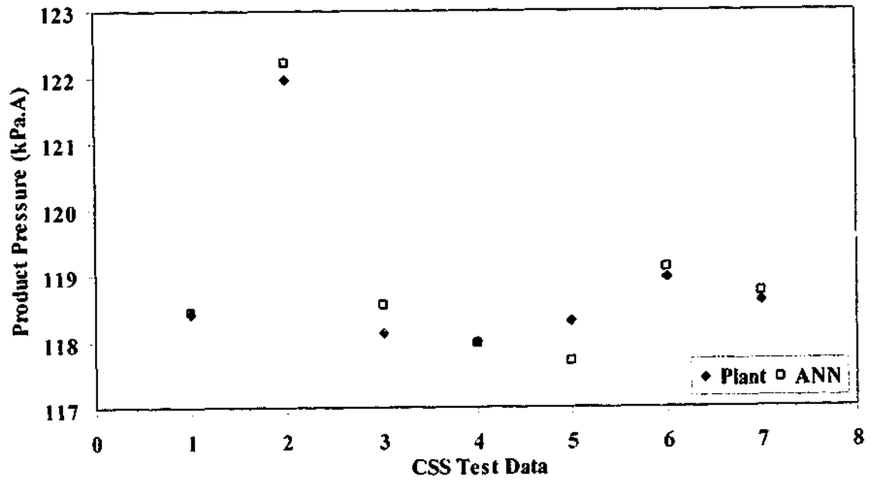

Figure 4.6c. Comparison of pilot plant product pressure with the trained ANN prediction.

Table 4.6a. Average sensitivity matrix for the O_2VSA process (open loop gain matrix).

	∂Oxygen Purity (%)	∂Production Rate (kgPDc)	∂Product Pressure (kPa.A)
∂Product Valve (%)	-0.510	0.217	-0.232
∂Purge Valve (%)	-0.614	0.646	0.639
∂Feed Valve (%)	-1.489	1.045	1.383
∂Ambient Temperature (°C)	0.278	0.059	-0.131
∂Inlet Temperature (°C)	-1.844	1.030	1.191
∂Inlet Pressure (kPa.A)	-0.002	0.012	0.335

For the region of operation studied, the open loop gain matrix reveals some interesting information. Changes in the feed valve position have the greatest impact on all of the output variables, as shown by the large gradients. Only the pairing of the purge valve to production rate resulted in a sensitivity close to that of the feed valve. The product valve, on the other hand, has a curiously modest influence on the output variables in comparison to the other valves. This is interesting, as industrial convention has typically been to use the product valve for purity control [Beh *et al.*, 2000] or in a cascade loop controlling both flow rate (slave loop) and purity (master loop). Table 4.6a also revealed that the ambient temperature and inlet pressure had only a minor influence on the output variables. This is a little deceptive since these variables were not deliberately varied in the experimental data set – the sensitivities are based on "naturally" occurring variations and probably have large errors associated with them. It is important to note that inlet temperature appears to have a large influence on system performance, even though PID control was used to regulate the output of a heater element situated in the feed tank. The difficulty of this task is due to the lack of proper mixing in the tank and the fact that the controller operates with continuous time whilst variable amounts of gas is provided to the adsorber beds during the feed and repressurisation steps only. This can cause up to a 3°C difference in temperature of the inlet stream depending on the disturbance experienced and highlights the sensitivity of the adsorbent to temperature fluctuations. This finding suggests that tight temperature control of the inlet gas would be beneficial to overall process control.

4.7 RELATIVE GAIN ANALYSIS

In multiple input multiple output systems, MIMO – such as the case with VSA, there is an added complexity of correct matching of control loop pairs (i.e. which manipulated variable should be used to control a particular target variable?). Quite often, in large systems, this choice is often not immediately obvious. For example - is it more appropriate to control the product purity with the product flow valve or would the bed purge valve serve as a better choice for an O_2 VSA system? Both variables have a strong influence on the product purity (as seen in the open loop responses in the previous section). Trial and error is one way to develop a "sense" of which loop pairings would be best but this is inefficient and time consuming. Bristol suggested that relative gain array, RGA, can be used to measure the influence a specific manipulated variable has over a specific controlled variable relative to other manipulated variables in the process [Shinskey, 1996]. Essentially the RGA is matrix of open loop gradients at a particular region of operation in ratio with the gradient coefficient obtained with all other loops closed (i.e. controlled variables constant and controllers in automatic and on set point). Mathematically, the relative gain, λ_{ij}, is expressed as

$$\lambda_{ij} = \frac{\left.\frac{\partial c_i}{\partial m_j}\right|_{m_k=\text{constant}, k\neq j}}{\left.\frac{\partial c_i}{\partial m_j}\right|_{c_k=\text{constant}, k\neq i}} \qquad (4.7a)$$

The relative gain array is expressed in matrix format, (Eq. (4.7b)), with the requirement that the sum of each row and column of the array should be 1.

$$\Lambda = \begin{array}{c|cccc} & m_1 & \cdot & \cdot & m_n \\ c_1 & \lambda_{11} & \cdot & \cdot & \lambda_{1n} \\ \cdot & \cdot & \cdot & \cdot & \cdot \\ \cdot & \cdot & \cdot & \lambda_{ij} & \cdot \\ \cdot & \cdot & \cdot & \cdot & \cdot \\ c_n & \lambda_{n1} & \cdot & \cdot & \lambda_{m} \end{array} \qquad (4.7b)$$

Experimentally, element λ_{ij} can be obtained by firstly perturbing, in open loop, the manipulated variable m_j resulting in the change in output c_i (and possibly of all other output variables). This same perturbation is made to m_j when all other loops are closed (controllers on and on set point) and observing the change in c_i and of all other controlled variables. To

overcome the limitations of perturbing a particular manipulated variable whilst keeping all other loops in control, the RGA can be evaluated directly from open loop data by utilising the following calculation procedure [McAvoy, 1983]

$$\Lambda = K \cdot (K^{-1})^T \tag{4.7c}$$

where K is the open loop gained determined by evaluating the open loop sensitivities using the ANN model and $(\cdot)$ is the *Hadamard* product (element by element multiplication). The power of this method for the purpose of process control is that information about the relative interaction between control loops at CSS can be easily quantified so that correct control loop pairings are made. Also, the magnitude and the sign of each component of the relative gain matrix provide insight into the stability and response of the loops. Table 4.7a provides a brief outline of the significance of the RGA values whilst references such as Shinskey (1996) and Liptak (1995) contain information, in greater detail, on how these values should be interpreted and of their applications.

As described by Eq. (4.7c), $\Lambda = f(K)$ and any deviation in the open loop gain elements due to process measurement errors and process/model errors would reflect on the K matrix and hence the overall RGA elements, Λ. Therefore, a method to determine the spread of the K elements is required. For this case study, it was assumed that the process/model mismatch is small compared to the errors in measurement (which is confirmed by the good approximation abilities of the ANN as shown in Figures 4.7a to 4.7c) and that the measurement errors of the input variables (X_i's) was negligible. Thus, only the measured outputs (O_k) would vary in an assumed normal distribution and hence the sensitivity, K, and the RGA, Λ, would vary normally. Based on the accumulated instrument errors, the error for the oxygen purity variable, production rate and product pressure was estimated to be $\pm 0.5\%O_2$, ± 1.01 kgPDc and ± 2 kPa respectively.

The absolute output variables oxygen purity, production rate and product pressure were perturbed in combinations about three states – no change in the output variable, a positive change in the output variable and a negative change in the output variable. This amounted to 3^3 data sets yielding 27 different sets of ANN weight coefficients from the various combinations. A last assumption was that the actual measured measured output variables represented the true universal population and hence the gain matrix shown in Table 4.6a is the universal mean. The standard deviation of $\partial Y_k/\partial X_i$ was assumed to be a third of the range of $\partial Y_k/\partial X_i$ over the 27 data sets. Table 4.7b shows the results of the estimation of the mean and standard deviation of the open loop gains.

Table 4.7a. Interpretation of the RGA values.

λ_{ij}	Qualitative Interpretation
< 0	Loop is conditionally stable. Closing this loop reverses the gain and the final response is opposite to the open loop response due to interaction from neighbouring loops (positive feedback dominates).
0	Loop pairing only responds when all other loops are closed due to interaction. Open loop gain is zero.
0 to 1	Interaction from neighbouring loops increases closed loop gain and extends period (all feedback loops are negative).
1	No control loop interaction. Completely decoupled.
> 1	Interaction from neighbouring loops reduces closed loop gain resulting in a sluggish response when other loops are in automatic (weak positive feedback loops are present).
∞ (> 100)	Suggests that the control loop is a strong function of neighbouring loops and cannot be independently controlled.

Table 4.7b. Open loop gain matrix for the CSS data showing the mean and standard deviation of the gains.

	∂Oxygen Purity (%)	∂Production Rate (kgPDc)	∂Product Pressure (kPa.A)
∂Product Valve (%)	$\mu_{11} = -0.510$; $\sigma_{11} = 0.005$	$\mu_{12} = 0.217$; $\sigma_{12} = 0.004$	$\mu_{13} = -0.232$; $\sigma_{13} = 0.006$
∂Purge Valve (%)	$\mu_{21} = -0.614$; $\sigma_{21} = 0.012$	$\mu_{22} = 0.646$; $\sigma_{22} = 0.005$	$\mu_{23} = 0.639$; $\sigma_{23} = 0.009$
∂Feed Valve (%)	$\mu_{31} = -1.489$; $\sigma_{31} = 0.003$	$\mu_{32} = 1.045$; $\sigma_{32} = 0.012$	$\mu_{33} = 1.383$; $\sigma_{33} = 0.009$

The distribution of RGA elements is then generated using a Monte Carlo method based on the deviation about a mean of the open loop gains. This involves randomly selecting, in a Gaussian fashion sets of open loop gain matrices and using each set to calculate the subsequent RGA matrix from Eq. (4.7c) above. The method used is based on the polar form of the Box and Muller (1958) transformation function which allows a set of uniformly distributed random variables to be transformed into a set of normally distributed random variables (RV). This procedure is described by Eqs. (4.7d) to (4.7f). Two uniformly distributed RV's, u_1 and u_2, are chosen between (0,1) producing two RV's x_1 and x_2 as shown in Eqs. (4.7d) and (4.7e).

$$x_1 = 2u_1 - 1 \tag{4.7d}$$

$$x_2 = 2u_2 - 1 \tag{4.7e}$$

The acceptance criteria of the random variables, x_1 and x_2, requires that $w < 1$ (Eq. (4.7f)).

$$w = x_1^{\,2} + x_2^{\,2} \tag{4.7f}$$

If this is true then two Gaussian RV's, g_1 and g_2, are generated by

$$g_1 = x_1\left(\frac{-2\log_e(w)}{w}\right)^{\frac{1}{2}} \tag{4.7g}$$

$$g_2 = x_2\left(\frac{-2\log_e(w)}{w}\right)^{\frac{1}{2}} \tag{4.7h}$$

The new value for each gain element k_{ij} is evaluated based on the normalised Gaussian RV's determined from the Eqs. (4.7g) and (4.7h) above and resulting in Eq. (4.7i).

$$k_{ij} = g_k\sigma_{ij} + \mu_{ij} \tag{4.7i}$$

Each RGA element, λ_{ij}, can be re-determined by calculation of Eq. (4.7c) using the updated value of k_{ij} from Eq. (4.7i). Therefore, by using a suitable population of Gaussian RV's, the standard deviation of each λ_{ij} can be determined. Figure 4.7a shows a plot of the standard deviation of RGA element λ_{33} as a function of the population size of the Gaussian random variables. For this study ten million Gaussian RV's were used which is sufficient as an estimate of the true population σ as Figure 4.7a revealed that for 300000 or more Gaussian RV's the standard deviation remains relatively constant. A summary of the calculation procedure for the mean and standard deviation of the RGA elements is shown in Figure 4.7b.

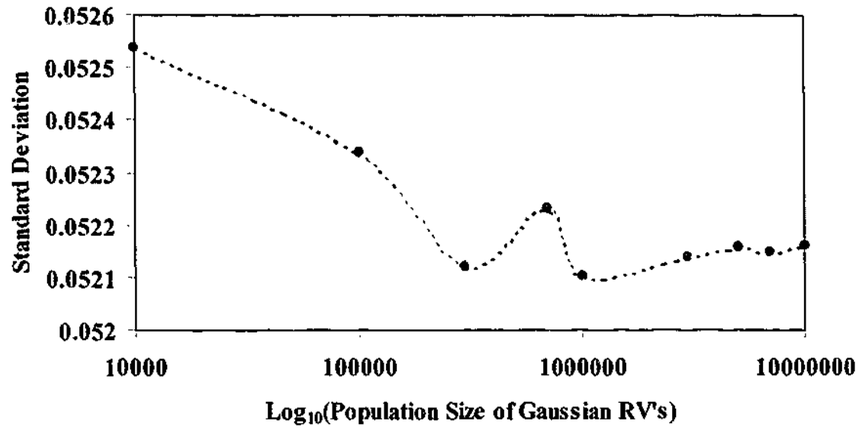

Figure 4.7a. Dependence of the standard deviation of RGA element λ_{33} as a function of the population size of the Gaussian random variables.

It is worthwhile noting that the method presented for obtaining the RGA deviations is analogous to that derived by Chen and Seborg (2002b). In that work, λ_{ij} was approximated by a first-order Taylor series and an analytical expression derived for the variance of λ_{ij} in terms of the covariance of K. The method presented in the present work, however, does not truncate higher-order terms and keeps the richness of the system intact. However, the opportunity cost of this scheme compared to the analytical method of Chen and Seborg (2002b) is the greater computing power required in generating a sufficient population of RV's. Nevertheless, the main difficulty is the determination of the standard deviation of $\partial Y_k/\partial X_i$, which has been addressed in this chapter unlike Chen and Seborg (2002b) who leave this as a user input. Table 4.7c shows the RGA matrix for the O_2 VSA process being studied along with the error range for each RGA element taken as one standard deviation of the nominal/mean value.

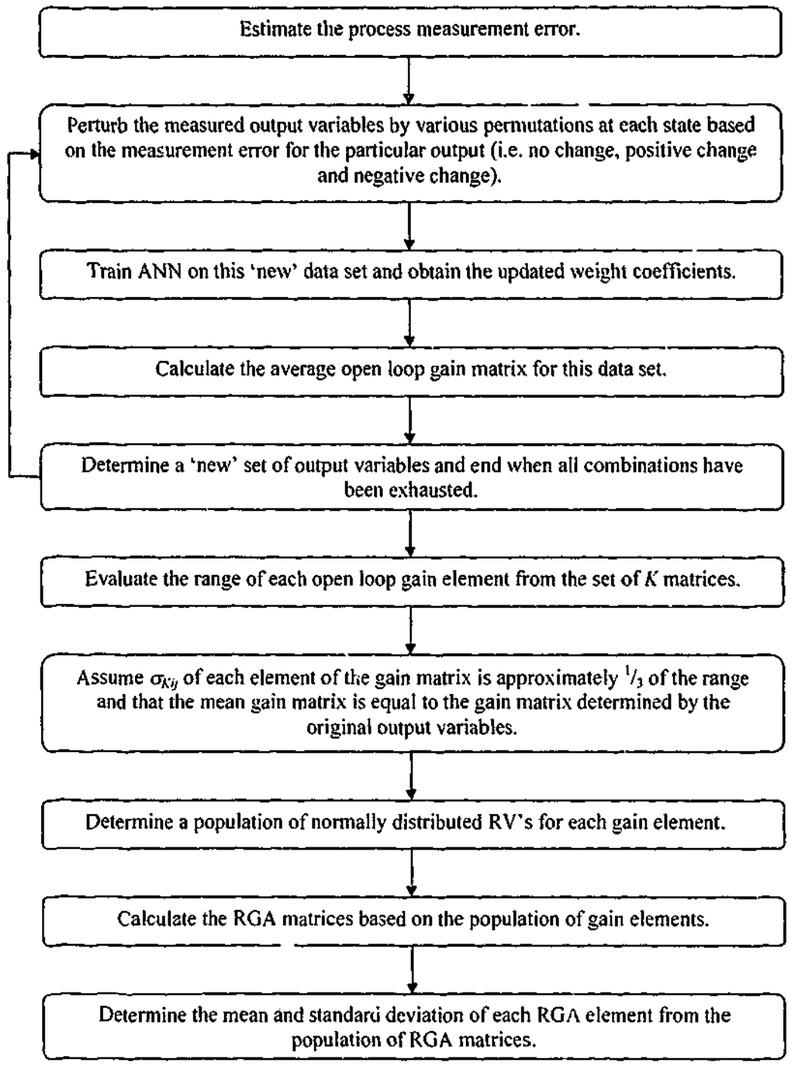

Figure 4.7b. A flow sheet detailing the calculation procedure for the mean and standard deviation of the RGA elements.

Table 4.7c. RGA matrix for CSS data showing the nominal/mean value and the error band of the RGA elements due to process measurement error taken as one standard deviation either side of the mean. Standard deviation determined by a population of ten million Gaussian RV's. Characters in bold is the suggested pairing.

	Oxygen Purity (%)	Production Rate (kgPDc)	Product Pressure (kPa.A)
Product Valve (%)	**0.543** $0.515 \le \lambda_{11} \le 0.571$	0.106 $0.084 \le \lambda_{12} \le 0.128$	0.351 $0.343 \le \lambda_{13} \le 0.359$
Purge Valve (%)	-1.578 $-1.679 \le \lambda_{21} \le -1.476$	**3.217** $3.075 \le \lambda_{22} \le 3.360$	-0.640 $-0.692 \le \lambda_{23} \le -0.588$
Feed Valve (%)	2.035 $1.934 \le \lambda_{31} \le 2.135$	-2.323 $-2.465 \le \lambda_{32} \le -2.181$	**1.288** $1.236 \le \lambda_{33} \le 1.341$

A negative RGA value suggests that the loop is conditionally stable as positive feedback dominates the loop (i.e. the open loop change has an opposite effect from the change if all other loops are in automatic and on set point). Hence, the pairings of the feed valve with production rate and purge valve with product pressure and oxygen purity should be avoided (refer to Table 4.7c). Ideally, for no loop interaction, the relative gain should have a value of unity and therefore the loops that produce RGA values closest to one should be chosen. A value greater than one indicates that interaction reduces the effectiveness of the control loop due to the presence of weak positive feedback loops. Based on the RGA matrix shown in Table 4.7c, this suggests the pairings of the feed valve with product pressure, the purge valve with production rate and the product valve with oxygen purity. However, the RGA matrix above indicated a significant amount of interaction from neighbouring loops (especially in the case of the product valve pairing with purity, which has a RGA of ~ 0.5) and warrants investigation of appropriate decoupling techniques. Also, an analysis of the determinant of the gain matrix at the nominal/mean value indicated a relatively small value of 0.211. This further suggests that the system is highly coupled as a determinant close to zero results in large changes in the RGA elements for small changes in the open loop gains. A final comment with regards to the RGA is that the effect of the process measurement error has a negligible impact on the absolute value of λ_{ij} and does not alter the pairings and therefore the chosen controller structure is appropriate for the region of operation.

In order to reduce the effects of interaction, Shinskey (1996) has suggested categorising the control loops into slow, fast or of similar dynamics and detuning the PID gains by its RGA

value. Chapters six and seven will address the issues involved with the use and implementation of these control loop pairings.

4.8 CONCLUDING REMARKS

Although the oxygen VSA process is highly complex, this study shows that a simple lumped model that can be solved easily by numerical means can describe trends in the bulk flows and pressures. The primary cause of mismatch between the model and pilot plant data is due to a fixed value for the composition used in the model (y_{N2} at the end of purge and evacuation steps is assumed equal to 0.77). The mismatch is also due, to a lesser extent, to the various assumptions, (isothermal behaviour, negligible axial pressure drop and ambient heat transfer, equilibrium conditions and constant feed pressure). Moreover for the region of interest, complications involving thermal effects can be essentially neglected and hence a simplification to the control problem can be made. Furthermore, future studies testing the action of control loops and the tuning of such loops can be made by perturbation of the product valve only as this has shown to yield similar dynamics to the application of a load disturbance on the product stream. It is also envisaged that monitoring of the axial thermal profiles at each instance in time, coupled with the measurements of the product flow, can provide valuable heuristic information on the movement of the adsorption front and the likely impact on product concentration. In terms of the control of the process, these two variables may make worthy candidates as process variables for feed forward control of the product purity loop.

In addition, an extension to the simple mechanistic model was made so that the product oxygen purity could be modelled. This empirically based relationship (with physical assumptions such as same cycle dynamics) for concentration was compared to plant response data and a purely empirical FODT model. The finding suggests that both models were able to approximate the purity variable with sufficient accuracy further simplifying the control problem and paves the way for use of online model-based control. In both cases, the principal cause of model error was attributed to the variable and less than ideal mixing profiles predominant in the product vessel. This perceived dead time tends to shift the output profile in time rather than alter its absolute value. Therefore, it is envisaged that by proper design of these vessels, benefits would be gained from the decreased downtime attributed to a reduction in process control problems and subsequently, resulting in customer satisfaction

The disadvantage of the FODT model, being largely empirical, is that the physics of the process is not captured. It requires, therefore, to be recalibrated for operation outside of its linear range, which may not be the case with the SoCAT model provided that experimental data is available over a wide range of operating conditions. For real-time implementation, however, the FODT model is much simpler to implement and less computationally intensive than the

simplified adsorption process model. This makes it attractive for the application of model predictive control methods where the change in process variable is predicted and in some cases the Jacobian matrix (which is known to require additional computing power) is calculated.

Similarly, both SoCAT and a second-order model (SODT) approximate the production rate variable quite readily and was shown to be a function of both the dynamics of the oxygen purity and product flow. It was also demonstrated, for this variable, that the reason for the negligible observed time delay is because this variable is largely dominated by the product flow.

In addition, an artificial neural network was successfully implemented to model the CSS responses of an oxygen VSA cycle to open loop step perturbations. The matrix of gain elements obtained from the ANN fit suggests that the system is highly coupled, with changes in valve position influencing all output variables to a significant extent. Also, it was found that the maintenance of a steady inlet temperature would uncouple the undesirable effects of a variable inlet temperature stream on process performance. The method of relative gain allows insight into the closed loop performance of the system under control from the sensitivity matrix. The results of this analysis suggested that the pairings of the feed valve with product pressure, the purge valve with production rate and the product valve with oxygen purity should be attempted. The RGA also indicated that due to the non-unity of the pairings, control loop decouplers should be designed to achieve optimal control. Finally, the application of Monte Carlo techniques to determine the variance of the RGA elements due to process measurement errors ensured the robustness of the RGA structure.

In conclusion, the very nature of the VSA process and its complexity makes it unlike other processes encountered in the field of process control. Certainly, step responses aid in the understanding of the dynamics of the system and perhaps controller tuning but the strong nonlinearities present in the process make it to be a challenging problem for the control engineer.

NOMENCLATURE

SoCAT Nomenclature

b_i, b_{oi}	1st site dual-site isotherm parameters (1/kPa)
C	a constant defined by Eqs. (4.4e) and (4.4f)
C_v	valve flow coefficient
d_i, d_{oi}	2nd site dual-site isotherm parameters (1/kPa)
k_i	mass transfer coefficient for oxygen and nitrogen (1/s)
$m_{1,2}$	1st and 2nd dual-site isotherm parameter (mol/kg)
M	adsorbent bed mass (kg)
n_i	nitrogen and oxygen adsorbed loading (mol/kg)

n_i^{eq}	nitrogen and oxygen adsorbed equilibrium loading (mol/kg)
N	moles of gas (mol)
P	pressure (kPa.A)
Q	volumetric flow rate through valve (m^3/s)
Q_{1i}	1st site dual-site isotherm parameter (J/mol)
Q_{2i}	2nd site dual-site isotherm parameter (J/mol)
R	universal gas constant (kJ/mol/K)
S_g	fluid specific gravity
t	time variable (s)
T	temperature (K)
V	volume (m^3)
y_i	mole fractions of nitrogen and oxygen
ε_b	bed voidage
τ_c	cycle time (s)

SoCAT Subcripts

1	feed tank inlet before control valve (m^3/s)
3	feed tank outlet after control valve (m^3/s)
3A	adsorbent bed 1 inlet (m^3/s)
4	product tank inlet after control valve (m^3/s)
4A	adsorbent bed 1 product (m^3/s)
6	product tank inlet after control valve (m^3/s)
8A	adsorbent bed 1 evacuation (m^3/s)
10A	adsorbent bed 1 purge (m^3/s)
A1	adsorbent bed 1
c	cycle
D	downstream of valve
F	feed tank
i	inlet stream or adsorbable component
o	outlet stream
P	product tank or make product step
U	upstream of valve

FODT Nomenclature

K_p	process gain (%O_2/%Valve Open)
IAE	integrated absolute error
O	change in product oxygen concentration (%O_2)

t	cycle number (cycle)
T	total number of cycles (cycles)
V	change in input variable (typically valve position) (%)
y	product composition (%)
τ_D	process time delay (cycles)
τ_p	process time constant (cycles)

FODT Subscripts

a	actual
m	model

RGA Nomenclature

c_i	i^{th} controlled variable
K	open loop gains (sensitivities)
m_j	j^{th} manipulated variable
λ_{ij}	relative gain array
Λ	relative gain matrix

Chapter Five

Frequency Response to Cyclic Disturbances

Frequency response analysis is a powerful method that can aid the understanding of process dynamics and can provide a richer source of information than step responses. Results from this study have demonstrated that reduced parameter models, such as SoCAT, can be utilised for plant monitoring and as the basis for model-based control to a sufficient degree of accuracy. The method of frequency response has further justified the analysis performed in Chapter 4 and confirms that a composition gradient, inherent in the product vessel of the pilot plant, was the principal cause of model error. It was also experimentally demonstrated that this perceived time delay was variable and a function of the oxygen molar flows into and out of the tank. However, due to the variability of the mixing characteristics present in the product tank and the negligible time delays of the oxygen production rate and product pressure, it became both impractical and unrealisable to employ frequency response techniques to analyse system stability and loop interaction.

5.1 INTRODUCTION

Perturbations due to load and process changes yield interesting system dynamics in the VSA process as characterised by their long time constants and nonlinear behaviour [Beh and Webley, 2003b]. From an industrial standpoint, it is these time-varying parameters that are of interest and in turn, the bugbear for both plant operators and control engineers alike. Frequency response represents a method by which the process can be characterised to determine the magnitude and phase of the output response, the system stability, the extent of interaction between variables and also employed as the basis for control loop tuning. In the field of adsorption, the application of frequency response techniques has been limited to the determination of the value of the mass transfer coefficient and diffusion characteristics [Park *et al.*, 1998b; Park *et al.*, 1998c; Petkovska and Do, 1998] with no application to industrial adsorption cycles to date.

In the case of oxygen VSA, there are several variables that contribute to the flows of mass and energy in the system such as composition, pressure, molar flow and thermal energy. The close coupling of these distributed variables causes process modelling to be both computationally intensive and complicated as discussed in Chapter 3, §3.1. More importantly, it is difficult when using such complex models, to assess the significance of each input parameter

(boundary conditions or the like) – the numerics and the volume of data generated can obscure the understanding of the process. It is the objective of this chapter to quantify the experimental trends observed and to highlight the variables of importance in this system. It is anticipated that a lucid understanding of the dynamic and cyclic steady state responses gained from this work will aid future development of reduced-parameter models for process modelling, process heuristics and model-based control.

The data presented in this chapter was gathered from a dual bed oxygen VSA pilot plant (Figure 2.1a, Chapter 2) running the cycle configuration shown in Figure 2.2c of Chapter 2. Once again, as employed in the previous chapter, SoCAT was used to quantify and explain the observed experimental trends. The chapter begins by discussing the implementation of the frequency response method and the perturbation scenarios. The chapter closes by discussing the open loop frequency results and concludes by highlighting the important findings.

5.2 IMPLEMENTATION OF THE FREQUENCY RESPONSE TECHNIQUE

The frequency response method used in this study involves injecting a sinusoidally varying input signal into the system and observing the variation of the output signals (see Figure 5.2a). If an input function is varied periodically by an amount ω (the angular frequency) as given by Eq. (5.2a)

$$A\sin(\omega t) \tag{5.2a}$$

then the corresponding output signal will also vary by an amount (assuming that the system is linear about the point of perturbation) determined by Eq. (5.2b).

$$B\sin(\omega t + \phi) \tag{5.2b}$$

The constant, ϕ, is the phase lag angle and represents a horizontal shift in time of the period of the output with respect to the input while B is the amplitude of the output variable.

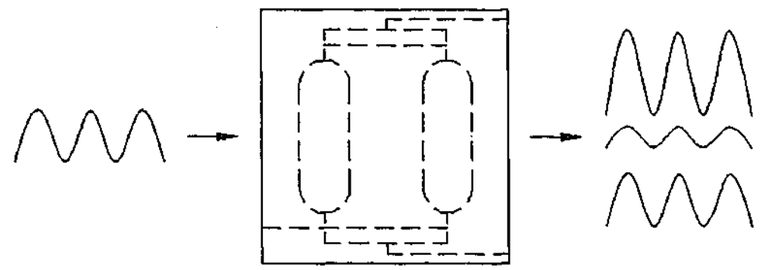

Figure 5.2a. Schematic showing the effect of a sinusoidal input on the output variables.

The power of frequency response methods lies in their simplicity of implementation and the ability to assess important information such as system dynamics and the response to periodic disturbances. This is because, unlike step response data, frequency responses are only valid when the system attains periodic stability, negating transient dynamics which can contain sensor noise and error (contrary to step responses where these factors can severely impact on the transient response) while maintaining dynamic information at CSS. Frequency techniques also allow examination of the system's closed loop stability, which is arguably the information of greatest importance to the control engineer. In addition, because of the multivariate nature of VSA systems, information on the closed loop stability is of specific importance when designing controllers and also to gauge the extent of loop interaction and deduce control loop pairings. Implementation of this methodology to the oxygen VSA process, however, will be primarily experimental with the lumped parameter model, SoCAT, used to explain the observed trends.

Typically, academic studies have concentrated on processes that are well-characterised and hence are described by appropriate transfer functions written in the Laplace domain [Luyben, 1986, Chen and Seborg, 2001], which allows the application of powerful analysis techniques. The VSA process for oxygen enrichment, however, is complex to the point that linearisation of the governing differential equations is difficult even in its reduced form as a lumped parameter system such as SoCAT. This complexity is coupled with the alternating boundary conditions that simulate the periodicity of the adsorption process. The last complication associated with these systems is that the manipulated and control variables of interest are only implicitly described in the governing conservation equations. Control valves are commonly used for the regulation of various output parameters and not for the manipulation of actual flow rates or pressures that are explicitly contained in the conservation equations. In the VSA system under investigation, the manipulated variables available for control are the feed valve, purge valve and product valve (refer to Chapter 2, Figure 2.1a). It is acknowledged that a relationship between flow/pressure can be developed such as the valve equation specified by the Fluids Control

Institute and utilised in Eqs. (4.3g) and (4.3h) in Chapter 4 but it is usually difficult to match the model to the process (e.g. unknown valve characteristics and C_v, important transients conditions not adequately captured). Furthermore, the output variables in an oxygen VSA process that directly impacts upon the customer and hence the variables selected for control the product purity, production rate and product pressure respectively. The product concentration and pressure are explicit terms in the conservation equations, however, the production rate variable is defined in terms of the product concentration and cyclic molar flow (refer to Eq. (4.5.4a) in Chapter 4) making an analytic frequency analysis of the conservation equations impossible.

Given the difficulties in establishing appropriate transfer function descriptions of this process, an experimental study was conducted by perturbing the three valves under investigation at various frequencies and gauging their influence on the system variables. Only periods of integer value were used because non-integer periods give rise to asymmetrical cycle operation. The shortest practical period used in this investigation, was a period of three. Shorter periods (one and two) yielded no changes in the valve position as both $sin(2\pi t)$ and $sin(\pi t)$ are zero. The amplitudes chosen for this cycle are the maximum controller action as developed in the previous chapter. The following scenarios were studied with reference to Figure 2.2c in Chapter 2 and perturbations initiated at a fixed point about a baseline cyclic steady state condition –

Case 1. The frequency response of the system to a sinusoidal feed valve perturbation of amplitude 5%. The valve position is updated once per cycle during the feed steps (steps 2 and 5). The output variables of interest are measured at the end of the feed step (step 2) during the cycle in which the valve change is made.

Case 2. The frequency response of the system to a sinusoidal purge valve perturbation of amplitude 3%. The valve position is updated once per cycle during the purge steps (steps 3 and 4). The output variables of interest are measured at the end of the feed step (step 2) at the cycle following the valve change.

Case 3. The frequency response of the system to a sinusoidal product valve perturbation of amplitude 10%. The valve position is updated once per cycle during the feed steps (steps 2 and 5). The output variables of interest are measured at the end of the feed step (step 2) during the cycle in which the valve change is made.

The responses measured were bed pressures, flow rates, temperature (axial and about the system), product composition and pressure as a function of absolute and cycle time.

5.3 OPEN LOOP RESULTS AND DISCUSSION

In this section the open loop frequency responses will be discussed and due to the extensive amount of data, only a representative sample of the various responses will be shown to demonstrate the method. Due to the batch nature of the process, each bed cycles through several steps but product is only provided during the feed step. Hence, it is of interest to only show the system variables at the end of the feed step during successive cycles for the first adsorbent bed (step 2, refer to Chapter 2, Figure 2.2c). Also, due to operation symmetry of the beds, the second adsorbent bed yielded similar results to the first at the end of its feed step condition (step 5 in this case, refer to Chapter 2, Figure 2.2c). Lastly, it is worthwhile noting that absolute time has been transposed to cycle time (as this is of the greatest interest from the perspective of the control engineer) and used in all of the subsequent discussion unless stated otherwise.

5.3.1 Bed and Product Tank Pressure Frequency Response

The result of the open loop data showed similar dynamic responses for both the bed and product tank pressures to the three input frequency variations. In order to aid brevity, only the end of step conditions of certain scenarios will be shown as representative of the runs investigated while a comparative summary between plant and model in terms of CSS amplitude is provided in Table 5.3.1a.

An observation of the experimental data revealed the inverse relationship between valve position and the product and bed pressure in the product valve perturbation scenario – as the product valve increased, bed pressure and hence product pressure decreased from its value at the previous cycle (refer to Figure 5.3.1a). This is expected for pressure driven flow. There was also an observed phase lag in both the adsorbent bed and product tank pressure, which asymptotes from –90° to zero as $\omega \rightarrow \infty$. The phase lag associated with the response of the product pressure to the cycling of the product valve can be explained by examination of Figure 5.3.1b. This graph illustrates the variation in the product tank pressure with time at CSS over the course of the valve cycle. It shows that when the product valve was at its lowest position, (the valve change was made at the start of the feed step of the first bed and maintained until the feed step of the first bed at the next cycle – 11 seconds to 70 seconds), the end of step product pressure only attained a maximum value at the next cycle (at 84 seconds). This phase lag was caused by the coupling of the second bed, which altered the initial conditions in the tank at the start of the feed step. A similar argument can be used to explain the time lag observed in bed pressure at the end of the feed step. An additional observation was that the actual feed step did not occur for a further four seconds in the simulation data presented – Figure 5.3.1b shows that the product tank pressure decreased to a minimum value before bed one was permitted to feed gas into it. This is consistent with the experimental data, which shows that this is anywhere between two and four

seconds. This "No Flow" condition prevented backflow from the product tank to the adsorbent beds and was implemented in the pilot plant by keeping the solenoid valves closed until the upstream pressure was less than the downstream. A similar set of logic exists in the numerical model.

On the other hand, both the feed and purge valve frequency responses exhibited a linearly proportional relationship with bed and product tank pressure. Opening the feed valve increased the amount of moles entering the bed and hence increased the overall bed and product pressure. For the scenario whereby the purge valve position was increased from the previous cycle, the pressure of the first adsorbent bed rose to a higher pressure at the start of the step. The cause of this effect was due to the greater number of moles of gas entering the first bed from bed two during step 5 (bed 1 receiving purge gas) at the previous cycle (remembering that the purge valve increase was made at $cycle_N$ at step 3 but its effects are only measured at the end of step 2 at $cycle_{N+1}$). Figure 5.3.1c, which represents the frequency of the end of step pressure of adsorbent bed one to a purge valve perturbation, is representative of the transient and CSS responses due to cycling of the feed and purge valves.

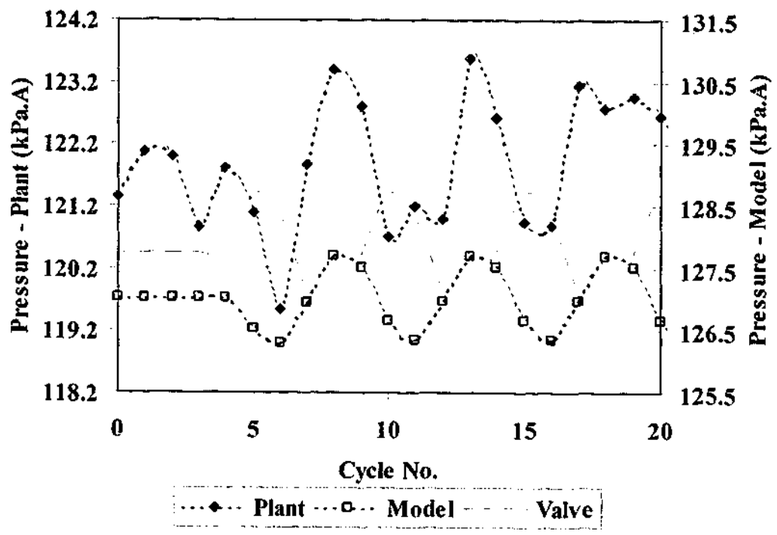

Figure 5.3.1a. Transient and CSS response of the product pressure at the end of step 2 to a product valve frequency perturbation (amplitude 10, period 5) initiated at cycle 5. CSS amplitude: pilot plant ~1.5 kPa; model 0.67 kPa.

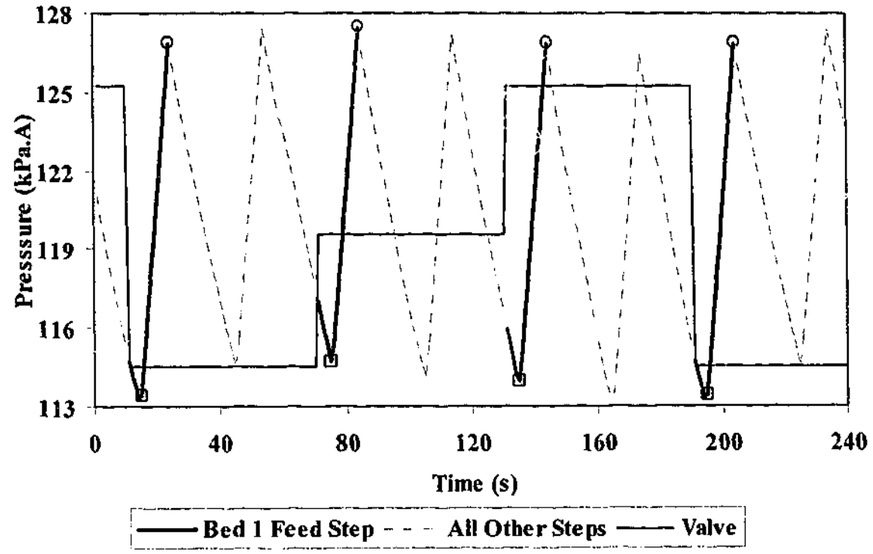

Figure 5.3.1b. CSS time variant frequency response of the product tank pressure in response to cycling of the product valve (amplitude 10, period 3) – model data. Squares represent the product pressure when bed 1 begins to feed gas into the product tank and while the circles represent the product tank pressure at the end of bed 1 feed step (step 2).

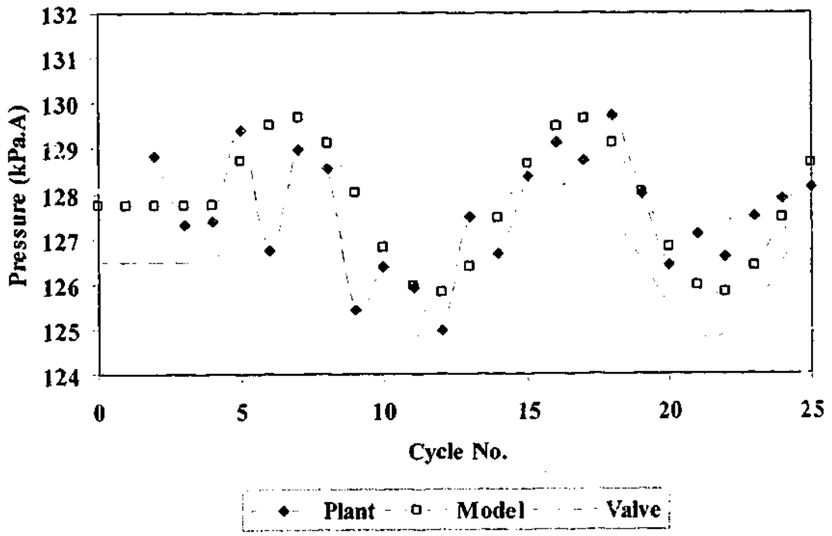

Figure 5.3.1c. Transient and CSS response of bed 1 pressure at the end of step 2 to a purge valve frequency perturbation (amplitude 3, period 10) initiated at cycle 5. CSS amplitude: pilot plant ~1.7 kPa; model 1.93 kPa.

For all three case studies, the response of the VSA plant was immediate and cyclic steady state was achieved within the next period of the valve cycle as demonstrated by Figure 5.3.1d. The model matches the experimental trends well during both CSS and transient operation although the pilot plant data was not as smooth (due to sensor error) as the predicted model response. However, in some situations there was a difference in the amplitude of the swing in both bed and product pressure between process and model as the valve in question cycled (see Figure 5.3.1c and Table 5.3.1a). These observed mismatches between process and model can be primarily attributed to the assumption of constant composition used in the lumped parameter model. In the real system a composition gradient exists axially through each bed. This resulted in a variation in the uptake of the adsorbable species at each axial location in the bed. Therefore, depending on the initial and boundary conditions. SoCAT may over or under predict the total amount adsorbed. An even larger mismatch resulted when the incorrect assumption of constant mole fraction was used to model the second bed whilst undergoing evacuation (desorption step). Not only was there an observed difference in the amplitude (refer to the middle rows in Table 5.3.1a) and the absolute values differs but the period varied also in some cases. Figure 5.3.1e illustrates an example of the typical response of the second bed to a cyclic perturbation. The overall variance in the bed pressure profile manifested itself in the product tank pressure and resulted in similar mismatches in terms of magnitude between plant and model as shown in Figure 5.3.1a. However, for the majority of the runs investigated SoCAT predicted amplitude changes of similar order to that of the plant as shown in Table 5.3.1a.

Lastly, the observed experimental and numerical results shows that the amplitude of the output signal of both the bed undergoing feed and the product pressure increased as ω decreased (i.e. the period increased – compare Figure 5.3.1c with Figure 5.3.1f and refer to Table 5.3.1a). No measurable difference in phase was observed between the bed undergoing feed and the product tank pressure. The variation in amplitude with ω was due to the time constant of the system. In the previous chapter it was shown that the response of the product vessel pressure converged within 5 cycles after a step disturbance in valve position. As the period became greater than the system time constant, a larger change in the output variable was be observed as the system had longer to respond.

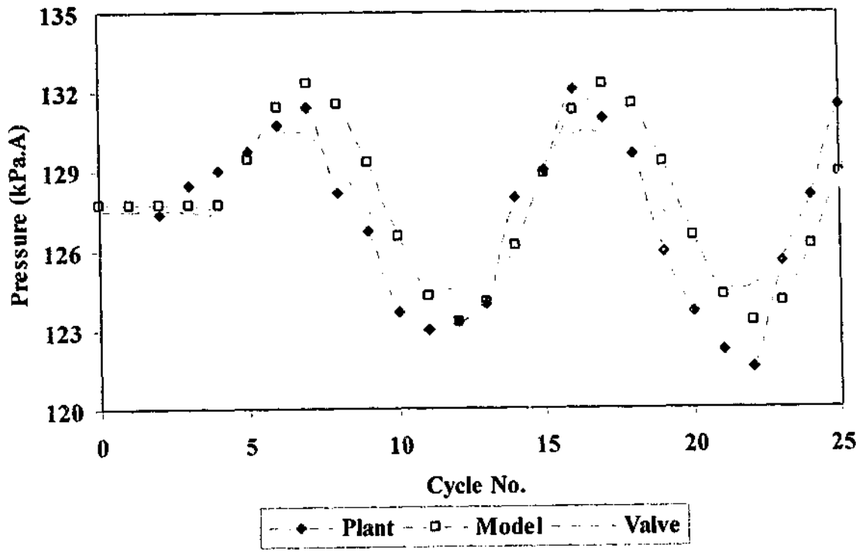

Figure 5.3.1d. Transient and CSS response of bed 1 pressure at the end of step 2 to a feed valve frequency perturbation (amplitude 5, period 10) initated at cycle 5. CSS was attained within the next period of the valve cycle. CSS amplitude: pilot plant ~5.3 kPa; model 4.49 kPa.

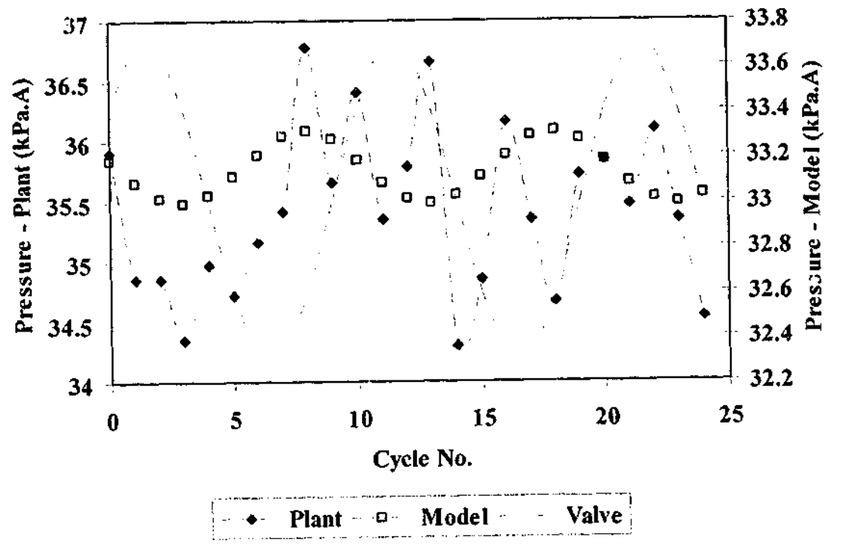

Figure 5.3.1e. CSS response of bed 2 pressure at the end of step 2 to a product valve frequency perturbation (amplitude 10, period 10). Pilot plant amplitude ~1.2 kPa and model 0.16 kPa.

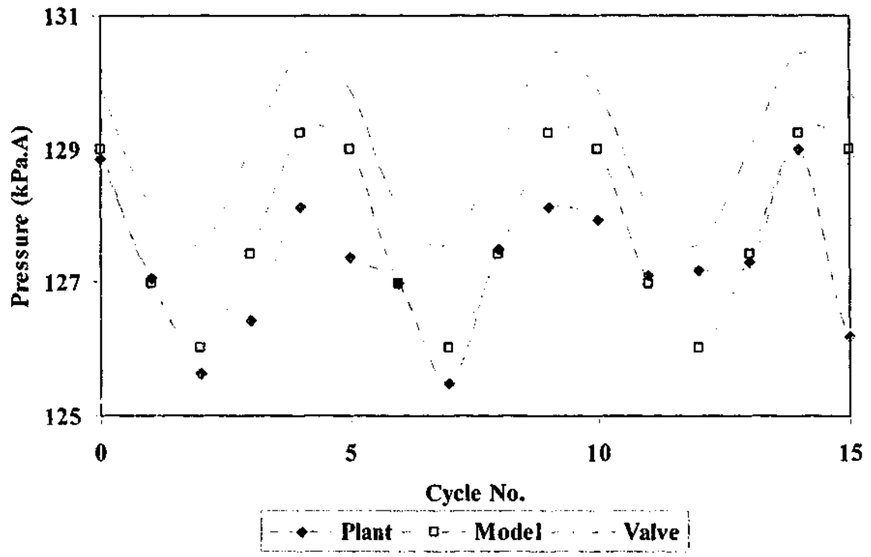

Figure 5.3.1f. CSS response of bed 1 pressure at the end of step 2 to a purge valve frequency perturbation (amplitude 3, period 5). Pilot plant amplitude ~1.7 kPa and model 1.62 kPa.

Table 5.3.1a. Comparison of the CSS amplitude between plant and model for the system pressures at the end of the feed step (step 2).

	Period (cycles)	Feed Valve (5% Amp.)		Purge Valve (3% Amp.)		Product Valve (10% Amp.)	
		Plant (kPa)	Model (kPa)	Plant (kPa)	Model (kPa)	Plant (kPa)	Model (kPa)
Bed 1 Pressure	5	3.7	3.12	1.7	1.62	1.5	0.65
	10	5.3	4.49	1.7	1.93	1.7	0.97
	15	5.4	4.81	1.7	2.01	1.9	1.09
Bed 2 Pressure	5	2.3	0.56	1.5	0.37	0.8	0.12
	10	1.8	0.73	1.6	0.34	1.2	0.16
	15	1.6	0.77	1.7	0.32	1.0	0.17
Product Pressure	5	2.9	3.02	1.8	1.61	1.5	0.67
	10	4.4	4.35	1.9	1.93	1.8	1.0
	15	4.8	4.67	2.0	2.01	2.2	1.11

5.3.2 Frequency Response of the System Flows

Figures 5.3.2a to 5.3.2d represents a summary of the responses to the three periodic disturbances in terms of the cyclic molar flows about the system. The discussion begins with reference to the feed flow variable. Figures 5.3.2a and 5.3.2b display differing behaviour of the model in response to the various disturbances. In the case of periodic cycling of the purge and product valve, the model predicted no change in the inlet molar flow, which was contrary to the observed response of the pilot plant (represented by Figure 5.3.2a and also shown in Table 5.3.2a). This discrepancy in the trends calculated by the simulator was primarily due to the pressure regulator valve located on the pilot plant whose dynamics was not modelled by SoCAT (refer to Chapter 4, §4.5.2). The absence of the pressure regulator in the model resulted in the development of choked flow conditions between the feed tank and the adsorbent beds, as the inlet tank was much higher pressures than the beds. Consequently, the model predicted constant volumetric flow rate at constant pressure and temperature and therefore a constant mole rate (since the feed tank pressure is constant). Use of the pressure regulator in the plant decreased the outlet pressure from the feed tank and permitted pressure-driven flow to occur. This was contrary to the feed valve perturbation case, which displayed periodic cycling captured by the numerical model (see Figure 5.3.2b and Table 5.3.2a). The cycling of the feed valve and hence the valve C_v, allowed the pressure regulator to be negated in this case as pressure-driven flow dominated the response. For the majority of variables such as product and vacuum flow, the numerical model predicted the transient and CSS trends with acceptable accuracy as presented in Figures 5.3.2c and 5.3.2d and Table 5.3.2a. The dynamic plots exhibited immediate response when the periodic disturbance was introduced and CSS was attained rapidly, generally within the next period of the input signal as shown in Figures 5.3.2b to 5.3.2c.

For all three scenarios, the product flow rate, arguably the most important of the three variables, did not display any measurable phase shift from the cyclic inputs and increased in amplitude for the most part with a reduction in frequency (once again as discussed in §5.3.1 due to the time constant of the system). In the case of the product and feed valve this is an easily explained phenomenon. This is because the product mole rate is proportional to the amount of feed gas entering the bed during the feed step and is directly correlated to the position of the feed/product valve which causes either more or less moles of gas to enter the system or imposes a back pressure on the process outlet. The purge valve disturbance was not so easily linked to the product flow however. The results show that both plant and model have a linear dependence between purge valve position and product flow. A similar trend was observed in §4.5.2 of Chapter 4 whereby the product mole rate was increased by ~30 mmole/cycle in response to a positive 3% step change in the purge valve position. The reason for this linear dependence is that an increase in the purge valve caused an overall rise in the pressure of the bed receiving purge gas. This bed, now operating at a higher pressure, provided product gas at a pressure

higher than the previous cycle during its feed step, which in turn raised the overall product pressure. The higher product pressure increased the driving force for flow at a constant valve C_v (as volumetric flow is proportional to the square root of ΔP) producing more product gas per cycle. This subsequently produced a greater end of step pressure than that of the previous cycle due to the higher initial product pressure.

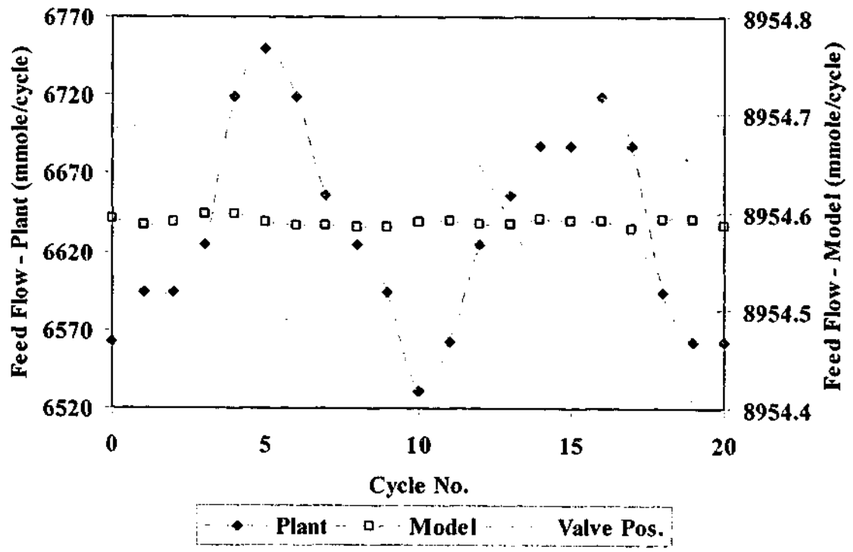

Figure 5.3.2a. CSS response of the feed flow variable at the end of step 2 to a purge valve frequency perturbation (amplitude 3, period 10). Pilot plant amplitude ~93 mmole/cycle and model 0.0 mmole/cycle.

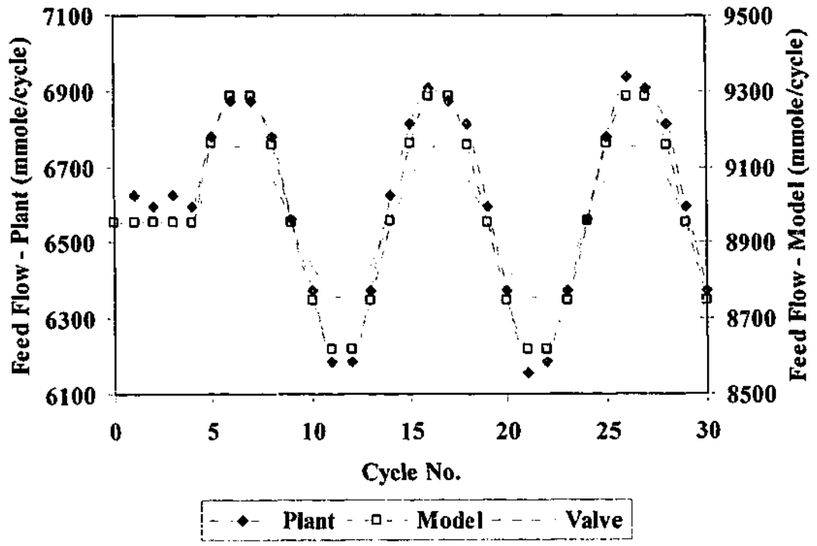

Figure 5.3.2b. Transient and CSS response of the feed flow variable at the end of step 2 to a feed valve frequency perturbation (amplitude 5, period 10) initated at cycle 5. CSS was attained within the next period of the valve cycle. Amplitude at CSS: pilot plant ~390 mmole/cycle; model 335 mmole/cycle.

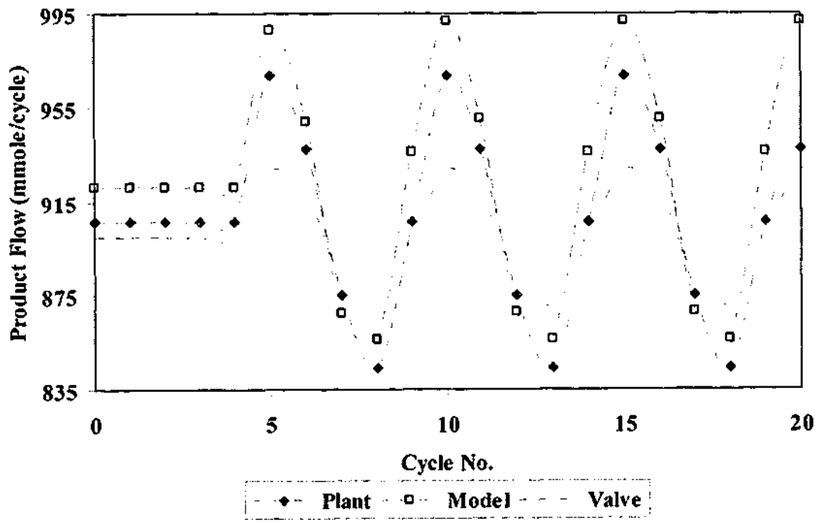

Figure 5.3.2c. Transient and CSS response of the product flow variable at the end of step 2 to a product valve frequency perturbation (amplitude 10, period 5) initated at cycle 5. CSS was attained within the next period of the valve cycle. Amplitude at CSS: pilot plant ~21.3 mmole/cycle; model 39.79 mmole/cycle.

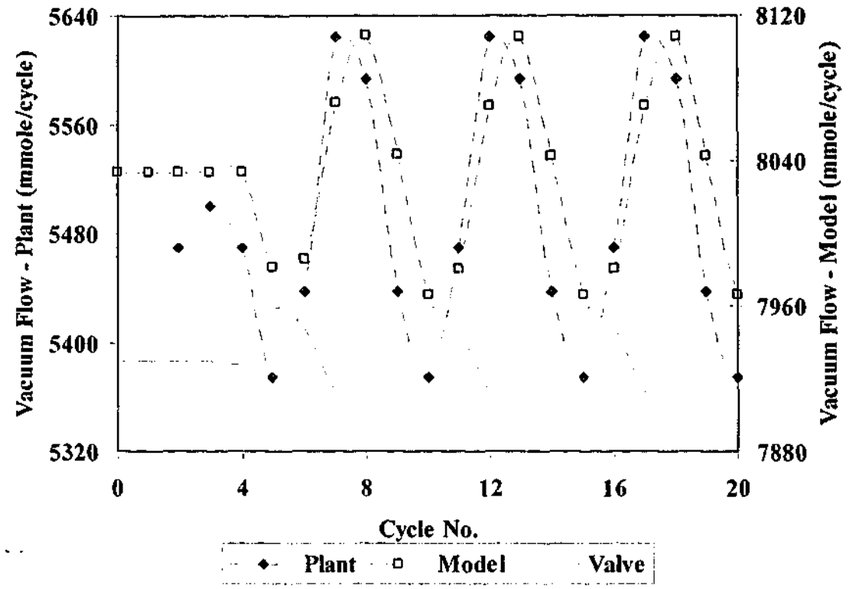

Figure 5.3.2d. Transient and CSS response of the vacuum flow variable at the end of step 2 to a purge valve frequency perturbation (amplitude 3, period 5) initated at cycle 5. CSS was attained within the next period of the valve cycle. Amplitude at CSS: pilot plant ~125 mmole/cycle; model 71.04 mmole/cycle.

Table 5.3.2a. Comparison of the CSS amplitude between plant and model for the system molar flows per cycle.

	Period (cycles)	Feed Valve (5% Amp.)		Purge Valve (3% Amp.)		Product Valve (10% Amp.)	
		Plant (mmole/ cycle)	Model (mmole/ cycle)	Plant (mmole/ cycle)	Model (mmole/ cycle)	Plant (mmole/ cycle)	Model (mmole/ cycle)
Feed Flow	5	406.3	334.98	78.1	0.0	31.3	0.0
	10	390.6	334.56	93.4	0.0	46.9	0.0
	15	375.0	349.44	109.4	0.0	31.3	0.0
Vacuum Flow	5	93.8	135.31	125.0	71.04	31.3	30.42
	10	140.6	197.29	125.0	67.24	46.9	43.54
	15	156.3	220.99	140.6	60.35	46.9	49.59
Product Flow	5	78.1	64.40	31.3	32.29	31.3	39.79
	10	109.4	95.93	31.3	42.36	46.9	61.10
	15	125.0	104.38	31.3	47.18	46.9	57.13

5.3.3 Product Composition Frequency Response

Although a range of frequencies was investigated for each valve perturbation, only the responses at a period of 10 cycles are presented and the results of a representative batch of frequencies summarised in Table 5.3.3a. A first-order model of the form discussed in Chapter 4, §4.5.3 was used to estimate the dead time and calculate the phase angle as described by Eq. (5.3.3a). This equation demonstrates that a phase lag can result even with negligible time delays. Also, the reader should note that some results from this section pertaining to the purge valve frequency response have been published [Beh and Webley, 2003d].

$$\phi = \left(\frac{180^\circ}{\pi}\right)\left[\tan^{-1}\left(-\omega\tau_p\right) - \omega\tau_D\right] \qquad (5.3.3a)$$

Figures 5.3.3a to 5.3.3c and Table 5.3.3a demonstrates the performance of the SoCAT purity model (detailed in Chapter 4, §4.4) for the prediction of the product concentration response in comparison with measured data. The model yields reasonable results with modest differences, capturing the frequency responses well (0.63% – 0.71% for the model compared to 0.39% measured by the pilot plant for the purge and product valves respectively). The feed valve case study experienced the greatest model error where the difference between the amplitude of the plant and model was up to 1.05% (as observed in feed valve period 5 run – see Table 5.3.3a). What is encouraging though, is that the observed trends, both transient and CSS, are captured by the model (model and plant both exhibit an increase in amplitude with decreasing frequency) and the phase angle predicted by the model matches experimental results. Table 5.3.3a also indicates that the phase angle decreased with an increase in the period of oscillation and was attributed to the time constant of the system (i.e. as ω decreased the system was permitted more time to respond due to smaller changes in valve position between cycles). Overall, the differences in the estimation of the absolute value of the composition variable are sufficiently small such that the application of this technique in the field for process monitoring or control would yield useable results as the oxygen purity is commonly permitted to drift within 1% to 2% of set point.

The reasons for the discrepancies between plant and model, alluded to in §4.5.3 of Chapter 4, can be summarised as follows:

1. Errors associated with the accuracy of the initial calibration of the SoCAT model was shown to differ, in terms of product flow, by up to 20 mmole/cycle, which correlates to a 0.6% difference between the absolute values of the plant and model (see Chapter 4).

2. Incorrect estimation of the control valve C_v boundary condition as input into SoCAT will cause incorrect prediction of the amplitude of the oxygen purity.

3. Reliability of the empirical fit and the experimental data. As indicated in Figure 4.4a of Chapter 4, the experimental data points showed a 2% scatter in purity for the same product flow. However, the model was able to correctly predict the transient responses, which is encouraging as signified in Figures 5.3.3a to 5.3.3c. As previously discussed in Chapter 4, for faster cycles such as rapid PSA, the assumption of 'instantaneous' product concentration leaving the adsorber vessels may no longer hold and model errors would be at their greatest.

4. The predominant cause of error between process and model is clearly highlighted from the frequency plots and has been attributed to poor mixing characteristics in the product tank. Unlike the step response case studies of Chapter 4 where the product stream purity showed 'instantaneous' movement or a transient response at the time of the disturbance (indicating that the composition dynamics within the product vessel are of an order greater than one), the frequency response data exhibited negligible transient dynamics as the change per cycle was less than that of a step test. The benefits of frequency response analysis is it permits investigation of the system dynamics at periodic stability where variables such as system dead times can be clearly observed and transient dynamics have ceased. In order to fit the SoCAT model to the pilot plant data the output of the model was delayed by the amounts shown in Table 5.3.3a. The variation in time delay indicated that the composition gradient present within the product tank varied as a function of the moles of oxygen and of the total moles entering and leaving the vessel. The common procedure used to analyse processes using frequency techniques is to fit and validate a model (either mechanistic or empirical) to experimental data and then develop a Nyquist curve (or Bode plot) at various frequencies once periodic stability has been achieved. The inability to characterise these nonidealities as a single, constant lumped parameter (i.e. the dead time, τ_D) therefore restricted the use of this technique in stability analysis as it was impractical to model the tank system in detail. Furthermore, nonidealities such as noise, sensor error and the presence of unknown and measured external disturbances inhibited the use of plant operating data for the development of frequency plots. Variables such as phase lags and dead times became difficult to determine from experimental data.

The individual responses shown in Figures 5.3.2a to 5.3.2c will now be discussed. The feed valve and product valve responses are conceptually simpler to envision and, as discussed in §4.5.3 of Chapter 4, cause direct movement of the adsorption front by allowing more and less

gas into or out of the adsorber column. The purge valve, on the other hand, is more difficult to comprehend and hence model. Its effect on the oxygen concentration profile are two-fold –

1. The purge valve varies the product concentration leaving the adsorber bed by shifting the position of the mass transfer zone axially (this may also cause some degree of dispersion of the adsorption front).

2. The purge valve alters the composition profile leaving each individual bed during the production step (steps 2 and 5 in Figure 2.2c) as purge gas of varying purity (typically high to low impurity) enters the bed receiving purge (as shown in steps 3 and 6 of Figure 2.2c).

For the purge valve case study, the oxygen purity exhibited a proportional relationship with valve position because the chosen amplitude of the perturbation, 3%, was significantly large for this region of operation (refer to Chapter 4, §4.5.3). Therefore, instead of purifying the bed receiving purge, nitrogen breakthrough was permitted and hence lowered the average composition per cycle.

Table 5.3.3a. Phase angle, amplitude and dead time estimation of the averaged oxygen concentration for the pilot plant and model to frequency perturbations.

Valve	K_p (%O_2/ %Valve Open)	τ_p (cycles)	Period (cycles)	τ_D (cycles)	ϕ (°)	Amplitude (% O_2)	
						Plant	Model
Feed (5% Amp.)	-0.765	5	5	3	-297	0.19	1.24
			10	4	-216	0.88	1.75
			15	4	-160	1.68	2.15
Purge (3% Amp.)	-0.3167	4	5	2	-223	0.20	0.32
			10	$1>\tau_D<2$	~-122	0.39	0.63
			15	2	-107	0.59	0.87
Product (10% Amp.)	-0.2925	6	5	3	-298	0.05	0.36
			10	4	-219	0.39	0.71
			15	5	-188	0.70	0.90

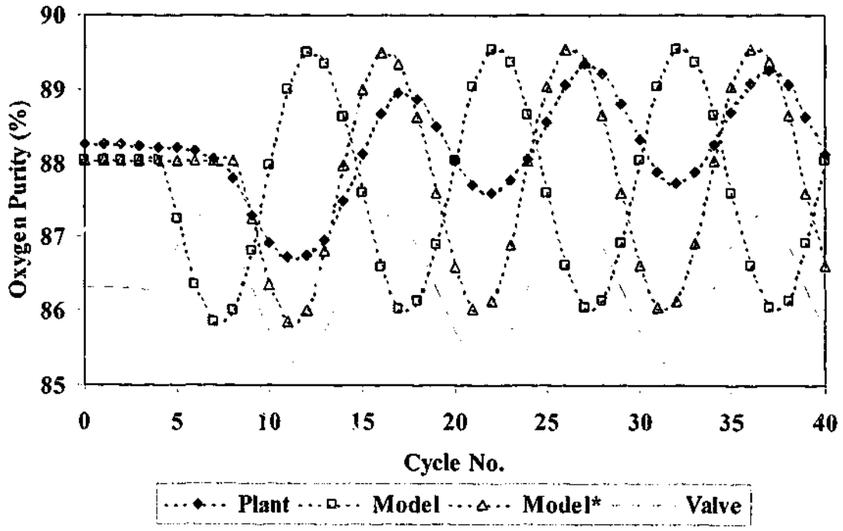

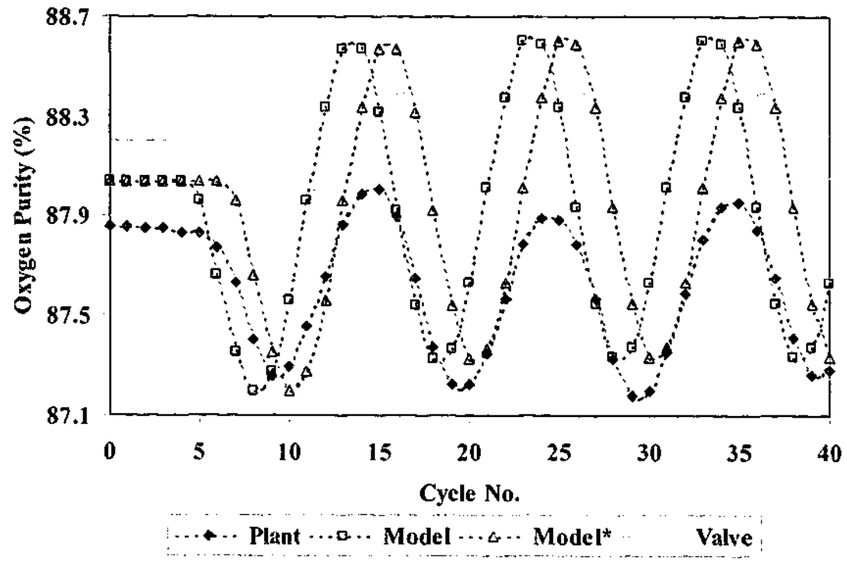

Figure 5.3.3. **(a) Cycle averaged oxygen purity response to a cyclic feed valve input of amplitude 5% and a period of 10 cycles. Pilot plant amplitude ~0.88%. Model amplitude ~1.75%.**

(b) Cycle averaged oxygen purity response to a cyclic purge valve input of amplitude 3% and a period of 10 cycles. Pilot plant amplitude ~0.39%. Model amplitude ~0.63%. Triangle data points shows the model output delayed by (a) four and (b) one cycles. Frequency perturbation initiated at cycle 5.

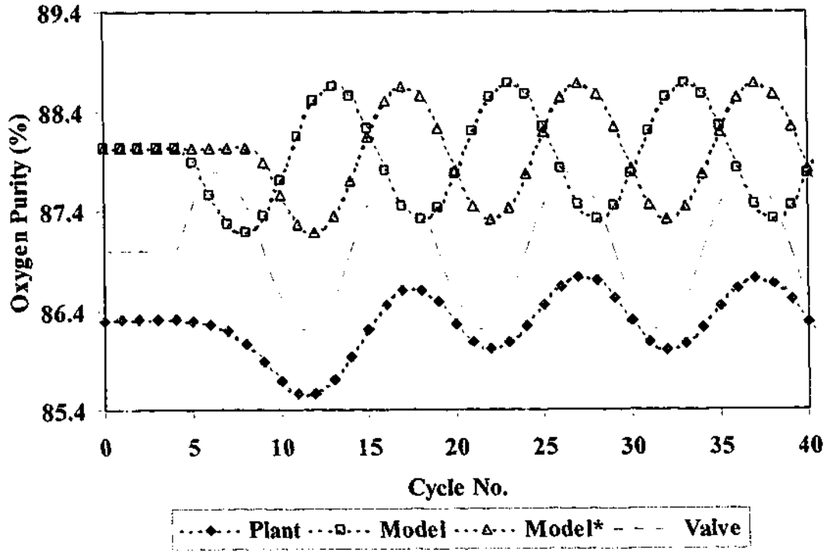

Figure 5.3.3c. **Cycle averaged oxygen purity response to a cyclic product valve input of amplitude 10% and a period of 10 cycles. Triangle data points shows the model output delayed by four cycles. Frequency perturbation initiated at cycle 5. Pilot plant amplitude ~0.39%. Model amplitude ~0.71%.**

5.3.4 Production Rate Frequency Response

Arguably, the production rate is considered to be the second most important variable in an adsorption process with parts of the literature devoted to its regulation and control [Rouge and Teuscher, 2001; Schaub *et al.*, 1995]. Both experimental and model responses of the oxygen production rate to periodic disturbances are shown in Figures 5.3.4a to 5.3.4c and summarised in Table 5.3.4a. The figures indicate that the response of this variable was dominated by the response of the product flow (refer to Eq. (4.5.4a) in Chapter 4, which describes production rate as a function of the product flow and the averaged product composition per cycle). As the feed, purge or product valve increased, the product rate follows in direct response with negligible phase lag at all frequencies as displayed by the figures presented in this section. In addition, the time delays associated with nonideal mixing conditions in the product tank, which was not modelled in SoCAT, contributed only modest errors to the response. This result was consistent with the step response data discussed in §4.5.4 of Chapter 4.

The product valve scenario, which revealed smaller amplitudes at lower frequencies (see Table 5.3.4a), produced a surprising anomaly. Intuitively, it was expected that an inverse effect

should have been observed as for the case with the feed and purge valve disturbances which revealed greater amplitudes at the lower frequencies for both the product flow and purity. The cause of these differences at various frequencies originated from the inverse response between the position of the product valve and the oxygen purity and the phase lag variation between frequencies. For instance, at lower frequencies the phase angle approached -180°, which results in the product flow being at its uppermost value and the oxygen purity at its lowest point at CSS (see Table 5.3.3a). Since production rate is a product of the two variables, the change in amplitude at the lower frequencies was not as pronounced as the higher frequency runs. On the other hand, at higher frequencies, when the product valve attained its lowermost position (which also coincides with the lowest point of the product flow), the oxygen purity had not yet achieved its lowest value since the phase lag was less than -180° (refer to Table 5.3.3a). This results in larger production rate amplitude changes with increasing frequency.

Table 5.3.4a. Comparison of the CSS amplitude between plant and model for the production rate variable.

Period (cycles)	Feed Valve (5% Amp.)		Purge Valve (3% Amp.)		Product Valve (10% Amp.)	
	Plant (kgPDc)	Model (kgPDc)	Plant (kgPDc)	Model (kgPDc)	Plant (kgPDc)	Model (kgPDc)
5	3.1	2.08	1.33	1.18	2.34	2.69
10	4.80	3.14	1.75	1.54	2.11	2.40
15	5.58	3.34	1.53	1.61	2.16	2.13

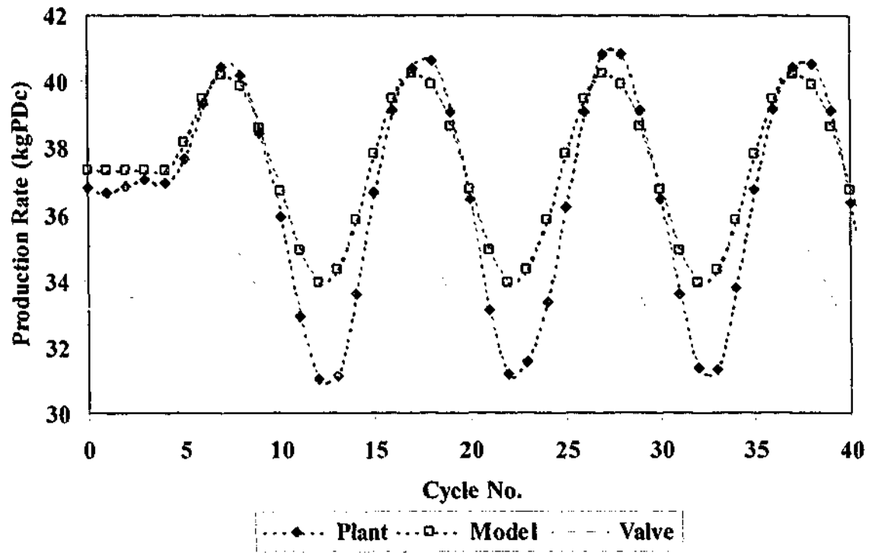

Figure 5.3.4a. Production rate response to a cyclic feed valve input of amplitude 5% and a period of 10 cycles. Frequency perturbation initiated at cycle 5. CSS amplitude: pilot plant ~4.80 kgPDc; model ~3.14 kgPDc.

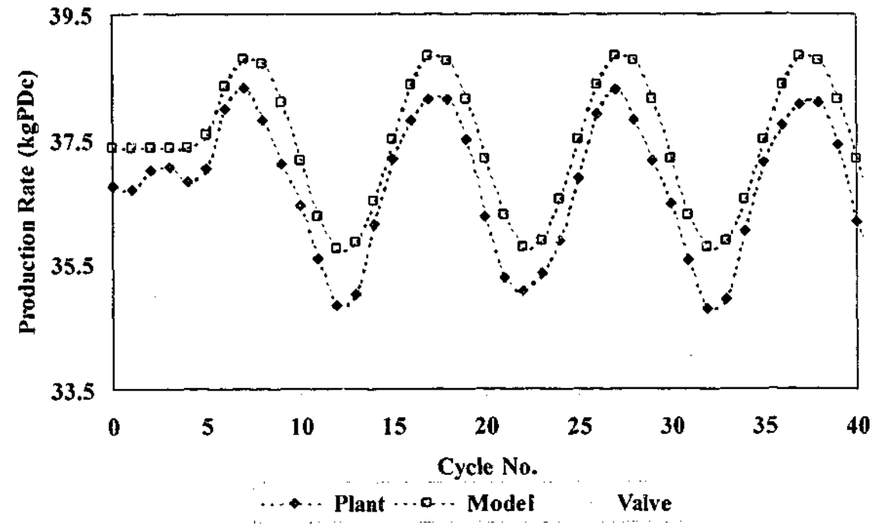

Figure 5.3.4b. Production rate response to a cyclic purge valve input of amplitude 3% and a period of 10 cycles. Frequency perturbation initiated at cycle 5. CSS amplitude: pilot plant ~1.75 kgPDc; model ~1.54 kgPDc.

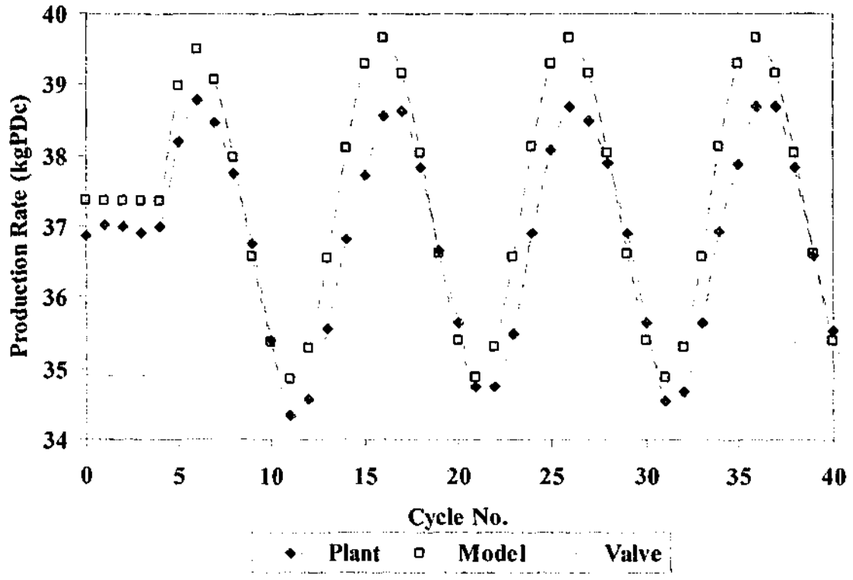

Figure 5.3.4c. Production rate response to a cyclic product valve input of amplitude 10% and a period of 10 cycles. Frequency perturbation initiated at cycle 5. CSS amplitude: pilot plant ~2.11 kgPDc; model ~2.40 kgPDc.

5.3.5 Frequency Response of the Thermal Profiles

For consistency and to aid brevity, plots of the thermal evolution presented in this section are selected from the feed valve perturbation case at various frequencies unless stated. This data has been determined as reasonably representative of the observed effects.

From the customer's perspective, temperature profiles and their evolution, are of no particular interest other than of physical curiosity. However, because adsorption is an exothermic process, examination of the thermal profiles provides insight into the movement of the thermal energy of the system and its closure. This is useful, as it is well known within the industry that seasonal and even diurnal variation can impact upon the performance of VSA/PSA plants. The results obtained from this study, however, indicated that for most of the periodic disturbances, the input signal had only marginal effect on the axial temperature profiles within the bed at constant inlet and ambient temperature. This in turn manifested itself in the oxygen purity variable, which displayed modest variations in amplitude and hence minor movement of the adsorption front as the valve in question cycles.

To illustrate this point, an examination of Figures 5.3.5a and 5.3.2b, which shows the response at high and low frequencies to a periodic feed valve perturbation in the main

adsorption section of the bed, indicated less variation in temperature at the higher frequencies for the same point in the bed (~1°C for the period 5 run and ~2°C for the period 10 run). This result was consistent with Table 5.3.3a, which also signified a modest variation in the oxygen concentration – the observed amplitude varied from approximately 0.19% to 0.88% at CSS for the period 5 and 10 runs respectively. In addition, Figures 5.3.5c and 5.3.5d shows the variation of the thermal mass at two distinct zones in the bed for the same period of oscillation. One sensor was positioned in the non-adsorbing zone (the cold-spot – located at the interface between the prelayer and the adsorbent layer) and the other in the oxygenated region (1.6m). Once again both thermocouples exhibited either negligible (at the cold-spot) or modest (~0.4°C at 1.6m) movement in temperature which indicated minimal heat of adsorption and/or convected thermal energy.

The transient response of the thermocouple located in the adsorption zone for the product and feed valve scenarios are presented in Figures 5.3.5e and 5.3.5f respectively. The transient response to the feed valve was similar to that at CSS (refer to Figure 5.3.5b), however, it is difficult to discern the response of the product valve input (Figure 5.3.5e). This is likely to be due to a difference in the relative movement of the thermal profile to a disturbance between the feed and product valve case studies (compare Figures 4.5.5b and 4.5.5d in Chapter 4 which showed differing thermal response across the bed for the same purity response).

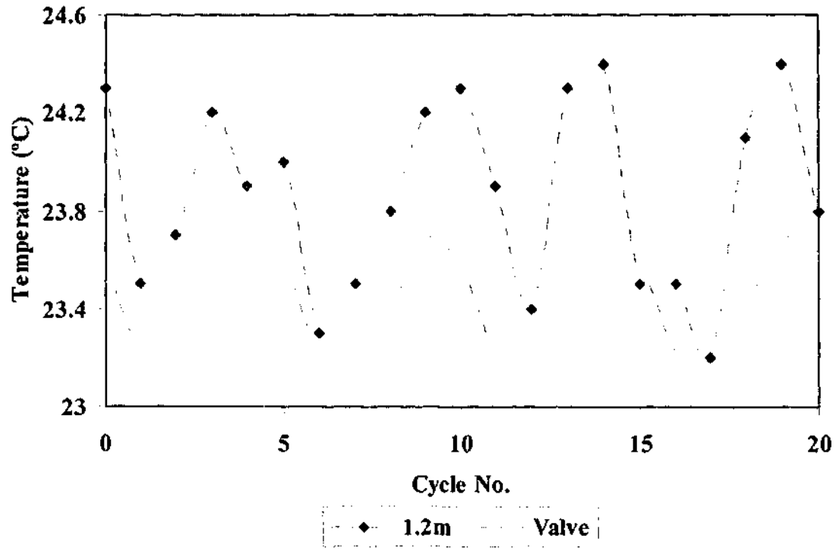

Figure 5.3.5a. CSS response of the thermal profile at an axial position of 1.2m in bed 1 at the end of step 2 to a feed valve frequency perturbation (amplitude 5, period 5).

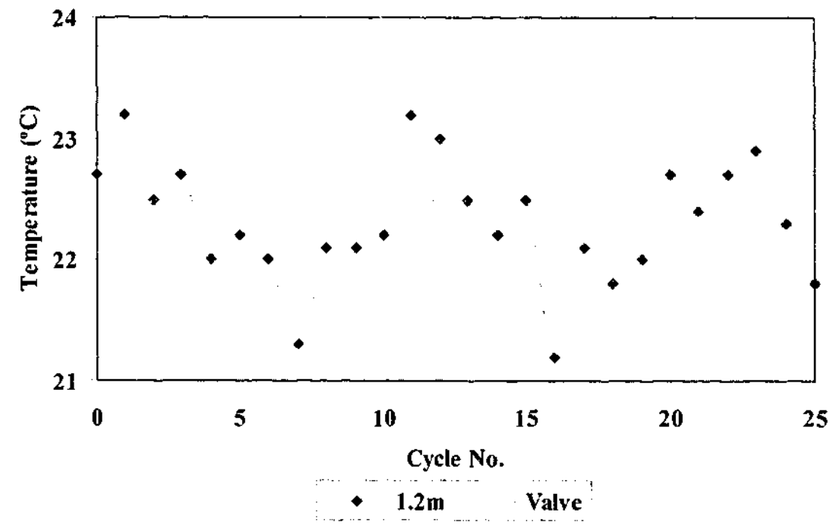

Figure 5.3.5b. CSS response of the thermal profile at an axial position of 1.2m in bed 1 at the end of step 2 to a feed valve frequency perturbation (amplitude 5, period 10).

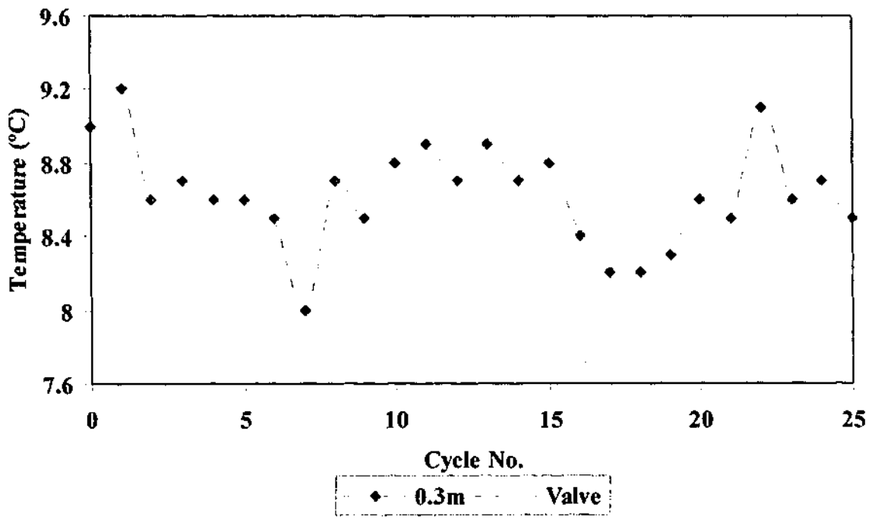

Figure 5.3.5c. CSS response of the thermal profile at an axial position of 0.3m ('cold-spot') in bed 1 at the end of step 2 to a feed valve frequency perturbation (amplitude 5, period 10).

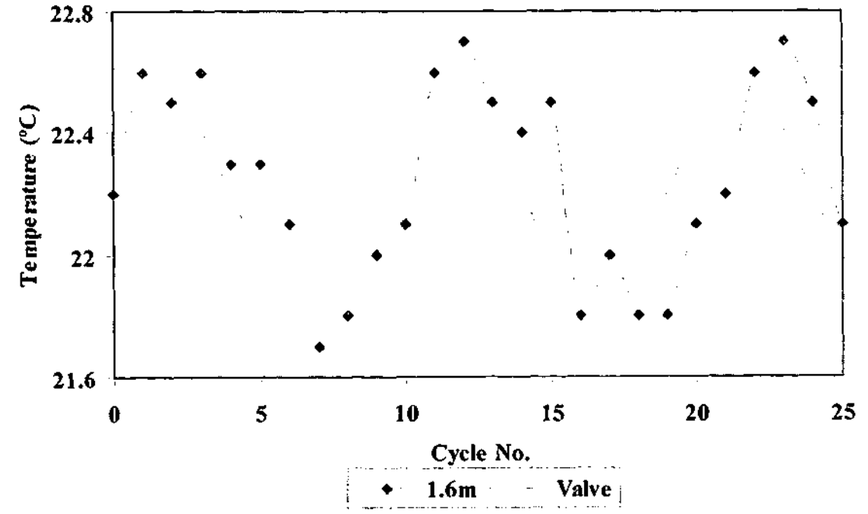

Figure 5.3.5d. CSS response of the thermal profile at an axial position of 1.6m in bed 1 at the end of step 2 to a feed valve frequency perturbation (amplitude 5, period 10).

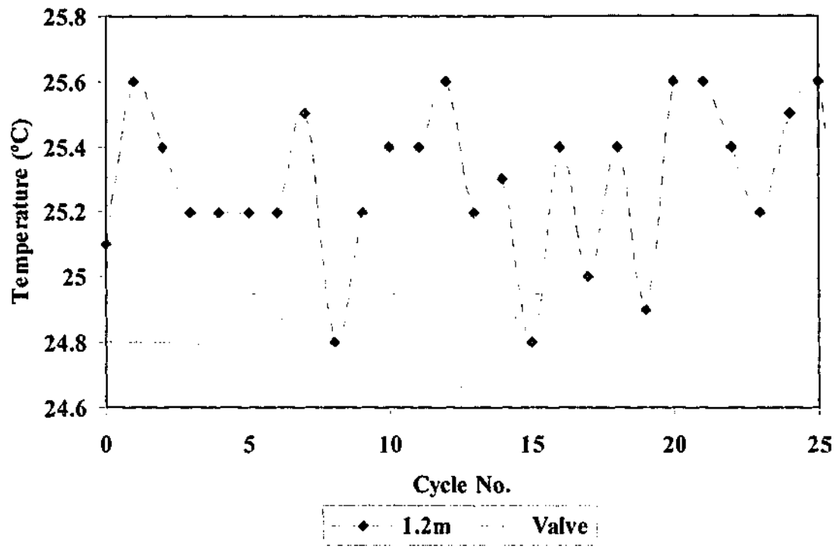

Figure 5.3.5e. Transient response of the thermal profile at an axial position of 1.2m in bed 1 at the end of step 2 to a product valve frequency perturbation (amplitude 10, period 10) initiated at cycle 5.

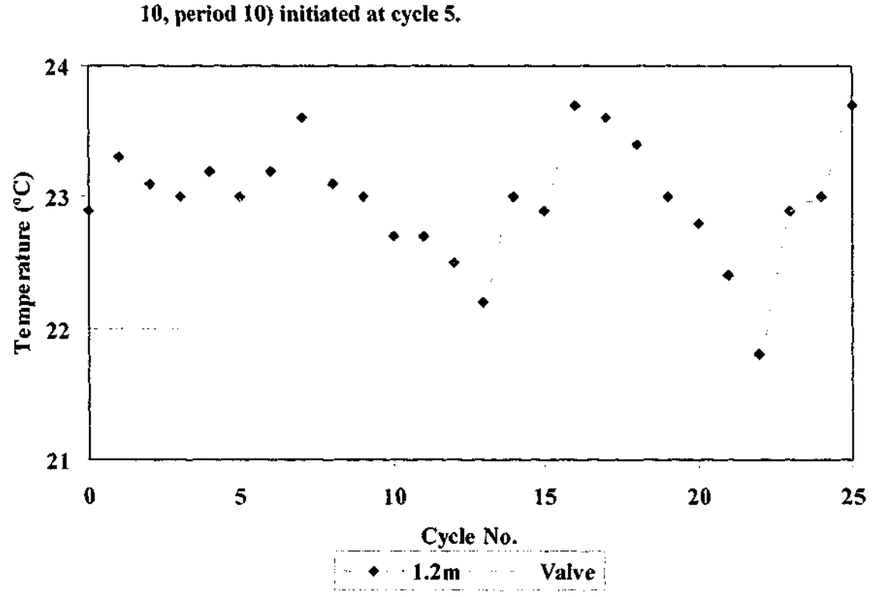

Figure 5.3.5f. Transient response of the thermal profile at an axial position of 1.2m in bed 1 at the end of step 2 to a feed valve frequency perturbation (amplitude 5, period 10) initiated at cycle 5.

5.4 CONCLUDING REMARKS

Three periodic case studies were examined in this chapter involving the feed, purge and product valves and further confirmed the utility of the lumped parameter model, SoCAT, in capturing the trends, (from transients through to the periodic steady state), observed in a pilot-scale oxygen VSA plant. As a result, the complexities involved in modelling such a system, which is highly nonlinear, can be attributed primarily to changes in bulk flow and pressure conditions (as suggested in Chapter 4 and supported through this study). In addition, this chapter has demonstrated the amplitudes of the periodic perturbations, which are also the perceived maximum controller actions, are within the linear range of operation allowing linear frequency analysis techniques to be used.

The observed responses can be summarised as follows. Firstly, it was demonstrated that a phase lag could result due to coupling of the adsorbent beds and the instance within the cycle when the measurement was made (refer to the discussion of the bed and product pressure). Also, product pressure and flow, the product oxygen purity and production rate all displayed inverse relationships between amplitude and frequency with the exception of the production rate response to the product valve. This was attributed to both the reverse action of purity with product valve position and also on the period of perturbation. Lastly, an examination of the temperature profiles indicated that there was negligible variation over the period of the perturbation further reinforcing the validity of the isothermal simulator.

The main cause of mismatch between plant and model was the assumption of a constant bulk composition highlighted by the pressure history of the adsorbent bed undergoing evacuation (desorption). Furthermore, additional sources of error were determined for the empirical purity model such as calibration of the valve flow coefficients and the availability of reliable experimental data in which to establish a relationship between total product flow and product concentration that caused predictive errors in the simple oxygen purity model. However, the primary cause of mismatch between process and model (that had been identified in Chapter 4 and confirmed through this study) was the inherent nonidealities that exist within product tank of the pilot plant. This is because once the transient dynamics ceased and periodic stability was attained, variables such as system dead times could be clearly observed, which further emphasises an advantage of frequency response methods over step response techniques. However, the dependence of the time delays in the system to process flows has unfortunately meant that it has not been possible to apply frequency response methods to analyse the closed loop stability and controller pairings and tunings.

In closing, this chapter suggests that most of the physics of the processes has been correctly assumed and emphasises the usefulness of SoCAT as the basis for a model-based control structure or for processes monitoring. Analysis of the system using frequency response enables

the practitioner to determine the parameters of importance and consequently develop reduced-order models for diagnostics, modelling and control.

NOMENCLATURE

A, B	amplitude of input and output signal respectively
t	time variable (s)
ϕ	phase angle (rad or deg)
ω	angular frequency (rad/s)

Chapter Six

Single Loop Control

The requirement for regulation of various design variables has become increasingly important as the use of PSA technology increases, spurring a greater effort in the application of process control theory. This chapter discusses the implementation and performance of both PID and a model-based control algorithm for PSA control of the pilot oxygen VSA plant. Single loop control of the oxygen purity variable (arguably the variable of most importance) will be the primary focus of this chapter. The intention is to demonstrate the practical application of PID to a periodic/batch system, to show the design and implementation of a novel model predictive controller and to compare the performance between PID and model predictive control for both load rejection and set point changes.

6.1 INTRODUCTION

Adsorption processes, such as PSA and VSA, have become common methods for the separation of various fluids as discussed in Chapter 1 and yet very little attention in the field of process control has been given to this important unit operation (as suggested in a literature search conducted in Chapter 1). The intent therefore of this chapter is to focus on the control of a method for air separation to produce a purified oxygen product. The industrial interest in control of these processes stems from the fact that disturbances can cause serious compromises in performance, which implies huge financial burdens to a customer. Table 1.5a in Chapter 1 highlights the consequences of controller failure from an industrial perspective and shows that in most cases where off-spec product is produced, expensive liquid oxygen (LOX) must be provided until controllability of the plant is once again achieved. From an academic perspective, these processes contain severe nonlinearities – they operate under unsteady state, non-equilibrium conditions and there is a relatively high degree of coupling between boundary conditions and the output (performance/design) variables. In addition to these complications, there is usually more than one variable of interest to control further escalating the control problem. The last difficulty associated with these systems is that most industrial VSA/PSA processes operate in a cyclic manner, which may spur some interest in this field, as the current control theory is still in its infancy in terms of control of periodic or batch processes.

Given the limitations of the previous efforts in the control of these processes, the objectives of this study are two-fold. In this chapter, various control schemes are demonstrated and applied for the control of the most important variable – the product oxygen concentration in an oxygen VSA process. The work presented in this chapter is based on previous research efforts by Beh and Webley (2003e) and Beh and Webley (2003f). Firstly, the practical implementation of a batch-wise PID algorithm will be discussed – this avoids the problems with continuous control (refer to Beh *et al.* (2000)). This batch-wise PID algorithm will then be applied on a pilot-scale oxygen VSA plant. The second objective is to present the design of a model predictive control (MPC) structure and demonstrate its application and performance on the same plant. The chapter will conclude by discussing the benefits and limitations of PID compared to the advanced control technique for a single loop system in terms of both load rejection and set point change.

6.2 CONTROLLER PAIRINGS AND CASE STUDIES

The VSA cycle utilised in this study is typical of current industrial practice and is implemented on a pilot oxygen VSA plant. Rather than utilising a simulation environment to test the controllers, it was envisaged that the less well-defined experimental conditions would provide a veritable and severe challenge for the controllers. Kershenbaum (2000) offers several reasons and advantages for testing controllers under laboratory or field conditions. A detailed description of both the VSA cycle (refer to Figure 2.2c) and the oxygen VSA pilot plant is contained in Chapter 2.

For single loop control the suggested pairing of the product valve, CV4 in Figure 2.2c of Chapter 2, with oxygen purity should be used. This has been established in §4.7 of Chapter 4 through the use of the method of relative gain (RGA) analysis and the robustness of these pairings tested by statistical means. The proposed control schemes sample once every cycle (i.e. $\Delta t_c = 1$) at the end of the feed step (step 2 in Figure 2.2c,) and the controller action is output at the same time updating the plant at the next cycle. For this reason, an in-house batch multiple loop PID controller was designed as most commercial algorithms function in real-time. Also, it was foreseen that incorporation of the model-based decoupling scheme (in Chapter 7 of this study) would be easier than modifying third-party software.

By using the control loop pairing mentioned above, the performance of each controller is tested by subjecting the process to a known and measurable disturbance and tracking the output of the plant and controller with time. Changes in ambient temperature, due to both diurnal and seasonal fluctuations, represent the most common disturbance in the field for an O_2 VSA process. This type of disturbance affects both the inlet stream temperature and the amount of heat lost or gained by the adsorbent beds and can alter the adsorptive capacity of the zeolite

sieve. It is through this mechanism that the performance of the process can vary. Other field disturbances commonly associated with changes in performance are fluctuations in inlet pressure and/or flow and fluctuations in downstream product pressure. The first two disturbance variables (temperature and inlet pressure/flow) are not easily implemented in the laboratory situation. Instead this investigation will focus on varying the system back pressure in a step-like manner from atmospheric conditions to 5 kPa above atmosphere. This test is performed in the laboratory by placing the product outlet into a tank of water, which is realistic as it simulates conditions observed in practice whereby a customer's downstream demand decreases or a pipe/filter blockage occurs. The scenarios investigated in this study are as listed below.

Case 1. Testing the load rejection performance of the control system by applying two sequential step changes in load, which represents a difficult task for any controller. This is accomplished by initiating a 5 kPa back pressure on the system for 40 cycles – implemented at cycle 5 and removed at the start of the feed step (step 2 in Figure 2.2c). This load disturbance represents a change in the system back pressure in field operation due to sudden variations in downstream requirements or pipe work blockages.

Case 2. Testing the performance of the controller to a 5% set point change in oxygen purity. The set point change is initiated at cycle 5 at the start of the feed step (step 2 in Figure 2.2c) and sustained throughout the course of the run. The set point change represents a situation whereby a customer's demand changes due to equipment maintenance or shutdown. It should be noted that this case is of lesser importance than the performance of the controllers under load disturbances as the main task of a controller is to maintain plant operation at its design condition.

6.3 PID CONTROL AND PRACTICAL IMPLEMENTATION

According to a recent study, more than 90% of all control loops are in the form of the PID algorithm with the use of this type of feedback control predicted to continue in the future [Åström and Hägglund, 2001]. The standard or non-interacting feedback PID control algorithm is arguably the most commonly practiced form of the algorithm and is described by Eq. (6.3a) below. Performance of this algorithm will be utilised as the basis for comparison against all other control techniques. To aid generality, as Chapter 7 will refer to this section, the controller is described in terms of a general $N \times N$ control structure where the half arrows on top of the variables represents vector quantities. The change in manipulated variable, $d\vec{m}(t)$, is given by

$$d\bar{m}(t) = \bar{K}_c\left(\bar{e}(t) + \frac{1}{\bar{\tau}_i}\int_0^t \bar{e}(t)dt + \bar{\tau}_d\frac{d\bar{e}(t)}{dt}\right) \tag{6.3a}$$

where t in this case is cycle number and the error is usually defined as

$$\bar{e}(t) = \bar{S}_p - \bar{c}(t) \tag{6.3b}$$

However, if the manipulated variable has an inverse influence on the variable to be controlled then the result of Eq. (6.3b) is multiplied by -1. Such is the case when the product valve is paired to control the outlet concentration. The non-interacting/standard PID algorithm described in Eq. (6.3b), is implemented in the full-position form as detailed in Eq. (6.3c) below. The manipulated variable is then updated with reference to its initial condition at the commencement of the controller action (Eq. (6.3d)).

$$\Delta m(t) = K_c\left[e(t) + \frac{\Delta t_c}{\tau_i}\sum_0^t e(t) + \frac{\tau_d}{\Delta t}\left(e(t) - e(t-\Delta t_c)\right)\right] \tag{6.3c}$$

$$m(t+\Delta t_c) = m_0 + \Delta m(t) \tag{6.3d}$$

where t is the cycle number, Δt_c the controller sampling interval and m_0 is the initial value of the manipulated variable at $t(0)$. This form of the PID algorithm is becoming more commonly used for a number of reasons. Firstly, the advantage of using the non-interacting controller above is that by adjusting the controller gain, K_c, the contribution of the integral and derivative terms also changes, which may ease loop tuning [GE Fanuc Automation, 1996]. Also, unlike the parallel algorithm where each of the PID terms are independent of each other, adjustment of the proportional gain does not affect the phase angle of the controller [Shinskey, 2002]. The positional algorithm was used as the digital form of the standard PID algorithm. This method has several distinct benefits over the velocity format, which is based on the rate of change in error. The most significant limitation of the velocity algorithm is its poor performance when noise is present in either the sensor measurement or inherent in the process [Liptak, pp.33, 1995] and plant data is typically noisy. It is for this reason that the positional form of the non-interacting algorithm was chosen although once tuned, the closed loop performance of the two is identical [Liptak, pp.33, 1995].

One of the properties of the PID algorithm is that it is simple to add non-linear characteristics that can assist the performance of the controller. This attractive feature, aside from its general ease of operation and variety of permutations, is another reason why this algorithm is so well utilised. For field implementation, the algorithm described above also contains the following features that are used for plant control.

1. Controller Dead Band

In most practical cases, exact control is not necessarily required due to instrument errors or allowable system tolerances. In this case, the process set point can span over a fixed range and if the system is operating within this region, the generated error term at the current sample interval is zero. Another benefit in setting the sample error to zero and defining the error as a function of the controller dead band is that wind-up of the integral term (in a PID algorithm) resulting in a 'controller-kick' is avoided. This is best described in Eqs. (6.3e) to (6.3g).

$$\text{If} \quad \left(S_p - DB_{\min}\right) \le c(t) \le \left(S_p + DB_{\max}\right) \quad \text{then} \quad e(t) = 0 \tag{6.3e}$$

$$\text{If} \quad c(t) < \left(S_p - DB_{\min}\right) \quad \text{then} \quad e(t) = \left(S_p - DB_{\min}\right) - c(t) \tag{6.3f}$$

$$\text{If} \quad c(t) > \left(S_p + DB_{\min}\right) \quad \text{then} \quad e(t) = \left(S_p + DB_{\min}\right) - c(t) \tag{6.3g}$$

It should be noted that this does not signify that the PID output is zero (refer to Eq. (6.3c)) as the accumulation of previous non-zero error samples will force a non-zero change in $m(t)$.

2. Clamps on the Manipulated Variable

In some instances, an engineer may wish to limit either the minimum or maximum range of movement of a particular input variable. Reasons for this can be to safeguard a reactor by preventing flow reaching dangerous levels or in the case of the oxygen VSA processes, limiting the minimum value of the purge valve so that sufficient purge gas is permitted to maintain product purity or to prevent the possibility of an over-pressure situation occurring, resulting in destruction of the adsorbent beds. This feature is mathematically described Eq. (6.3h).

$$m_{\min} \le m(t) \le m_{\max} \tag{6.3h}$$

3. Slew Rate Clamps

As discussed in the section above, the engineer may also wish to limit the movement of the manipulated variable over the controller sample period. This, in essence, dampens the controller response to infrequent disturbances or large set point changes and is given by Eq. (6.3i).

$$\frac{dm_{min}}{dt} \leq \frac{dm}{dt} \leq \frac{dm_{max}}{dt} \tag{6.3i}$$

PID Controller Tuning

The PID tuning procedures used in this study are based on those first derived by Zeigler and Nichols (1942). A first-order-plus-dead time (FODT) dynamic model of the process was fit and validated with experimental data obtained through step [Beh and Webley, 2003b] and frequency responses. Equation (6.3j) describes the form of the FODT model, which was solved in terms of deviation variables ($O \equiv$ change in product oxygen concentration and $V \equiv$ change in product valve position).

$$\frac{dO(t)}{dt} + \frac{1}{\tau_p} O(t) = \frac{K_p}{\tau_p} V(t - \tau_D) \tag{6.3j}$$

where K_p is the process gain, τ_p the process time constant, τ_D the system time delay and t in this case has the time units of cycle number (i.e. $t \in$ N, where N = 0, 1, 2, 3, ...). Figure 6.3a shows the response of both the FODT model and pilot plant to a load disturbance and reveals satisfactory correlation between the two.

The initial controller gains were calculated based on the slopes of the FODT response curve for a 1% change in input and further refined through process simulation by minimising the integrated absolute error (IAE) (Eq. (6.3k)).

$$\text{IAE} = \int_0^t |e(t)| dt \tag{6.3k}$$

6.4 MODEL PREDICTIVE CONTROL STRUCTURE AND IMPLEMENTATION

An alternative structure to the PID algorithm is model predictive control with several informational survey papers discussing this subject in terms of the theory and theoretical developments, its application and its future prospects [Bequette, 1991; Froisy, 1994; Garcia *et al.*, 1989; Henson, 1998; Mayne *et al.*, 2000; Qin and Badgwell, 1997; Qin and Badgwell, 2003]. Algorithms such as dynamic matrix control (DMC) [Cutler and Ramaker, 1980], internal model (IMC) [Garcia and Morari, 1982] and the Smith predictor [Smith, 1957] represent some of the better established and studied MPC structures that have been applied to a fairly broad range of process control problem with reasonable amount of success. There has been, however, some contention in the past between the proponents of PID and MPC [Shinskey, 2001] but the benefits of this technology, attested by past applications [Froisy, 1994; Garcia *et al.*, 1989; Cutler and Ramaker, 1980; Qin and Badgwell, 1997; Qin and Badgwell, 2003], cannot be ignored and is the primary reason why model-based control was investigated for the VSA process. In this study, the use of traditional MPC structures will not be employed, instead the development of a unique MPC controller will be discussed as it was envisaged that implementation of this controller would better suit this process. Nevertheless, the established MPC formats do lend themselves to future research in this area.

Figure 6.4a depicts the block diagram of the MPC controller developed for the regulation of a general N x N process. It should be noted that the study of this control scheme is still in its infancy and therefore its full potential has yet to be realised. In the heart of the MPC controller is the predictive algorithm represented by the transfer function G_{FF} in Figure 6.4a. This architecture differed from the structure inherent in other MPC controllers in that the set point was not altered by the difference between the model and process output. Instead, the MPC controller predicted the future plant input by direct inversion of the process model such that the predicted error was minimised as described by Eq. (6.4a).

$$\bar{f}_{min} = \bar{e}(t) = \bar{S}_p - \bar{c}_{FF}(t) = 0 \tag{6.4a}$$

The output variable, c_{FF}, is defined as

$$\bar{c}_{FF}(t) = \bar{c}(t)_{measured} + \Delta\bar{c}_{FF}(t) = 0 \tag{6.4b}$$

where Δc_{FF} was determined by integration of a numerical process model. Δc_{FF} was calculated initially by using the PID algorithm to guess a value for Δm_{FF} (as $\Delta c_{FF} = g(\Delta m_{FF})$) and then an

unconstrained nonlinear search for Δm_{FF} was conducted such that Eq. (6.4a) was satisfied. This method relied upon the use of a multidimensional or a single degree of freedom search in the case of single loop control, Newton-Raphson scheme coupled with a line search algorithm [Press *et al.*, 1997]. The established value of Δm_{FF} was filtered through a first-order filter, G_f, to dampen the predictive controller output as described by Eq. (6.4c).

$$\frac{d(\Delta \bar{m}_f(t))}{dt} + \frac{1}{\bar{\tau}_f}\Delta \bar{m}_f(t) = \frac{1}{\bar{\tau}_f}\Delta \bar{m}_{FF}(t) \tag{6.4c}$$

The new manipulated variable was sent to the process at the next sample interval as

$$\bar{m}_{FF} = \bar{m}_0 + \Delta \bar{m}_f \tag{6.4d}$$

where m_0 was updated with the value of the manipulated variable at the end of each set point trajectory. Experience has shown that if m_0 was not updated, the controller performance was both erratic and highly oscillatory.

Recognising that it is physically unrealistic to achieve the desired value within the next sample interval due to the time constant and the inherent system time delays, the set point was altered in a smooth manner such that it progressed from the current operating value to the nominal desired value over a fixed time horizon. In this case, a linear set point trajectory was utilised and implemented in the following form

$$\bar{S}_p = \left(\frac{\bar{S}_{p,nom} - \bar{c}_0}{\bar{T}}\right)t + \bar{c}_0 \tag{6.4e}$$

Equation (6.4e) is represented in Figure 6.4a as the transfer function G_{SP} and the gradient was automatically updated at the end of each time horizon.

The utility of the MPC controller stems from the fact that it is able to predict the plant output due to the process model that it is based on. However, process/model mismatch can cause unstable controller action and can manifest itself in four ways. The first source of mismatch is the process model, which may not be an accurate depiction of the system (physics of the system is not properly described) or secondly, the process has time delays that cannot be accurately identified. The dead time of the system is a noninvertible component and cannot be incorporated into the inverted process model of the MPC controller. If the time delay is large, it may cause significant differences in the derivatives calculated by the model inducing controller failure. The

third source of mismatch is due to scheduling, which occurs when the MPC controller is initiated when the process is not at steady state. Integration of the process model will generate a difference in output between the controller and the plant. The last and major cause of variance between process and model is due to differences in boundary conditions that are not captured in the model. Unmeasured load disturbances represent the primary source of variances in boundary condition (even if a perfect model was used with negligible scheduling errors). This is shown as an input to the actual process, G_p, in Figure 6.4a as the load, L, which enters with its own dynamics, G_L. In other words, the change in plant output, Δc_P, is a function of all the boundary conditions such that $\Delta c_P = f(\Delta m_1, \ldots, \Delta m_j, L_1, \ldots, L_n)$. For the single loop case, because $\Delta m_j|_{j \neq 1} = 0$, the controller process model is only a function of Δm_1 (i.e. $\Delta c_m = g(\Delta m_1)$). It can be seen that $\Delta c_P = \Delta c_m$ only if all the disturbance variables, L_n, are zero. In order to minimise the effects of mismatches, a feedback controller, G_{FB}, was placed in parallel with the MPC structure such that its output is additive to that of G_{FF} as shown in Figure 6.4a. For this particular control architecture, a PID algorithm of the form described in Eq. (6.3c) was used in the feedback mode.

The process model utilised by the MPC controller was a simple first-order differential equation describing the dynamics of the concentration variable for the single loop case [Beh and Webley, 2003b]. It was implemented in terms of a deviation variable and of similar form to Eq. (6.3j) with the time delay element, τ_D, (a noninvertible element) removed.

The remaining item of importance in Figure 6.4a is the block diagram showing "< >". This symbolises the manipulated variable limiters such as the maximum and minimum value and slew rate clamps as described in the PID algorithm section. The option of placing dead bands about the set point was omitted from the MPC structure because the action of the dead band is to constrain the input variable and hence the controller's region of search. If the dead band on one or more variables were set unknowingly large, the control action would be artificially hindered and a global minimum (i.e. the ability to set the error vector, Eq. (6.4a), to zero) may not ever be found.

MPC Controller Tuning

For this MPC controller, the primary tunable parameters are the set point time horizon, T, and the time constant of the first-order filter, τ_f. Controller tuning involved setting these values such that the IAE was minimised through simulation studies. Once the appropriate parameters had been achieved, the gains of the feedback controller, G_{FB} were set. Generally, these gains should be sufficiently small and were only used to compensate for the differences between process and model and to dampen oscillatory behaviour on the approach to steady state.

As a last point of note, one may notice the generality of this MPC structure as it permits the user to define the extent of the contribution of the feedback action. This feature may be useful in certain applications (i.e. by utilising larger filter time constants the contribution of the feedback controller would increase).

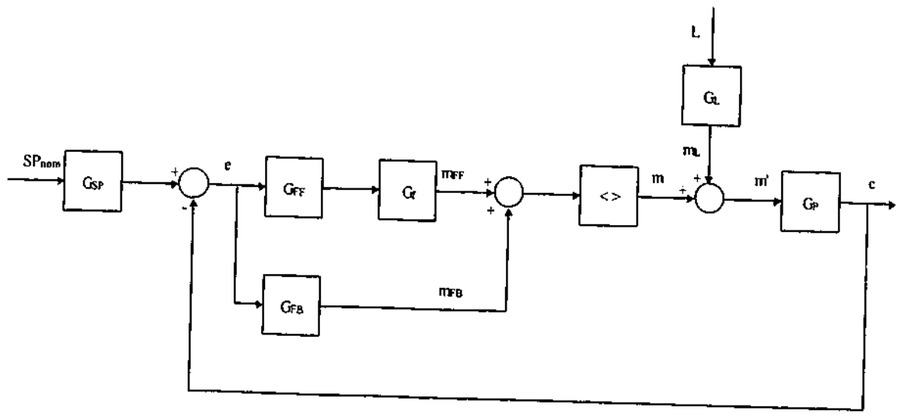

Figure 6.4a. Block diagram of the proposed MPC control structure.

6.5 RESULTS AND DISUSSION

Table 6.5a summarises the performance of each of the controllers in terms of both load rejection and set point change and compares the performance of the controllers in the simulation environment and in the field. The value in brackets under the MPC simulation IAE refers to the MPC controller without assistance from the feedback controller, which reveals marginally worse performance than if feedback action was implemented. The results of each case study will be discussed in detail below.

Table 6.5a. Controller performance.

Controller Type	Plant IAE	Simulation IAE
Load Rejection		
No Control	179	168
PID	89	72
MPC	104	86 (90)
Set Point Change		
PID	39	41
MPC	122	81

Case 1. Response to a 5 kPa product load disturbance.

Figure 6.5a shows the system response to a load disturbance entering as a pulse at cycle 5 for 40 cycles with no controller action causing the oxygen purity to increase by 4% – 4.5% from its baseline value. The FODT model used to study the dynamics of the controllers whilst offline shows reasonable correlation to the plant characteristics. This was not captured by the IAE values in Table 6.5a, which indicated a modest difference between the plant IAE and simulation. This difference can be attributed to the oxygen purity variable not returning to its initial value before the disturbance but instead being offset by approximately 0.4% from cycles 50 to 100. The cause of this offset may be due to other disturbances such as ambient changes or more likely, slight variations in the inlet pressure or flow, which signifies the sensitivity of the system to process perturbations. It is for this reason that the set point for the controllers varied slightly between each run in Figures 6.5b to 6.5e by about 1%.

As expected, the load rejection characteristics of both the single loop PID and MPC controllers revealed a significantly improved IAE compared to the case with no control as shown in Figures 6.5b and 6.5c. Both controllers were able to attain set point within 25 cycles from the initiation of the product load change. However, the PID algorithm resulted in a better response exhibiting smoother transitions to cyclic steady state than the MPC controller (which only attained a stable value between cycles 150 to 200). This was not truly indicative of the performance of the MPC controller, as improved tuning may result in a more complementary or

better match to that of PID. What is promising though, is that the process is able to follow the set point trajectory planned for it by the MPC algorithm.

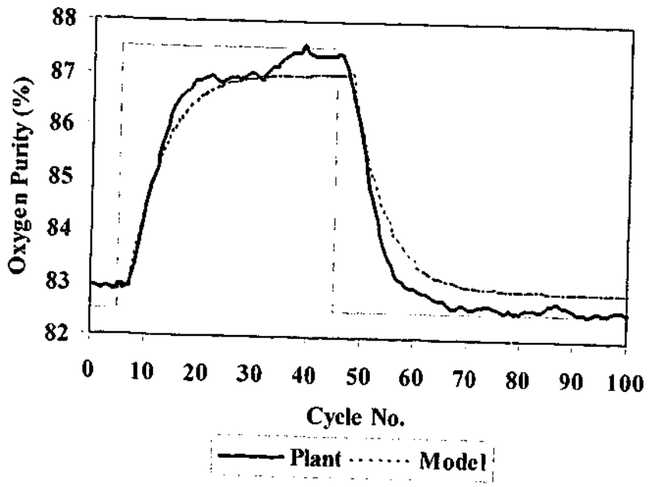

Figure 6.5a. **Response of the product oxygen variable with no control. IAE_{Plant} = 179, IAE_{Model} = 168.**

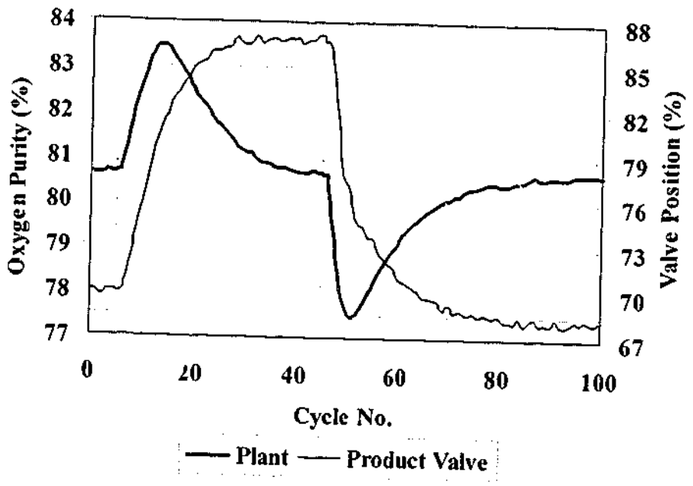

Figure 6.5b. **Single loop PID control of the oxygen purity variable using the product valve. Set point 80.65%, IAE = 89.**

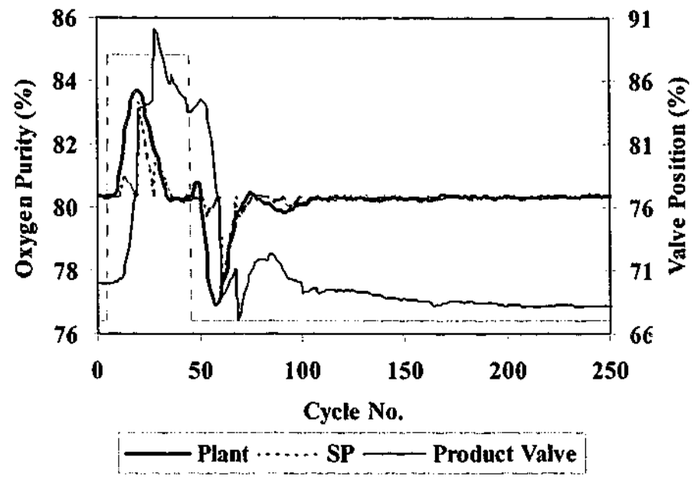

Figure 6.5c. **Single loop MPC control of the oxygen purity variable using the product valve. Set point 80.35%, IAE = 104.**

Case 2. 5% O_2 set point change.

The system response for the second case study whereby the set point was stepped by 5%, revealed a greater difference in performance between the PID and MPC algorithm. It is worthwhile noting that both controllers were tuned for load rejection and these same controller parameters were used during the set point tests. Figure 6.5d shows that the PID algorithm closes the product valve within 5 cycles and hence the product concentration increased as the adsorption front was pushed back further into the bed. It then maintained this value indefinitely until set point was reached. The MPC controller, on the other hand, exhibited an oscillatory motion until the nominal set point was attained (refer to Figure 6.5e). This was in part due to the set point trajectory taken and the sensitivity of the controller to noise and model errors. It is conceivable that process noise and model mismatch was the cause of the difference between the IAE in the simulation case and the actual controller performance as shown in Table 6.5a. As for the load rejection scenario, the plant follows the set point trajectory relatively well.

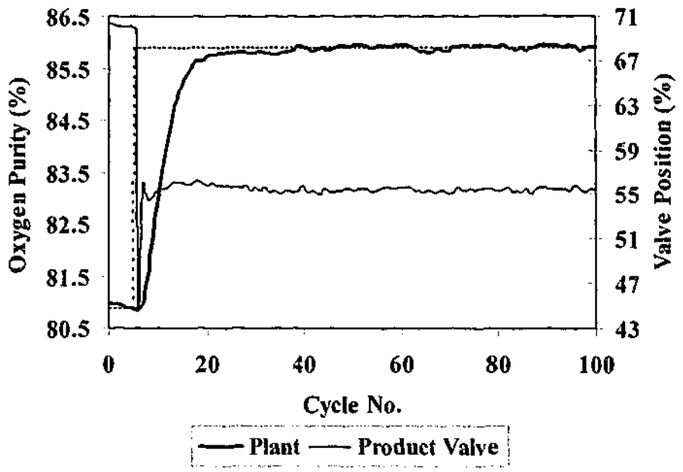

Figure 6.5d. Single loop PID control of the oxygen purity variable using the product valve. Set point change 80.9% to 85.9%, IAE = 39.

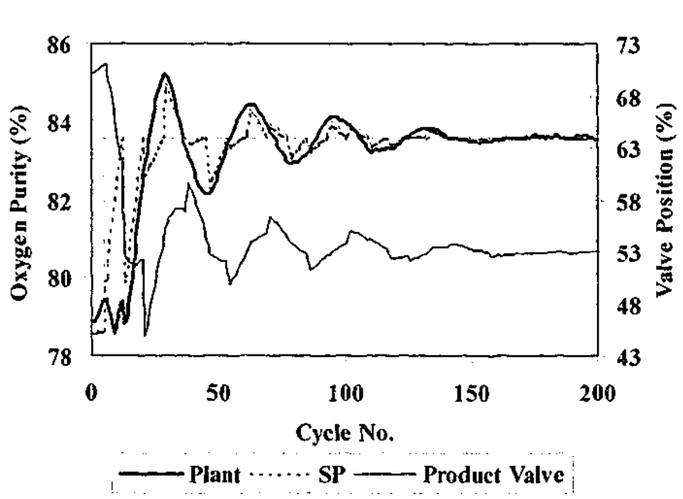

Figure 6.5e. Single loop MPC control of the oxygen purity variable using the product valve. Set point change 78.6% to 83.6%, IAE = 122.

6.6 CONCLUDING REMARKS

In this chapter an alternative method for the implementation of control algorithms on periodic process was presented. It is based on cycle time rather than real-time, which in the past has exhibited poor control [Beh *et al.*, 2000]. Also, a novel MPC control structure was developed (which differed from traditional MPC algorithms) and compared to PID. In terms of load rejection, the performance of the PID and MPC algorithm were fairly close but the PID controller gave far superior performance in terms of set point change for the same controller parameters. In this case, it is concluded that for single loop control of this process, PID is better than the proposed MPC algorithm with its simple process model. The use of higher order/mechanistic models and/or traditional MPC controllers, such DMC [Cutler and Ramaker, 1980], IMC [Garcia and Morari, 1982], the Smith predictor [Smith, 1957] or other model-based control algorithms (such as generic model control (GMC) [Lee and Sullivan, 1988]) may produce superior performance to single loop PID. A last point to note is that the oxygen VSA process studied in this region of operation exhibited linear behaviour but at higher product concentrations, inverse responses may result due to the movement of large thermal gradients as well as sharper changes in the product oxygen purity. In this situation standard PID may fail whereas an MPC structure may maintain stable operation and control if its process model was able to predict the trends correctly.

NOMENCLATURE

c	process output/controlled variable
DB	controller dead band
e	error
IAE	integrated absolute error
K_c	PID proportional gain
m	manipulated variable
S_p	set point
t	controller time interval (cycles)
T	set point time horizon (cycles)
Δc	change in output/controlled variable
Δt_c	controller sample interval (cycles)
Δm	change in manipulated variable
τ_d	PID derivative time (cycles)
τ_f	MPC filter time constant (cycles)
τ_i	PID integral time (cycles)

Subscripts

0	initial value
f	filter
FF	feedforward (MPC) controller

Chapter Seven

Multiple Loop Control

The control of adsorption systems is still in its infancy although the use of this technology has become quite widespread in the chemical engineering community motivating the need to research the application of control theory to these processes. This chapter represents the first study in the open literature on the multiple loop control of an oxygen vacuum swing adsorption process with realistic cycle conditions. The data gathered from this study was obtained through implementation of the various control systems on a pilot-scale plant representative of field operation.

7.1 INTRODUCTION

The motivation for the study of control of vacuum and pressure adsorption (VSA/PSA) processes and in particular oxygen VSA, has been outlined in Chapter 1 and the cyclic control of the product concentration was investigated in Chapter 6. The focus of this chapter is to extend the controllers proposed in the previous chapter to regulate multiple control objectives. It should be noted that because the application of control theory is still in its infancy in this area, this work is classed as an application study. Furthermore, it is not claimed that this research effort is a wholly seminal or completely authoritative document on the general control of these processes but it does represent the very first endeavour, in the open literature, to tackle multiple loop control issues. The intent, therefore, of this work is to demonstrate the application and performance of both PID and model predictive control (MPC) in multiple loop mode for the control of an industrially representative oxygen VSA cycle, implemented on a pilot-scale plant. In addition, the work presented in this chapter is based on previous research efforts by Beh and Webley (2003e) and Beh and Webley (2003g). To achieve this goal, a series of objectives were planned and are listed as follows. The first objective of this work will be to demonstrate the application of decentralised, multiple loop PID with and without an explicit decoupling algorithm. Secondly, the practical implementation of multivariate MPC will be discussed and the performance of all the control systems compared.

This chapter is organised in the following manner. Firstly, the control loop pairings are discussed and the load disturbance case study is summarised. The development of a simplified process model for use in controller tuning and as a predictive model in both the control loop

decoupling algorithm and the MPC controller is subsequently described. Design of an explicit loop decoupling algorithm will follow this section and tuning of the multiple loop PID and MPC algorithms are discussed. The chapter concludes by reporting the performance of the control schemes, implemented on a pilot-scale plant discussed in Chapter 1 (refer to Figures 2.1a and 2.2c), in relationship to a load disturbance.

7.2 CONTROLLER MODEL DEVELOPMENT AND VALIDATION

Before the controller model is discussed the control loop pairings are outlined. Table 7.2a shows the manipulated and controlled variable pairings listed in order of decreasing importance. These pairings have been established in Chapter 4 (refer to Table 4.7c) through the use of the method of relative gain (RGA) analysis and robustness of these pairings have been tested by statistical means. The proposed control schemes sampled once every cycle (i.e. $\Delta t_c = 1$) at the end of the feed step (step 2 in Figure 2.2c, Chapter 2) and the controller action was output at the same time updating the plant at the next cycle. For this reason, an in-house batch multiple loop PID controller was designed as most commercial algorithms function in real-time. Also, it was foreseen that incorporation of the model-based decoupling scheme would be easier than modifying third-party software.

Table 7.2a. The control loop pairings to be studied.

Manipulated Variable	Controlled Variable
Product Valve	End of Feed Step Oxygen Purity
Purge Valve	Oxygen Production Rate
Feed Valve	End of Feed Step Product Pressure

As practiced in Chapter 6, each control structure was tested by subjecting the process to a product stream back pressure through the use of a 5 kPa load disturbance via a water tank. The set point responses will not be investigated in this study as the controllers have been tuned for load rejection and use of these parameters for set point tracking led to highly oscillatory and unstable behaviour. In field operation, load rejection is the critical performance variable, as the customer normally requires that the plant operate at its design state.

In the discussion to follow, the description of the development of the process model pertains to both the loop decoupling algorithm and the MPC controller. Accurate estimation of the system transfer function matrix $\mathbf{G_m}$ requires the development of a detailed mechanistic model to correctly describe the complex interaction between the various controlled and manipulated

variables with time. The use, however, of these complicated models, defeated the purpose of real-time application as discussed in Chapter 4. In order to decrease these computational burdens but still retain some knowledge of the process dynamics, a first-order linear approximation to $\mathbf{G_m}$ was introduced for modelling of the oxygen purity and product pressure variables whilst production rate was modelled in second-order form. This is due to the production rate variable being a derived quantity, defined in terms of the product concentration and cyclic molar flow. To reiterate from previous chapters, the units used for large industrial VSA installations are tonnes per day of contained oxygen (TPDc) but will be re-defined for this study as kilograms per day of contained oxygen (kgPDc) because of much reduced capacity of the pilot plant as given by Eq. (7.2a).

$$PR = \frac{0.0864 M_{O_2}}{\tau_c}\left(\int_t^{t+\tau} n_p y_{o_2} dt\right) \tag{7.2a}$$

where M_{O2} is the molar mass of oxygen (taken to be 31.999 kg/kmol), τ_c is the cycle time, y_{O2} is the mole fraction of oxygen in the product, n_p is the instantaneous molar product flowrate and t represents continuous time. From Eq. (7.2a), two first-order differential equations are adjusted to fit the measured responses of the purity and cyclic molar flow. The product per cycle of these two first-order equations was multiplied by the constant terms outside the brackets in Eq. (7.2a), determining the production rate for that cycle. Equation (7.2b) describes the form of the first-order differential equation used to model the adsorption system, which is written in terms of the deviation variables and integrated using a 5th order Runge Kutta scheme with a time step of 0.001.

$$\frac{d(\Delta o_{ij})}{dt} + \frac{1}{\tau_{ij}}\Delta o_{ij} = \frac{k_{ij}}{\tau_{ij}}\Delta m_j \tag{7.2b}$$

Estimation of the time constant, τ_{ij}, and the open loop gain, k_{ij}, had been established through open loop step response studies of either the process or a detailed model (refer to Chapters 4 and 5).

The overall influence of a set of changes in input values was assumed to be additive as described by Eq. (7.2c).

$$\Delta c_i = \sum_{j=1}^{J} \Delta o_{ij} \tag{7.2c}$$

Equations (7.2b) and (7.2c) are diagrammatically described for a 3 x 3 system in Figure 7.2a, which shows the sets of differential equations, g_{ij}, to be integrated on a cyclic basis.

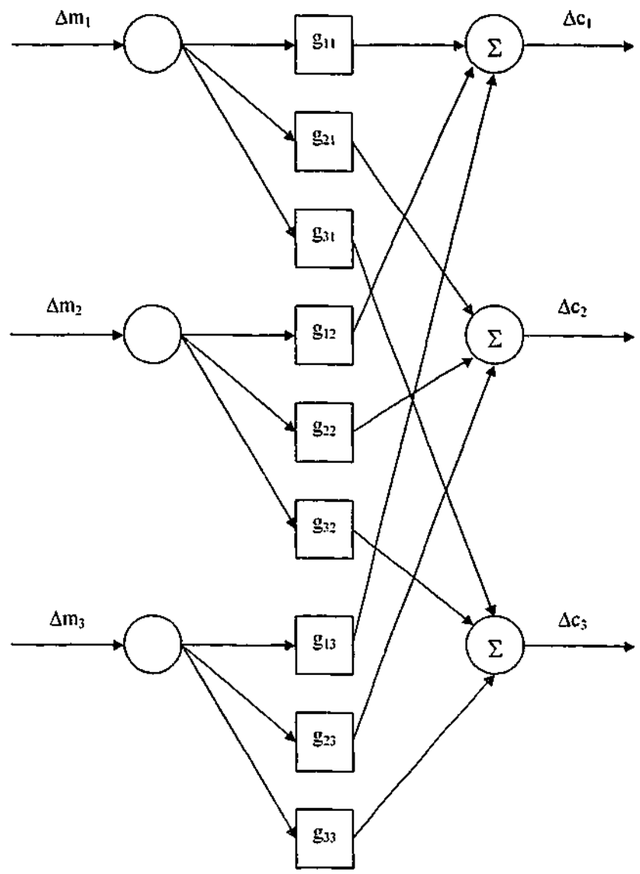

Figure 7.2a. Block diagram showing the elements and the structure of the estimated dynamic transfer function matrix, G_m, to be used in both the loop decoupler and MPC algorithm.

Validation of the process models used in the controller algorithms is shown in Figures 7.2b to 7.2d and summarised in Table 7.2b. The integrated absolute error (IAE) had an equivalent definition as in Eq. (6.3k) of Chapter 6. It should be noted, however, that the simulation results contained a time delay for the oxygen purity and production rate variables of three cycles and one cycle respectively, which was not represented in the controller model. This is because dead

time is a noninvertible element and therefore a process/model mismatch was inherently present in the controller model. The one cycle delay employed to model production rate was due to the sampling interval of the controller and is discussed in detail in §7.4. Nevertheless, the process model containing the time delays is used for tuning purposes and performance estimation of the PID and MPC controllers. This simplified adsorption process model satisfactorily characterised both the oxygen purity and production rate variables to a useable degree (refer to Figures 7.2b and 7.2c). Some reasons for the experimentally measured time delays of the product purity variable had been discussed in Chapters 4 and 5. The results revealed that the amount of dead time was a function of the flow characteristics entering and leaving the product vessel and caused by less than ideal mixing conditions in the tank. Variability of the time delay was a significant cause of difference between the process and controller models. This simplified empirical model, on the other hand, correctly predicted the inverse behaviour of the production rate response to a load perturbation, which showed this variable firstly decreasing and then asymptotically increasing to a steady value. Only product pressure had not been accurately captured by the simple model due to noise in the sensor signal (refer to Figure 7.2d and Table 7.2b). It is anticipated that control issues will arise due to the deviation in this signal but no effort will be made to dampen or filter the signal in this preliminary investigation. The overall trend, nevertheless, shows that the first-order model approximated the average value to an adequate degree.

Table 7.2b. Comparison of simulation and plant IAE to a 5 kPa product load disturbance.

Process Variable	Plant IAE	Simulation IAE
No Control		
Oxygen Purity	179	168
Production Rate	95	94
Product Pressure	84	58
Average IAE	120	107

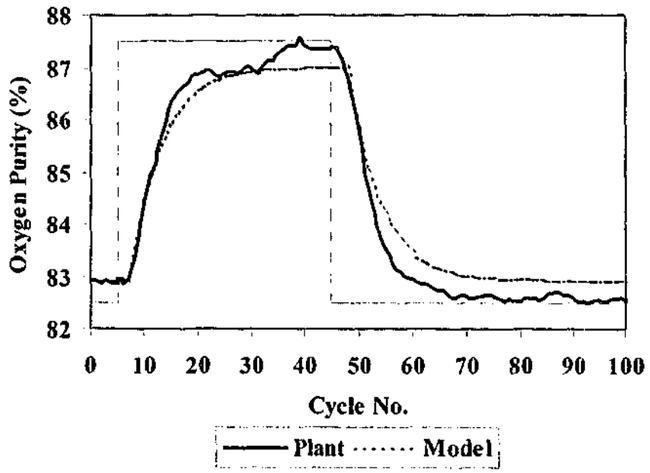

Figure 7.2b. Response of the product oxygen variable to a 5 kPa load disturbance with no control. $IAE_{Plant} = 179$, $IAE_{Model} = 168$.

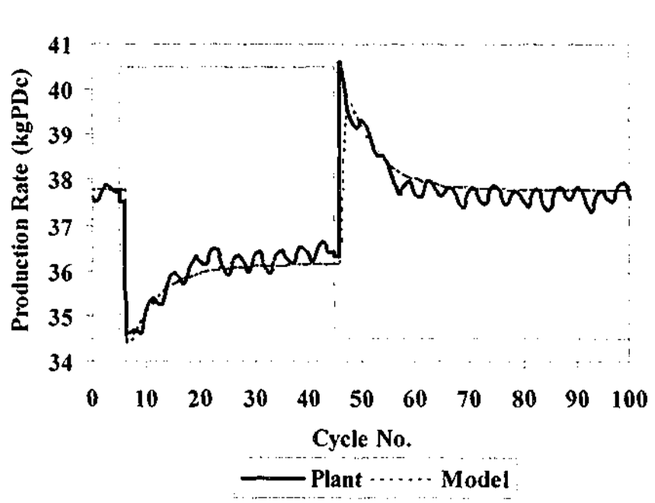

Figure 7.2c. Response of the product production rate variable to a 5 kPa load disturbance with no control. $IAE_{Plant} = 95$, $IAE_{Model} = 94$.

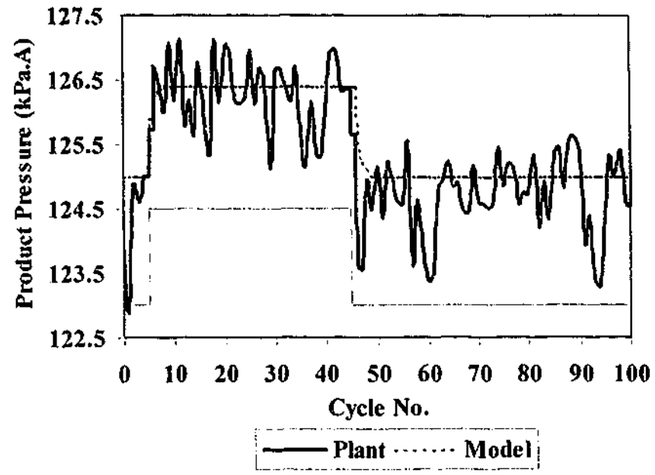

Figure 7.2d. Response of the product pressure variable to a 5 kPa load disturbance with no control. $IAE_{Plant} = 84$, $IAE_{Model} = 58$.

7.3 DECOUPLER DESIGN AND DERIVATION

In Chapter 4 the sensitivity of the controlled variables to the manipulated variables was investigated, and revealed a significant extent of coupling and severe interactions between each control loop. In an attempt to minimise this loop interaction, an explicit decoupling strategy was developed to enable better performance of the decentralised feedback controllers. The application of the method had been discussed in previous work [McAvoy, 1979; Weischedel and McAvoy, 1980; Shinskey, 1996] and was extended for a general N x N control system and applied to the batch O_2 VSA process in this chapter.

Derivation of the control loop decoupling strategy begins with the following definition of the control variable with respect to a change

$$\vec{c}_{m+dm} = \vec{c}_m + d\vec{c} \tag{7.3a}$$

where $\vec{c}$ is the vector of controlled variables either before or after the change in manipulated variable m. This vector of changes in the controlled variable, $d\vec{c}$, for a 3 x 3 system is given by

$$d\bar{c} = \mathbf{G}_P \cdot d\bar{m} = \begin{bmatrix} g_{P11} & g_{P12} & g_{P13} \\ g_{P21} & g_{P22} & g_{P23} \\ g_{P31} & g_{P32} & g_{P33} \end{bmatrix} \cdot \begin{bmatrix} dm_1 \\ dm_2 \\ dm_3 \end{bmatrix} = \begin{bmatrix} \frac{\partial c_1}{\partial m_1} & \frac{\partial c_1}{\partial m_2} & \frac{\partial c_1}{\partial m_3} \\ \frac{\partial c_2}{\partial m_1} & \frac{\partial c_2}{\partial m_2} & \frac{\partial c_2}{\partial m_3} \\ \frac{\partial c_3}{\partial m_1} & \frac{\partial c_3}{\partial m_2} & \frac{\partial c_3}{\partial m_3} \end{bmatrix} \cdot \begin{bmatrix} dm_1 \\ dm_2 \\ dm_3 \end{bmatrix} \tag{7.3b}$$

where $\mathbf{G}_P$ is the system's square, dynamic closed-loop gain matrix of each of the transfer functions g_{Pij}. The objective of the control loop decoupler algorithm was to minimise or prevent closed loop interaction (i.e. $g_{Pij} = 0$ where $i \neq j$). This would mean that the off-diagonal terms in Eq. (7.3b) would be zero so that m_1 only affects c_1 and so forth. To diagonalise the real process, Eq. (7.3b) can be rewritten as

$$d\bar{\hat{c}} = \hat{\mathbf{G}}_P \cdot d\bar{m} = \mathbf{P}^{-1} \cdot \mathbf{G}_P \cdot \mathbf{P} \cdot d\bar{m} \tag{7.3c}$$

The equation above, however, is not realisable, as the process would need to be physically altered to accommodate the eigenvector $\mathbf{P}$ (or $\mathbf{P}^{-1}$). An alternative method is, by inclusion of a process model, to incorporate the effects of the off-diagonal elements in the input of the process (i.e. modify the dm vector such that the output interaction is minimised). The general form for the N x N control system can be expressed in terms of the manipulated variable using an explicit decoupling strategy for all three control loops as described in Equation (7.3d) below.

$$d\hat{m}_i = \Delta m_i - \sum_{j \neq i}^{J} \Delta m_j \frac{g_{mij}}{g_{mii}} \tag{7.3d}$$

Equation (7.3d) represents the i^{th} manipulated variable whose value has been adjusted by consideration of all other j^{th} manipulated variables in product with the ratio of the derivative of the off-diagonal component, g_{mij}, and the derivative of the i^{th} variable, g_{mii}. A process model, $\mathbf{G}_m$ as described in the preceding section, was used to estimate the derivatives of the real system and the "decoupled" controller output was transmitted to the process as

$$d\bar{\hat{c}} = \mathbf{G}_P \cdot d\bar{\hat{m}} \tag{7.3e}$$

Equations (7.3d) and (7.3e) shows that the decoupling strategy works in conjunction with any arbitrary decentralised control structure (i.e. the process controller calculates Δm) but it is applied only to the multiple loop PID algorithm in this investigation.

The severity of loop interaction in the process under study preempts the suitability of this method. The large (> 1.0) relative gains (RGA) determined in Chapter 4 and the existence of process model errors suggests that instability of the control system may result if full loop decoupling is used [McAvoy, 1979; Weischedel and McAvoy, 1980]. An alternative method to full decoupling as described in Eqs. (7.3d) and (7.3e), is partial or one-way decoupling. This involves the use of the process model to decouple only one or more loops of interest but not all. The product oxygen concentration is arguably the variable of greatest importance in an industrial oxygen VSA process and one-way decoupling of this variable may induce better controller performance than full decoupling as the mean RGA value for the pairing of the product valve with purity was less than one (~ 0.54 refer to Table 4.7c, Chapter 4), although the interaction of the other manipulated variables may cause stability issues to arise. Application of one-way decoupling by McAvoy (1979) has shown that it is less sensitive to process model mismatches than full decoupling. Equation (7.3f) mathematically describes the application of one-way decoupling for a 3 x 3 control system such as that studied in this chapter.

$$\begin{bmatrix} \hat{c}_1 \\ \hat{c}_2 \\ \hat{c}_3 \end{bmatrix} = \mathbf{G}_P \cdot \begin{bmatrix} \Delta m_1 - \left(\Delta m_2 \frac{g_{m12}}{g_{m11}} + \Delta m_3 \frac{g_{m13}}{g_{m11}} \right) \\ \Delta m_2 \\ \Delta m_3 \end{bmatrix} \tag{7.3f}$$

It is realised that control loop decoupling may not truly decouple the control loops but it may compensate the control loops in a favourable manner. The use of both one-way and full, explicit decoupling will be investigated in this chapter noting that application of this control technique to this process has not been shown in the current literature.

7.4 CONTROLLER TUNING

The complexity in developing a general method for tuning decentralised controllers has undergone much research as shown in the current literature. In terms of batch controller tuning, however, information relating to this area has been somewhat limited. It is not the intention in this chapter to provide a survey of all the relevant articles in the current literature on this subject but to discuss and reference some of the more important developments.

Arguably the most well-known technique and the method used as the basis for comparison against other developments, is the biggest log-modulus tuning (BLT) by Luyben (1986). This procedure is relevant only for processes that are open loop stable and can be utilised on systems that are either well-characterised (available in transfer function form) or available in a frequency response format. Luyben's method is an extension of the classical Nyquist stability criterion for single-input-single-output (SISO) systems by defining a multivariable closed loop modulus, $L_{cm,max}$. The initial controller gains are calculated from Ziegler-Nichols (1942) settings by assuming loop independence and are decreased by a factor F which in turn becomes an optimisation problem to find K_c and T_i such that $L_{cm,max} = 2N$ is satisfied (where N is the system order – e.g. $N = 3$ for a 3 x 3 control problem). The original BLT method has been subsequently extended to include derivative action and accounts for the nonsymmetric nature of multiloop interactions [Monica *et al.*, 1988].

Other methods that are fundamentally similar to BLT involve shaping the Gershgorin bands by utilisation of the Nyquist stability analysis such that the closed loop system remains stable and interaction is minimised [Ho *et al.*, 1997; Chen and Seborg, 2001; Chen and Seborg, 2002c]. An extension of the SISO iterative continuous cycling method to multiple-input-multiple-output (MIMO) PI tuning through application of the Nyquist array method [Lee *et al.*, 1998], provides an alternative procedure to the tuning of decentralised controllers. The remaining traditional approach to multiple loop controller tuning has been to formulate the control problem by direct synthesis of the process model (if available) and controller to obtain the appropriate gains [Chen and Seborg, 2002a; Skogestad, 2003].

The methods for decentralised, multiple loop controller tuning proposed above were not utilised in this study. Listed below are various reasons why such tuning rules were not practised to develop initial estimates of the PID gains.

- In all current tuning procedures a time delay is assumed to exist, which is a legitimate assumption in most cases if applied in continuous time. A batch system, on the other hand, completes its operations after a number of steps have been realised. Such is the case with adsorption processes which are inherently cyclic and therefore control should be implemented in terms of cycle time (i.e. on a per cycle basis) and not real-time. This change from continuous time to cycle time can remove delays attributed to sensors, actuators and the system causing the application of most tuning strategies to fail as a dead time is required as input. The product pressure variable is an example of this condition where zero dead time is "experienced" by the system as a disturbance manifests itself when the process variable is measured by the control system at the end of the step (refer to Table 7.2a). On the other hand, the perceived dead time may disappear or appear as a result of the definition of the point at which control action occurs, severely affecting the controller settings (refer to §5.3.1

of Chapter 5 which demonstrates how this peculiarity occurs). Another example of ... re this situation can occur is measurement of the production rate variable as alluded to in §7.2. If a perturbation occurs at any point within a cycle when the process was initially at steady state, the production rate will also alter during that cycle. Since the final production rate value is updated at the end of the cycle (refer to Eq. (7.2a) which reveals that PR is integrated over a cycle), a measurement of this variable at any time other than at the end of a cycle would record its value at the previous cycle. As indicated in Table 7.2a, the production rate is measured at the end of step 2 and updated for the next cycle by the control system at a similar time instant. In this case, the production rate variable is artificially delayed by one cycle. Zero time delay would result if control action occurred at the end of the cycle.

- A further problem encountered with batch systems is that a process variable may exhibit a variable dead time, which is the predicament of the product oxygen concentration. In this case, the oxygen purity time delay varies as a strong function of inlet and outlet flow due to non-ideal mixing characteristics in the pilot plant product vessel and is discussed in detail in Chapters 4 and 5 – the dead time fluctuates between one to five cycles in the experimental region. Calculation of the controller gains, therefore, can also vary over a large range whether one or five cycles are used as the delayed amount.

As mentioned previously, academic studies have concentrated on processes that are well-characterised and hence are described by appropriate transfer functions written in the Laplace domain [Luyben, (1986); Monica *et al.*, 1988; Ho *et al.* 1997; Chen and Seborg, 2001; Chen and Seborg, 2002c]. This allowed the application of powerful mathematical techniques to analyse the results and in some cases, allowed the direct determination of controller settings [Chen and Seborg, 2002a; Skogestad, 2003). The inability to properly characterise the VSA process, as discussed above, has led to a somewhat ad hoc methodology whereby the initial PID settings were based upon the well-known methods of Zeigler and Nichols (1942) by assuming independence of each control loop. Fixed values of the time delay for each variable were also assumed. Each PID controller was enabled sequentially and the loops detuned in simulation experiments to minimise the IAE and ensure stable control loop behaviour with all controllers in automatic. This is, in principal, similar to although less rigorous than the sequential closing technique proposed by Mayne (1973). The product concentration loop, being of most importance, was tuned more aggressively than the other two control loops with a dead time of one cycle assumed during the initial calculation of gains for the product pressure variable. This procedure ensured that the controllers were stable if all controllers were in closed loop mode but did not guarantee the stability of the control system should a particular loop be put into manual.

These same gains, calculated for the PID system, were utilised by the full and one-way decoupling algorithms.

The tuning strategy for the MPC controller involved a similar iterative process with its structure described in detail in §6.4 of Chapter 6. In this case the feedback (PID) controller was initially disabled and an experimental database of time horizon and filter time constant was built using process model information for the first (oxygen purity) loop. Once suitable controller settings were selected, the second and third loops were tuned sequentially by varying the tunable parameters (i.e. time horizons and filter time constants). The gains for the feedback controller, as discussed in Chapter 6 of this study, are the last to be altered and are set sufficiently small so that process/model differences are compensated for and oscillatory behaviour dampened. As with the PID controller, the product purity control loop was tuned more aggressively than the rest.

7.5 RESULTS AND DISUSSION

The results of the performance of the controllers in terms of load rejection are tabulated in Tables 7.5a and 7.5b below and the dynamics of the response variables shown in Figures 7.5a to 7.5l. The predicted IAE based on simulation trials (Table 7.5b) using the simple process models discussed previously in this chapter showed similar absolute values and trends when compared to the plant trials in Table 7.5a. The largest difference occurred with the product pressure variable, which was attributed to the noise in the actual process signal as indicated in Figure 7.2d. Otherwise, the qualitative trend of decreasing IAE from the loop of most importance (oxygen purity) to the least important (product pressure) was captured in the simulation study. This included the prediction of the unstable control loop behaviour of both the full and one-way decoupling strategies, which was attributed to the sensitivity of this method to differences between process and model [McAvoy, 1979]. The inability to model the change in boundary condition due to the load disturbance being the primary cause of mismatch.

Table 7.5a. Controller performance on the VSA pilot plant.

Controller Type	Oxygen Purity IAE	Production Rate IAE	Product Pressure IAE	Average IAE
No Control	179	95	84	120
PID	136	85	66	96
Full Decoupling*	N.A.	N.A.	N.A.	N.A.
1 Way Decoupling*	N.A.	N.A.	N.A.	N.A.
MPC	129	88	101	106

*Unstable

Table 7.5b. Controller performance in simulation studies.

Controller Type	Oxygen Purity IAE	Production Rate IAE	Product Pressure IAE	Average IAE
No Control	168	94	58	107
PID	98	49	34	61
Full Decoupling*	N.A.	N.A.	N.A.	N.A.
1 Way Decoupling*	N.A.	N.A.	N.A.	N.A.
MPC	96	60	47	68

*Unstable

The responses shown in Figures 7.5a to 7.5l will now be discussed individually and in terms of each control scheme. It should be noted that the set points between each run vary slightly. The reason for this is that it was experimentally difficult to establish exactly the same baseline conditions due to slight variations in the inlet pressure or flow, inlet temperature and ambient conditions. Nevertheless, each experiment was conducted while the process was at cyclic steady state (CSS) and the length of time of each run was shorter than the time constants of the various external disturbances.

The effect of the product load disturbance with no control was to increase the system back pressure and to push the adsorption front further into the bed, creating a rich oxygenated zone near the top. This ultimately increased the oxygen concentration and product pressure and causes a decrease in the production rate. Removal of the load disturbance caused the system to return to its original state (refer to Figures 7.2b to 7.2d). The goal of the controller was to counter this perturbation by moving the manipulated variables to a new state such that the original baseline conditions (i.e. the set points) are maintained. The PID controllers, being decentralised linear controllers, attempt to regulate each output variable independent of each other. For example the results for the control of the output variables under coupled PID, presented in Figures 7.5a to 7.5c, shows that as the purity begins to increase in response to the disturbance, the product valve began to increase to maintain set point. Section 4.5.3 of Chapter 4 demonstrated that the product valve, which has an inverse relationship with purity, induces movement of the mass transfer zone that either increases or decreases the final product concentration. Similar arguments can be qualitatively constructed to explain the action of the purge and feed valves responses to their controlled variables (refer to sections 4.5.1 and 4.5.4 of Chapter 4). Figures 7.5a to 7.5c shows that PID achieves reasonable control for all output variables and highlights the benefits of implementing a workable control structure as the IAE was lower for each controlled variable than if no controller was present. As expected, the system response for each variable differed which was simply attributed to process dynamics.

The figures indicated that set point was attained within 35, 20 and 30 cycles from initiation of the disturbance for each of the three variables respectively.

Unlike PID, the use of full and one-way decoupling combined with PID showed unsatisfactory results. In both cases, the boundary condition step change caused unstable response with the full, explicit decoupling strategy generating a trip condition in the pilot plant within 20 cycles of the load disturbance. Figures 7.5d and 7.5f clearly shows the full decoupler algorithm driving the product and feed valves fully closed which in turn caused the purge valve to saturate (Figure 7.5e). It is for this reason that all the controlled variables attained ambient condition or reach a zero state. As hypothesized in an earlier section of this chapter, one-way decoupling may produce more favourable results than full decoupling. The response of this control scheme is shown in Figures 7.5g to 7.5i. Unlike the full decoupling method, one-way decoupling did not terminate plant operation but as the process/model errors accumulated, even after the disturbance was removed, the controller outputs saturated (cycle 220 showed the major increase) leading to different operating states.

Marginally better or equivalent performance is indicated in Tables 7.5a and 7.5b and Figures 7.5j and 7.5k by the MPC algorithm over PID for the oxygen purity and production rate loops. The main reason for the lower purity IAE was due to less overshoot upon removal of the disturbance as the product valve attains a maximum value of around 77% compared to 88% in the case of PID. Cyclic steady state was achieved within 35 to 40 cycles from the withdrawal of the product load. A similar argument can be advanced for the production rate variable. The performance limiting variable for the MPC scheme was product pressure. Figure 7.5l shows that set point was not achieved during the load disturbance with the likely cause being noise in the product pressure signal resulting in unfavourable set point trajectories and dampening the aggressiveness of the controller. Furthermore, because centralised control was practised, the calculated set point trajectory of the pressure variable influenced the output of the optimisation algorithm. The consequence of this was that the magnitudes of the manipulated variables of the other loops were also affected. Suppressing the oscillatory motion of this variable by redefining the variable to be in terms of an average product pressure or filtering the sensor signal may result in an IAE close to that of the simulation run of 47. A final point to note is that the feed valve shown in Figure 7.5l indicated that it was still linearly increasing. This is not as it seems as both the controlled variable and the valve exhibit steady behaviour after 250 cycles. The time scale was chosen to allow comparison with the PID experiments.

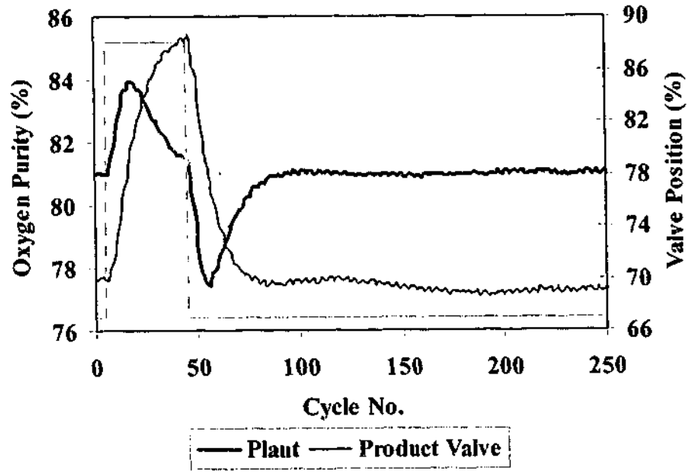

Figure 7.5a. Multiple loop PID control of the oxygen purity variable using the product valve. Set point 81%, IAE = 136.

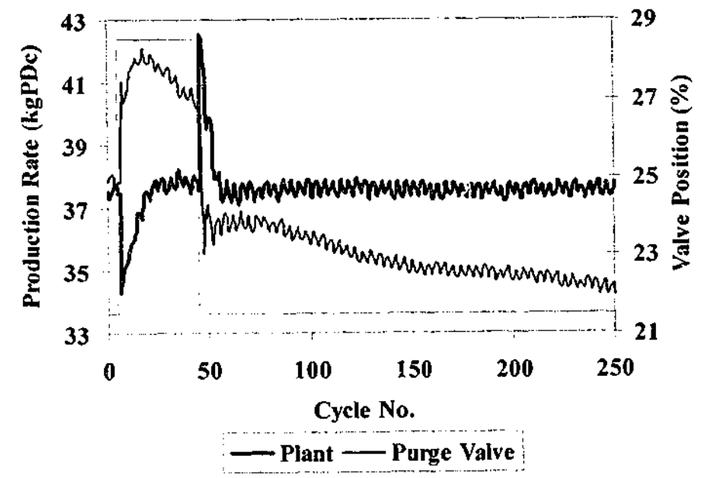

Figure 7.5b. Multiple loop PID control of the production rate variable using the purge valve. Set point 37.5 kgPDc, IAE = 85.

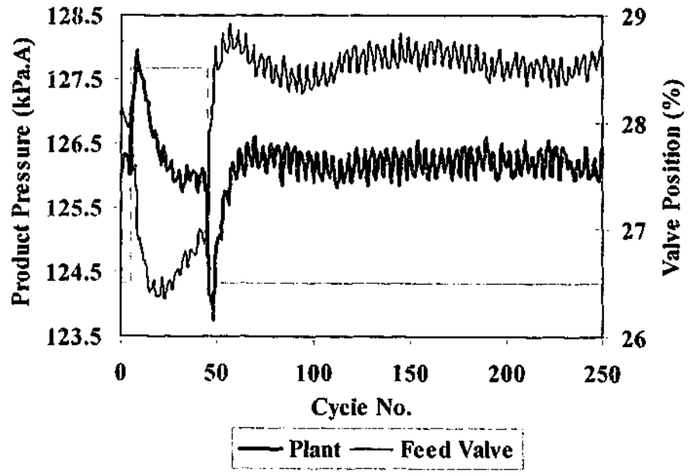

Figure 7.5c. Multiple loop PID control of the product pressure variable using the feed valve. Set point 126.2 kPa.A, IAE = 66.

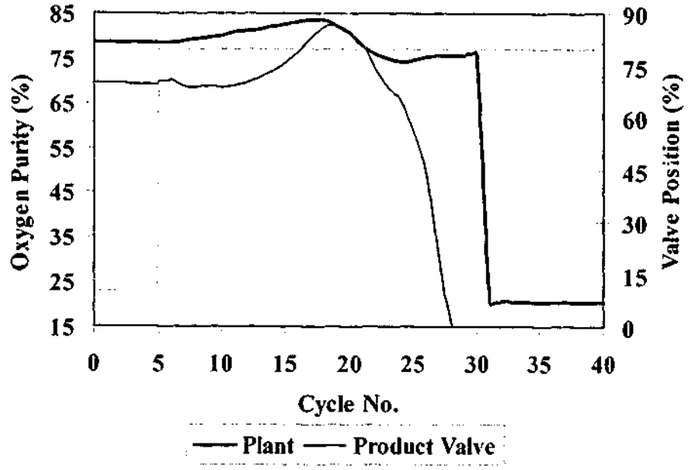

Figure 7.5d. Multiple loop PID control with full decoupling of the oxygen purity variable using the product valve. Set point 78.5%, IAE = unstable.

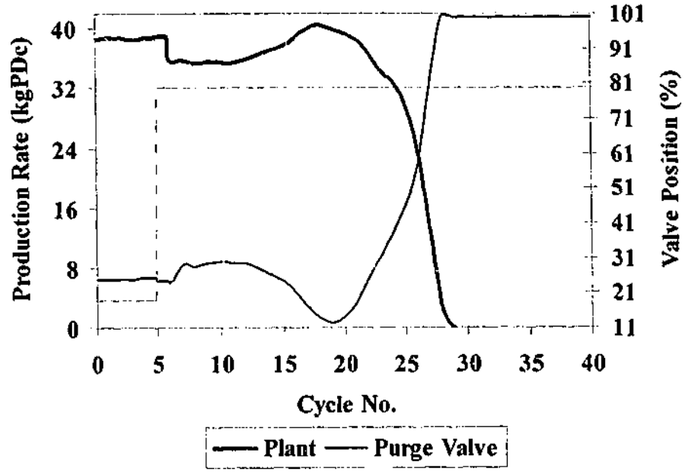

Figure 7.5e. Multiple loop PID control with full decoupling of the production rate variable using the purge valve. Set point 38.7 kgPDc, IAE = unstable.

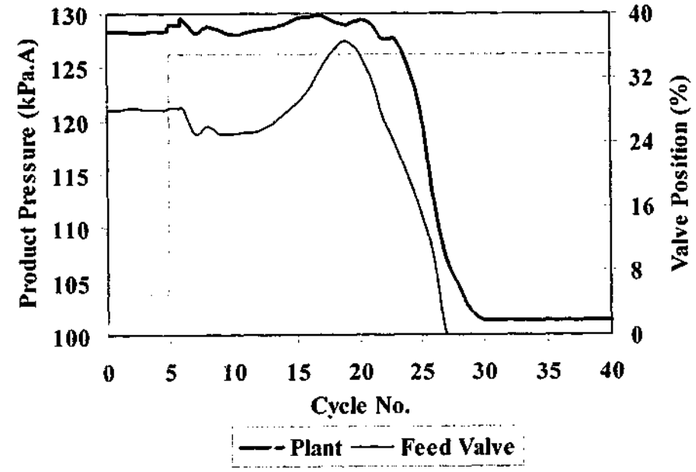

Figure 7.5f. Multiple loop PID control with full decoupling of the product pressure variable using the feed valve. Set point 128.25 kPa.A, IAE = unstable.

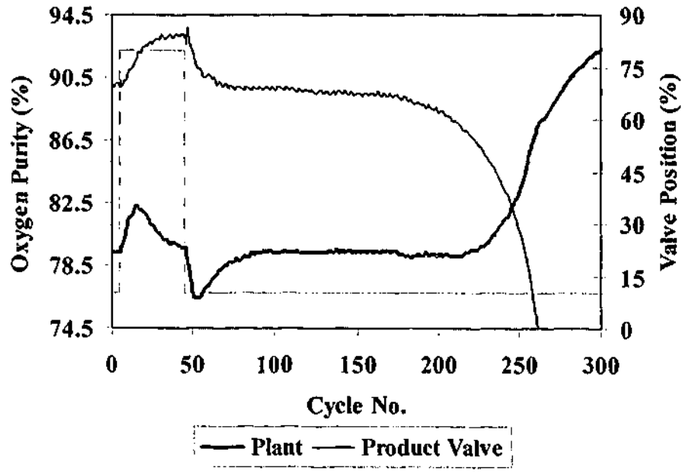

Figure 7.5g. Multiple loop PID control with one-way decoupling of the oxygen purity variable using the product valve. Set point 79.4%, IAE = unstable.

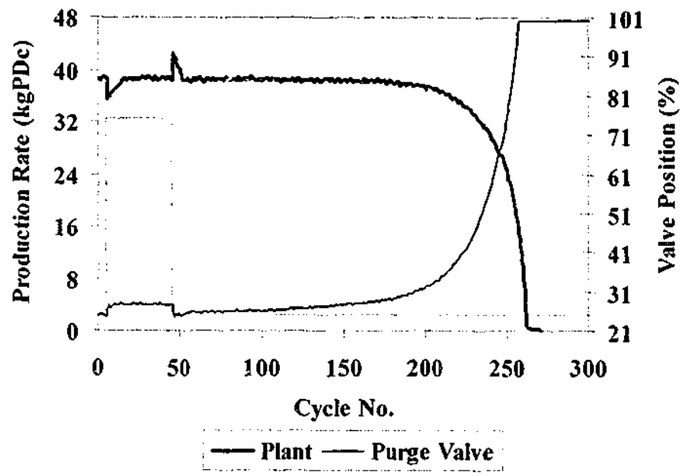

Figure 7.5h. Multiple loop PID control with one-way decoupling of the production rate variable using the purge valve. Set point 38.65 kgPDc, IAE = unstable.

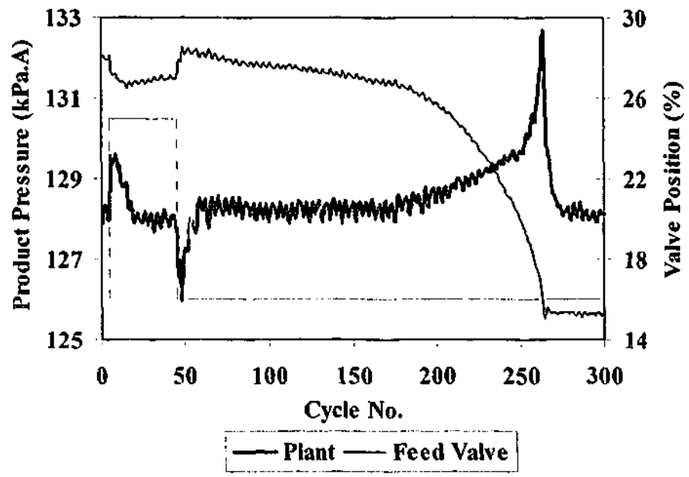

Figure 7.5i. Multiple loop PID control with one-way decoupling of the product pressure variable using the feed valve. Set point 128.1 kPa.A, IAE = unstable.

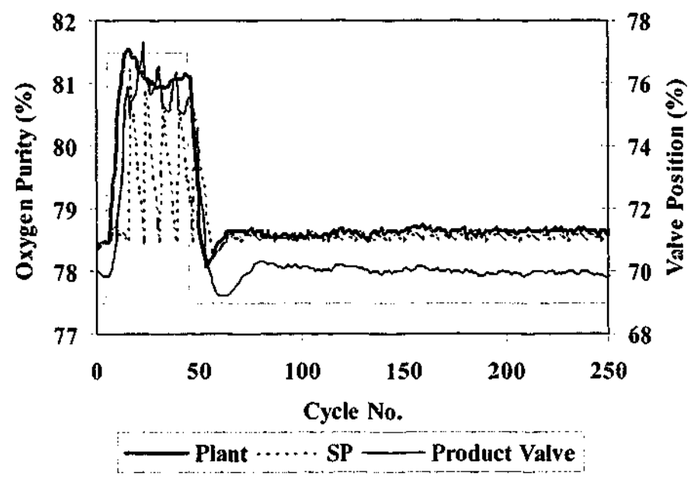

Figure 7.5j. Multivariate MPC control of the oxygen purity variable using the product valve. Set point 78.5%, IAE = 129.

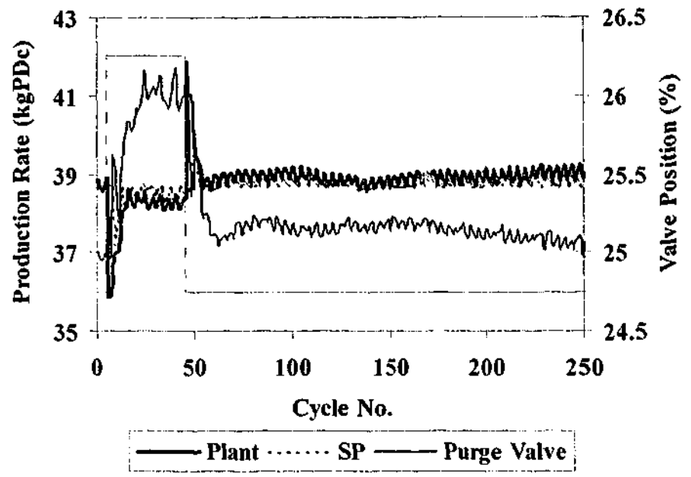

Figure 7.5k. Multivariate MPC control of the production rate variable using the purge valve. Set point 38.7 kgPDc, IAE = 88.

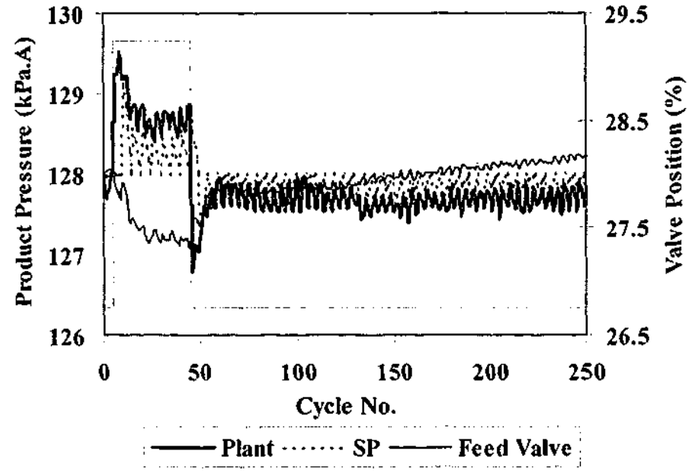

Figure 7.5l. Multivariate MPC control of the product pressure variable using the feed valve. Set point 128.0 kPa.A, IAE = 161.

7.6 CONCLUDING REMARKS

The results obtained from this preliminary study into the control of the oxygen VSA process can be summarised in the following manner –

(a) Tuning using a sequential/iterative method via simulation runs on a simple empirical process model produced sufficiently well-tuned feedback (PID) and centralised (MPC) controllers. As shown in the figures, the response to a load disturbance was worse without control.

(b) The control loop pairings obtained from an analysis in §4.7 of Chapter 4 analysis have proved to be robust for this process about its particular operating regime.

(c) Comparisons between the PID and MPC controllers indicate comparable performance characteristics.

(d) Noise in the pressure signal has a negative influence over the movement of the MPC controller output. It has been suggested that methods for damping the noise should be investigated to obtain better controller performance as indicated in the simulation studies.

(e) Both experimental and modelling work reveals that the use of full and one-way decoupling strategies combined with decentralised (PID) control resulted in unstable loop behaviour. As theorised in previous studies [McAvoy, 1979] and experimentally demonstrated through this work, one-way decoupling showed less sensitivity to model errors.

As emphasised in Chapter 6 and reiterated again here, this study presented some preliminary findings only and attempted to address some of the practical implementation issues. Although no conclusive evidence showing superiority in performance was discovered between PID and the unique MPC structure used, this does not imply that PID and MPC are equivalent in all multiple loop situations. It is hypothesized that for cycles operating in highly nonlinear regimes (such as higher product concentrations), PID because of its linear decentralised nature, may fail where MPC may succeed. Finally, the use of traditional MPC architectures may exhibit exceptional performance over PID and is a motivating element for further research in this area.

NOMENCLATURE

IAE	integrated absolute error
k	open loop gain
K_c	PID proportional gain

m	manipulated variable
M_{O2}	molar mass of oxygen (kg/kmol)
n_p	instantaneous molar product flowrate (ALPM)
PR	production rate (kgPDc)
t	controller time interval (cycles); real-time (s)
y_{O2}	oxygen mole fraction
Δc	change in output/controlled variable
Δt_c	controller sample interval (cycles)
Δm	change in manipulated variable
Δo	controller sample interval (cycles)
τ	system time constant (cycles)
τ_c	cycle time (cycles)

Chapter Eight

A Simple Method to Construct the Composition Profile

In this chapter, a simplified energy balance equation to aid online measurement of the adsorbed phase nitrogen loading in industrial-scale pressure and vacuum swing adsorption systems consisting of one preferentially adsorbed component was proposed. Implementation of this technique to current and future plants requires the addition of thermocouples (which are relatively inexpensive) located axially through the bed and pressure transmitters at the bottom and top of the bed. The advantages of this methodology is that the composition front can be accurately inferred from direct measurements of the local pressure and temperature and used as the basis for process monitoring and diagnostics of plant purity, recovery and production rate.

8.1 INTRODUCTION

Knowledge of the location of the adsorbate front and its associated mass transfer zone, MTZ, can be utilised as a powerful diagnostic tool for both the plant engineer and operator. Its importance stems from the fact that process performance, especially product concentration, is a strong function of the axial composition profile in the bed. Therefore, being able to determine this online would be a very useful aid in both daily plant maintenance and trouble-shooting. However, current technology does not permit direct in-situ measurement of composition. All modern oxygen sensors measure the gas concentration, which is a derived parameter being a function of pressure, temperature and mole fraction. In a VSA cycle, all of these fundamental parameters are time variant during each step of the process. Spurious results would occur with state-of-the-art oxygen analysers even with pressure and temperature compensation. Furthermore, vacuum conditions are experienced during certain steps of the VSA cycle and this causes difficulties in extracting a sample for analysis. Ingenious methods would need to be invented in order to capture the gas at a particular point of the cycle for analysis in real-time or as a post processing step.

Given the impracticalities and failings of various numerical efforts and the inability to accurately measure the gas composition, this chapter, which is based on previous work [Beh and Webley, 2003a], seeks to demonstrate how, with certain assumptions and the measurement of

axial temperatures and pressures, a simplification to the solution of mass and energy balances describing a bulk separation PSA/VSA process can be made. This knowledge can then be utilised to accurately estimate the loading in the bed and thus the position of the adsorbate front. The added advantage of this technique is that it can be readily applied in field operation and forms part of a diagnostic tool for the process engineer for the determination of plant performance.

The motivation for the development of this technique originated from the observations of the axial temperature profiles in both the field and numerical simulation of the VSA process for oxygen enrichment. Consider Figures 8.1a and 8.1b shown below for the 'low' and 'high' purity cases where both scenarios are operated under similar conditions however, a single boundary condition, the position of the feed valve, was the main difference in this example. It is quite clear that the drop in purity (from 85.4% to 81.5%) due to the feed valve change has manifested itself to some degree in the axial temperature measurements. The thermocouples near the top of the bed (1.6m to 1.8m) reinforced this observation showing less temperature swing for the 'high' purity case (Figure 8.1b) than the 'low' purity run (Figure 8.1a). The main reason for the observed temperature swing (~ 1.6°C at 1.7m) at the top of the bed in the 'high' purity example was the convection of thermal energy out of the bed during the feed step and then back into the bed during the receive purge step. Oxygen adsorption was minimal in this case due to the nitrogen selective properties of the lithium-based zeolite used. In Figure 8.1a, more moles of nitrogen were allowed out of the bed and hence contaminating the product stream giving rise to the 'low' purity case. The higher observed temperature swings (~ 2.1°C at 1.7m) was in part due to the additional nitrogen molecules adsorbing and desorbing from the sieve surface and the convected thermal energy. Therefore, it was surmised that knowledge of the position and extent of these temperature swings could aid in prediction of the adsorption front. Previous researchers such as Matz and Knaebel (1987) and Beh and Webley (2003b), had proposed to use the axial temperature gradients for control or as a heuristic to monitor plant performance respectively.

In a similar way, recent work by Bitzer *et al.* (2000) and Bitzer and Zeitz (2002b) had demonstrated the use of a distributed parameter observer to infer the spatial concentration profiles utilising pressure and temperature measurement from the process to correct the outputs of the observer. Their work was limited to trials on an in-house simulator as the equations describing the observer were too computationally intensive for real-time application (the observer required the solution of the three conservation PDE's along with other ODE's describing momentum and uptake). Also, their method was dependent on correctly setting the initial conditions of the observer which, if incorrectly estimated, may result in highly erroneous computation of the associated adsorption front.

This chapter is ordered in the following manner. Firstly, a description of the development of simplified adsorption process model will be discussed and an expression for the time-

variant spatial composition profile obtained. This simple adsorption process model will be implemented on a typical industrial cycle, which was simulated on an experimentally verified in-house process simulator. The cycle is summarised in a separate section and the results of the estimations of the composition profiles by the simple model will be presented. The chapter will conclude by highlighting its applications and limitations.

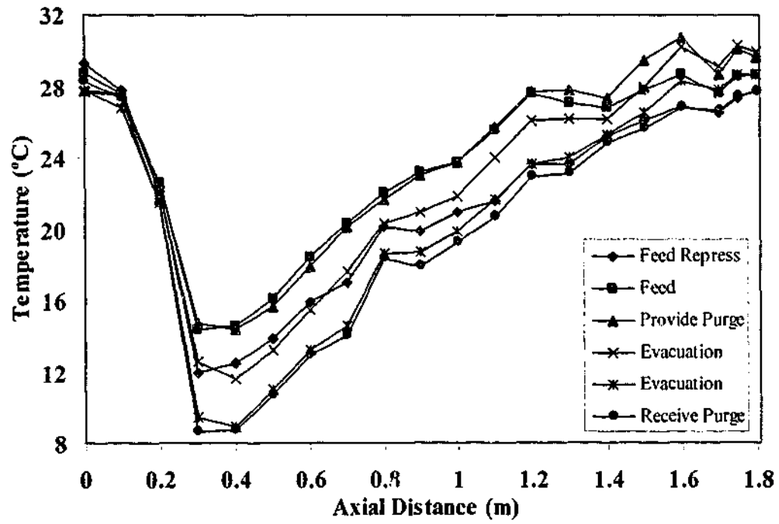

Figure 8.1a. **Cyclic steady state, end of step axial temperature profiles of a single bed taken from pilot plant studies – dual bed, 6 step, 60 second cycle with a single adsorbent layer on top of an inert prelayer. 'Low' purity (81.5%) case.**

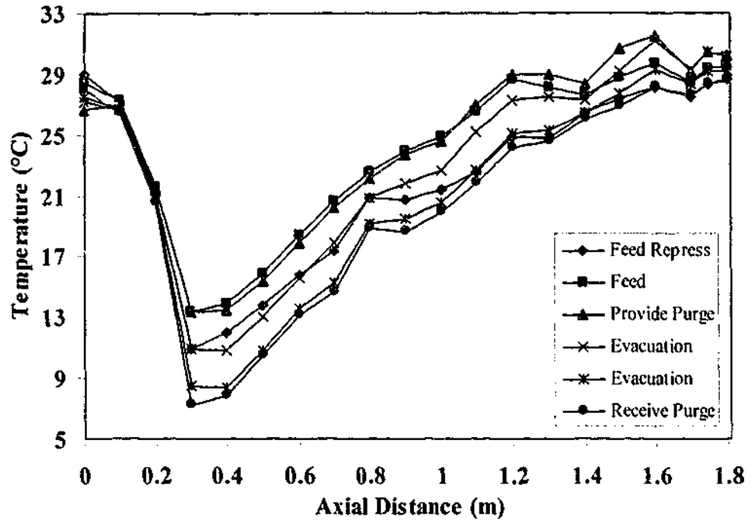

Figure 8.1b. Cyclic steady state, end of step axial temperature profiles of a single bed taken from pilot plant studies – dual bed, 6 step, 60 second cycle with a single adsorbent layer on top of an inert prelayer. 'High' purity (85.4%) case.

8.2 DEVELOPMENT OF A SIMPLIFIED ADSORPTION PROCESS MODEL

The proposed mechanistic model is restricted to conditions in which the thermal and concentration waves are coincident [Basmadjian, pp. 57-59, 1997]. For the simulation conditions, binary components consisting of oxygen and nitrogen was assumed with their behaviour described by the ideal gas law. Furthermore, the following additional assumptions were made to allow the development of the model:

- The only adsorbable species is nitrogen. This is a reasonable assumption as zeolite synthesis technology is producing sieves with better selectivities and adsorptive capacity (compare the isotherms for nitrogen and oxygen shown in Figure 8.3c for a lithium zeolite) [Hutson *et al.*, 1999; Yang, 2000].
- Convective heat flux is ignored (i.e. $\partial T/\partial z = 0$) as it has been observed that the change in temperature over a cycle is not a strong function of the convection of thermal energy [Wilson and Webley, 2002b].
- The effect of temperature on the gas density can be ignored (e.g. ΔT over a cycle is ~10°C and therefore $T_{initial}/(T_{initial} + \Delta T) \approx 1$ causing $\rho_g \equiv$ constant).

- The accumulation of energy in the gas and adsorbed phases is negligible in comparison with the solid/bed (i.e. $\rho_s C_{ps} >> \rho_g C_{pg}$).
- Adiabatic operation.
- Second-order effects such as axial dispersion and conduction are negligible.
- Energy conservation considerations are based on enthalpy changes only and thus kinetic energy variations are ignored.
- Local equilibrium between the gas and solid phases – a good assumption for 'slow' cycles.

The equilibrium isotherm for gas adsorption is a function of pressure, temperature and mole fraction

$$n_i^{eq} = f(P, y, T) \tag{8.2a}$$

and for a binary system containing nitrogen and oxygen the isotherm equation, the dual-site Langmuir equation was used to describe the equilibrium loading on the sieve

$$n_i^{eq} = \frac{m_1 b_{oi} e^{\frac{Q_{1i}}{RT}} Py}{1 + b_{oi} e^{\frac{Q_{1i}}{RT}} Py + b_{oj} e^{\frac{Q_{1j}}{RT}} P(1-y)} + \frac{m_2 d_{oi} e^{\frac{Q_{2i}}{RT}} Py}{1 + d_{oi} e^{\frac{Q_{2i}}{RT}} Py + d_{oj} e^{\frac{Q_{2j}}{RT}} P(1-y)} \tag{8.2b}$$

Let $A = m_1 b_{oi} e^{\frac{Q_{1i}}{RT}} P$; $B = b_{oi} e^{\frac{Q_{1i}}{RT}} P$; $C = b_{oj} e^{\frac{Q_{1j}}{RT}} P$; $D = m_2 d_{oi} e^{\frac{Q_{2i}}{RT}} P$; $E = d_{oi} e^{\frac{Q_{2i}}{RT}} P$; $F = d_{oj} e^{\frac{Q_{2j}}{RT}} P$

Equation (2a) can be re-written as

$$n_i^{eq} = \frac{Ay}{1 + By + C(1-y)} + \frac{Dy}{1 + Ey + F(1-y)} \tag{8.2c}$$

and re-arranged in terms of y to yield

$$y = \frac{(b - n_i^{eq} d) \pm \sqrt{(n_i^{eq} d - b)^2 - 4(n_i^{eq} c - a)(n_i^{eq} e)}}{2(n_i^{eq} c - a)} \tag{8.2d}$$

where $a = AE - AF + BD - CD$; $b = A + AF + D + CD$; $c = BE - BF - CE + CF$; $d = E - F + B + BF - C - 2CF + CE$; $e = 1 + F + C + CF$

Finally, the energy balance can be written in terms of the accumulation of energy in the solid and the generation or loss of heat from adsorption or desorption respectively (a first-order approximation). This was a reasonable assumption as it has been established in previous work [Wilson and Webley, 2002b], that the temperature variation at a point in the bed was due to a very small convective term and a significantly larger adsorptive term. This assumption is encapsulated in the following expression (Eq. (8.2e)) which shows that the temperature change at a point in the bed is a manifestation of the change in loading at that point. Hence, the application of this method to the inert prelayer would yield spurious results.

$$\rho_s C_{p_s} \left.\frac{dT}{dt}\right|_z = \rho_s \Delta H_i \left.\frac{dn_i}{dt}\right|_z \tag{8.2e}$$

Equation (8.2e) can be expressed in terms of the adsorptive uptake rate as

$$\left.\frac{dn_i}{dt}\right|_z = \frac{C_{p_s}}{\Delta H_i} \left.\frac{dT}{dt}\right|_z \tag{8.2f}$$

The resulting equation (Eq. (8.2f)), suggests that the adsorbent isotherm is essentially captured by the temperature time derivative provided that a fairly accurate value of the heat of adsorption, ΔH_i, is available. Integrating Eq. (8.2f) gives

$$n_{i,t+\Delta t} = \frac{C_{p_s}}{\Delta H_i}\left(T_{t+\Delta t} - T_t\right) + n_{i,t} \tag{8.2g}$$

Equation (8.2g) reveals that the amount adsorbed can be determined independent of pressure and composition by measurements of temperature alone. However, this equation requires an initial condition to be established for the mole fraction, temperature and pressure at each point in the bed. The initial amount loaded is then calculated using an isotherm relationship such as shown in Eq. (8.2b). Assuming that the process is operating near-equilibrium conditions, $n_{i,t+\Delta t} \approx n_i^{eq}$, the composition at a particular point is evaluated by solving for the positive real root (that is less than unity) of Eq. (8.2d).

It is worthwhile to note that certain isotherm models such as the Freundlich and Toth models, cannot be manipulated to produce an explicit expression for the composition as shown in Eq. (8.2d) for the dual-site Langmuir equation. This is because of the power relationship between the amount adsorbed and the composition. Nonlinear solution techniques such as Newton-Raphson or the Secant rule bounded between 0 and 1 are required. Furthermore, if the isotherm model adopted is favourable and the operation of the adsorber is within the horizontal portion of the isotherm, then integration of Eq. (8.2a) in terms of y is necessary to yield the correct solution. Equation (8.2h) describes this solution strategy whereby Eq. (8.2a) is expanded using the chain-rule for derivatives in terms of time and the right hand side of Eq. (8.2f) is substituted for the uptake rate (refer to Eq. (8.2i)). Equation (8.2i) can then be integrated numerically by employing the Runge-Kutta method to provide the temporal composition profile at a particular point in the bed.

$$\left.\frac{dn_i}{dt}\right|_z = \left(\frac{\partial n_i}{\partial P}\right)_{y,T} \left.\frac{dP}{dt}\right|_z + \left(\frac{\partial n_i}{\partial y}\right)_{P,T} \left.\frac{dy}{dt}\right|_z + \left(\frac{\partial n_i}{\partial T}\right)_{y,P} \left.\frac{dT}{dt}\right|_z \tag{8.2h}$$

$$\left.\frac{dy}{dt}\right|_z = \frac{\left[\left.\frac{dT}{dt}\right|_z \left(\frac{C_{p_s}}{\Delta H} - \left(\frac{\partial n_i}{\partial T}\right)_{y,P}\right) - \left(\frac{\partial n_i}{\partial P}\right)_{y,T} \left.\frac{dP}{dt}\right|_z\right]}{\left(\frac{\partial n_i}{\partial y}\right)_{P,T}} \tag{8.2i}$$

An additional note is that the solution method for composition and loading as presented above, can be extended to include binary systems. The analysis begins by expressing the total amount adsorbed as the sum of the contributions from the each of the species i and j (refer to Eq. (8.2j)). Once again, equilibrium conditions had been assumed and hence the functions $f()$ and $g()$ represent the appropriate isotherm relationship. Also for a binary system, the relationship between the composition of species i and species j is given by $y_j = 1 - y_i$.

$$N = n_i^{eq} + n_j^{eq} = f(P, y_i, T) + g(P, y_j, T) = f(P, y_i, T) + g(P, (1 - y_i), T) \tag{8.2j}$$

The energy balance equation. Eq. (8.2e), is also modified to account for the additional species, j as shown in Eq. (8.2k) below.

$$\rho_s C_{p_s} \left.\frac{dT}{dt}\right|_z = \rho_s \Delta H_i \left.\frac{dn_i}{dt}\right|_z = \rho_s \left[\Delta H_i \left.\frac{dn_i}{dt}\right|_z + \Delta H_j \left.\frac{dn_j}{dt}\right|_z\right] \tag{8.2k}$$

Once again, by taking the derivative of the isotherm in terms of time and expanding using the chain-rule, the uptake rate in Eq. (8.2k) can be approximated as shown in Eq. (8.2l) below.

$$C_{ps}\left.\frac{dT}{dt}\right|_z = \Delta H_i\left[\left(\frac{\partial n_i}{\partial P}\right)_{y_i,T}\left.\frac{dP}{dt}\right|_z + \left(\frac{\partial n_i}{\partial y_i}\right)_{P,T}\left.\frac{dy_i}{dt}\right|_z + \left(\frac{\partial n_i}{\partial T}\right)_{y_i,P}\left.\frac{dT}{dt}\right|_z\right] + \Delta H_j\left[\left(\frac{\partial n_j}{\partial P}\right)_{y_i,T}\left.\frac{dP}{dt}\right|_z + \left(\frac{\partial n_j}{\partial y_i}\right)_{P,T}\left.\frac{dy_i}{dt}\right|_z + \left(\frac{\partial n_j}{\partial T}\right)_{y_i,P}\left.\frac{dT}{dt}\right|_z\right] \quad (8.2l)$$

The final expression, Eq. (8.2m), can be integrated to obtain a value for species *i* and then used to calculate the composition of component *j* at a point in the bed.

$$\left.\frac{dy_i}{dt}\right|_z = \frac{C_{ps}\left.\frac{dT}{dt}\right|_z - \Delta H_i\left[\left(\frac{\partial n_i}{\partial P}\right)_{y_i,T}\left.\frac{dP}{dt}\right|_z + \left(\frac{\partial n_i}{\partial T}\right)_{y_i,P}\left.\frac{dT}{dt}\right|_z\right] - \Delta H_j\left[\left(\frac{\partial n_j}{\partial P}\right)_{y_i,T}\left.\frac{dP}{dt}\right|_z + \left(\frac{\partial n_j}{\partial T}\right)_{y_i,P}\left.\frac{dT}{dt}\right|_z\right]}{\left(\frac{\partial n_i}{\partial y_i}\right)_{P,T}\left(\Delta H_i + \Delta H_j\right)} \quad (8.2m)$$

The last point to note is that it is not possible to extend this method beyond two components as the number of unknowns becomes more than the number of equations relating to them (i.e. no obvious method of relating the composition of a third component with the first and second species).

8.3 THE VSA CYCLE AND SIMPLIFIED MODEL IMPLEMENTATION

The VSA cycle simulated in this chapter bears the main characteristics typical of industrial practice. The numerical process simulator, MINSA (described in §3.1 of Chapter 3), was used to model the adsorption system consisting of a dual bed, five-step, 60 second cycle as a single bed cycle depicted in Figure 8.3a. The ternary air separation system comprising of nitrogen, oxygen and argon was modelled as a binary mixture of nitrogen and oxygen within MINSA as argon was assumed to behave similarly to oxygen [Miller, 1973]. Therefore, the boundary condition at the inlet to the adsorbers comprises of 78% nitrogen and 22% oxygen. The adsorbent was

simulated using the isotherm of a commercially available lithium-based zeolitic sieve (9.1kg/bed) with an inert prelayer (0.5kg/bed). In industry, the prelayer's function is to remove moisture from the air stream, preventing contamination of the main bed. Whilst a dry inlet air stream was simulated, the prelayer was retained in order to duplicate the unusual temperature profiles created by a prelayer of material in a bulk gas separation system [Wilson *et al.*, 2001].

Figure 8.3a, shows the various steps within the cycle, step times, flow direction and control valves and is a numerical implementation of the dual bed cycle depicted in Figure 2.2c of Chapter 2. Being a semi-batch process, product off-take occurred during step two, with the flow into the bed controlled by valve CV1 and product flow controlled by valve CV4. Desorption of the adsorbate (nitrogen in this case) occurred during step four and was regulated via valve CV2. The purge step, here shown in steps three (provide purge) and five (receive purge), was important for the maintenance of product purity. It forces contaminants (nitrogen) in the fluid phase down from the top of the bed and allowes further adsorbate desorption to occur by lowering the partial pressure of nitrogen around the sieve. Control of the product purge stream was via valve CV3. Pressurising the bed with dry air in step one completed the cycle. The various steps are operated by applying square wave boundary conditions that essentially turned the flows at the bottom and top of the bed either on or off. This simulated the fixed C_v switch valves used in industrial plants.

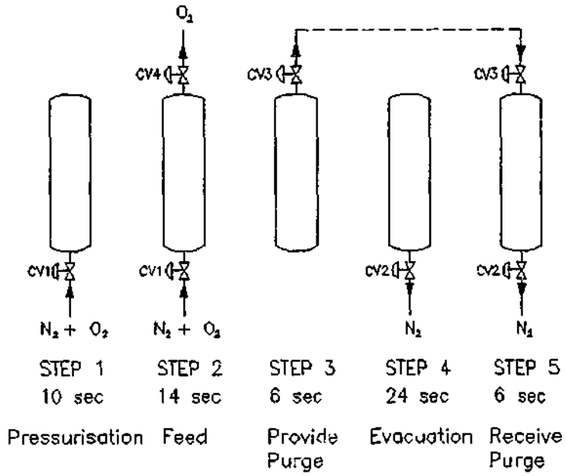

Figure 8.3a. Numerical simulation of a dual bed 6 step cycle using a single bed 5 step simulator.

Implementation of the simplified adsorption model to determine the composition profile was relatively straightforward and is described by way of schematic in Figure 8.3b. It shows that

initial conditions are to be specified. In order for the method to predict accurate results, the initial conditions of the model should match that of the plant (or MINSA in this case). This can be easily achieved in the field by initially purging the beds with a gas of known composition (e.g. dry air) at constant pressure and temperature until saturated and equilibrated. The remaining piece of information required for solution of the simple model was the measurement of the plant's pressure and temperature profile at each instance in time from start-up. These measured parameters are then used to solve Eqs. (8.2b) and (8.2g) to yield the instantaneous local composition (Eq. (8.2d)). Alternatively, Eqs. (8.2i) or (8.2m) can be integrated to determine the fluid phase mole fraction.

The last point to note is that although the method proposed is conservative (Eq. (8.2f) closes at CSS), the boundary conditions are unknown in the simple model. Incorporation of the boundary condition requires compliance with the component mass balance at CSS where the integrated inlet flow less the product flow equals the integrated flow of gas exiting the system as desorbate over a cycle. This desorbate stream is equivalent to the change in adsorbate loading over a cycle plus the change in the fluid phase composition over a cycle. A mathematical description of the situation outlined is shown in Eq. (8.2n).

$$\int_0^z (n_{i,0} - n_{i,\tau})\frac{\rho_s \pi D^2}{4}dz + \int_0^\tau \left[\int_0^z \frac{P_{z,t}u_{z,t}\varepsilon_b y_{z,t}}{RT}dz\right]dt = \int_0^\tau \frac{P_{0,t}u_{0,t}y_{0,t}}{RT}dt - \int_0^\tau \frac{P_{L,t}u_{L,t}y_{L,t}}{RT}dt \quad (8.2n)$$

Solution of the spatial adsorbate profile and composition (the terms on the left hand side of Eq. (8.2n)) at the end of the cycle was solved by iterative methods. For a bulk separation process, the solution was underspecified as there are several solutions to Eq. (8.2n) (i.e. various configurations of the composition and loading profile that still satisfied the mole balance). The primary reason for this failure to yield a convenient solution is that the right hand side of Eq. (8.2n) only describes bulk properties whereas the local composition at each point in the bed is of primary interest (i.e. Eq. (8.2n) is *ill-posed*). Hence, specification of incorrect initial conditions without input of the boundary conditions results in a vertical shift of the predicted composition profile either up or down by the difference in the error between the actual and guessed initial conditions. However, since the method is independent of the axial position (y is calculated locally with time at each sensor location), any errors in the estimated initial conditions would not propagate to affect the composition calculation of the other sensors at different axial locations.

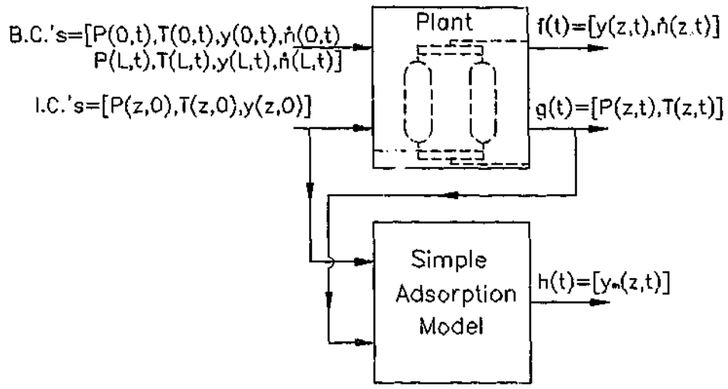

Figure 8.3b. Schematic showing the implementation strategy of the simple adsorption process model on the plant.

The MINSA input conditions for the cycle shown in Figure 8.3a is presented in Table 8.3a along with the isotherm information for nitrogen and oxygen plotted in Figure 8.3c. Performance parameters at cyclic steady state are shown in Table 8.3b for this cycle. This CSS condition will be utilised as the basis for the baseline case study. In order to test the accuracy of the model in capturing dynamic trends, a 5% step change in the feed valve C_v was performed and the composition profiles of both MINSA and the simple model tracked with time. This shift in the valve position represented an increase in inlet flow and/or pressure which is a common disturbance in field operation. For this study, the bed was discretised into twenty-three nodes with three nodes in the prelayer. Also, it was assumed that the location of the temperature and pressure sensors coincided with the nodal positions and that there was an equivalent amount of sensors as there are nodes in the adsorbent bed (i.e. twenty sensor points were used). Furthermore, it was assumed that pressure sensors were available at the very bottom and top of the beds, which corresponded with the wall values calculated by the numerical simulator. Finally, the integral absolute error, IAE, was used as a measure of performance of the simple model in comparison with MINSA and is given by Eq. (8.2o).

$$IAE = \int_0^\tau |y_a - y_m| dt \quad (8.2o)$$

Table 8.3a. Numerical simulation input parameters.

Bed and Adsorbent Properties	
Total Bed Height (mm)	1810
Internal Bed Diameter (mm) and Wall Thickness (mm)	104 x 6 w.t.
Adsorbent	Lithium zeolitic sieve
Prelayer Length (mm)	300
Prelayer	Alumina, 2.5mm beads
Particle Diameter, d_p, (mm)	1.4
Bed Voidage, ε_b	0.37
Pellet Voidage, ε_p	0.60
Solid Density, ρ_s, (kg/m^3)	710
Solid Heat Capacity, C_{ps}, (J/kg/K)	1000
Site-Weighted Heat of Adsorption (J/mole)	ΔH_{N2}=18573 ; ΔH_{O2}=11968
Numerical Model Parameters	
No. of Nodes in Adsorbent Bed and Prelayer	20 ; 3
CSS Mass Balance Closure Tolerance (%)	$5x10^{-3}$
CSS Energy Balance Closure Tolerance (%)	$1x10^{-5}$

Table 8.3b. CSS performance information of the 5 step, dual bed oxygen VSA cycle studied.

Cycle Time (seconds)	60
Feed Gas (mmole/cycle)	8428
Evacuation Gas (mmole/cycle)	7172
Product Gas (mmole/cycle)	1256
Product Oxygen Purity (%)	85.72
Production Rate (kg/day)	50
Product Recovery (%)	58.10
Mass Balance Closure (gmole)	$-6.542x10^{-8}$
Energy Balance Closure (kJ)	$1.2x10^{-12}$
End of Step Pressures	**kPa.A**
Step 1 - Feed Repressurisation	100.97
Step 2 - Feed + Product	121.72
Step 3 - Provide Purge Gas	106.62
Step 4 - Evacuation	38.86
Step 5 - Receive Purge Gas	43.95

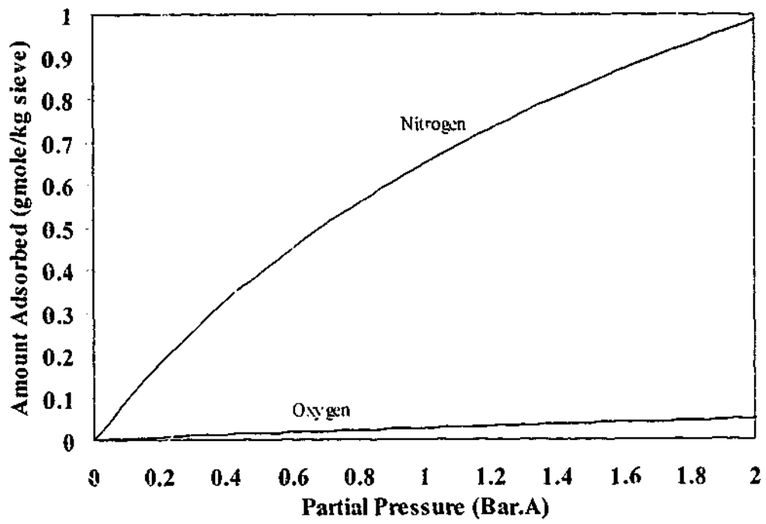

Figure 8.3c. The isotherm for the lithium based zeolite used in this study shown at 300K.

8.4 DISCUSSION OF THE EXPERIMENTAL RESULTS

The discussion of the results begins with an analysis of Figure 8.4a, which shows the performance of the model in capturing the composition profile 'measured' in the MINSA simulation environment at cyclic steady state. Three scenarios were investigated – pressure sensors available at each of the twenty axial locations, a linear pressure gradient through the bed and negligible pressure drop through the bed. The initial condition used for this study was established from the CSS baseline values obtained from MINSA. In the first case, the mole fraction profile of the model matched MINSA quite well with the IAE calculated as 1.05. The assumption of a linear pressure profile that was determined by fitting a curve between the pressure measured at the bottom and top of the bed also yielded reasonable correlation with actual values. In this case, the IAE was marginally smaller than that for the first case (0.94). However, what the IAE figure did not indicate was the sensitivity of the simple method to changes in pressure during each step as observed in Figure 8.4a. As the system moves from one step to the next, the composition profile showed sudden jumps in value although it was much more damped if the axial pressure profile was measurable. This trend is further highlighted when the assumption of negligible pressure drop was made. Using only the pressure measurement at the bottom of the bed, the difference between the actual (MINSA) profile and the estimated profile was accentuated. For this case, the IAE was 6.40 and Figure 8.4a shows this significant difference. These three scenarios emphasize the importance of being able to correctly measure or estimate the pressure profile in the bed even for a cycle such as this one, which was operating close to equilibrium conditions. Obviously, for faster cycles, such as rapid PSA (RPSA) systems, the assumption of equilibrium would fail and differences between the process and model would be further stressed. However, for most oxygen VSA systems, the assumption of a linear pressure gradient afforded a reasonable estimate.

Figure 8.4b further validated the assumption of linear pressure gradients, which shows that the simple model approximated the 'measured' conditions well at the end of the two most important steps of the cycle – end of feed and end of receive purge. The reason the model allowed a better prediction of the shape of the composition front during the end of the receive purge step than the feed step was because adsorption occurred throughout the bed in the purge step. This was indicated by the end of the bed receiving purge where adsorbate breakthrough of the bed providing purge gas occurred – the nitrogen mole fraction increased at the end of the bed receiving purge gas. In addition, the rather low CSS product purity pointed to saturation of the beds during the cycle operation. For the portions of the bed where no or very little adsorption occurred, the simple method failed and errors between measurement and prediction resulted since the model predicted that the change in temperature was solely due to nitrogen ad/desorption. During the feed step, the thermal variation with time at certain points in the bed

was principally due to convective heat transfer because the adsorbent at that point was either saturated with adsorbate (bottom of the bed) or in the oxygenated zone (top of the bed). These are the regions where the model approximations exhibited the greatest error as observed in Figure 8.4b for the feed step. Nevertheless, it is clear that the mass transfer zone began at around 1.14m into the bed followed by the shock-like decrease in the nitrogen mole fraction, which was correctly predicted by the model.

Figure 8.4c shows the simple technique employed in a dynamic situation. It was assumed in this simulation that the initial profile in the bed was known and that it was at mass and thermal equilibrium (Cycle 0). A 5% step change to the feed valve position at the start of the feed step was made at Cycle 1 and the profiles of MINSA and the simple model tracked with time until Cycle 10 where the product purity had dropped by 23.74% to 61.98% (from 85.72%). It is worthwhile noting that once the initial conditions for the model was predetermined, the predicted final conditions were used as the initial conditions for the model on the next cycle. The model was not re-calibrated against the full numerical model at any stage during the dynamic run. Once again, differences between measurement and model were highlighted by the assumption of a single adsorbable species and negligible convective heat transfer. However, the overall shape of the front had been correctly approximated. Figures 8.4d and 8.4e compare the model prediction at various points in the bed and showed that the best correlation occurred at the locations within the MTZ. Thus, at 0.34m, for example, the model predicted a rising mole fraction with cycle number when in fact it was constant at the feed gas composition of 0.78. The reason for the difference becomes obvious upon examination of Eq. (8.2i). In order for no change in composition to occur with time at a given point, the following situation has to be satisfied:

$$\left.\frac{dy}{dt}\right|_z = \left.\frac{dT}{dt}\right|_z \left(\frac{C_{ps}}{\Delta H} - \left(\frac{\partial n_i}{\partial T}\right)_{y,P}\right) - \left(\frac{\partial n_i}{\partial P}\right)_{y,T} \left.\frac{dP}{dt}\right|_z = 0 \qquad (8.4a)$$

or in other words

$$\left.\frac{dT}{dt}\right|_z \left(\frac{C_{ps}}{\Delta H} - \left(\frac{\partial n_i}{\partial T}\right)_{y,P}\right) = \left(\frac{\partial n_i}{\partial P}\right)_{y,T} \left.\frac{dP}{dt}\right|_z \qquad (8.4b)$$

The temperature gradient with time was non-zero at 0.34m due to convective heating from the inlet gas stream. This convective temperature variation caused the simple model to calculate a change in composition, which it assumed was solely due to adsorption. Hence, at this point in the bed the left-hand side of Eq. (8.4b) is greater than the right-hand side and produced a

positive increase in composition as observed in Figure 8.4d. However, the determination of the mole fraction was independent of the spatial coordinate and therefore errors, such as that described previously, were not permitted to propagate through the calculation for the rest of the bed.

Nevertheless, aside from the errors, which were modest on the whole, the success of this method in a dynamic situation whereby an unknown disturbance (to the simple model) was applied revealed the relative power of this technique as an online diagnostic tool for field operation. The reason that this method was able to capture the time-varying composition profile despite the convective term (which shapes the temperatures and hence composition profiles in the bed) being absent, is because it is implicitly combined with the adsorptive term through measurement of the axial temperatures. It has been established that if Eq. (8.2e) was solved numerically together with the mass conservation balance, then a flat temperature profile would result and hence produce an erroneous estimation of the composition gradient [Wilson, 2001].

The final issue to be resolved is whether the assumption of a single adsorbale species was sufficient to model the air separation process and avoid the complexity of solving Eq. (8.2m). A simple test of this assumption is to calculate the temperature rise at a point in the bed over half a cycle, assuming only nitrogen or oxygen was ad/desorbing, and comparing this result with the measured change. This technique is summarised in Eqs. (8.4c) and (8.4d). The results are plotted and shown in Figure 8.4f. From this graph, it is clear that the assumption of nitrogen adsorption yielded very good correlation with the actual values. This was attributed to the high selectivity and adsorptive capacity of the lithium based molecular sieve for nitrogen and the bulk gas adsorption property of the air separation process for oxygen enrichment. Thus, the heat generation due to the adsorption of oxygen was insignificant when compared with that of nitrogen (i.e. $\rho_s \Delta H_{N2} \Delta n_{N2} >> \rho_s \Delta H_{O2} \Delta n_{O2}$) because oxygen is not a strongly adsorbed component. On the other hand, this assumption would not hold in the case of a binary mixture whereby both species shared similar capacities.

$$\int_0^{\frac{\tau}{2}} dT_{i,j} = \frac{\Delta H_{i,j}}{C_{p_s}} \int_0^{\frac{\tau}{2}} dn_{i,j} \tag{8.4c}$$

$$T_{i,j}\Big|_{\frac{\tau}{2}} - T_{i,j}\Big|_0 = \frac{\Delta H_{i,j}}{C_{p_s}} \left(n_{i,j}\Big|_{\frac{\tau}{2}} - n_{i,j}\Big|_0 \right) \tag{8.4d}$$

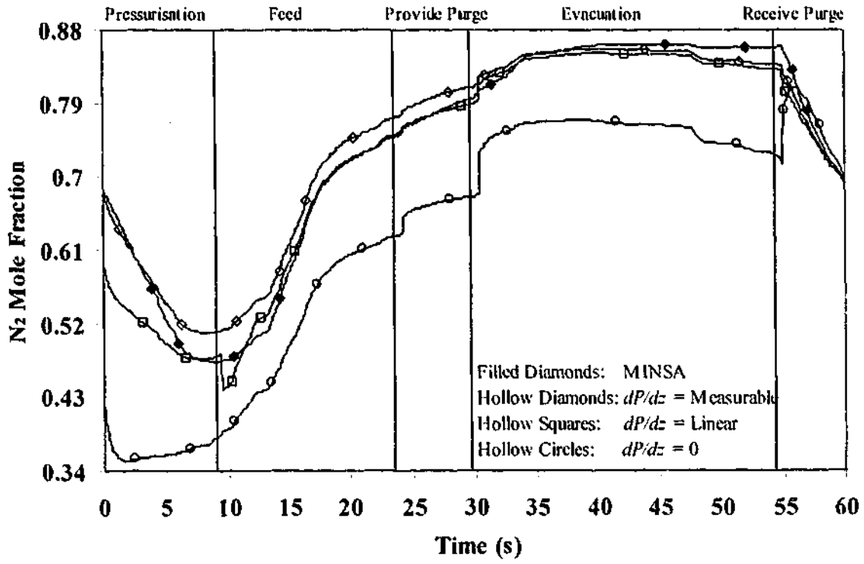

Figure 8.4a. Performance of various assumptions of pressure drop in capturing the N_2 mole fraction profile at an axial distance of 1.11m compared to the actual (MINSA) profile over a cycle at CSS.

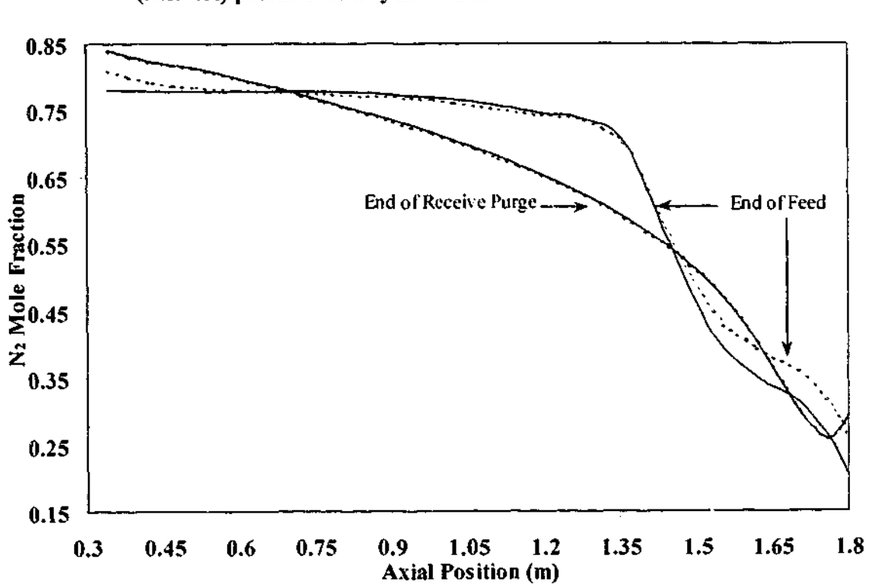

Figure 8.4b. CSS comparison between performance of the model and MINSA in the estimation of the N_2 mole fraction profile at the end of the feed (step 2) and receive purge steps (step 5) assuming a linear pressure gradient. Continuous lines correspond to MINSA while the dashed lines pertain to the simple model.

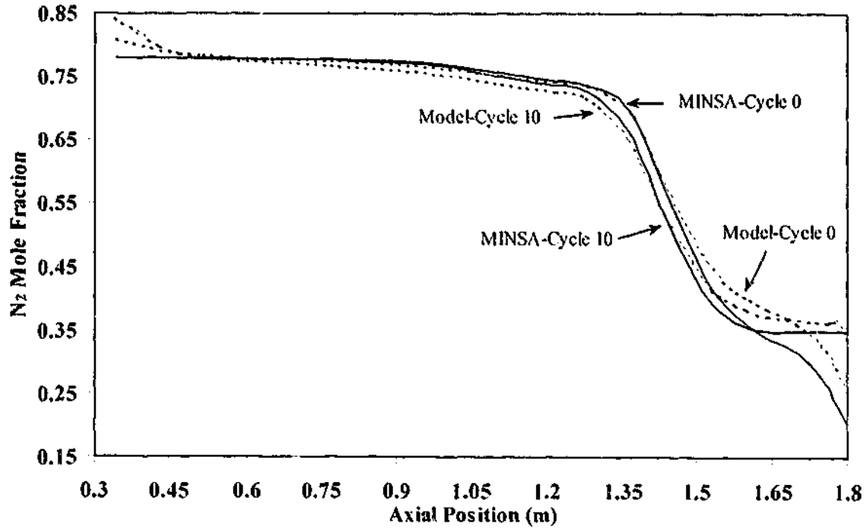

Figure 8.4c. **Comparison between performance of the model and MINSA in the estimation of the dynamic N_2 mole fraction profile at the of feed step (step 2) assuming a linear pressure gradient. Continuous lines correspond to MINSA while the dashed lines pertain to the simple model.**

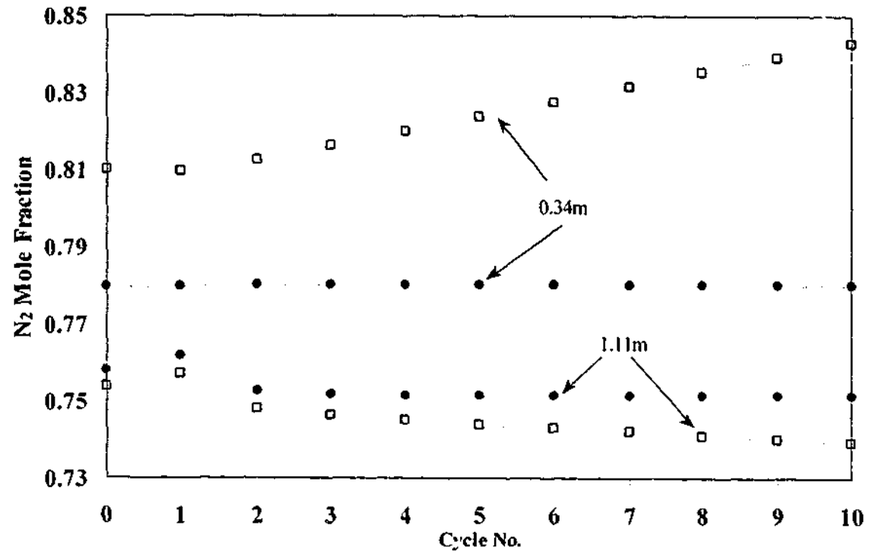

Figure 8.4d. **Movement in the N_2 mole fraction profile with cycle following a 10% step change in the feed valve position initiated at cycle 1. Comparison between model and MINSA values at a point outside the MTZ (0.34m) and a point close to the inception of the MTZ (1.11m). Filled circles correspond to MINSA data while the hollow squares are model estimations.**

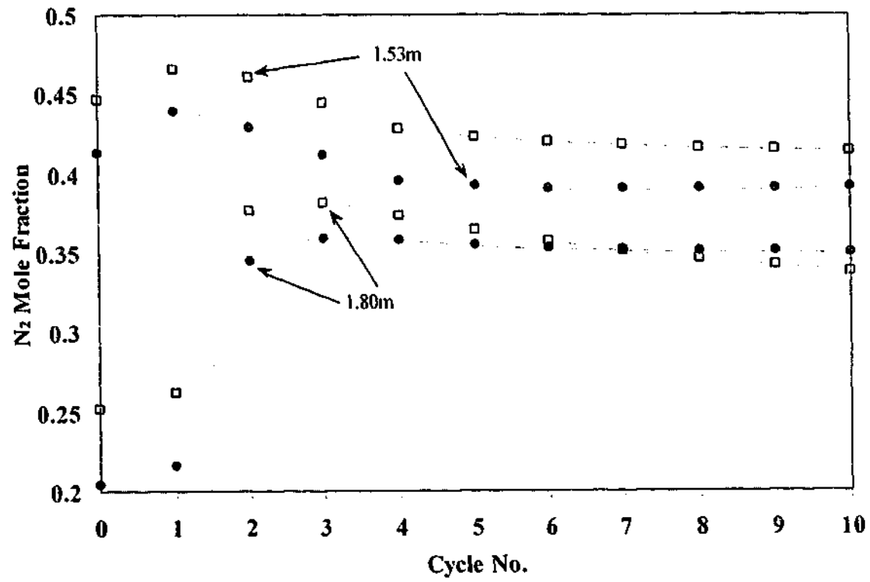

Figure 8.4e. **Movement in the N_2 mole fraction profile with cycle following a 10% step change in the feed valve position initiated at cycle 1. Comparison between model and MINSA values at a point within the MTZ (1.53m) and a point close to the boundary of the MTZ (1.80m). Filled circles correspond to MINSA data while the hollow squares are model estimations.**

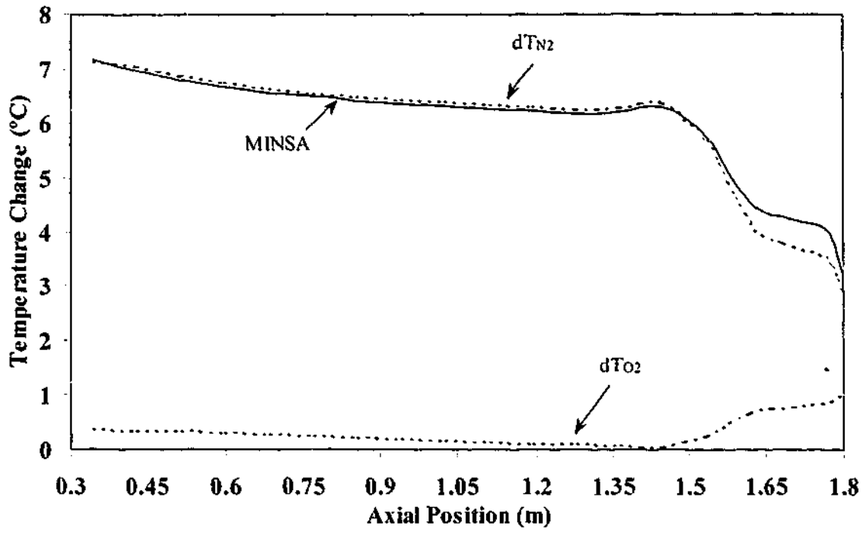

Figure 8.4f. Comparison of the ΔT calculated over the bed for half a cycle when assuming the ad/desorption of nitrogen or oxygen compared with 'measured' values from MINSA. C_{ps} = 1000 J/kg/k; ΔH_{N2} = 18573 J/mol; ΔH_{O2} = 11968 J/mol.

8.5 CONCLUDING REMARKS

Presentation has been made of a practical technique capable of implementation online with some accuracy to allow inference of the time-variant composition gradient in an adsorption bed. The method used a combination of natural observations (measurements of plant pressures and temperatures) and mathematical algorithms to allow expeditious calculation of the loading and composition. The method is cheap (the cost of thermocouples is insignificant compared to other capital costs) and simple to implement. Coupled with plant operating and design heuristics, this procedure allowed the identification of instrument failure be it pressure or temperature and sieve contamination due to impurities present in the inlet stream or through radial leaks into the beds. It may also provide heuristics to the plant engineer on making informed decisions on changes to boundary conditions (such as control valves and step times) and assist in the diagnosis of system disturbances (such as valve failure and inlet pressure disturbances).

The main limitation of this technique is that it is only valid for bulk separation processes consisting of single or binary component adsorption (such as oxygen VSA or PSA operations whereby one component is strongly adsorbed) because of the inherent assumption of

coincidence of the mass and thermal wave fronts. Additional errors would occur if the temperature sensor was placed in non-adsorbing locations such as in the prelayer or in a saturated or oxygenated zone as the model assumed up to two strongly adsorbed components with no convective heat transfer. For bulk separations involving more than two adsorbable components, (for example in hydrogen PSA), it is foreseeable that decoupling the temperature signals would be extremely difficult. In addition, with the future trend tending towards shorter cycle times and smaller sieve particle sizes, pressure drop becomes increasingly important and in this scenario, the assumption of a linear pressure gradient may begin to deteriorate. In this case the technique may have to be extended to include direct measurement of the spatial pressure profile.

To ensure reliable performance in field implementation, a sufficient number of thermocouples were required in the main adsorption layer especially about the mass transfer zone such that an accurate map of the composition front can be constructed (say by linearly interpolating between sensor points or through the use of spline fitting methods). Furthermore, field implementation would have to consider the effects of the sensor error band and measurement noise. To enable dynamic tracking of the composition profile, a known initial condition was required at each location in the bed. This can be achieved in practice by initially purging the bed with a gas of known composition (such as air) while the plant was shutdown due to maintenance, etc.

The final limitation of this technique is that it can not be used to extrapolate through in the temporal domain, as current measures of the primary parameters are required for solution of the differential equation. Therefore use of this method in a feedforward structure requires extending its use to predict the temperature and pressure profiles.

NOMENCLATURE

b_{oi}	1st site dual-site isotherm parameters (1/kPa)
C_{ps}	adsorbent heat capacity (J/kg/K)
d_{oi}	2nd site dual-site isotherm parameters (1/kPa)
D	adsorber bed internal diameter (m)
$m_{1,2}$	1st and 2nd dual-site isotherm parameter (mol/kg)
n_i^{eq}	equilibrium loading of the adsorbable species (nitrogen) (mol/kg)
N	total adsorbed amount (mol/kg)
P	pressure (kPa.A)
$Q_{1,2}$	dual-site isotherm parameter (kJ/kmol)
R	universal gas constant (kJ/kmol/K)
t	time variable (s)

T	temperature (K)
u	superficial velocity (m/s)
y_i	mole fraction of the adsorbable species (nitrogen)
z	axial position (m)
ΔH	heat of adsorption (kJ/kmol)
ε_b	adsorber bed voidage
ρ_s	adsorber bed density (kg/m^3)
τ	cycle time (s)

Subscripts

a	actual measurement
i, j	first and second adsorbable component
L	adsorber bed length (m)
m	model estimation

Chapter Nine

Conclusions and Recommendations for Future Work

9.1 CONCLUSIONS

The work undertaken in this study investigated the dynamic response of the oxygen vacuum swing adsorption system and attempted to characterise the features important for process control to aid development of simple mechanistic and empirical models. Both numerical and experimental resources, (through the use of a VSA pilot plant), had been utilised to achieve this goal. The second part of this investigation presented the development and implementation of various controllers (decentralised and centralised) and demonstrated their performance through pilot plant studies. The third objective was to develop a method based on plant observations as a heuristic tool to aid operators and engineers in the field. Conclusions gathered from this research effort are summarised below.

- The existing oxygen VSA pilot plant had been redesigned to be more mechanically robust to allow for continuous cyclic operation. The new beds had been demonstrated to be reasonably adiabatic and hence representative, in operation, of industrial columns. Furthermore, the employment of inlet temperature control, enhanced feed pressure regulation and refined flow metering equipment improved the control over fixed variables and permitted the gathering of reliable data.

- The bulk pressure and flow effects in a VSA process can be satisfactorily modelled using a system of coupled isothermal tanks with ad/desorption. This simplified mechanistic model provided adequate prediction of the variables of greatest interest to the customer. Distributed, rigorous numerical models were useful as predictive design tools but were overly complicated and required extensive computing resources for model-based control and online process monitoring. Empirical methods, such as artificial neural networks, shared the same computational dilemmas as detailed numerical simulations as a large database of operating conditions was required to permit sufficient regression. Thus, the use of the current ANN algorithm to model dynamic responses was limited.

- The simple coupled tank model was extended to include the product vessel composition variable by assuming the adsorbers responded instantaneously (within one cycle) and by

fitting an empirical relationship between product flow per cycle and oxygen purity. The data showed reasonable agreement between process and model with non-uniform mixing being the principal factor for the mismatch.

- The experimental investigation coupled with various analysis tools such as ANN's, Monte Carlo techniques and RGA analysis, yielded information on appropriate controller pairings, the extent of control loop interaction and robustness of the closed-loop control system.

- A novel MPC controller was developed and utilised for both single and multiple loop control of the experimental oxygen VSA process.

- Comparisons under load rejection criteria between PID and MPC showed comparable performance in single and multiple conditions.

- PID exhibited superior performance over this particular MPC algorithm under set point response in single loop mode.

- Explicit decoupling of decentralised controllers, whether full or one-way, proved to be prone to model errors causing instabilities or severely reducing performance.

- A simple method for the prediction of axial composition profiles in binary bulk separation processes was derived. With the simplifying assumptions, this model exhibited favourable agreement with numerical data thus, highlighting its usefulness as a technique for process monitoring and diagnostics.

9.2 RECOMMENDATIONS FOR INDUSTRIAL IMPLEMENTATION

The various modelling and control techniques presented in this thesis can readily be applied in field operation. Throughout this study, the practical application of this work was always kept in mind and hence many simplifications were made to the problem at hand. The author has the following recommendations for industrial implementation of the control and modelling strategies presented in this thesis.

- Most industrial PSA/VSA units are built with commercial PLC's and these computers generally come with PID control algorithms specific to the vendor. Implementation of the control methods presented in this thesis required that the control algorithm actuate once

during the cycle and at a particular point in the cycle (i.e. at the end of adsorber A's feed step). The commercial PID packages, however, typically actuate at every sweep or scan as most common unit operations are continuous systems. Therefore, use of these vendor supplied algorithms requires detuning of controller gains and hence, damping the controller response to disturbances. For this study, in-house control software was developed with many of the nonlinear options such as slew rates and clamps made available as with most commercial PLC's. This alternative method, however, did not provide a straightforward communication protocol with the PLC – it is the PLC that updates the process boundary conditions. Instead the control software communicated with a SCADA system which then updated register values in the PLC. Another option would include careful programming of the PLC logic such that the commercial control code would only be refreshed once per cycle with Δt set to one. Altering the controller sample period does not achieve this same effect. An equivalent implementation strategy can be followed for the application of MPC controllers in the field.

- Tuning a controller for optimal output requires exact knowledge of both the PID control algorithm and the digital implementation of the algorithm. From the author's experience, this level of detail seemed to be always lacking either in process control papers, controller manuals and process control texts.

- Implementation of model-based controllers and process monitoring tools such as the method for the determination of the composition gradient requires higher level languages. It would be overly complicated to program this out in most PLC's as ladder logic and sequential function charts are low level languages requiring direct manipulation of processor memory. A personal computer (PC), therefore, is required to execute the program with a communication protocol established between the PLC and software. The addition of the PC can compromise robustness of the supervisory control system, as PC-based operating environments are less robust than the PLC.

9.3 PROSPECTS FOR FUTURE RESEARCH

To reiterate, this work represents a preliminary investigation into the dynamic characterisation of the oxygen VSA process and implementation of various process control algorithms. Consequently, there remains a plethora of fields not covered in this research due to strict time constraints. The following is a list of areas of research on this topic recommended by the author that may prove to be both academically and industrially beneficial.

- Investigation into multivariate tuning rules for batch systems. Currently, frequency response analysis is the only method available to tune PID controllers in multiple loop processes if transfer function descriptions are unavailable. The limitation of frequency analysis is that it is time consuming and impractical in field operations although its use is possible on established models (empirical or mechanistic). This study also demonstrated that there were cases where zero or variable time delay may occur, which caused the current loop tuning techniques to fail as dead time was required as an input.

- Refinement of the proposed MPC controller. This would include a theoretical study into control tuning and performance limitations through the possible use of direct synthesis of the controller and simple process models.

- Application of traditional model-based controllers for the control of VSA/PSA processes. Although not included in this thesis, the use of model predictive controllers such as dynamic matrix control (DMC) [Cutler and Ramaker, 1980], Internal Model Control (IMC) [Garcia and Morari, 1982; Morari and Zafiriou, 1989], the Smith Predictor [Smith, 1957] and model-based methods such as generic model control (GMC) [Lee and Sullivan, 1998], may produce superior performance to PID. Also, a method originated by Shinskey (2001b) termed PID with dead time compensation has had some success in field operation but only under single loop control. This controller had been shown to have a similar transfer function to IMC under certain conditions and testing this method under VSA operation and extending it to multiple loop systems may prove beneficial to industrial interests.

- Application of mechanistic process models such as MINSA or SoCAT or even the analytical models based on the Method of Characteristics [Abbott, 1966] for other PSA applications such as trace component removal, in a model predictive structure. The advantage with these systems compared to bulk gas separation processes is that assumptions and simplifications can be made to the governing equations such as isothermal operation and constant axial fluid velocity. This results in a reduction in the computational requirements whilst maintaining a reasonable predictive accuracy.

- Further investigation into various dynamic empirical models such as FODT and ANN's for use in predictive control architectures. It is likely that other ANN algorithms, other than backpropagation MLP's, would be more suited to the training of large sets of time-series data.

- Research into improved nonlinear solution or optimisation algorithms for real-time numerical process model inversion in model-based controllers. This is important for the practical application of advanced centralised control schemes.

- This study has limited itself to the use of control valves for plant regulation. Other boundary conditions such as cycle and step times have so far been kept constant. Use of these variables as candidates for control of these systems could be investigated. Cycle time, for the control of medical generators, is currently being tested by a group at the Institut für Systemdynamik und Regelungstechnik, Universitat Stuttgart [Bitzer *et al.* (2001); Bitzer and Zeitz (2002a); Bitzer *et al.* (2002)] but they have restricted themselves to the control of a single variable – oxygen purity. The study of cycle and step times with multiple loop objectives would, therefore, prove both interesting and of industrial significance.

- So far, only the oxygen VSA system has been investigated but there are other equally important process applications of VSA/PSA technology where control theory is limited. Hydrogen PSA is one such system whereby multi-component adsorption occurs over several (six to eight) adsorbent beds. Such a process would be a formidable challenge and a real test for a control system.

- The coupling of control objectives with optimisation goals. In many control problems, the problem is formulated with a view to regulate the controlled variables such that their desired values (usually the design conditions) are met at steady state. By constraining the problem through the use of a primary objective such the minimisation of total energy or work in the transient period in which control action is taken may have financially rewarding benefits to the customer. This may involve the use of the Lyapunov analysis on dynamically stability causing controller pairings to switch in order to minimise the global function as well as any secondary objectives.

- The PSA Challenge – A "Real" Control Problem. Currently, the control of batch processes has not received much attention although many industrial processes operate in a batch manner. VSA and PSA processes are now common and important unit operations that are in essence, batch systems. Furthermore, the sparse amount of literature available on control of various adsorption processes has made it difficult to compare controllers as each process operated under different cycle configurations, boundary conditions and differing number of adsorber beds. In order to create research and academic interest in these processes, a generic adsorption process model could be developed. This model, which would be typical of current industrial practice, would contain in detail all the modelling parameters, initial and boundary conditions as well as the magnitude and dynamics of various disturbances. The model would also have been rigorously tested against both experimental data (pilot plant and perhaps breakthrough studies) and a detailed numerical model. The use of this model would serve as a bench mark for future controllers. It would also allow communities of researchers, who do not have direct access to PSA plants or models but who would be genuinely interested in studying the control aspects of these processes, to investigate the application of various control theories to VSA/PSA processes. This would enable researchers to compare, on an even par, the benefits and limitations of their control strategies against others in the field. It is envisaged that this may finally provide industry with a robust and practical controller, which can be utilised in real-time on their plants.

References

Abel, A.D., W.E. Waldron and T.F Wells, "Control of Product Withdrawal from a Sorptive Separation System", **U.S. Patent 4,995,889**, 1991

Abbott, M.B., *An Introduction to the Method of Characteristics*, Thames & Hudson, London, 1966

Åström, K. and T. Hägglund, *PID Controllers: Theory, Design, and Tuning*, 2nd Ed., ISA, USA, 1995

Åström, K.J. and T. Hägglund, "The Future of PID Control", *Control Engineering Practice*, **9**, 1163-1175, 2001

Asztalos, S., "Valve Control of an Adsorption Process", **U.S. Patent 4,360,362**, 1982

Aylsworth, A.C., K. Adriance and G.R. Miller, "Apparatus and Method for Controlling Output of an Oxygen Concentrator", **U.S. Patent 5,746,806**, 1998

Baksh, M.S.A and F. Notaro, "Method for Production of Nitrogen Using Oxygen Selective Adsorbents", **U.S. Patent 5,735,938**, 1998

Basheer, I.A. and Y.M. Najjar, "Predicting Dynamic Response of Adsorption Columns with Neural Nets", *Journal of Computing in Civil Engineering*, **10**, 31-39, 1996

Basmadjian, D., *The Little Adsorption Book : A Practical Guide for Engineers and Scientists*, CRC Press, New York, 1997

Beh, C.C.K. and P. Ranganathan, "Comments on "An Artificial Neural Network as a Model for Chaotic Behavior of a Three-Phase Fluidized Bed"", *Chaos, Solitons and Fractals*, **17**, 985-986, 2003

Beh, C.C.K., K.A. Smith and P.A. Webley, "Dynamic Modelling Using Neural Networks. Case Study – Pilot Scale VSA Process for Oxygen Production", *Smart Engineering System Design: Neural Networks, Fuzzy Logic, Evolutionary Programming, Data Mining and Complex Systems*, C. H. Dagli, A.L. Buczak, J. Ghosh, M.J. Embrechts, O. Ersoy, and S. Kercel (Eds.), ASME Press, New Jersey, **11**, pp. 551-556, 2001a

Beh, C.C.K., K.A. Smith and P.A. Webley, "The VSA Process for Oxygen Enrichment: Process Description and Dynamic Modeling Using Neural Networks", *International Journal of Smart Engineering System Design*, **5**, 1-9, 2003

Beh, C.C.K., R.S. Todd, P.A. Webley, "Capturing Mass Transfer Effects Using Neural Network Models. Case Study - Breakthrough Fronts for N_2/O_2 Separation", *Proceedings of the Sixth World Congress in Chemical Engineering*, Paper No. 228, ISBN 0 7340 2201 8, 2001b

Beh, C.C.K. and P.A. Webley, "On-Line Modelling of an Oxygen Vacuum Swing Adsorption Process Using Neural Networks", *Proceedings of the Sixth World Congress in Chemical Engineering*, Paper No. 226, ISBN 0 7340 2201 8, 2001

Beh, C.C.K. and P.A. Webley, "Open Loop Dynamics of an Oxygen Vacuum Swing Adsorption Process", *AIChe Annual Meeting*, November, Paper No. 121e, 2002

Beh, C.C.K. and P.A. Webley, "A Method for the Determination of Composition Profiles in Industrial Air Separation, Pressure Swing Adsorption Systems", *Adsorption Science and Technology*, **21**, 35-52, 2003a

Beh, C.C.K. and P.A. Webley, "The Dynamics and Characteristics of an Oxygen Vacuum Swing Adsorption Process to Step Perturbations. Part 1. Open Loop Responses", *Adsorption Science and Technology*, **21**, 319-347, 2003b

Beh, C.C.K. and P.A. Webley, "The Dynamic Response and Characteristics of an Oxygen Vacuum Swing Adsorption Process to Step Perturbations. Part 2. Sensitivity Analysis and Controller Pairings", *Adsorption Science and Technology*, **21**, 349-362, 2003c

Beh, C.C.K. and P.A. Webley, "A Practical Method for the Dynamic Determination of the Product Oxygen Concentration in Pressure-Swing Adsorption Systems", *Industrial and Engineering Chemistry Research*, in press, 2003d

Beh, C.C.K. and P.A. Webley, "Control of Periodic Adsorption Processes – A Review and Some Recent Developments", *Proceedings of the 31st Annual Australasian Chemical Engineering (Chemeca) Conference*, September, Paper No. 253, 2003e

Beh, C.C.K. and P.A. Webley, "Control of the Oxygen Vacuum Swing Adsorption Process. Part 1. Single Loop Control", *Control Engineering Practice*, submitted for review, 2003f

Beh, C.C.K. and P.A. Webley, "Control of the Oxygen Vacuum Swing Adsorption Process. Part 2. Multiple Loop Control", *Control Engineering Practice*, submitted for review, 2003g

Beh, C., S. Wilson, P. Webley and J. He, "The Control of the Vacuum Swing Adsorption Process for Air Separation", *Proceedings of the Second Pacific Basin Conference on Adsorption Science and Technology*, D. Do (Ed.), World Scientific, Singapore, pp. 663-667, 2000

Bequette, B.W., "Nonlinear Control of Chemical Processes: A Review", *Industrial and Engineering Chemistry Research*, **30**, 1391-1413, 1991

Bhat, N.V. and T.J. McAvoy, "Determining Model Structure for Neural Models by Network Stripping", *Computers and Chemical Engineering*, **16**, 271-281, 1992

Bitzer, M. and M. Zeitz, "Process Control Scheme for a 2-Bed Pressure Swing Adsorption Plant", *Proceedings of the European Symposium on Computer Aided Process Engineering – 12 (ESCAPE–12)*, J. Grievink and J. van Schijndel (Eds.), Elsevier Science, **10**, pp. 451-456, 2002a

Bitzer, M. and M. Zeitz, "Design of a Nonlinear Distributed Parameter Observer for a Pressure Swing Adsorption Plant", *Journal of Process Control*, **12**, 533-543, 2002b

Bitzer, M., F.J. Christophersen and M. Zeitz, "Periodic Control of a Pressure Swing Adsorption Plant", *Proceedings of the IFAC Workshop on Periodic Control Systems*, S. Bittanti and P. Colaneri (Eds.), pp. 85-90, 2001

Bitzer, M., A. Fehn and M. Zeitz, "State Profile Estimation for a Nonisothermal Adsorption Process by a Nonlinear Distributed Parameter Observer", *Proceedings of the IFAC Symposium on Advanced Control of Chemical Processes (ADCHEM 2000)*, L.T. Biegler, A. Brambilla and C. Scali (Eds.), Elsevier Science, **1**, pp. 287-292, 2000

Bitzer, M., W. Lengerer, M. Stegmaier, G. Eigenberger and M. Zeitz, "Process Control of a 2-Bed Pressure Swing Adsorption Plant and Laboratory Experiment", *CHISA 2002, Proceedings of the 15th International Congress of Chemical and Process Engineering*, Paper No. 833, 2002

Box, G.E.P., W.G. Hunter and J.G. Hunter, *Statistics for Experimenters*, John Wiley & Sons, Inc., New York, 1978

Box, G.E.P. and M.E. Muller, "A Note on the Generation of Random Normal Deviates", *Annals of Mathematical Statistics*, **29**, 610-611, 1958

Brasquet, C. and P. Le Cloirec, "Modelling of the Breakthrough Curves of Organic Compounds in Activated Carbon Cloth Filters by the Utilization of Neural Networks", *Proceedings of the Second Pacific Basin Conference on Adsorption Science and Technology*, D. Do (Ed.), 14-18 May, World Scientific, Singapore, pp. 356-360, 2000

Brown, P.N., G.D. Byrne and A.C. Hindmarsh, "VODE: A Variable-Coefficient ODE Solver", *Siam Journal of Scientific and Statistical Computing*, **10**, 1038-1051, 1989

Carsky, M. and D.D. Do, "Neural Network Modeling of Adsorption of Binary Vapour Mixtures", *Adsorption*, **5**, 183-192, 1999

Cassidy, R.T. and E.S. Holmes, "Twenty-five Years of Progress in "Adiabatic" Adsorption Processes", *AIChe Symposium Series*, **80**, 68-75, 1984

Chahbani, M.H. and D. Tondeur, "Pressure Drop in Fixed-Bed Adsorbers", *Chemical Engineering Journal*, **81**, 23-24, 2001

Chen, D. and D.E. Seborg, "Multiloop PI/PID Controller Design Based on Gershgorin Bands", *Proceedings of the American Control Conference*, June 25-27, pp. 4122-4127, 2001

Chen, D. and D.E. Seborg, "PI/PID Controller Design Based on Direct Synthesis and Disturbance Rejection", *Industrial and Engineering Chemistry Research*, **41**, 4807-4822, 2002a

Chen, D. and D.E. Seborg, "Relative Gain Array Analysis for Uncertain Process Models", *AIChE Journal*, **48**, 302-310, 2002b

Chen, D. and D.E. Seborg, "Design of Decentralized PI Control Systems Based on Nyquist Stability Analysis", *Journal of Process Control*, **13**, 27-39, 2002c

Chiang, A.S.T., "An Analytical Solution to Equilibrium PSA Cycles", *Chemical Engineering Science*, **51**, 207-216, 1996

Cutler, C.R. and B.L. Ramaker, "Dynamic Matrix Control – A Computer Control Algorithm", *Joint Automatic Control Conference*, Part I, Paper No. WP5-B, 1980

Dabrowski, A., "Adsorption – From Theory to Practice", *Advances in Colloid and Interface Science*, **93**, 135-224, 2001

Doong, S.J. and L.A. Brenskelle, "Pressure Swing Adsorption Process Turndown Control", **U.S. Patent 5,733,359**, 1998

Doong, S.J. and P. Propsner, "Effect of Operation Symmetry on Pressure Swing Adsorption Process", *Adsorption*, **4**, 149-158, 1998

Ergun S., "Fluid Flow Through Packed Columns", *Chemical Engineering Progress*, **48**, 89-92, 1952

Farooq, S., D.M. Ruthven, K.S. Knaebel, *Pressure Swing Adsorption*, VCH Publishers, New York, 1994

Faur-Brasquet and P. Le Cloirec, "Modelling of the Flow Behaviour of Activated Carbon Cloths Using a Neural Network Approach", *Chemical Engineering and Processing*, **42**, 645-652, 2003

Faur-Brasquet, C., P. Monneyron and P. Le Cloirec, "A Comparison of Ideal Adsorbed Solution Theory and Neural Networks to Model Multicompoinent Adsorption onto Activated Carbon Cloths in Aqueous Solution", *Proceedings of the Sixth World Congress in Chemical Engineering*, Paper No. 100, ISBN 0 7340 2201 8, 2001

Fogler, H.S., *Elements of Chemical Reaction Engineering*, 2nd Ed., Prentice Hall, New Jersey, 1992

Froisy, J.B., "Model Predictive Control: Past, Present and Future", *ISA Transactions*, **33**, 235-243, 1994

Garcia, C.E. and M. Morari, "Internal Model Control. 1. A Unifying Review and Some New Results", *Industrial & Engineering Chemistry Process Design & Development*, **21**, 308-323, 1982

Garcia, C.E, D.M. Prett and M. Morari, "Model Predictive Control: Theory and Practice – A Survey", *Automatica*, **25**, 335-348, 1989

Garson, G.D., "Interpreting Neural-Network Connection Weights", *AI Expert*, **6**, 47-51, 1991

Gaskell, P.H. and A.K.C. Lau, "Curvature-Compensated Convective Transport: SMART, A New Boundedness-Preserving Transport Algorithm", *International Journal of Numerical Methods Fluids*, **8**, 617-, 1988

Gedeon, T.D., "Data Mining of Inputs: Analysing Magnitude and Functional Measures", *International Journal of Neural Systems*, **8**, 209-218, 1997

GE Fanuc Automation, *Series 90-30/20/Micro Programmable Controllers Reference Manual*, GFK-0467H, October, 1996

Glueckauf, E. and J.I. Coates, "Theory of Chromatography. Part IV. The Influence of Incomplete Equilibrium on the Front Boundary of Chromatograms and on the Effectiveness of Separation", *Journal of the Chemical Society*, 1315-1321, 1947

Golden, T., P.J. Battavio, Y.C. Chen, T.S. Farris and J.N. Armor, "Oxygen Selective Desiccants", **U.S. Patent 5,135,548**, 1992

Golden, T., W.C. Kratz, M.N. Mead, T.S. Farris and J.N. Armor, "Oxygen Selective Adsorbents", **U.S. Patent 5,447,557**, 1995

Grader, R.J., "Pressure Swing Adsorption Process for Supplying Oxygen Under Variable Demand Conditions", **U.S. Patent 4,643,743**, 1987

Graupe, D., *Principles of Artificial Neural Networks*, World Scientific, London, 1997

Gunderson, J. "Automatic Control for PSA System", **U.S. Patent 4,725,293**, 1988

Hassoun, M.H., *Fundamentals of Artificial Neural Networks*, The MIT Press, London, 1995

Haykin, S., *Neural Networks – A Comprehensive Foundation*, 2nd Ed., Prentice Hall, Inc., New Jersey, 1999

Hecht-Nielsen, R., "Theory of the Backpropagation Neural Network", *Proceedings of the 1989 IEEE International Joint Conference on Neural Networks*, Piscataway, New Jersey, Vol. I, pp. 593-608, 1989

Henson, M.A., "Nonlinear Model Predictive Control: Current Status and Future Directions", *Computers and Chemical Engineering*, **23**, 187-202, 1998

Ho, W.K., T.H. Lee and O.P. Gan, "Tuning of Multiloop Proportional-Integral-Derivative Controllers Based on Gain and Phase Margin Specifications", *Industrial and Engineering Chemistry Research*, **36**, 2231-2238, 1997

Hornik, K., M. Stinchcombe and H. White, "Multilayer Feedforward Networks are Universal Approximators", *Neural Networks*, **2**, 359-366, 1989

Hornik, K., M. Stinchcombe and H. White, "Universal Approximation of an Unknown Mapping and Its Derivatives Using Multilayer Feedforward Networks", *Neural Networks*, **3**, 551-560, 1990

Hutson, N.D., S.U. Rege and R.T. Yang, "Mixed Cation Zeolites: Li_x Ag_y -X as a Superior Adsorbent for Air Separation", *AIChE Journal*, **45**, 724-734, 1999

International Electrotechnical Commission, *Batch Control – Part1: Models and Terminology*, **IEC 61512-1**, IEC, Geneva, Switzerland, 1997

Kershenbaum, L. "Experimental Testing of Advanced Algorithms for Process Control: When is it Worth the Effort?", *Transactions of the IChemE*, **78**, 509-521, 2000

Klatt, K.U., F. Hanisch, G. Dünnebier and S. Engell, "Model-Based Control of a Simulated Moving Bed Chromatographic Process for the Separation of Fructose and Glucose", *Journal of Process Control*, **12**, 203-219, 2002

Klatt, K.U., F. Hanisch, G. Dünnebier and S. Engell, "Model-Based Optimization and Control of Chromatographic Processes", *Computers and Chemical Engineering*, **24**, 1119-1126, 2000

Knaebel, K.S. and F.B. Hill, "Pressure Swing Adsorption: Development of an Equilibrium Theory for Gas Separations", *Chemical Engineering Science*, **40**, 2351-2360, 1985

Koch, W.R., "Control System for Air Fractionation by Selective Adsorption", **U.S. Patent 4,539,019**, 1985

Koros, W.J. and R. Mahajan, "Pushing the Limits on Possibilities for Large Scale Gas Separation: Which Strategies?", *Journal of Membrane Science*, **175**, 181-196, 2000

Kowler, D.E. and R.H. Kadlec, "The Optimal Control of a Periodic Adsorber", *AIChE Journal*, **18**, 1207-1219, 1972

Kumar, R., "Vacuum Swing Adsorption Process for Oxygen Production - A Historical Perspective", *Separation Science and Technology*, **31**, 877-893, 1996

Kumar, R. and S. Sircar, "Adiabatic Sorption of Bulk Single Adsorbate from an Inert Gas - Effect of Gas-Solid Mass and Heat Transfer Coefficients", *Chemical Engineering Communications*, **26**, 319-338, 1984

LaCava, A.I., Shirley, A.I. and Ramachandran, R., "How to Specify Pressure-Swing Adsorption Units", *Chemical Engineering*, **June**, 110-118, 1998

Lee, J., W. Cho and T.F. Edgar, "Multiloop PI Controller Tuning for Interacting Multivariable Processes", *Computers and Chemical Engineering*, **22**, 1711-1723, 1998

Lee, P.L. and G.R. Sullivan, "Generic Model Control (GMC)", *Computers and Chemical Engineering*, **12**, 573-580, 1988

Leonard, B.P., "A Stable and Accurate Convective Modeling Procedure Based on Quadratic Upstream Interpolation", *Computer Methods in Applied Mechanics and Engineering*, **19**, 59-98, 1979

LeVan, M.D., "Pressure Swing Adsorption: Equlibrium Theory for Purification and Enrichment", *Industrial and Engineering Chemistry Research*, **34**, 2655-2660, 1995

Lewandowski, J., N.O. Lemcoff and S. Palosaari, "Use of Neural Networks in the Simulation and Optimization of Pressure Swing Adsorption Processes", *Chemical Engineering Technology*, **21**, 593-597, 1998

Li, D.L, Y.J. Tang, J.L. Yang, C.G. Zhang and D.G. He, "Programmable Control and Operation Equipment of Swing Pressure Adsorption Process", **U.S. Patent 5,240,481**, 1993

Liptak, B.G. (Editor-in-chief), *Instrument Engineers' Handbook. Process Control*, 3rd Ed., Butterworth-Heinemann Ltd, London, 1995

Luyben, W.L., "Simple Method for Tuning SISO Controllers in Multivariable Systems", *Industrial & Engineering Chemistry Process Design & Development*, **25**, 654-660, 1986

Masters, T., *Practical Neural Network Recipes in C++*, Academic Press Inc., London, 1993

Man, K.F., K.S. Tang and S. Kwong, *Genetic Algorithms: Concepts and Designs*, Springer, London, 1999

Matz, M.J. and K.S. Knaebel, "Temperature Front Sensing for Feed Step Control in Pressure Swing Adsorption", *Industrial and Engineering Chemistry Research*, **26**, 1638-1645, 1987

Mayne, D.Q., "The Design of Linear Multivariable Systems", *Automatica*, **9**, 201-207, 1973

Mayne, D.Q., J.B. Rawlings, C.V. Rao and P.O.M. Scokaert, "Constrained Model Predictive Control: Stability and Optimality", *Automatica*, **36**, 789-814, 2000

McAvoy, T.J., "Steady-State Decoupling of Distillation Columns", *Industrial & Engineering Chemistry Fundamentals*, **18**, 269-273, 1979

McAvoy, T.J., *Interaction Analysis*, Instrument Society of America, Research Triangle Park, NC, 1983

McCombs, N.R., "Capacity Control System for Pressure Swing Adsorption Apparatus and Associated Method", **U.S. Patent 5,474,595**, 1995

McCombs, N.R., "Pressure Swing Adsorption Apparatus and Method", **Patent WO 98/57728**, 1998

Michael, K.P., "Industrial Gas: Surveying Onsite Supply Options", *Chemical Engineering*, **January**, 72-79, 1997

Miller, G.W., "Adsorption of Nitrogen, Oxygen, Argon and Ternary Mixtures of These gases in 13X Molecular Sieve", *AIChe Symposium Series*, **83**, Paper No. 259, 28-39, 1973

Miller, G.W., Jr. Gray and L. Robert, "Pressure Swing Adsorption Product Purity Control Method and Apparatus", **U.S. Patent 4,693,730**, 1987

Monica, T.J., C.C. Yu and W.L. Luyben, "Improved Multiloop Single-Input/Single-Output (SISO) Controllers for Multivariable Processes", *Industrial and Engineering Chemistry Research*, **27**, 969-973, 1988

Morari, M. and E. Zafiriou, *Robust Process Control*, Prentice-Hall, Englewood Cliffs, New Jersey, 1989

Myers, W.P., T.A. Torzala and J.W. Henneman, "Pneumatically Actuated Electronic Control for a Fluid Mixture Adsorption Separator", **U.S. Patent 4,322,228**, 1982

Nagrath, D., B.W. Bequette and S.M. Cramer, "Evolutionary Operation and Control Chromatographic Processes", *AIChE Journal*, **49**, 82-95, 2003

Naheiri, T., "Pressure Swing Adsorption Gas Flow Control Method and System", **U.S. Patent 6,183,538**, 2001

Natarajan, S. and J.H. Lee, "Repetitive Model Predictive Control Applied to a Simulated Moving Bed Chromatography System", *Computers and Chemical Engineering*, **24**, 1127-1133, 2000

Nikravesh, M. and A.R. Kovscek and T.W. Patzek, "Identification and Control of Industrial-Scale Processes via Neural Networks", *Proceeding of the Fifth International Conference on Chemical Process Control*, J.C. Kantor, C.E. Garcia and B. Carnahan (Eds.), CACHE and AIChE, **93**, pp. 284-287, 1997

Notaro, F., J.T. Mullhaupt, F.W. Leavitt, M.W. Ackley, "Adsorption Process and System Using Multilayer Adsorbent Beds", **U.S. Patent 5,810,909**, 1998

Otawara, K., L.T. Fan, A. Tsutsumi, T. Yano, K. Kuramoto and K. Yoshida, "An Artificial Neural Network as a Model for Chaotic Behavior of a Three-Phase Fluidized Bed", *Chaos, Solitons and Fractals*, **13**, 353-362, 2002

Otawara, K., L.T. Fan, A. Tsutsumi, T. Yano, K. Kuramoto and K. Yoshida, "Reply to Comments on an Artificial Neural Network as a Model for Chaotic Behavior of a Three-Phase Fluidized Bed", *Chaos, Solitons and Fractals*, **17**, 987, 2003

Park, J.H., J.N. Kim, S.H. Cho, J.D. Kim and R.T. Yang, "Adsorber Dynamics and Optimal Design of Layered Beds for Multicomponent Gas Adsorption", *Chemical Engineering Science*, **53**, 3951-3963, 1998a

Park, I.S., M. Petkovska and D.D. Do, "Frequency response of an adsorber with modulation of the inlet molar flow-rate - I. A semi-batch adsorber", *Chemical Engineering Science*, **53**, 819-832, 1998b

Park, I.S., M. Petkovska and D.D. Do, "Frequency response of an adsorber with modulation of the inlet molar flow-rate - II. A continuos flow adsorber", *Chemical Engineering Science*, **53**, 833-843, 1998c

Parkinson, G., R. D'Aquino and G. Ondrey, "O_2 Breathes New Life into Processes", *Chemical Engineering*, **September**, 28-31, 1999

Petkovska, M. and D.D. Do, "Nonlinear Frequency Response of Adsorption Systems: Isothermal Batch and Continuous Flow Adsorbers", *Chemical Engineering Science*, **53**, 3081-3097, 1998

Petzold, L., "Automatic Selection of Methods for Solving Stiff and Non-Stiff Systems of Ordinary Differential Equations", *Siam Journal of Scientific and Statistical Computing*, **4**, 136-148, 1983

Pietruszewski, J.J., "Turndown Control for Pressure Swing Adsorption", **U.S. Patent 4,140,495**, 1979

Press, W.H., S.A. Teukolsky, W.T. Vetterling and B.P. Flannery, *Numerical Recipes in Fortran 77*, 2nd Ed., Press Syndicate of the University of Cambridge, 1997

Qin, S.J. and T.A. Badgwell, "An Overview of Industrial Model Predictive Control Technology", *Proceeding of the Fifth International Conference on Chemical Process Control*, J.C. Kantor, C.E. Garcia and B. Carnahan (Eds.), CACHE and AIChE, **93**, pp. 232-256, 1997

Qin, S.J. and T.A. Badgwell, "A Survey of Industrial Model Predictive Control Technology", *Control Engineering Practice*, **11**, 733-764, 2003

Ray, M.S., "Adsorptive and Membrane-type Separations: A Bibliographical Update (1999)", *Adsorption Science and Technology*, **18**, 439-468, 2000

Reich, Y. and S.V. Barai, "A Methodology for Building Neural Networks Models from Empirical Engineering Data", *Engineering Applications of Artificial Intelligence*, **13**, 685-694, 2000

Rouge, D. and N. Teuscher, "PSA or VSA Unit Having Jointly-Controlled Production Output and Production Pressure", **U.S. Patent 6,270,556**, 2001

Ruthven D. M., *Principles of Adsorption and Adsorption Processes*, John Wiley and Sons, New York, 1984

Ruthven, D.M., "Past Progress and Future Challenges in Adsorption Research", *Industrial and Engineering Chemistry Research*, **39**, 2127-2131, 2000

Schaub, H.R., J. Smolarek, F.W. Leavitt, L.J. Toussaint and K.A. LaSala, "Tuning of Vacuum Pressure Swing Adsorption Systems", **U.S. Patent 5,407,465**, 1995

Schebler, B.J. and R.F. Hart, "Oxygen Partial Pressure Controller for a Pressure Swing Adsorption System", **U.S. Patent 4,589,436**, 1986

Sereno, C. and A. Rodrigues, "Can Steady-State Momentum Equations be Used in Modelling Pressurization of Adsorption Beds?", *Gas Separation & Purification*, **7**, 167-174, 1993

Servido, J.L., R.E. Tucker, J. Murphy, "Pneumatic Circuit Control for Pressure Swing Adsorption Systems", **U.S. Patent 5,183,483**, 1993

Shaw, A.M., F.J. Doyle II and J.S. Schwaber, "A Dynamic Neural Network Approach to Nonlinear Process Modelling", *Computers and Chemical Engineering*, **21**, 371-385, 1997

Shelley, S., "Out of Thin Air", *Chemical Engineering*, **June**, 30-39, 1991

Sherwood, T.K., R.L. Pigford, C.R. Wilke, *Mass Transfer*, McGraw-Hill, New York, 1975

Shinskey, F.G., *Process Control Systems: Application, Design, and Tuning*, 4th Ed., McGraw-Hill Co., 1996

Shinskey, F.G., "Process Control: As Taught Vs as Practiced", *Industrial Engineering Chemistry Research*, **41**, 3745-3750, 2001a

Shinskey, F.G., "PID-Deatime Control of Distributed Processes", *Control Engineering Practice*, **9**, 1177-1183, 2001b

Shinskey, F.G., *Personal Communications*, E-mail correspondence, 16:10:13 (GMT-0400), 12 August, 2002

Shirley, A.I. and A.I. LaCava, "PSA System with Product Turndown and Purity Control", **U.S. Patent 5,258,056**, 1993

Skogestad, S. "Simple Analytical Rules for Model Reduction and PID Controller Tuning", *Journal of Process Control*, **13**, 291-309, 2003

Sircar, S., "Control System and Method for Air Fractionation by Vacuum Swing Adsorption", **U.S. Patent 4,472,177**, 1984

Sircar, S., "Publications on Adsorption Science and Technology", *Adsorption*, **6**, 359-365, 2000

Sircar, S., "Applications of Gas Separation by Adsorption for the Future", *Adsorption Science and Technology*, **19**, 347-366, 2001

Sircar, S. "Pressure Swing Adsorption", *Industrial and Engineering Chemistry Research*, **41**, 1389-1392, 2002

Sircar, S. and B.F. Hanley, "Production of Oxygen Enriched Air by Rapid Pressure Swing Adsorption", *Adsorption*, **1**, 313-320, 1995

Sircar, S. and J.R. Hufton, "Why Does the Linear Driving Force Model for Adsorption Kinetics Work?", *Adsorption*, **6**, 137-147, 2000

Smith, O., "Closer Control of Loops with Dead Time", *Chemical Engineering Progress*, **53**, 217-219, 1957

Smith, A.R. and J. Klosek, "A Review of Air Separation Technologies and Their Integration with Energy Conversion Processes", *Fuel Processing Technology*, **70**, 115-134, 2001

Smolarek, J., "Control of Pressure Swing Adsorption Operations", **U.S. Patent 5,042,994**, 1991

Stinchcombe, M. and H. White, "Universal Approximation Using Feedforward Networks with Non-Sigmoid Hidden layer Activation Functions", *Proceedings of the 1989 IEEE International Joint Conference on Neural Networks*, 18-22 June, Piscataway, New Jersey, Vol. 1, pp. 613-617, 1989

Stocker, J. and M. Whysall, "Pressure Swing Adsorption Control Method and Apparatus", **U.S. Patent 4,761,165**, 1988

Subramanian, D. and J.A. Ritter, "Equilibrium Theory for Binary Solvent Vapor Recovery by Pressure Swing Adsorption: Conceptual Process Design for Separation of the Lighter Component", *Chemical Engineering Science*, **53**, 1295-1305, 1998

Sundaram, N., "Training Neural Networks for Pressure Swing Adsorption Processes", *Industrial and Engineering Chemistry Research*, **38**, 4449-4457, 1999

Tan, Z., "PSA Process with Dynamic Purge Control", **U.S. Patent 5,529,607**, 1996

Tchaban, T., M.J. Taylor and J.P. Griffin, "Establishing Impacts of the Inputs in a Feedforward Neural Network", *Neural Computing & Applications*, **7**, 309-317, 1998

The International Society for Measurement and Control, *Batch Control – Part 1: Models and Terminology*, **ISA-S88.01-1995**, ISA, Research Triangle Park, N.C., 1995

Tien, C., *Adsorption Calculations and Modeling*, Butterworth-Heinemann, Boston, 1984

Todd, R.S., *Mass Transfer in Rapid Pressure Swing Adsorption Systems*, PhD Thesis, Department of Chemical Engineering, Monash University, 2003

Todd, R.S., C.C.K. Beh, S.J. Wilson and P.A. Webley, "Simplified Modelling of Pressure Driven Flow in Pressure Swing Adsorption Process", *Proceedings of the Melbourne Graduate Fluids Conference*, 5 July, pp. 5-8, 2001a

Todd, R.S., J. He, P.A. Webley, C.C.K. Beh, S.J. Wilson and M.A. Lloyd, "Fast Finite Volume Method for PSA/VSA Cycle Simulation –Experimental Validation", *Industrial and Engineering Chemistry Research*, **40**, 3217-3224, 2001b

Watson, C., R.D. Whitley and M.L. Meyer, "Multiple Zeolite Adsorbent Layers in Oxygen Separation", **U.S. Patent 5,529,610**, 1996

Webley, P., Beh, C., J. He, Wilson, S., and Todd, S., "Numerical Simulation and Experimental Validation of Multiple-Layer, Non-Isothermal, Bulk gas Pressure Swing Adsorption", *Proceedings of the Second Pacific Basin Conference on Adsorption Science and Technology*, D. Do (Ed.), 14-18 May, World Scientific, Singapore, pp. 658-662, 2000

Webley, P.A. and He, J. "Fast Solution-Adaptive Finite Volume Method for PSA/VSA Cycle Simulation. 1. Single Step Simulation", *Computers and Chemical Engineering*, **23**, 1701-1712, 2000

Weischedel, K. and T.J. McAvoy, "Feasibility of Decoupling in Conventionally Controlled Distillation Columns", *Industrial & Engineering Chemistry Fundamentals*, **19**, 379-384, 1980

Wilson, S.J., *Thermal Profiles in Oxygen VSA – Modelling, Observations and Optimisation*, PhD Thesis, Department of Chemical Engineering, Monash University, 2001

Wilson, S.J., C.C.K. Beh, P.A. Webley and R.S. Todd, "The Effects of a Readily Adsorbed Trace Component (Water) in a Bulk Separation PSA Process: The Case of Oxygen VSA", *Industrial and Engineering Chemistry Research*, **40**, 2702-2713, 2001

Wilson, S.J. and P.A. Webley, "Perturbation Techniques for Accelerated Convergence of Cyclic Steady State (CSS) in Oxygen VSA Simulations", *Chemical Engineering Science*, **57**, 4145-4159, 2002a

Wilson, S.J. and P.A. Webley, "Cyclic Steady State Axial Temperature Profiles in Multilayer, Bulk Gas PSA – The Case of Oxygen VSA", *Industrial and Engineering Chemistry Research*, **41**, 2753-2765, 2002b

Xinggui, Z., Lianghong, L., Yingchun, D., Weikang, Y. and Hudson, J.L., "On-Line Prediction of a Fixed-Bed Reactor Using K-L Expansion and Neural Networks", *Chinese Journal of Chemical Engineering*, **4**, 299-305, 1998

Yang, R.T., *Gas Separation by Adsorption Processes*, Butterworth, Boston, 1987

Yang, R.T., "New Adsorbents for Gas Separation by Weak Chemical Bonds", *Proceedings of the Second Pacific Basin Conference on Adsorption Science and Technology*, D. Do (Ed.), pp. 21-25, World Scientific, Singapore, 2000

Yang, M., J. Hubble, A.D. Lockett and R.R. Rathbone, "A Neural Network Model for Prediction of Binary Adsorption Using Single Solute and Limited Binary Solute Adsorption Data", *Separation Science and Technology*, **31**, 1259-1265, 1996

Ziegler, J.G. and N.B. Nichols, "Optimum Settings for Automatic Controllers", *Transactions of the ASME*, **64**, 759-768, 1942

Zone, I.R. and N.F. Kirkby, "Controlling the Pressure Swing Adsorption Process", *The 1994 IChemE Research Event*, 844-846, 1994

Zorzetto, L.F.M., Maciel Filho, R. and Wolf-Maciel, M.R., "Process Modelling Development Through Artificial Neural Networks and Hybrid Models", *Computers and Chemical Engineering*, **24**, 1355-1360, 2000

Zurada, J.M., *Introduction to Artificial Neural Systems*, West Publishing Co., New York, 1992

Zurada, J.M., A. Malinowski and I. Cloete, "Sensitivity Analysis for Minimization of Input Data Dimension for Feedforward Neural Network", *Proceedings of the 1994 IEEE International Symposium on Circuits and Systems*, 30 May-2 June, **6**, pp. 447-450, 1994

Appendix A.

Instrumentation and Equipment Specification

Component	Tag	Type & Model	Manufacturer	Range & Error/Size
Vacuum Pump and Electric Motor		Rotary Vane, KSV65	Kinney	
Vacuum Pump Oil		Kinlube 220	Tuthill Corporation	
Vacuum Pump Oil Filter Element		W920/17	Mann	
Air Dryer with Filtration System		NaX PSA Dryer, Pneudri DM015	Domnick Hunter	
Oxygen Analyser	AIT2	Paramagnetic, 1440C	Servomex	0 – 100% O_2; ±1% O_2
Humidity Meter (not shown on P&ID)	AIT4	HMP 36	Vaisala	0 – 100%RH; ±1% RH
Vacuum Line Filter				100 micron
Feed Supply Tank		Carbon Steel		60L
Product Surge Tank		Carbon Steel		60L
Feed Tank Heater Element		U-TC-0055, Single Phase, 240V	Stokes Synertec	1500W
Feed Tank Heater Controller		91e	Eurotherm	
Variac for Heater Controller		W20, 240V	Warburton Franki	
Feed Tank Upstream Pressure Regulator		R24-400-RNLG	Norgren	Max Outlet 8.6 Bar
Feed Tank Downstream Pressure Regulator		R24-400-RNCG	Norgen	Max Outlet 2.1 Bar
Feed Pressure Transmitter	P1	½" 22D7	Bourdon Sedeme	0.965 - 250 kPa.A; ±0.5 kPa
Pressure Transmitter	P2	½" 22D7	Bourdon Sedeme	0 – 250 kPa.A; ±0.5 kPa
Product Pressure Transmitter	P4	½" 23D7	Bourdon Sedeme	101.295 – 200 kPa.A; ±0.5 kPa
Vacuum Pressure Transmitter	P5	½" 22D7	Bourdon Sedeme	3.245 – 250 kPa.A; ±0.5 kPa
Product Tank Pressure Transmitter	P6	½" 22D7	Bourdon Sedeme	2.9 – 250 kPa.A; ±0.5 kPa
Bed-to-Bed Pressure Transmitter	P7	½" 22D7	Bourdon Sedeme	0.955 – 250 kPa.A; ±0.5 kPa

Component	Tag	Type & Model	Manufacturer	Range & Error/Size
Feed Tank Pressure Transmitter	P8	½" GS4200	Genspec	0 – 10 Bar.G; ±0.5 Bar.G
Bed 1 Pressure Transmitter	PB1	½" 22D7	Bourdon Sedeme	1.5 – 250 kPa.A; ±0.5 kPa
Bed 2 Pressure Transmitter	PB2	½" 22D7	Bourdon Sedeme	0 – 250 kPa.A; ±0.5 kPa
Bed 3 Pressure Transmitter	PB3	½" 22D7	Bourdon Sedeme	1.125 – 250 kPa.A; ±0.5 kPa
Bed-Bed Differential Pressure Transmitter	DP1	EJA110	Yokogawa	-100 – 100 kPa.A; ±1 kPa
Feed Flow Meter	FIT1	Annubar, GNT-10	Fisher Rosemount	½"
Feed Flow Differential Pressure Transmitter	DP2	IDP10-A22A21D-M1	Foxboro	0 – 7.5 kPa.A; ±0.1 kPa
Product Flow Meter	FIT4	½" Laminar Plate, PVHL-50LPM	Cole Palmer	0 – 50 LPM; ±2% (BFSL)
Vacuum Flow Meter	FIT5	Annubar, GNT-10	Fisher Rosemount	½"
Vacuum Flow Differential Pressure Transmitter	DP4	IDP10-A22A21D-M1	Foxboro	0 – 7.5 kPa.A; ±0.1 kPa
Feed Control Valve	FCV1	Linear Trim 4, CV=4.0, ATO, 3-15 psi.G	Badger Meter, Inc.	¾"
Bed-to-Bed Control Valve	FCV2	Linear Trim 4, CV=4.0, ATO, 3-15 psi.G	Badger Meter, Inc.	¾"
Product Repress Control Valve	FCV3	Linear Trim A, CV=2.5, ATO, 3-15 psi.G	Badger Meter, Inc.	½"
Product Control Valve	FCV4	Linear Trim H, CV=0.13, ATO, 3-15 psi.G	Badger Meter, Inc.	¼"
Vacuum Control Valve	FCV5	Linear Trim 5, CV=5.0, ATO, 3-15 psi.G	Badger Meter, Inc.	1"
Thermocouple	T1	T-type, Junction Exposed Wire	RS Components	-40 – 40°C; ±1°C
Thermocouple	T2	T-type, Junction Exposed Wire	RS Components	-40 – 40°C; ±1°C
Thermocouple	T3	T-type, Junction Exposed Wire	RS Components	-40 – 40°C; ±1°C
Thermocouple	T4	T-type, Junction Exposed Wire	RS Components	-40 – 40°C; ±1°C

Component	Tag	Type & Model	Manufacturer	Range & Error/Size
Thermocouple	T5	T-type, Junction Exposed Wire	RS Components	-40 – 40°C; ±1°C
Thermocouple	T6	T-type, Junction Exposed Wire	RS Components	-40 – 40°C; ±1°C
Thermocouple	T7	T-type, Junction Exposed Wire	RS Components	-40 – 40°C; ±1°C
Thermocouple	T8	T-type, Junction Exposed Wire	RS Components	-40 – 40°C; ±1°C
Thermocouple	T9	T-type, Junction Exposed Wire	RS Components	-40 – 40°C; ±1°C
Thermocouple	T10	T-type, Junction Exposed Wire	RS Components	-40 – 40°C; ±1°C
Thermocouple	T11	T-type, Junction Exposed Wire	RS Components	-40 – 40°C; ±1°C
Thermocouple	T12	T-type, Junction Exposed Wire	RS Components	-40 – 40°C; ±1°C
Thermocouple	T13	T-type, Junction Exposed Wire	RS Components	-40 – 40°C; ±1°C
Thermocouple	T14	T-type, Junction Exposed Wire	RS Components	-40 – 40°C; ±1°C
Thermocouple	T15	T-type, Junction Exposed Wire	RS Components	-40 – 40°C; ±1°C
Thermocouple	T16	T-type, Junction Exposed Wire	RS Components	-40 – 40°C; ±1°C
Thermocouple	T17	T-type, Junction Exposed Wire	RS Components	-40 – 40°C; ±1°C
Thermocouple	T18	T-type, Junction Exposed Wire	RS Components	-40 – 40°C; ±1°C
Thermocouple	T19	T-type, Junction Exposed Wire	RS Components	-40 – 40°C; ±1°C
Thermocouple	T20	T-type, Junction Exposed Wire	RS Components	-40 – 40°C; ±1°C
Thermocouple	T21	T-type, Junction Exposed Wire	RS Components	-40 – 40°C; ±1°C
Thermocouple	T22	T-type, Junction Exposed Wire	RS Components	-40 – 40°C; ±1°C

Component	Tag	Type & Model	Manufacturer	Range & Error/Size
Thermocouple	T23	T-type, Junction Exposed Wire	RS Components	-40 – 40°C; ±1°C
Thermocouple	T24	T-type, Junction Exposed Wire	RS Components	-40 – 40°C; ±1°C
Vacuum Pressure Relief Valve	PRV5	1" Brass Body		Relief @ 20 kPa.A
Product Repress Isolation Valve	KV1	Manual Ball, 3 piece S.S.	Kingston	¾"
Feed Isolation Valve	KV2	Manual Ball, 3 piece S.S.	Kingston	1"
Vacuum Isolation Valve	KV3	Manual Ball, 3 piece S.S.	Kingston	1"
Vacuum Isolation Valve	KV4	Manual Ball, 3 piece S.S.	Kingston	1"
Product Isolation Valve	KV5	Manual Ball, 3 piece S.S.	Kingston	¼"
Product Isolation Valve	KV6	Manual Ball, 3 piece S.S.	Kingston	¼"
Product Isolation Valve	KV7	Manual Ball, 3 piece S.S.	Kingston	¼"
Vacuum Isolation Valve	KV8	Manual Ball, 3 piece S.S.	Kingston	1"
Bed 1 Feed Valve On/Off	KV11	554-25D195-1-1	Gemu	1" Angle Seat
Solenoid Valve for above		324-2M1254-1-24VDC	Gemu	Single Acting
Bed 1 Vacuum Valve On/Off	KV12	554-25D195-1-1	Gemu	1" Angle Seat
Solenoid Valve for above		324-2M1254-1-24VDC	Gemu	Single Acting
Bed 1 Product Valve On/Off	KV13	554-20D195-1-0	Gemu	¾" Angle Seat
Solenoid Valve for above		324-2M1254-1-24VDC	Gemu	Single Acting
Bed 1 Purge Valve On/Off	KV14	554-20D195-1-0	Gemu	¾" Angle Seat
Solenoid Valve for above		324-2M1254-1-24VDC	Gemu	Single Acting
Bed 2 Feed Valve On/Off	KV21	554-25D195-1-1	Gemu	1" Angle Seat
Solenoid Valve for above		324-2M1254-1-24VDC	Gemu	Single Acting
Bed 2 Vacuum Valve On/Off	KV22	554-25D195-1-1	Gemu	1" Angle Seat
Solenoid Valve for above		324-2M1254-1-24VDC	Gemu	Single Acting
Bed 2 Product Valve On/Off	KV23	554-20D195-1-0	Gemu	¾" Angle Seat

Component	Tag	Type & Model	Manufacturer	Range & Error/Size
Solenoid Valve for above		324-2M1254-1-24VDC	Gemu	Single Acting
Bed 2 Purge Valve On/Off	KV24	554-20D195-1-0	Gemu	¾" Angle Seat
Solenoid Valve for above		324-2M1254-1-24VDC	Gemu	Single Acting
Bed 3 Feed Valve On/Off	KV31	554-25D195-1-1	Gemu	1" Angle Seat
Solenoid Valve for above		324-2M1254-1-24VDC	Gemu	Single Acting
Bed 3 Vacuum Valve On/Off	KV32	554-25D195-1-1	Gemu	1" Angle Seat
Solenoid Valve for above		324-2M1254-1-24VDC	Gemu	Single Acting
Bed 3 Product Valve On/Off	KV33	554-20D195-1-0	Gemu	¾" Angle Seat
Solenoid Valve for above		324-2M1254-1-24VDC	Gemu	Single Acting
Bed 3 Purge Valve On/Off	KV34	554-20D195-1-0	Gemu	¾" Angle Seat
Solenoid Valve for above		324-2M1254-1-24VDC	Gemu	Single Acting
PLC & SCADA				
CPU		IC693CPU352	GE Fanuc Automation	
Power Supply		IC693PWR321	GE Fanuc Automation	
Ethernet Interface Module		HE693THM884	GE Fanuc Automation	
Thermocouple Module, 8 Channel		IC693CMM321	GE Fanuc Automation	
Analogue Input/Output Module, 2 Out/4 In		IC693ALG442	GE Fanuc Automation	
Analogue Output Module, 8 Channel		IC693ALG392	GE Fanuc Automation	
Analogue Input Module, 8 Channel		IC693ALG223	GE Fanuc Automation	
Digital Input Module, 16 Channel		IC693MDL634	GE Fanuc Automation	
Digital Output Module, 16 Channel		IC693MDL940	GE Fanuc Automation	
High Speed Counter Module, 16 Channel		IC693APU300	GE Fanuc Automation	

Component	Tag	Type & Model	Manufacturer	Range & Error/Size
PLC Programmer		LM90 Logicmaster ver. 9.01	GE Fanuc Automation	
SCADA Software		Citect ver. 5.21, Service Pack E	Ci Technologies	

Appendix B.

Oxygen VSA Pilot Plant P&ID

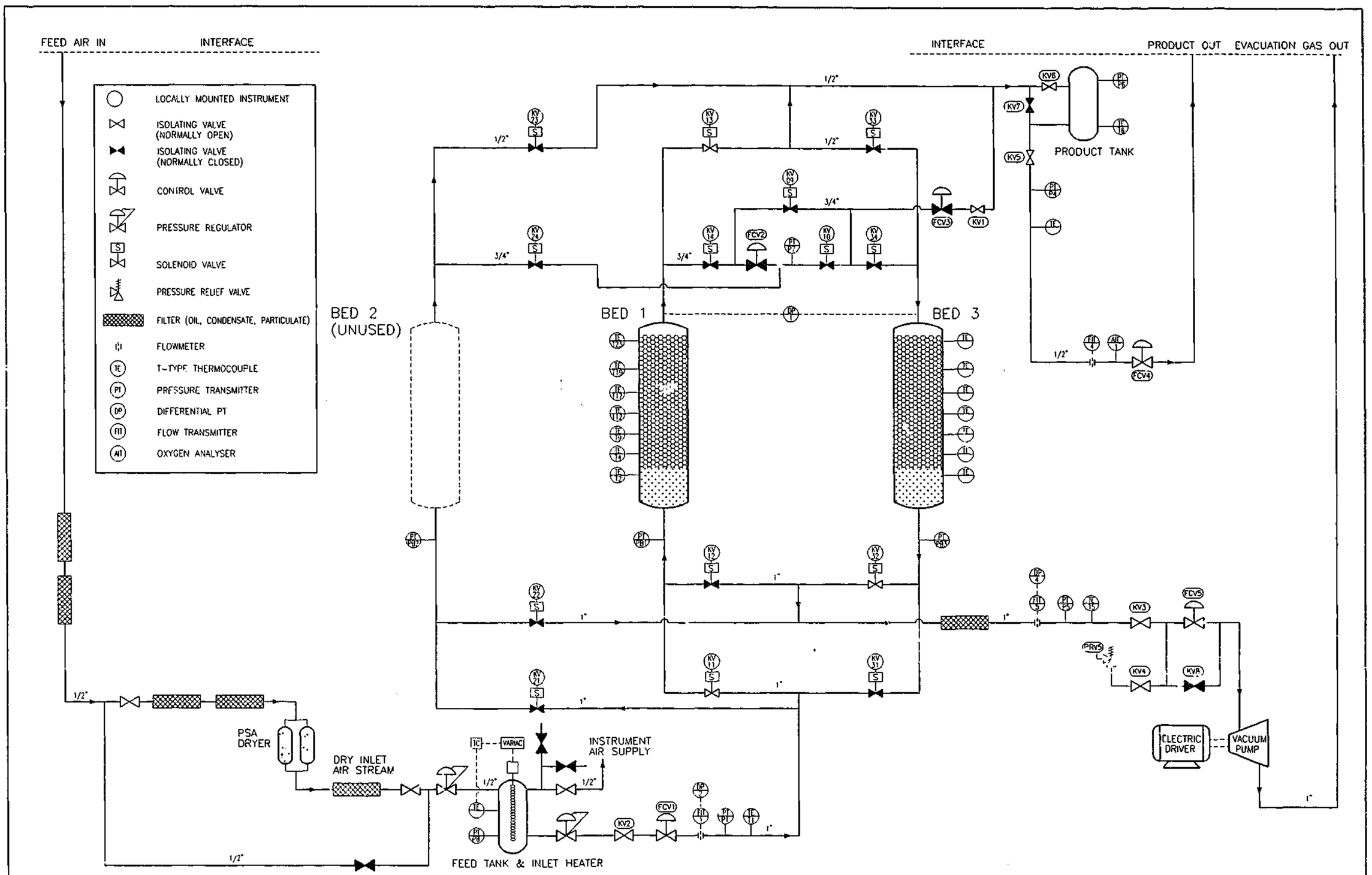

NOTES:

1. P&ID SHOWN IN TERMS OF OPERATIONAL BEDS 1 & 3 THIS DIFFERS FROM FIGURE 2.1a WHICH HAS BEEN GREATLY SIMPLIFIED TO AID PERCEPTION OF THE PROCESS
2. DUAL BED CYCLE DEPICTED – BED 1 FEED; BED 3 EVACUATION

P&ID O_2 VSA PILOT PLANT DEPT. OF CHEMICAL ENGINEERING MONASH UNIVERSITY	CHECKED: SIMON WILSON	AUTHORIZED: PAUL WEBLEY
	DRAWN: CHRIS BEH	VSA–01 C

Appendix C.

Adsorber Column Details

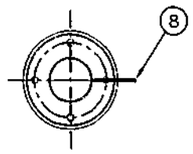

SECT. Y–Y

NOZZLE ORIENTATION

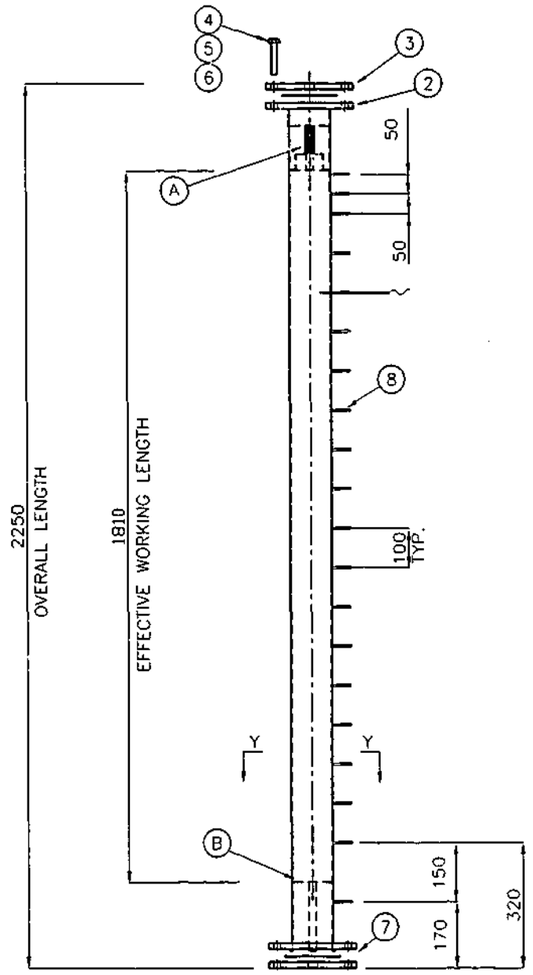

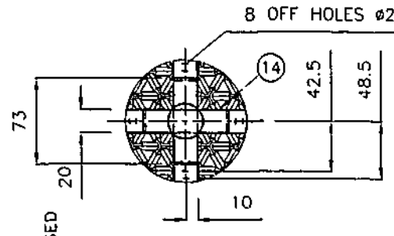

SECT. X–X

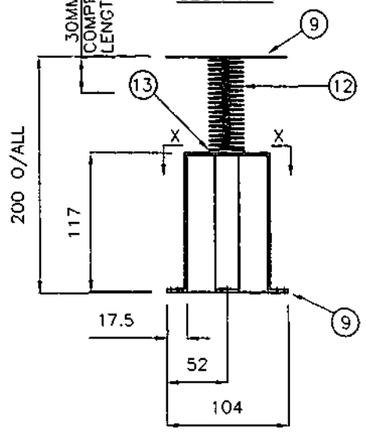

A. SIEVE COMPACTOR

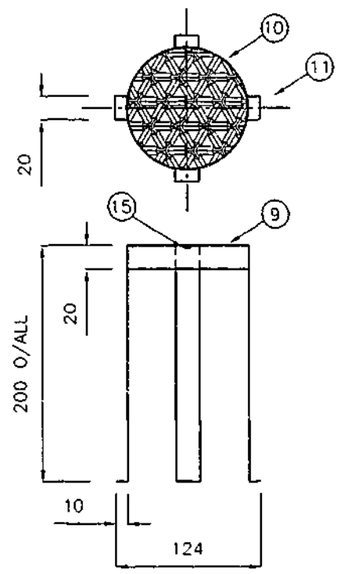

B. FLOW SPREADER

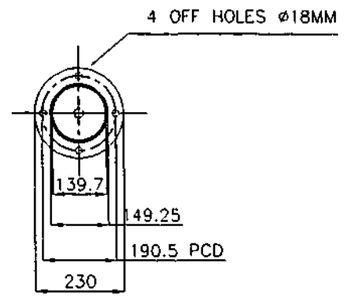

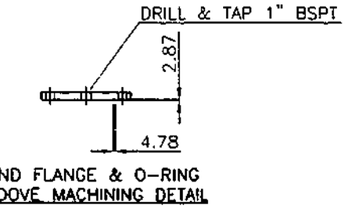

BLIND FLANGE & O–RING GROOVE MACHINING DETAIL

ITEM	DESCRIPTION	QTY/LENGTH
1	110 O.D. PVC PIPE, STORM WATER (3 w.t.)	2210
2	225NB SO FLANGE, PVC, 15mm	2
3	225NB BL FLANGE, PVC, 15mm	2
4	BOLT, CS, M16 x 60MM	8
5	WASHER, FLAT, CS, M16	16
6	NUT, HEX, CS, M16	8
7	O–RING, RUBBER, BS254, 139.3 I.D. x 3.53 W	2
8	THERMOCOUPLE CONNECTION, ø5 O.D. HOLE	30
9	SCREEN, 0.8MM APERTURE x ø.45, ø104 O.D.	3
10	FLAT, CS, 20 x 1 x 345LG	1
11	FLAT, CS, 20 x 1 x 220LG	4
12	SPRING, k=4kN/m, 80LG	1
13	ROUND, CS, ø30 x 3LG	1
14	FLAT, CS, 20 x 2 x 347LG	2
15	FLAT, CS, 5 x 1 x 107LG	1

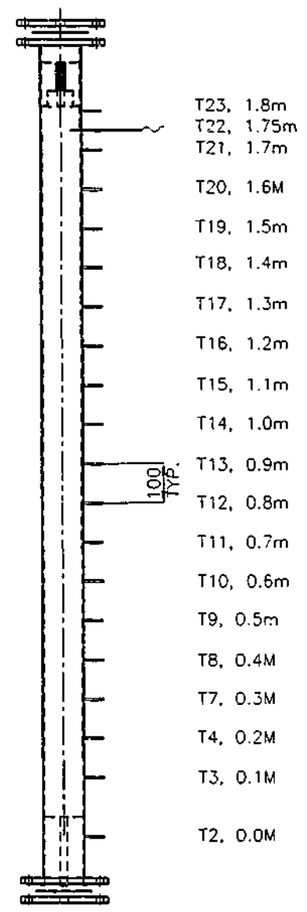

THERMOCOUPLE LOCATION

SCALE 1:16

ADSORBER COLUMN DETAILS
O_2 VSA PILOT PLANT
DEPT. OF CHEMICAL ENGINEERING
MONASH UNIVERSITY

CHECKED: SIMON WILSON

AUTHORIZED: PAUL WEBLEY

DRAWN: CHRIS BEH

VSA–03 C

Appendix D.

Sieve Regeneration Furnace

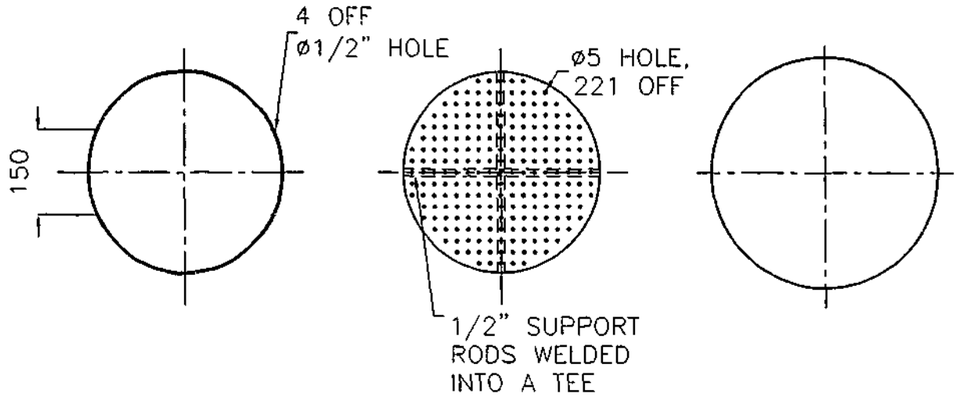

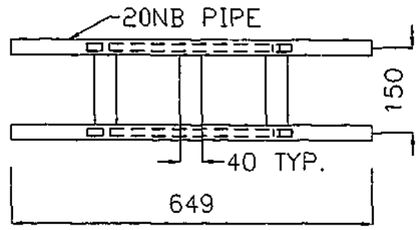

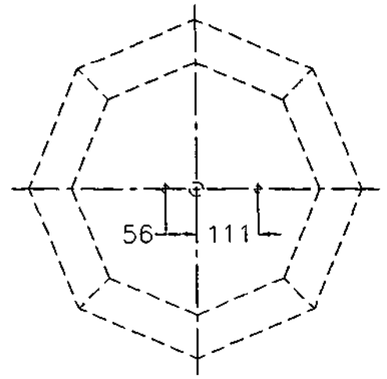

FURNACE LID

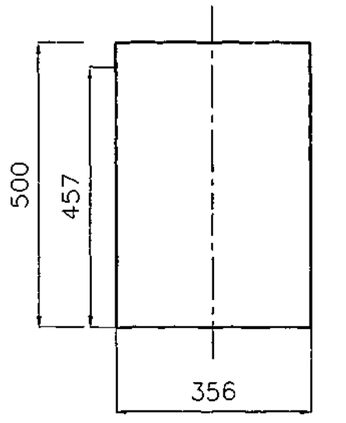

ITEM 1

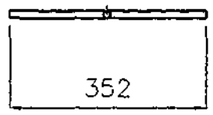

ITEM 2

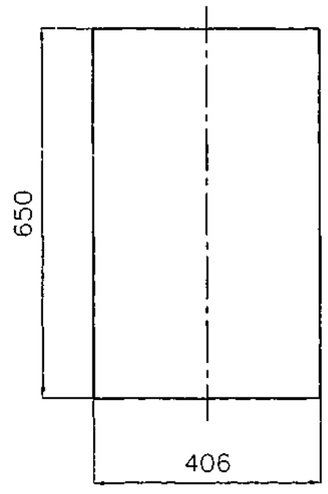

ITEM 3

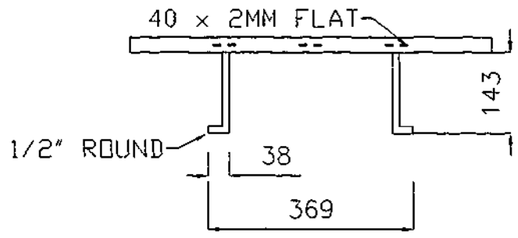

LIFTER

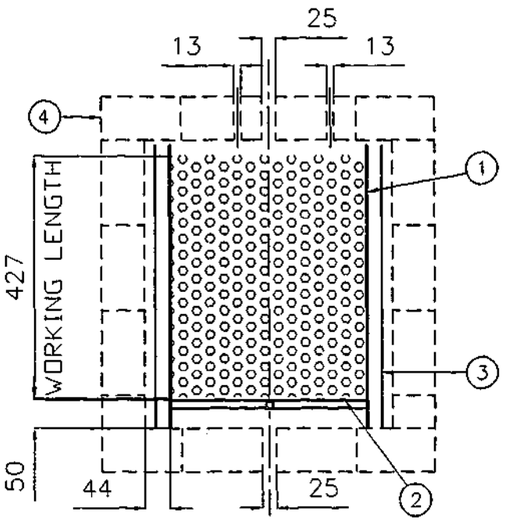

FURNACE X-SECT. GA

NOTES:
1. 41.5L WORKING VOLUME
2. ITEM 2 TO BE WELDED TO ITEM 1
3. 80 MICRON SCREEN TO BE TACK WELDED ON ITEM 3
4. FURNACE LID TO BE HINGED (AS IN STANDARD DESIGN)
5. 1" HOLES ALLOWED FOR IN LID AND BOTTOM OF FURNACE
6. 2 OFF 1/2" HOLES ALLOWED FOR IN LID OF FURNACE
7. TILES TO BE CLAD (INSIDE) ON FURNACE FLOOR - SMOOTH FINISH
8. TETLOW TO SUPPLY SHIMADEN SR72 TEMPERATURE CONTROLLER, SHIMADEN SR72 OVER TEMPERATURE CONTROLLER & SOLID STATE RELAYS

ITEM	DESCRIPTION	QTY/LENGTH
1	356 x 1.6 w.t. WELDED PIPE S.S. 304	500
2	1.6MM S.S. SHEET	1
2	1/2" ROD 352	2
3	406 x 1.2 w.t. SPIRAL LOCK SEAM GALV.	650
4	FURNACE - No. 4 OCTAGONAL KILN, BY TETLOW	1

SCALE 1:11

SIEVE REGENERATION FURNACE
O_2 VSA PILOT PLANT
CHEMICAL ENGINEERING
MONASH UNIVERSITY

CHECKED: RICHARD TODD

AUTHORIZED: PAUL WEBLEY

DRAWN: CHRIS BEH

VSA-04 A